Microfluidic Integration of Multi-Step Bioanalytical Assays

Leah Michele Dignan

Fallston, Maryland

B.S. Chemistry, St. Mary's College of Maryland, 2016

A Dissertation presented to the Graduate Faculty of the University of Virginia in Candidacy for the Degree of Doctor of Philosophy

Department of Chemistry

University of Virginia

July 2022

_____

_____

_____

_____

Abstract

Molecular diagnostics are powerful analytical tools that permit acquisition of useful biochemical information across numerous sectors, including forensic human identification, toxicology, ancestral genotyping, and disease diagnosis. Despite significant recent advances, the vast majority of these bioanalytical techniques remain tethered to benchtop laboratory instrumentation operated by trained analysts via time-consuming, labor-intensive workflows. The growing demand for alternative technologies, especially those amenable for use at the point-of-need, is evidenced by an increase in the translation of microfluidic academic research efforts into commercially-available products. Among these, centrifugal microfluidic 'lab-on-a-disc' (LoaD) platforms are especially promising as powerful, portable alternatives for rapid, cost-efficient, and convenient biomolecular processing by nontechnical personnel on-site, eliminating laboratory dependence entirely.

Molecular diagnostics involving nucleic acids are among the most rapidly growing areas for the development of fieldable analytical tools. However, successful analysis of genetic material requires effective purification from biological samples, a step that has garnered much less attention than downstream amplification and detection techniques. Consequently, nucleic acid preparation is often overlooked and omitted from LoaD strategies entirely, despite the aim for comprehensive translation of the benchtop workflow. This body of work describes research efforts to develop highly integrated, rotationally-driven microfluidic tools to be employed at the point-of-need. For reference, chapter one describes existing centrifugal microfluidic approaches to nucleic acid sample preparation and describes their application in the few sample-to-answer systems that autonomously perform all processes required for genetic analysis. Much of the work highlighted in this dissertation is focused on efforts to expand the repertoire of such microfluidic methods, including the preconcentration of biological targets, cellular/virion lysis, and extraction or purification methods. Chapter two describes the development of a LoaD for dynamic solid phase extraction (SPE) of high-purity polynucleic acids; the preparation mode demonstrated compatibility with a

panel of ubiquitous nucleic acid amplification tests. Similarly, chapter three is centered on the characterization, optimization, and microfluidic adaptation of viral preconcentration and subsequent RNA extraction, specifically intended for rapid pathogen detection. Both of these automatable, portable techniques stand to considerably advance capabilities for centrifugal microfluidic genetic analysis outside of traditional laboratory settings.

The comprehensive reliance of these LoaDs on rotational forces to direct flow confers a high degree of portability; yet, this fluidic control modality has also been cited as a key reason that very few *sample-to-answer* systems exist. Explicitly, leveraging centrifugal force provides unidirectional flow, whereby fluid moves radially outward towards the disc periphery and no further on-board processing is possible. Novel methods for on-disc liquid transport towards the center of rotation would enable sequential integration of nucleic acid preparation, amplification, and detection. Chapter 4 describes a biocompatible method for radially inward fluid displacement that relies on on-board gas generation and allows further rotationally-controlled processing, ultimately permitting increased assay complexity. Chapter 5 explores a second novel method for microfluidic flow control for LoaDs based on embedded cellulosic membranes to enable immunodetection of opioids. These novel flow control methods increase the capabilities of LoaD systems by facilitating the performance of increasingly complex bioassays without compromising portability.

Chapter 6 highlights the potential applications and implications of the techniques described in chapters two through five, future avenues for research exploration, and persistent challenges to be overcome.

Acknowledgements

I am extremely grateful to everyone who has supported me throughout, and prior to, my time at the University of Virginia. First, this achievement would not have been possible without Dr. James Landers – I feel incredibly lucky to have worked under your guidance for the last five years. When I first came to Charlottesville, I was immediately drawn to your application-driven work, which was clearly rooted in creating solutions for tangible, real-world problems. I am so grateful for the opportunity to participate in such impactful, cutting-research, as well as the support, motivation, and opportunities you've given me along the way. Thank you for giving me latitude in designing my research projects, chances to travel the world, truly unique collaborations, and occasions to sit at the table with world-renowned scientists. The high caliber of work ethic and dedication you demonstrate, and expect, has driven my immense growth as a scientist during this journey, which was among the most challenging, yet rewarding, of my life. I will carry these memories with me, and I'll always be incredibly proud to have graduated from your group.

There are numerous additional educators that sparked and sustained my love for science. Of special note, I thank Gretchen White for generating my initial interest in pursuing a career in chemistry. Though it has been several years since high school, I still clearly, and fondly, recall your enthusiasm, optimism, and selfless donation of your resources and time to your students. You made an indelible mark on my professional trajectory. I am also especially grateful for Dr. Andy Koch for fostering my love of research, sense of scientific curiosity, and confidence in the laboratory. The experience I gained working with you has proven invaluable as I continue to grow as a scientist. I would also like to express my appreciation for Dr. Chris Holstege, who provided me with unique, memorable experiences and opportunities throughout continued collaboration over the

years. Despite your numerous roles and commitments, you've been immeasurably generous with your already limited time.

To each of the talented scientists I've worked with in the Landers Lab, thank you for your expertise and insights, which shaped not only the work herein but also my perspective as a scientist. Beyond that, your consistent generosity, kindness, support, humor, and encouragement were integral, especially in particularly challenging times. For their specific contributions to the research in this dissertation, I'm especially grateful to Dr. Shane Woolf, Rachelle Turiello, Jeff Hickey, Aeren Nauman, Christopher Tomley, Isaac Buell, Isabella Mighell, and William Treene. Your dedicated efforts were each instrumental to the completion of the work described in the following chapters.

To my family, I could not imagine having reached this milestone without your continued encouragement, advice, and love. Mom and dad – as long as I can remember, you've been there, whole-heartedly nurturing and supporting my creative and academic goals. Thank you for always believing in me and making me feel like I can do anything. I also want acknowledge the family I have found during my time in Charlottesville. I was immeasurably fortunate to work alongside and form deep, meaningful friendships with such creative, driven, motivated, kind, and warm-hearted women that I'm certain will continue long past our time shared here. To Fermin, mi alma gemela – you are the kindest, most patient, understanding, dependable, and selfless partner I could have ever imagined. Thank you for being there for me, no matter what, and always making me smile. I love you so much, and I can't wait to see where the future takes us.

Dedication

In loving memory of my grandmother, Lola Keys. Thank you for your unconditional love and unshakeable belief in me.

“Hey girl, go for it all. It is there for the picking.”

I carry you always in my heart.

Table of Contents

List of Figures

1. Introduction

1.1. Background

Despite significant recent advances, the vast majority of nucleic acid-based diagnostic techniques remain tethered to benchtop laboratory instrumentation operated by trained analysts via time-consuming, labor-intensive workflows.[1-2] Mandatory performance of a multiplicity of processing steps in centralized facilities limits throughput, increases turnaround times, and ultimately hinders rapid acquisition of actionable information across a variety of sectors – for instance in administering treatment for disease or intoxication.[1, 3] The growing need for alternative diagnostic technologies, especially those that may be performed at the point-of-need (PoN), was magnified by the COVID-19 pandemic, and is evidenced by increasing emphasis on translation of academic research into viable commercial devices.[4] Among these developing technologies, microfluidic systems, including micro total analysis systems (μTAS)[5-6] and "LabCD"[7-8] or lab-on-a-disc (LoaD)[9] platforms, have been explored extensively for in situ nucleic acid (NA) processing across numerous applications.[10-11] In this vein, **Chapters 2-5** describe the development of microscale alternatives to traditional laboratory-based techniques.

1.2. Centrifugal Microfluidics

Among microfluidic approaches, centrifugal systems (e.g., LoaDs) are widely regarded as potentially the most promising for PoN integration of complex processes.[12-14] Following the landmark Anderson et al. publication in 1969 detailing the first small-scale centrifugal analytical device,[15] academic efforts towards development of rotationally-driven microsystems have steadily increased.[13] More recently, LoaDs have exhibited high potential to become a standard tool for mainstream diagnostics, with several major

diagnostic companies (e.g., 3M, Abaxis, Roche, Samsung) having brought centrifugal microsystems to market.[13, 16] Microfluidic integration eliminates complex, laborious, and time-consuming operations, reduces cost, minimizes contamination risk, and enables use outside of traditional analytical settings by nontechnical personnel due to simplicity of operation, ease of automation, portability, and versatility.[9, 13, 17-19] Rotationally-controlled inertial fluid propulsion requires only a simple motor to drive flow, on the scale of nanoliters to milliliters, through a self-contained network of channels and chambers within the disc and without bulky external pumps or high voltage power supplies (**Figure 1-1A**).[13, 16, 20] Within a rotational frame of reference, a fluid with density ρ experiences a centrifugal force (f_ω) defined by:

$$f_\omega = \rho r \omega^2$$

when located at distance r relative to the center of rotation and spinning at a given frequency ω. Centrifugal force acts radially outward from the center of rotation (CoR); though fluid velocity depends not only on f_ω, but also on the design of device microfeatures (e.g., channel geometry) and some fluidic properties, including viscosity (η).[21-22]

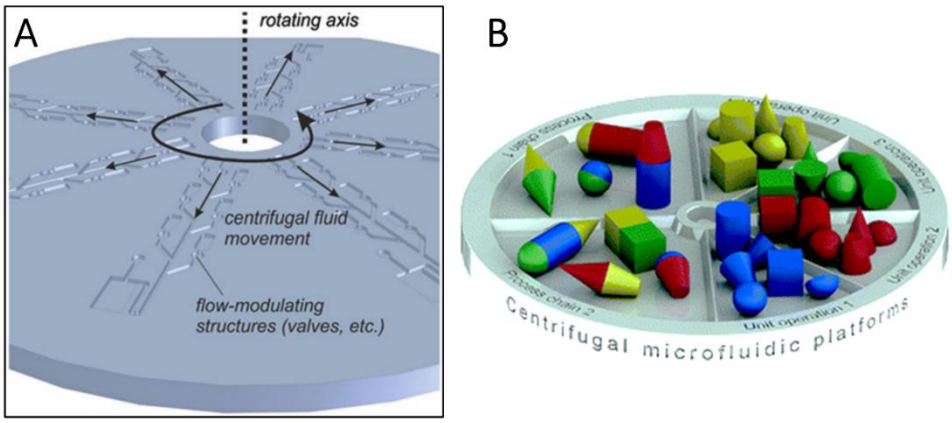

Figure 1-1. Operational principles of LoaD systems. (A) Schematic depiction of centrifugally-driven fluidics. Flow is driven radially outwards relative to the rotating axis, or center of rotation, and is modulated by architectural features (e.g., chambers, channels, and valves) within the microdevice. Such flow modulating structures permit performance of basic functionalities, or unit operations, such as mixing, metering, or aliquoting. Adapted from [20]. (B) Unit operations, depicted as individual, single-color shapes, can be combined and performed sequentially to yield process chains (multi-colored, combined shapes) that mimic laboratory processes. Adapted from [13].

Interestingly, unlike other pumping modes (e.g., electrokinetic pumping), centrifugally-driven flow is largely independent of many other physicochemical properties of the sample fluid, such as ionic strength, pH, and conductivity.[23] This makes LoaD systems amenable to the processing of a myriad of samples, including aqueous solutions, organic solvents, surfactants, and biofluids (e.g., blood, urine, mucus, and semen).[21] Thus, LoaD systems are uniquely well-situated for development with a wide variety of applications and amenable to the automation of diverse tools for biomarker analysis in samples of human origin.[16]

The broad range of applicability of these systems is matched by an enormous breadth of basic functionalities, or "unit operations", that, when used in conjunction, enable highly integrated centrifugal microfluidic systems capable of mirroring functionalities, or "process chains" of conventional benchtop instrumentation (**Figure 1-1B**). Many of these unit operations, including centrifugation, fluid flow, reagent/sample reconstitution, mixing, and filtration, are easily controlled by intrinsic inertial pseudoforces acting on fluids and particles within the LoaD during rotation.[13] However, centrifugation alone is insufficient to perform certain unit operations, and an extrinsic force must be applied. For instance, a central focus of **Chapters 2-3** involves the application of an external magnetic field to manipulate paramagnetic particles within microsystems. Among centrifugal unit operations, valving is perhaps the most essential in allowing for spatiotemporal control over fluid flow and successful sequential integration of individual unit operations into process chains found in existing laboratory workflows (e.g., NA extraction).[13, 16]

1.3. Sample-to-Answer Systems: Definition and Motivation

Development of advanced sample-to-answer centrifugal microfluidic systems for NA analysis constitutes a highly active research area slated for continued growth; fully-integrated molecular diagnostic systems have been described as the 'holy grail' of the μTAS field.[16] In both academic publications and commercial market penetration, clear trends have emerged towards complex, fully-integrated, and self-contained sample-to-answer LoaDs.[13] Despite appearing ubiquitously in scientific literature, the phrase "sample-to-answer" lacks a single, universally accepted definition. We argue that in order to qualify as sample-to-answer, a microfluidic system, comprised of the LoaD itself and the associated "spin stand" or platform, must accept raw, wholly unprocessed samples and perform all process chains required for NA analysis within integrated microfluidic circuits, ideally autonomously, but minimally must be easy to operate with no specialized training or tools. (**Figure 1-2**).[9, 13, 16, 24] Such systems allow for truncation of traditional multi-day workflows that involve transport between several locations (e.g., hospitals and laboratories) to only hours (or less) on-site by non-technical personnel (**Figure 1-3A**).

Explicitly, true sample-to-answer NA analysis in LoaD systems requires microfluidic integration and performance of on-disc NA preparation, amplification, and detection in a predefined sequence without intermittent intervention (**Figure 1-3B**).[1, 25] However, successful on-disc NA preparation from biofluids (e.g., urine, blood, sputum)

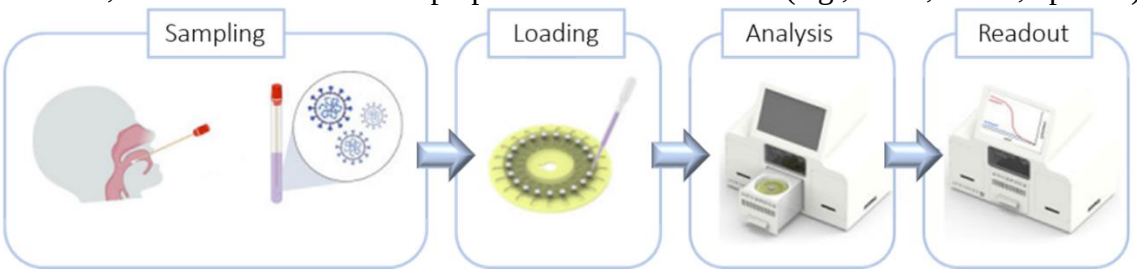

Figure 1-2. Diagrammatic sample-to-answer LoaD depiction. Following (e.g., nasopharyngeal swab) collection, unprocessed sample material is added to a LoaD microdevice and placed into the associated platform ("spin stand") for automated performance of all required assay process chains prior to displaying results. Adapted from [42].

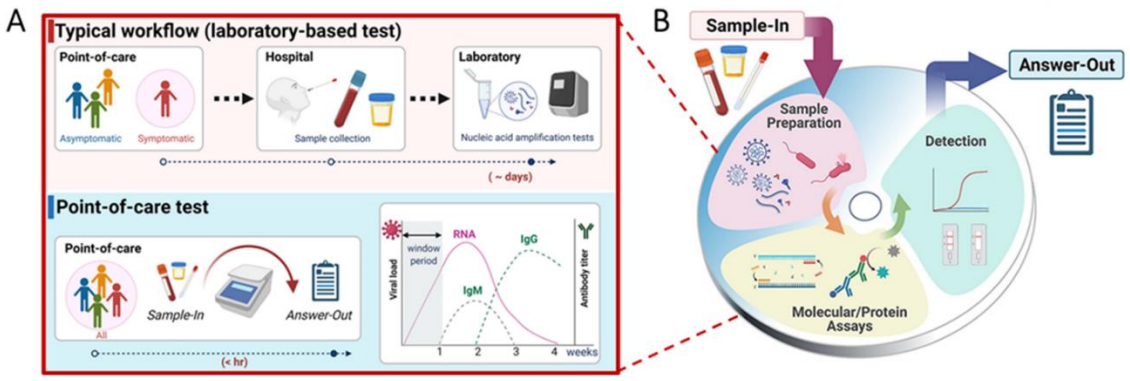

Figure 1-3. Schematic representation of PoN sample-to-answer LoaDs. (A) Typical workflows involve transport between numerous facilities (e.g., hospitals, laboratories) and days-long analytical intervals. PoN tests are capable of performing the traditional workflow on-site in a much shorter interval, hours or less. (B) Sample-to-answer LoaD capable of sequentially performing in-line sample preparation, a bioassay, and detection/readout. Adapted from [24].

requires intricate architectures, elaborate protocols, and has traditionally received less research attention than amplification.[25-28] Consequently, this step is, unfortunately, often overlooked and omitted from microfluidic workflows that aim to comprehensively translate benchtop techniques to the PoN.[10, 28-35] From a practical perspective, NA preparation traditionally necessitates highly manual and laborious processes for lysis and NA extraction (NAE), which are difficult to integrate with PoN workflows, regardless of the automation and portability of downstream amplification and/or detection methods. One recent LoaD system was developed with special focus on ensuring the amplification method was truly fieldable by using commercial hand warming packets for heating during NA amplification;[34] however, off-disc lysis required some degree of reliance on traditional equipment and manual sample handling.[34] Another example in which the practical limitations of manual sample preparation are explicitly evident can be found in consideration of a LoaD system intended for identification of common nut-derived allergens.[35] In this case, heavy emphasis was placed on the simple, convenient, and instrument-free detection afforded by colorimetric loop-mediated isothermal amplification (LAMP) and the intention for use in food inspection departments (e.g., not conventional

laboratories).[35] However, more careful dissection of the comprehensive assay workflow shows that, prior to LoaD processing, genetic material from the allergens was first manually isolated via exposure to liquid nitrogen, grinding in a mortar and pestle, enzymatic (Proteinase K; ProK) cellular lysis (30 min.), two sequential liquid-liquid extractions (each 15 min.), NA precipitation in isopropanol (10 min.), washing, desiccation, and finally resuspension.[35] Not only was this protocol extremely laborious, it required more time than the microfluidic detection assay (60 min.) and provided explicit demonstration that, in the absence of integrated NA preparation, seemingly simple, automatable LoaDs for nucleic acid amplification tests (NAATs) may belie exceedingly more complex and manual workflows. Further, many published LoaD systems misleadingly claim fully integrated or sample-to-answer workflows, yet require some measure of in-tube pre-processing.[1, 31, 36-38] Semantics are important as well; one group described sample-to-answer analysis of "real samples," which they defined as milk already spiked with bacteria and mixed with numerous chemical constituents (lysis buffer, ethanol, and a chaotrope) in-tube.[37] If LoaD systems are reasonably expected to be used at the PoN by non-technical personnel, easy sampling and pretreatment strategies must be considered and included on-disc.[4, 24]

Some LoaD systems mitigate the difficulty of integrating NA preparation by leveraging direct amplification chemistries, including only upstream lysis, not NAE.[13] Direct amplification LoaDs have been successfully utilized for pathogen detection, including in biological matrices (e.g., urine, milk),[39-42] and comprise a large constituency of the relatively few commercialized devices branded as sample-to-answer systems by companies including 3M,[43] GenePOC Inc.,[13] and DiaSorin Molecular, LLC.[9, 16] While true

that forgoing NAE eases implementation, this omission effectively limits the utility of these systems to select applications and sample types, such as those with high target prevalence and/or low amounts of amplification inhibitors.[13] Though the term "sample-to-answer" may be used to describe these microfluidic systems, their scope of use is incredibly narrow. Direct amplification methods also require extensive chemistry optimization and/or engineered enzymes and may also not be amenable for use with certain sample types.[1, 39, 44] For instance, direct amplification from blood samples would prove difficult, as genomic and pathogenic DNA exist at concentrations of only approximately 10^6–10^7 copies/mL and 10–10^2 copies/mL, respectively; successful detection of these NAs generally requires upstream target preconcentration and purification.[16] In fact, the development of a practical, yet reliable, method for DNA preparation from peripheral blood remains a key obstacle in the creation of PoN nucleic acid amplification tests (NAATs) for bloodborne pathogens (e.g., malaria).[28, 31, 45] Conversely, very few niche applications require only NAE, not lysis, to comprehensively address NA analysis. For example, cell-free DNA, a key biomarker in precision oncology, drug resistance, and overall health, can be extracted directly from peripheral blood.[46-48]

In summation, enabling robust, sample-to-answer centrifugal microsystems broadly capable of handling complex biofluids requires inclusion of complete, in-line NA preparation workflows carefully tailored to the intended sample type, volume, and target for detection.[24] Existing centrifugal microfluidic process chains for both lysis and NAE are discussed in the following section.

1.4. Microfluidic NA Preparation Process Chains

1.4.1. Lysis

Lysis is the critical initial step of virtually all molecular genetic tests, whereby rupture of cell/viral membranes makes NAs accessible.[24, 49] Efficient lysis, yielding a high quantity of intact genetic material, is crucial for the success of downstream NAATs.[26-27] Despite a plethora of available methods, microfluidic integration of simple, yet efficient, cell lysis has universally remained a key obstacle towards inclusion of sample preparation in LoaDs;[18, 28] lysis is still frequently performed in-tube prior to assay initiation.[10, 19, 30-35, 38] Broadly, membrane lysis may be performed using mechanical, chemical, or thermal methods; each of these approaches, either in isolation or conjunction, have been demonstrated in LoaD systems.[24] The most appropriate approach for a given application should be selected through careful consideration of multiple parameters, including time, required equipment, interference with downstream post-processing, and sample/cell type.[24]

Chemical methods rely on detergents, enzymes, osmotic shock, and/or other reagents to degrade membranes and constitute the most common lysis strategies, especially for mammalian cells.16, 18-19 Most commercial DNA extraction kits leverage detergents and/or enzymes to lyse cells while chemically stabilizing sample

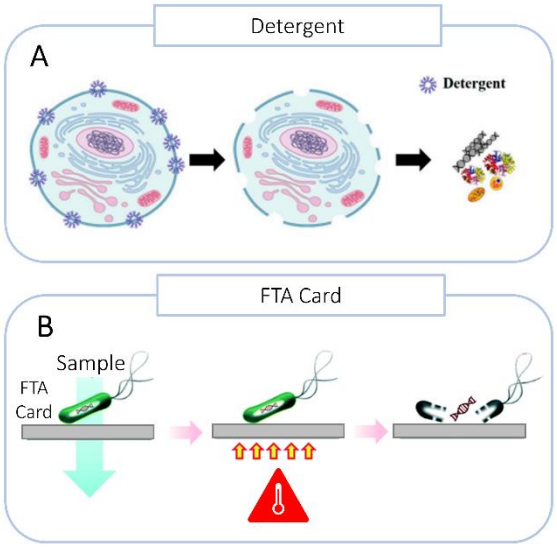

Figure 1-4. Graphical depiction of chemical lysis methods. (A) Chemical lysis is commonly performed via disruption of cellular membranes via exposure to detergents and/or enzymes, making intracellular components, including NAs, available for processing. Adapted from [50]. (B) Bacterial preconcentration and lysis is achieved via capture on an FTA card, which contains denaturants, and heating. Adapted from [51].

pH and reducing nuclease activity (**Figure 1-4A**).[18-19, 50] This approach has been recently demonstrated in a LoaD system that combined several chemical reagents (Tris-HCl, Triton X-100, Tween-20, and octylphenoxy-poly(ethoxyethanol)) to ensure the lysate remains at a LAMP-compatible pH, protect liberated single-stranded RNA, and preserve polymerase activity.[42] In addition to these high-bandwidth approaches, more specialized methods tailored to individual applications have been explored. For instance, one LoaD system achieved on-board lysis via integration of a portion of a Flinders Technology Associates (FTA) card – a specialized type of filter paper with embedded denaturation agents to lyse bacteria and immobilize the liberated genetic material (**Figure 1-4B**).[51] A second, out-of-the-box approach leverages a chimeric peptidoglycan hydrolase (endolysin) that targets distinct bonds in Staphylococcus aureus peptidoglycan to provide genus-specific lysis for downstream methicillin-resistant staphylococcus aureus (MRSA) detection.[52]

Enzymatic approaches to cellular lysis may be thermally expedited, however heating may damage NAs, increases hardware complexity and cost, and usually requires the addition of pressure-resistant valves.[16, 49] Though passive, rotationally-controlled valves are used widely in biomedical microdevices due to simple operation and integration,[16] they are not well-suited for on-disc heated chemical lysis for multiple reasons. First, they operate via a physically open format that fails to provide the pressure resistance essential for reliable fluid containment.[16] Additionally, strict reliance on surface tension hinders spatiotemporal control over the delivery of required reagents, buffers and detergents, which possess exceedingly variable fluidic properties.[1] Sacrificial active valves provide more robust pressure-resistant alternatives largely independent of rotational frequency, precise location on the disc, and sample composition.[16] These strategies permit

the reliable on-disc heating necessary for lysis and ease the integration of complex on-disc assays in general.[53] For instance, thermally-aided on-disc ProK lysis, both in solution[54] and directly from solid substrates (e.g., buccal swab cuttings),[55] has been enabled via active pneumatic pumping[54] and laser valving methods[49, 55] for flow control. Further, other active methods, including wax valving strategies,[11] have also been used in conjunction with chemical lysis. Regardless, chemical lysis methods are often the easiest to implement, including at the microscale,[16, 18] but reagent carryover into lysates may inhibit downstream post-processing (e.g., neutralization is generally required downstream of alkaline lysis to ensure amplification compatibility).[16, 56] Further, chemical methods alone are insufficient for processing bacteria, especially gram-positive species, and tissues; these samples require mechanical lysis.[40, 57]

Mechanical lysis is achieved via physical disruption of membranes through freeze-thaw cycles, grinding, centrifugation, sonication, and/or bead-beating.[19] The majority of on-disc strategies utilize bead-beating methods to lyse cells through collisions, shearing, and friction (**Figure 1-5A**). In fact, the first LoaD lysis system fully dependent on centrifugally-induced forces lysed cells using glass beads alone by alternating rotational directions to induce collisions and shearing (**Figure 1-5B**).[58] This simple, yet effective, strategy has since been augmented through incorporation of magnetically-actuated components to increase impact number and frequency, thereby increasing NA yield.[40-41, 59] Generally, some magnetically-susceptible object (e.g., metal disc,[59] stir bar[40-41]) is added to the sample chamber along with the beads such that exposure to some extrinsic magnetic force causes increased agitation of the beads and cells (**Figure 1-5C-D**). Chemical lysis agents, such as alkaline solutions,[59] can be added but are not necessary.[41] For both gram-

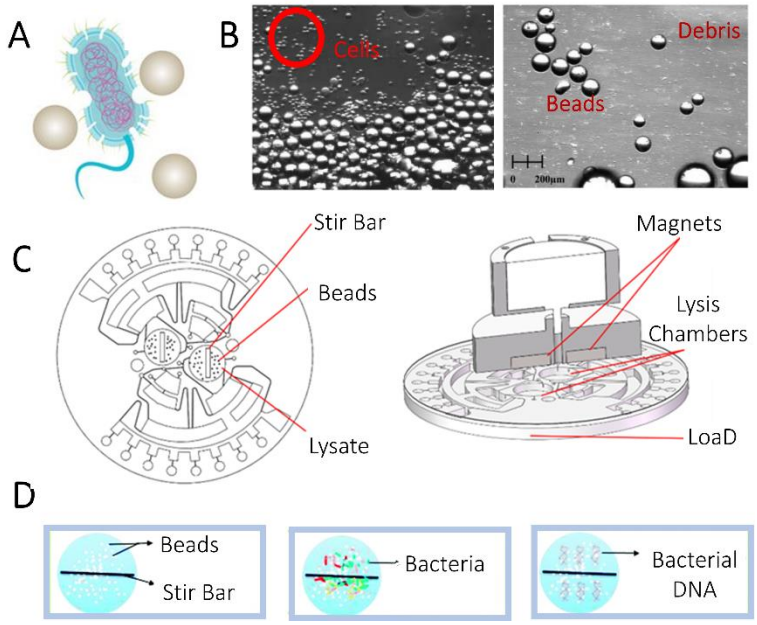

Figure 1-5. Microfluidic mechanical lysis via bead-beating. (A) Bacterial cells are commonly lysed through collisions with particles. Adapted from [59]. (B) Microscopic images of cells before bead-beating (left); cells and beads are the smaller and larger circles, respectively. After lysis (right), cells have been ruptured, debris is apparent in solution. Adapted from [58]. (C) Example LoaD that leverages integrated bead-beating assisted by on-board magnetic stir bars, shown with external permanent magnets used for actuation. Adapted from [41]. (D) Schematic liberation of bacterial DNA via magnetically-assisted bead-beating. Adapted from [40].

positive and gram-negative bacteria, lysis efficiencies of greater than 95% in ≤5 minutes have been reported.[40-41] A more complex approach involves pathogen immunocapture via antibody-coated beads, which are subsequently laser-irradiated to lyse the on-board bacteria via simultaneous heat-shock and mechanical collisions between the thermally excited beads.[53] These approaches are often faster and cheaper than chemical lysis methods and do not introduce inhibitory compounds to the sample, but require substantial additional instrumentation and are more likely to damage genetic material.[18]

1.4.2. Extraction

With the exception of direct amplification methods (discussed in Section 1.3), NAE is crucial for provision of purified, amplification-ready NAs compatible with varied downstream post-processing modalities.[19] In light of the growing demand for PoN genetic analysis, and the accompanying recognition that microfluidic integration of NAE is

essential for realization of sample-to-answer PoN LoaDs, increased recent attention has been placed on this previously neglected area. Yet, successful microfluidic adaptation of laboratory-based NAE workflows that traditionally require highly trained analysts, complex, expensive benchtop instrumentation, and lengthy workflows (up to 3 hours) remains a major bottleneck towards fully-integrated, sample-to-answer solutions.[19, 53] As also true for lysis (Section 1.4.1), selection of the on-disc NAE strategy governs the method's potential for integration with downstream amplification and the speed of detection for the entire process. Regardless, on-disc NAE for sample-to-answer analysis should be simple, rapid, scalable, fully automated, free of cross-contamination, and seamlessly integrated with microfeatures for amplification.[31]

Despite early and sustained laboratory acceptance, liquid-liquid extractions, including phenol-chloroform and cetyltrimethylammonium bromide, have key operational limitations (e.g., hazardous reagents, requirement for specialized glassware, non-automatable steps) that make them impractical for integration with PoN LoaD systems.[19] Most microfluidic NAE approaches instead rely on solid phase extraction (SPE), an approach that is considerably easier to integrate at the microscale.[19] Broadly, in SPE, a solid material (e.g., ion-exchange resin, gel, silica structures) is used to selectively separate NAs from undesired components in a liquid solution (e.g. lysate) by exploiting chemical or physical properties to first bind, then eventually release NAs.[26, 30] This reversible complexation (bind-wash-elute) can be simply controlled by adjusting pH and/or salt concentration.[19] Despite relatively simple operational principles, SPE methods traditionally require numerous manual manipulation steps (e.g., pipetting), that intrinsically create time- and labor-intensive protocols that require complex, carefully

orchestrated microfeatures and associated workflows for LoaD integration.[54] Among solid phases, unmodified silica is most popular (including in commercial systems[4]) due to stability, biocompatibility, and cost-efficient, yet effectual, SPE of high-purity NAs.[25, 60] Further, the versatility of silica fabrication means that it may possess various shapes (particles, gels, powders, microbeads, membranes, micropillars, and monoliths), layering formats, chemical compositions, and filtering capacities for flexible microscale implementation.[19]

Regardless of format, silica-based SPE involves a three step, bind-wash-elute workflow. Initial NA-silica binding occurs in high ionic strength solutions of chaotropic salts (e.g., guanidinium thiocyanate, guanidinium hydrochloride), which strengthen hydrogen bonding interactions and offer the additional benefit of denaturing proteins, such as nucleases.[13, 61] The solid phase is then washed with alcohol, such as ethanol, to remove organic sample contaminants (proteins, metabolites, membrane lipids, etc.) and residual lysis reagents. Both chaotropic salts and ethanol are known PCR inhibitors and significant carryover to eluate is possible.[54] Thus, additional wash steps are often incorporated to ensure inhibitor removal, complicating and extending NA processing. Finally, purified NAs are eluted from the solid phase in a hypo-osmotic solution, such as 1X Tris-EDTA or deionized water.[26, 30] Strict spatiotemporal control over liquid reagent delivery, retention, and removal from the solid phase is imperative for successful implementation of this stepwise silica-based SPE workflow at the microscale. Like lysis, extraction requires solutions (e.g., buffers, ethanol, etc.) with wildly varying fluidic properties that limit passive valve efficacy.[1] Performance of these flow control modalities has been shown to be variable and unreliable in NAE LoaDs, resulting in sub-par assay success rates.[62]

Broadly, silica-based SPE can be divided into column-based methods, where fluid flows through a packed silica bed, or dynamic SPE (dSPE) strategies, in which freely moving silica-coated particles, or beads, are manipulated through the sample.

The preponderance of existing microfluidic strategies utilize dSPE methods over packed-bed (e.g., column, filtration) approaches due to rapid analysis, relatively facile automation, and requirements for only minimal, inexpensive peripheral hardware, essential for cost-efficient, portable, PoN technologies.[19, 26-27] Centrifugal forces can be leveraged to facilitate solid phase interaction with NAs, namely through "shake mode" mixing; alternating the orientation of disc rotation induces back-and-forth bead deflection within a single chamber to facilitate NA capture.[63 17, 47-48, 64-65] Still, the typical format for inducing solid phase – NA interactions during downstream NAE is via magnetism, whereby the silica beads are endowed with magnetic cores (e.g., magnetite) to impart tunable, robust control over subsequent collection and movement.[19, 25] For instance, in several LoaDs, after binding, the beads are magnetically transported through a succession of distinct chambers, each containing a different buffer for washing, and eventually elution (**Figure 1-6A**).[25, 31, 47, 64-66] Conversely, the 'bind-wash-elute' NAE workflow may be performed in a single chamber with magnetically-controlled bead sweeping during each step to maximize bead-solution interaction (**Figure 1-6B**).[17, 55, 62] Magnetic control may also be used to ensure magnetic beads remain in a chamber during fluidic transfer steps, essential for maximizing recovery.[17] NAs obtained via such methods exhibit demonstrated suitability for a variety of applications, including forensic human identification, pathogen detection, and biomarker analysis.[47, 55, 62, 64-65]

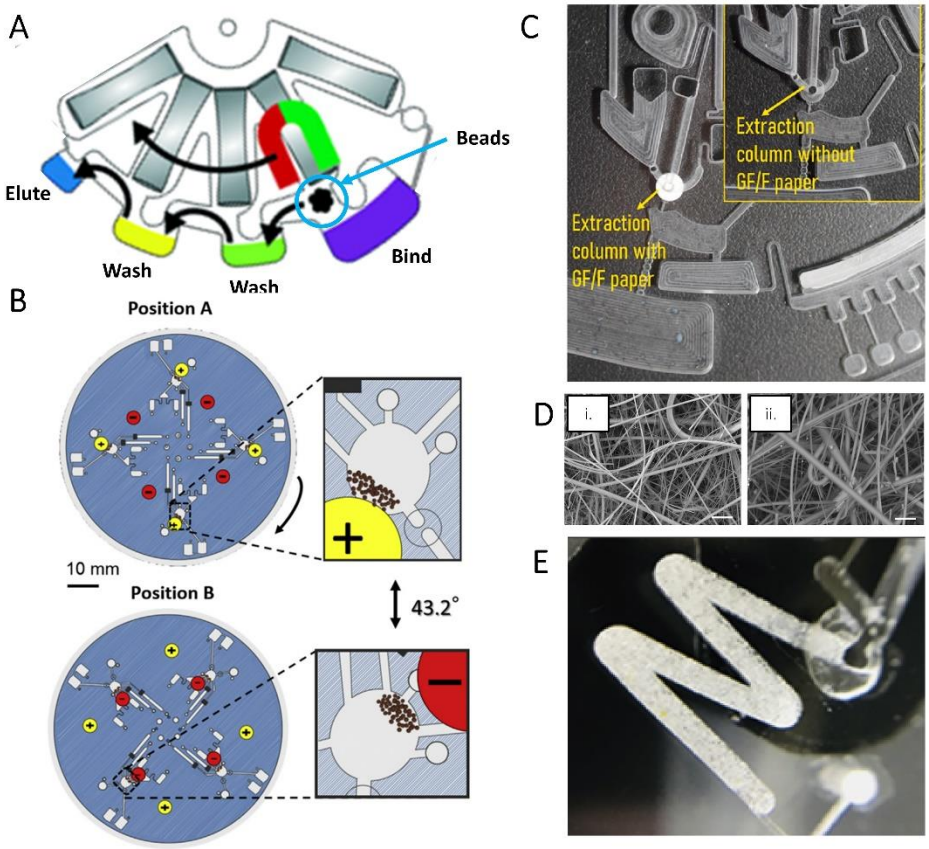

Figure 1-6. On-disc silica-based NAE methods. (A) dSPE achieved via successive bead transfer between chambers containing solutions for NA binding, washing, and elution. Adapted from [65]. (B) Depiction of a microdevice for multiplexed DNA extraction that relied on sequentially passing a series of solutions through a single chamber that housed beads. Bead migration through the chamber, controlled by changing the angular relation of this chamber to external permanent magnets ensured bead-solution interaction. Adapted from [62]. (C) Image of a microdevice with an embedded glass microfiber membrane for SPE. Adapted from [10]. (D) Scanning electron microscope images of (i) the extraction matrix from a QIAamp DNA Mini Kit and (ii) Whatman GF/D glass microfiber membrane that demonstrate similar morphologies. Adapted from [54]. (E) On-disc packed-bed silica microcolumn for SPE. Adapted from [36].

Filtration-based methods for silica SPE, though less common, have also been recently implemented in LoaD systems. Efforts that most closely match existing commercial kits involve on-disc integration of silica components taken directly from Qiagen spin columns.[11, 32] Additional membranes were included for either mechanical support (polycarbonate,[11] PTFE[32]) or in-line filtration (cotton[11]) of insoluble debris components that could obstruct interstitial spaces within the silica. Alternatively, custom NAE membranes have been constructed;[1, 34] in one iteration, one group of researchers added a Zeolite suspension on top of a Whatman paper membrane.[34] Similarly, other

groups have utilized embedded glass microfiber membranes, well suited as NAE columns due to large available surface areas for NA capture (**Figure 1-6C**).[10, 33, 54, 67] Whatman glass-filter membranes (e.g., GF/F, GF/D) are comprised of intertangled, micron-size glass microfibers and exhibit similar morphologies to the matrix used in the QIAamp DNA MiniKit (**Figure 1-6D**).[54] However, these membranes are generally much thinner (GF/F – 420 µM) than those used in the QIAamp columns (1700 µM), making them less likely to completely recover NAs.[54] While stacking GF/F membranes has been exp lored to increase column length, and thereby improve NA recovery,[54] this is more commonly achieved on-disc using silica-packed channels (Figure 1-6E).[14, 36, 38, 61, 68] One publication described an extraction channel filled with ground glass membrane,[14] but most approaches use packed silica beads.

Though silica-based SPE constitutes the majority of on-disc NAE approaches, alternatives have emerged. One especially unique approach involved a slidable centrifugal disc (slip chip) where an FTA card is slid through various chambers to facilitate lysis, NA adsorption, washing, and finally amplification.[51] More widely recognized methods involve NA binding and release from modified amine solid phases, such as chitosan, modulated by tuning pH. In acidic regimes (pH = 5), positively charged amines electrostatically interact with negatively charged NAs. Above neutral pH, however, the amines are neutralized and NAs are released.[30, 69] Low-molecular weight chitosan also inhibits RNases – an advantage over silica phases.[19] Charge-switchable magnetic beads can be used for NAE in LoaDs via workflows that mirror those used with silica solid phases, described above. In one example, after ensuring that the lysate was sufficiently acidic (pH = 5), parasitic DNA was captured on ChargeSwitch® beads during batch mode mixing.[31] The beads were then magnetically

transferred into a wash chamber, then to a final chamber where NAs were desorbed under alkaline conditions (pH = 8.8).[31] Magnetically-susceptible hydrogel nanoparticles represent a second alternative solid phase with demonstrated preparation of amplification-ready NAs from biological matrices.[70] In this case, nanoparticles interacted with pathogens in solution via embedded affinity baits,[70] but antibodies are the most common recognition elements added to functionalized nanoparticles (e.g., streptavidin – biotin linkages).[71] Analyte enrichment prior to lysis improves downstream detection sensitivity, important for development of reliable diagnostic tools.[70-71]

It should be noted that the methods described above have been discussed broadly for use with NAs. Lysis liberates NAs indiscriminately, and many NAE matrices, including silica, can be used to co-extract both DNA and RNA.[19] Extraction specificity is therefore not determined via assay workflow, rather by inclusion of either DNase I or RNase A to recover either RNA or DNA, respectively.[19] However, there are specific considerations that should be given to RNA isolation. RNA is chemically less stable than DNA and is rapidly destroyed by ubiquitous, endogenous RNases; incorporation of strong denaturants into assay workflow aids in obtaining intact RNA.[19] Specific approaches have leveraged chemical differences to preferentially isolate RNA; magnetic beads functionalized with oligo-dTs bind 3' poly-A tails of eukaryotic mRNA to permit selective isolation.[30]

1.5. Sample-to-Answer LoaDs: Discussion and Perspective

Despite the difficulties regarding sample preparation integration discussed above, several examples of centrifugal systems capable of performing comprehensive, sample-to-answer genetic analysis have been described since 2015.[14, 17, 40-41, 51-52, 64-66] Interestingly, each was designed specifically for pathogen detection, namely those that cause respiratory

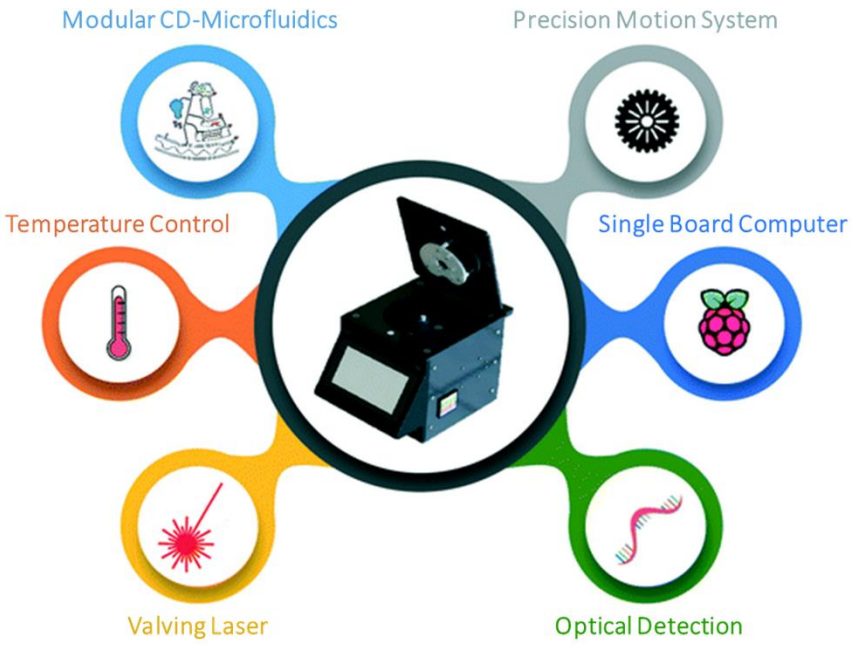

Figure 1-7. Exemplary spin stand for sample-to answer LoaD control. In addition to the microdevice itself, a spin stand capable of autonomously conducting all assay unit operations, such as disc rotation, heating, valving, and detection, is required for practical PoN implementation. Adapted from [59].

infections,[14, 52, 65-66] bloodborne viruses (specifically Hepatitis B)[17], foodborne bacteria,[41, 51, 64] and bacteria in urine.[40] This s ingularity in focus highlights the recent push towards developing simple, rapid NAAT-based PoN diagnostic tools brought to the forefront during the COVID-19 pandemic; demand for testing greatly outpaced laboratory capabilities, and traditional consumables (e.g., SPE kits) became supply chain limited.[4, 33, 72-74] To allow for practical PoN use, each of the published sample-to-answer systems detailed here included both a fully-integrated microdevice and a portable mechatronic system (spin stand) for comprehensive assay automation (**Figure 1-7**).[14, 17, 40-41, 51-52, 64-66] Commercial platforms (Qiagen Lake Constance's "LabPlayer") have been developed to ease LoaD automation, but they may not cover all required functionalities, especially in sample-to-answer workflows. In these cases, a commercial platform must either be augmented or a custom "spin stand" tailored to a particular assay must be developed de novo. The multidisciplinary engineering required to construct such an instrument often creates logistical barriers

towards development of true sample-to-answer systems that contribute to the current existence of relatively few examples.

A subset of the sample-to-answer diagnostic systems that have been published leveraged direct amplification from raw samples, bacterial lysis, and amplification of pathogenic genetic material in the lysate without the need for NAE. As mentioned in Section 1.3, omission of NAE from on-disc workflow eases assay integration but requires carefully optimized, custom chemistries and narrows potential applications.[1, 13, 39, 44] Nonetheless, Liu et al. developed a microdevice for sequential mechanical lysis (bead-beating) followed by loop-mediated isothermal amplification (LAMP) with colorimetric readout.[41] Chen et al. designed a similar fully integrated LoaD that also leveraged bead-beating for lysis and isothermal recombinase polymerase amplification (RPA).[40] We included this work as a sample-to-answer system despite inclusion of upstream, off-disc bacterial preconcentration, as this step improves sensitivity but is not strictly necessary.[40] In arguably the best example of bridging the "world-to-chip" interface among the sample-to-answer systems discussed here, Schulz et al. designed a LoaD capable of accepting an intact nasal swab, then rehydrating and solubilizing the adsorbed bacteria for on-disc processing (**Figure 1-8A,B**).[52] Staphylococcus spp. bacteria in solution were then selectively lysed using a chimeric endolysin and genetic markers for antibiotic resistance were amplified isothermally via RPA.[52] The entire assay was complete in only one hour, a fraction of the traditional 60-hour analytical interval. Not only do Schulz et al. smartly address sample acceptance, they also include on-disc reagent storage. Amplification reagents were stored as a lyophilized pellet, whereas liquid reagents (e.g., buffers) were contained in stickpacks, tubular composite-foil pouches with frangible seals that enable

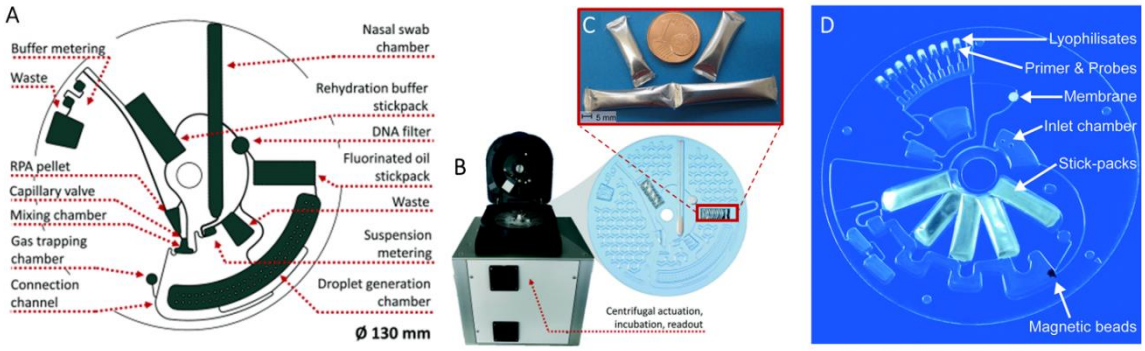

Figure 1-8. Sample-to-answer LoaD with comprehensive on-board reagent storage. (A) Microfluidic architecture that enabled swab acceptance, rehydration, cell lysis, and direct RPA amplification of genetic markers for antibiotic resistance. Amplification reagents were dried and stored on-board. Adapted from [52]. (B) Spin stand for automation of the LoaD shown in A, in which liquid reagents are stored in stickpacks. Adapted from [52]. (C) Image of stickpacks for liquid reagent storage. Adapted from [75]. (D) A LoaD with total on-board storage of dried and liquid reagents using desiccation and stickpacks, respectively. Adapted from [65].

release of reagents via centrifugally-applied pressure (**Figure 1-8C**).[52, 75] Though not included in our definition of sample-to-answer systems, the extent of on-board reagent storage integrated during device fabrication is an important consideration that greatly affects the practicality of PoN implementation. Some systems technically capable of sample-to-answer analysis require reagent preloading by pipette prior to assay initiation, but a more user-friendly option involves comprehensive incorporation of reagents during device fabrication such that the only step required at the PoN is sample loading (**Figure 1-8D**).[14, 17] Amplification reagents, including primers and enzymes, and even magnetic silica beads used for NAE, may be stored on-disc, either freeze-dried or otherwise desiccated, with stability of at least one year.[17, 52, 64, 66] During the assay, these dried components were rehydrated by liquid reagents (e.g., buffers) that were also stored on-board.[25, 52, 64-66] In some instances, all reagents were stored on-disc, completely obviating manual reagent handling in the entirety of assay workflow.[52, 65-66] From a practical perspective, these systems are most representative of those that could feasibly be commercialized for PoN use.

Numerous sample-to-answer NA LoaDs with NAE included were also recently published. With the exception of one centrifugal "slip chip" that leveraged an FTA card for bacterial lysis and DNA extraction upstream of single-temperature recombinase-aided amplification (**Figure 1-9A**),[51] all of these microdevices (published since 2015) incorporated silica-based NAE. Of these, all except one (Liu et al.[14]) (**Figure 1-9B**) achieved NA dSPE by magnetically transferring silica beads between chambers (discussed in Section 1.4.2) (**Figure 1-9C-D**). Though this was unsurprising given that this strategy was the most common NAE approach in LoaDs,[19, 26-27] it is worth noting that in these systems, lysis and NAE depend entirely on application of extrinsic magnetic forces and are wholly independent from centrifugal fluidic control.[64-66] Stated another way, despite LoaD formats, NA preparation process chains in these systems were necessarily controlled by external forces, not centrifugation, to allow for comprehensive integration (**Figure 1-9C-D).** These assay design choices point to a key roadblock towards development of sample-to-answer NA LoaDs which can be attributed to the foundational operational principles underlying centrifugal microfluidics as a whole. Because centrifugally-driven fluid flow is directed radially outward relative to the center of rotation (CoR) in these systems, the number of unit operations that may be successively implemented is effectively limited by device radius.[13] Further, NAE occurred along the disc periphery where centrifugal force, which acts radially outward only, could no longer be used to drive fluid movement.[17, 64-66]

It has long been understood that integration of novel, alternative, non-centrifugal unit operations to drive flow in any direction, but particularly radially inward, would permit integration of more complex, comprehensive on-disc assays.[13, 76] This is certainly the case

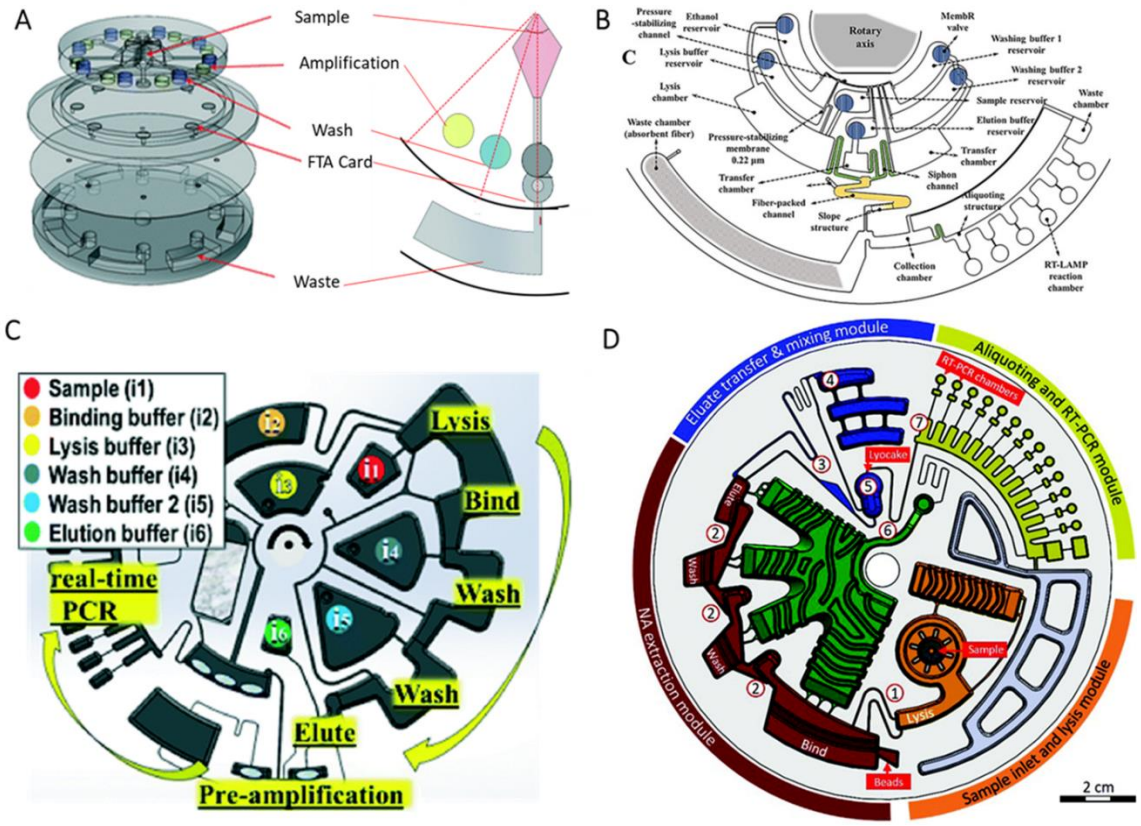

Figure 1-9. Fully-integrated NA processing architectures with SPE. (A) Centrifugal "slip chip" in which bacterial lysis, NAE, and isothermal amplification were performed directly on FTA cards, slid between separate chambers. Adapted from [51]. (B) LoaD that leverages membrane resistant (membR) valves to perform sequential flow of a lysate prepared on-disc, wash solutions, and an elution buffer through a packed silica column prior to on-disc colorimetric LAMP for detection of avian flu. Adapted from [14]. (C) Sample-to-answer LoaD encompassing mechanical lysis, dSPE, and real-time PCR-based bacterial detection from human serum samples. Adapted from [64]. (D) Fully automated centrifugal system for detection of respiratory pathogens (bacteria and viruses). This LoaD uses all the same process chains as the device in (C), but includes total on-board reagent storage. Adapted from [66].

when considering enabling continued downstream centrifugal, on-disc post-processing in these sample-to-answer LoaDs.[17, 64-66] Three such systems[63-65] leveraged centrifugo-dynamic inward pumping, specifically via a strategy described by Zehnle et al (**Fig. 1-10**).[76] Briefly, after lysis and bind-wash-elute NAE, the purified NA eluate was centrifugally pumped into a dead-end, peripheral chamber, compressing, and therefore pressurizing, the air originally contained there. Rapid deceleration decreased the centrifugally-generated hydraulic pressure exerted on the compressed air, allowing it to expand to pneumatically force the bulk eluate radially inward into a collection chamber closer to the CoR.[76] This approach was controlled solely via rotation, intrinsically available

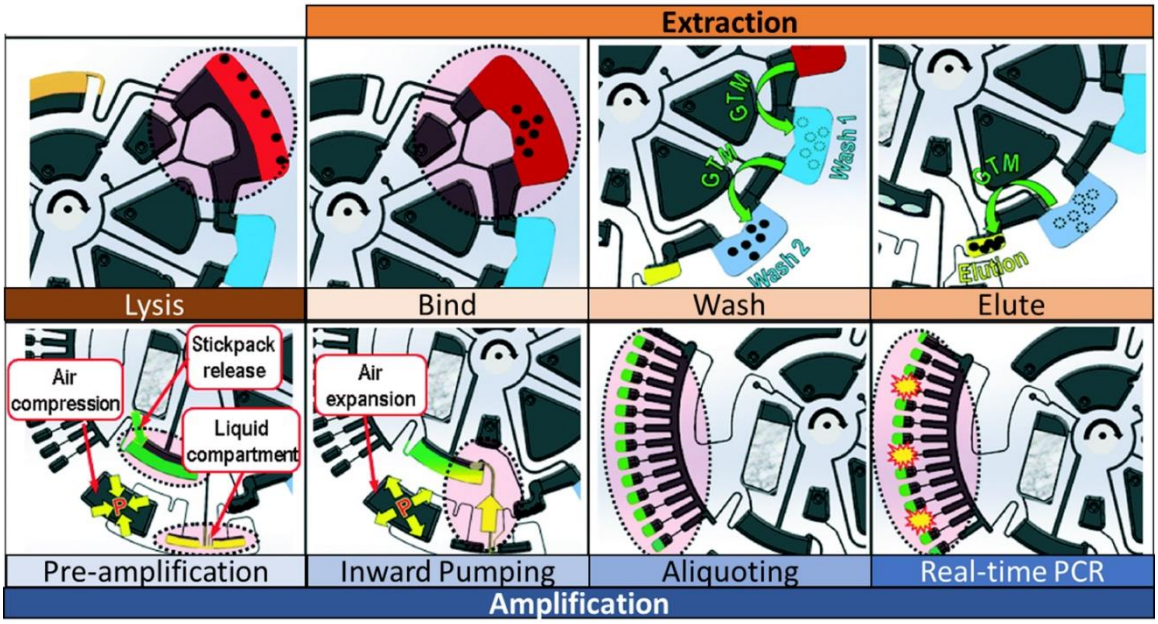

Figure 1-10. Sample-to-answer LoaD with magnetically-controlled dSPE. After on-disc lysis and NA binding, magnetically-susceptible silica-coated beads were transferred between various chambers for washing and NA elution. To facilitate downstream amplification, the eluate was displaced radially inward via centrifugally-controlled hydraulic compression, and subsequent expansion, of an air bubble on-disc. The NA solution was then mixed with amplification reagents and metered into numerous chambers for parallel RT-PCR amplification. Adapted from [64].

via spin stands, such that no specialized external equipment, reagents, or surface modifications were required.[76] Inward fluid displacement was also effectively achieved by Liu et al. using a different strategy, namely by changing the direction in which centrifugal force acted on fluid within their double rotation axis system (**Figure 1-11**).[17] Here, up to four LoaDs, each with a spindle motor that can rotate them individually, were loaded into a single turntable, also controlled by a spin motor.[17] The orientation of each microdevice may be adjusted prior to rotating the turntable to drive flow. Both of these approaches, namely inward fluid displacement and changing the CoR, effectively overcome the steric constraints that frequently preclude centrifugal integration of all process chains for complex assays to permit downstream amplification and detection.[13]

As mentioned above, recent focus has involved supplanting PCR-based amplification with alternative isothermal methods due to simplified hardware requirements

resulting from single-temperature heating.[13, 24, 38] It is unsurprising, therefore, that the two oldest sample-to answer LoaDs discussed here (Stumpf et al.,[65] Czilwick et al.[64]) used real-time PCR amplification. Of the remaining seven more recent sample-to-answer LoaDs highlighted in this section,[14, 17, 40-41, 51-52, 66] only two (Li et al.[17] and Rombach et al.[66]) leveraged PCR-based methods. Though powerful and ubiquitous, these assays rely on expensive fluorescence detection hardware and require relatively long analytical intervals; each of the LoaDs that used multiplexed PCR required upwards of 3 hours for assay completion.[64-66] A large portion of this time was devoted to cycling between denaturation and annealing temperatures at slow rates ranging from 0.7 – 1.0 ˚C/s.65 Isothermal techniques obviate this issue entirely via single-temperature amplification, which simplifies hardware and greatly decreases required analytical time.[77-79] For example, the total assay interval for each of the sample-to-answer LoaDs with isothermal amplification was between 40 and 70 minutes.[14, 40-41, 51-52] Due to reduced equipment requirements and analysis time, as well as compatibility with colorimetric detection in some instances (e.g., LAMP), we expect that in the future, a majority of fieldable sample-to-answer LoaDs will incorporate isothermal NAATs.

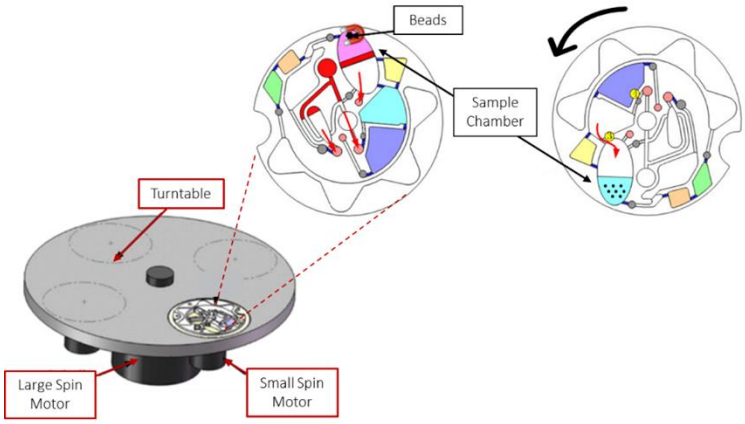

Figure 1-11. Changing CoR to enable comprehensive NA processing. Sequential reagent addition and removal from a single chamber containing magnetic beads was enabled by changing the direction of centrifugal force within the microdevice. To achieve this, up to four LoaDs were loaded onto a turntable, which spun to drive flow. The orientation of the microdevices could be changed via smaller motors within the turntable prior to its rotation using the large motor. Adapted from [17].

In summation, comprehensive NA analysis integration on LoaDs has been enabled via rapidly expanding capabilities in techniques for on-disc fluid pumping, valving, and magnetic manipulation of on-board components (e.g., beads).[13, 80] Recently, and perhaps resulting from the COVID-19 pandemic, increased research effort has been allocated to on-disc NA preparation methods (Section 1.4). Integration of such strategies with microfluidic amplification and detection is essential for development, and eventual commercialization, of portable centrifugal diagnostic tools. On-board storage of both liquid and solid reagents is key in providing LoaDs with fully automated, autonomous sample-to-answer workflows required for practical PoN use. Notably, this review was not intended to focus so heavily on diagnostics, but the majority of recent research driving development of sample-to-answer centrifugal NA processing devices has been concentrated in this arena. Expansion of field-forward genetic analysis LoaD techniques and translation into other disciplines, such as forensic science, has the potential to be transformative in untethering NAATs from centralized laboratories entirely.

1.6. Research Goals and Concluding Remarks

This dissertation is centered on adapting existing laboratory-based workflows for molecular testing to centrifugal microsystems to meet the distinct need for on-site analysis that is currently unmet in forensic and clinical settings alike. The primary focus (**Chapters 2-4**) involves development of methods for nucleic acid preparation in LoaD devices, a research area that has been historically underdeveloped.[26-28] This introductory chapter serves to contextualize this work by describing the current state of the field, namely existing methods for cell lysis, NAE, and their integration with downstream, on-disc post-processing. Specifically, **Chapter 2** focuses on a method for direct-from-swab cellular

lysis and subsequent dSPE within a single centrifugal microsystem. This method is robust, simultaneously co-extracting both DNA and RNA with reliable laser-actuated valving for a variety of applications spanning from clinical diagnostics to forensic human identification. **Chapter 3** describes how many of the principles initially explored in **Chapter 2** were subsequently leverages to the develop and optimize a novel, streamlined method for magnetic nanoparticle-based SARS-CoV-2 virion preconcentration, with subsequent simultaneous lysis and RNA isolation. This method was readily amenable for field-forward usage (e.g., temporary testing clinics) and exhibits the potential to decrease both the analytical interval for infection detection and strain on diagnostic laboratories.[81] Notably, after thorough characterization and optimization, this assay was eventually adapted to a LoaD system.[70] Both of these methods stand to make significant impacts as alternatives to conventional, laboratory-based, supply-chain limited workflows and could be automated for use by nontechnical personnel.

However, upon completion of both assays, purified NA eluates were located at the disc periphery, where further on-disc centrifugal processing was not possible, as seen in many of the sample-to-answer systems discussed in Section 1.5. In these instances, due to assay complexity and the number of process chains required, methods for inward fluid displacement (IFD) were, for the most part, essential.[76] However, the IFD approaches discussed previously possessed operational shortcomings that hinder practical, widespread implementation. Incorporation of two distinct rotation axes increases hardware complexity and cost, as well as instrument size – all detrimental to PoN use.[17] The centrifugo-dynamic inward pumping used in the published sample-to-answer systems relied on passive valving, which permitted backflow during displacement that harmed recovery and ultimately

limited reliability.[16, 64-66] To address these and other shortcomings, **Chapter 4** describes the development and characterization of a novel, actively-valved method for strict spatiotemporal control over inward fluid displacement based on carbon dioxide (CO_2) evolved from an on-board acid-base reaction. We demonstrate successful downstream NAATs following gas-driven inward fluid displacement of NAs prepared on-disc using out-of-the-box enzymatic chemistry for single-step cell lysis and isolation of amplification-ready NAs. These strategies offer improved, automatable methods for on-disc NA preparation that could be performed outside of centralized facilities and exhibit the potential for PoN use and integration with downstream post-processing for sample-to-answer use.

This introductory chapter was focused on NA-based analyses, but immunoassays also constitute a powerful class of analytical tools that have been used extensively for simple, specific, and rapid on-site testing.[82-83] However, lateral-flow immunoassays (LFIs), the most common fieldable format, possess key operational limitations due to reliance on capillary flow – namely poor control over flow and mixing, prevention of automation, and small or variable sampling volumes.[84-86] To address these issues, **Chapter 5** details the development of a centrifugal microfluidic device for performance of colorimetric enzyme-linked immunosorbent assays (ELISAs).[87] ELISAs provide precise, yet relatively cost-efficient, quantitative detection, but, like NA analysis, are largely tethered to operation by highly trained analysts using highly manual workflows and benchtop instrumentation.[88-89] Embedded membranes, not unlike those used for flow control in one sample-to-answer NA LoaD,[14] provided for rotationally-controlled retention, incubation, and elution of the numerous sequential reagents required for successful immunodetection. The bandwidth of

our approach is demonstrated through opiate detection in both buffer and mock clinical samples. Thus, with continued development, this approach has potential for varied application across forensic and toxicological applications and the PoN by non-technical personnel, including law enforcement and clinicians.

In summation, the chapters that follow highlight challenges encountered and progress made towards development of fieldable, bioanalytical alternatives to laboratory-based analyses. The bulk of the work described in this dissertation pertains to NA analysis, but there are also insights included regarding LoaD immunoassay adaptation and novel methods for on-disc flow control that were imperative for success of these assays at large. Finally, **Chapter 6** describes remaining challenges, ongoing efforts to overcome them, and future directions for continued pursuit.

1.7. References

1. Loo, J.; Kwok, H., Leung, C.; Wu, S.; Law, I.; Cheung, Y.; Cheung, Y.; Chin, M.; Kwan, P.; Hui, M., Sample-to-answer on molecular diagnosis of bacterial infection using integrated lab-on-a-disc. *Biosensors and Bioelectronics* **2017,** *93*, 212-219.

2. Jung, W.; Han, J.; Choi, J. W.; Ahn, C. H., Point-of-care testing (POCT) diagnostic systems using microfluidic lab-on-a-chip technologies. *Microelectronic Engineering* **2015**, *132*, 46-57.

3. Krauss, S. T.; Woolf, M. S.; Hadley, K. C.; Collins, N. M.; Nauman, A. Q.; Landers, J. P., Centrifugal microfluidic devices using low-volume reagent storage and inward fluid displacement for presumptive drug detection. *Sensors and Actuators B: Chemical* **2019,** *284*, 704-710.

4. Li, Z.; Bai, Y.; You, M.; Hu, J.; Yao, C.; Cao, L.; Xu, F., Fully integrated microfluidic devices for qualitative, quantitative and digital nucleic acids testing at point of care. *Biosensors and Bioelectronics* **2021,** *177*, 112952.

5. Reyes, D. R.; Iossifidis, D.; Auroux, P. A.; Manz, A., Micro total analysis systems. 1. Introduction, theory, and technology. *Analytical Chemistry* **2002,** *74* (12), 2623-2636.

6. Manz, A.; Graber, N.; Widmer, H. M., Miniaturized total chemical analysis systems: a novel concept for chemical sensing. *Sensors and actuators B: Chemical* **1990,** *1* (1-6), 244-248.

7. Madou, M. J. and Kellogg, G. J. In LabCD: a centrifuge-based microfluidic platform for diagnostics, Systems and Technologies for Clinical Diagnostics and Drug Discovery, International Society for Optics and Photonics: 1998; pp 80-93.

8. Ducrée, J.; Haeberle, S.; Lutz, S.; Pausch, S.; Von Stetten, F.; Zengerle, R., The centrifugal microfluidic Bio-Disk platform. *Journal of Micromechanics and Microengineering* **2007,** *17* (7), S103.

9. Van Nguyen, H.; Nguyen, V. D.; Nguyen, H. Q.; Chau, T. H. T.; Lee, E. Y.; Seo, T. S., Nucleic acid diagnostics on the total integrated lab-on-a-disc for point-of-care testing. *Biosensors and Bioelectronics* **2019,** *141*, 111466.

10. Van Nguyen, H.; Phan, V. M.; Seo, T. S., A portable centrifugal genetic analyzer for multiplex detection of feline upper respiratory tract disease pathogens. *Biosensors and Bioelectronics* **2021,** *193*, 113546.

11. Wang, Y.; Li, Z.; Huang, X.; Ji, W.; Ning, X.; Liu, K.; Tan, J.; Yang, J.; Ho, H. P.; Wang, G., On-board control of wax valve on active centrifugal microfluidic chip and its application for plasmid DNA extraction. *Microfluidics and Nanofluidics* **2019,** *23* (10), 1-11.

12. Foudeh, A. M.; Didar, T. F.; Veres, T.; Tabrizian, M., Microfluidic designs and techniques using lab-on-a-chip devices for pathogen detection for point-of-care diagnostics. *Lab on a Chip* **2012,** *12* (18), 3249-3266.

13. Strohmeier, O.; Keller, M.; Schwemmer, F.; Zehnle, S.; Mark, D.; von Stetten, F.; Zengerle, R.; Paust, N., Centrifugal microfluidic platforms: advanced unit operations and applications. *Chemical Society Reviews* **2015,** *44* (17), 6187-6229.

14. Liu, Q.; Zhang, X.; Chen, L.; Yao, Y.; Ke, S.; Zhao, W.; Yang, Z.; Sui, G., A sample-to-answer labdisc platform integrated novel membrane-resistance valves

for detection of highly pathogenic avian influenza viruses. *Sensors and Actuators B: Chemical* **2018,** *270*, 371-381.

15. Anderson, N. G., The development of automated systems for clinical and research use. *Clinica Chimica Acta* **1969,** *25* (2), 321-330.

16. Gorkin, R.; Park, J.; Siegrist, J.; Amasia, M.; Lee, B. S.; Park, J.-M.; Kim, J.; Kim, H.; Madou, M.; Cho, Y.-K., Centrifugal microfluidics for biomedical applications. *Lab on a Chip* **2010,** *10* (14), 1758-1773.

17. Li, L.; Miao, B.; Li, Z.; Sun, Z.; Peng, N., Sample-to-answer hepatitis B virus DNA detection from whole blood on a centrifugal microfluidic platform with double rotation axes. *ACS Sensors* **2019,** *4* (10), 2738-2745.

18. Jahromi, A. K.; Saadatmand, M.; Eghbal, M.; Yeganeh, L. P., Development of simple and efficient Lab-on-a-Disc platforms for automated chemical cell lysis. *Scientific Reports* **2020,** *10* (1), 1-13.

19. Obino, D.; Vassalli, M.; Franceschi, A.; Alessandrini, A.; Facci, P.; Viti, F., An Overview on Microfluidic Systems for Nucleic Acids Extraction from Human Raw Samples. *Sensors* **2021,** *21* (9), 3058.

20. Castillo-León, J.; Svendsen, W. E., Lab-on-a-Chip devices and micro-total analysis systems: a practical guide. Springer: 2014.

21. Madou, M.; Zoval, J.; Jia, G.; Kido, H.; Kim, J.; Kim, N., Lab on a CD. *Annual Review of Biomedical Eng*ineering **2006,** *8*, 601-628.

22. Zoval, J. V.; Madou, M. J., Centrifuge-based fluidic platforms. *Proceedings of the IEEE* **2004,** *92* (1), 140-153.

23. Duffy, D. C.; Gillis, H. L.; Lin, J.; Sheppard, N. F.; Kellogg, G. J., Microfabricated centrifugal microfluidic systems: characterization and multiple enzymatic assays. *Analytical Chemistry* **1999,** *71* (20), 4669-4678.

24. Sunkara, V.; Kumar, S.; Sabaté Del Río, J.; Kim, I.; Cho, Y.-K., Lab-on-a-Disc for Point-of-Care Infection Diagnostics. *Accounts of Chemical Research* **2021,** *54* (19), 3643-3655.

25. Sciuto, E. L.; Petralia, S.; Calabrese, G.; Conoci, S., An integrated biosensor platform for extraction and detection of nucleic acids. *Biotechnology and Bioengineering* **2020,** *117* (5), 1554-1561.

26. Ali, N.; Rampazzo, R. C. P.; Costa, A. D. T.; Krieger, M. A., Current nucleic acid extraction methods and their implications to point-of-care diagnostics. *BioMed Research International* **2017,** *2017*.

27. Wu, J.; Kodzius, R.; Cao, W.; Wen, W., Extraction, amplification and detection of DNA in microfluidic chip-based assays. *Microchimica Acta* **2014,** *181* (13-14), 1611-1631.

28. Dineva, M. A.; Mahilum-Tapay, L.; Lee, H., Sample preparation: a challenge in the development of point-of-care nucleic acid-based assays for resource-limited settings. *Analyst* **2007,** *132* (12), 1193-1199.

29. Mariella, R., Sample preparation: the weak link in microfluidics-based biodetection. *Biomedical Microdevices* **2008,** *10* (6), 777-784.

30. Kim, J.; Johnson, M.; Hill, P.; Gale, B. K., Microfluidic sample preparation: cell lysis and nucleic acid purification. *Integrative Biology* **2009,** *1* (10), 574-586.

31. Choi, G.; Prince, T.; Miao, J.; Cui, L.; Guan, W., Sample-to-answer palm-sized nucleic acid testing device towards low-cost malaria mass screening. Biosensors and *Bioelectronics* **2018,** *115*, 83-90.

32. Wang, G.; Tan, J.; Tang, M.; Zhang, C.; Zhang, D.; Ji, W.; Chen, J.; Ho, H. P.; Zhang, X., Binary centrifugal microfluidics enabling novel, digital addressable functions for valving and routing. *Lab on a Chip* **2018,** *18* (8), 1197-1206.

33. Van Nguyen, H.; Seo, T. S., High-throughput human DNA purification on a centrifugal microfluidic device for rapid forensic sex-typing. *Biosensors and Bioelectronics* 2021, *181*, 113161.

34. Zhang, L.; Tian, F.; Liu, C.; Feng, Q.; Ma, T.; Zhao, Z.; Li, T.; Jiang, X.; Sun, J., Hand-powered centrifugal microfluidic platform inspired by the spinning top for sample-to-answer diagnostics of nucleic acids. *Lab on a Chip* **2018,** *18* (4), 610-619.

35. Yuan, D.; Kong, J.; Li, X.; Fang, X.; Chen, Q., Colorimetric LAMP microfluidic chip for detecting three allergens: peanut, sesame and soybean. *Scientific Reports* **2018,** *8* (1), 1-8.

36. Van Nguyen, H.; Nguyen, V. D.; Lee, E. Y.; Seo, T. S., Point-of-care genetic analysis for multiplex pathogenic bacteria on a fully integrated centrifugal microdevice with a large-volume sample. *Biosensors and Bioelectronics* **2019,** *136*, 132-139.

37. Oh, S. J.; Park, B. H.; Choi, G.; Seo, J. H.; Jung, J. H.; Choi, J. S.; Seo, T. S., Fully automated and colorimetric foodborne pathogen detection on an integrated centrifugal microfluidic device. *Lab on a Chip* **2016,** *16* (10), 1917-1926.

38. Oh, S. J.; Seo, T. S., Combination of a centrifugal microfluidic device with a solution-loading cartridge for fully automatic molecular diagnostics. *Analyst* **2019,** *144* (19), 5766-5774.

39. Choi, G.; Jung, J. H.; Park, B. H.; Oh, S. J.; Seo, J. H.; Choi, J. S.; Seo, T. S., A centrifugal direct recombinase polymerase amplification (direct-RPA) microdevice for multiplex and real-time identification of food poisoning bacteria. *Lab on a Chip* **2016,** *16* (12), 2309-2316.

40. Chen, J.; Xu, Y.; Yan, H.; Zhu, Y.; Wang, L.; Zhang, Y.; Lu, Y.; Xing, W., Sensitive and rapid detection of pathogenic bacteria from urine samples using multiplex recombinase polymerase amplification. *Lab on a Chip* **2018,** *18* (16), 2441-2452.

41. Liu, D.; Zhu, Y.; Li, N.; Lu, Y.; Cheng, J.; Xu, Y., A portable microfluidic analyzer for integrated bacterial detection using visible loop-mediated amplification. *Sensors and Actuators B: Chemical* **2020,** *310*, 127834.

42. Tian, F.; Liu, C.; Deng, J.; Han, Z.; Zhang, L.; Chen, Q.; Sun, J., A fully automated centrifugal microfluidic system for sample-to-answer viral nucleic acid testing. *Science China Chemistry* **2020,** *63* (10), 1498-1506.

43. The Direct Amplification Disc. https://www.focusdx.com/integrated-cycler/dad-intl/ (Accessed March 8, 2022).

44. Fuehrer, H. P.; Fally, M. A.; Habler, V. E.; Starzengruber, P.; Swoboda, P.; Noedl, H., Novel nested direct PCR technique for malaria diagnosis using filter paper samples. *Journal of Clinical Microbiology* **2011,** *49* (4), 1628-1630.

45. Kolluri, N.; Klapperich, C.; Cabodi, M., Towards lab-on-a-chip diagnostics for malaria elimination. *Lab on a Chip* **2018,** *18* (1), 75-94.

46. Xu, Z.; Qiao, Y.; Tu, J., Microfluidic Technologies for cfDNA Isolation and Analysis. *Micromachines* **2019,** *10* (10), 672.

47. Hu, F.; Li, J.; Peng, N.; Li, Z.; Zhang, Z.; Zhao, S.; Duan, M.; Tian, H.; Li, L.; Zhang, P., Rapid isolation of cfDNA from large-volume whole blood on a centrifugal microfluidic chip based on immiscible phase filtration. *Analyst* **2019,** *144* (14), 4162-4174.

48. Kim, C. J.; Park, J.; Sunkara, V.; Kim, T.-H.; Lee, Y.; Lee, K.; Kim, M.-H.; Cho, Y.-K., Fully automated, on-site isolation of cfDNA from whole blood for cancer therapy monitoring. *Lab on a Chip* **2018,** *18* (9), 1320-1329.

49. Seo, M. J.; Yoo, J.-C., Lab-on-a-Disc platform for automated chemical cell lysis. *Sensors* **2018,** 18 (3), 687.

50. Shehadul Islam, M.; Aryasomayajula, A.; Selvaganapathy, P. R., A review on macroscale and microscale cell lysis methods. *Micromachines* **2017,** *8* (3), 83.

51. Wang, S.; Cai, G.; Duan, H.; Qi, W.; Lin, J., Automatic and multi-channel detection of bacteria on a slidable centrifugal disc based on FTA card nucleic acid extraction and recombinase aided amplification. *Lab on a Chip* **2022,** *22* (1), 80-89.

52. Schulz, M. et al. Point-of-care testing system for digital single cell detection of MRSA directly from nasal swabs. *Lab on a Chip* **2020,** *20* (14), 2549-2561.

53. Cho, Y. K.; Lee, J. G.; Park, J. M.; Lee, B.-S.; Lee, Y.; Ko, C., One-step pathogen specific DNA extraction from whole blood on a centrifugal microfluidic device. *Lab on a Chip* **2007,** *7* (5), 565-573.

54. Brassard, D.; Geissler, M.; Descarreaux, M.; Tremblay, D.; Daoud, J.; Clime, L.; Mounier, M.; Charlebois, D.; Veres, T., Extraction of nucleic acids from blood: unveiling the potential of active pneumatic pumping in centrifugal microfluidics

for integration and automation of sample preparation processes. *Lab on a Chip* **2019,** *19* (11), 1941-1952.

55. Dignan, L. M.; Woolf, M. S.; Tomley, C. J.; Nauman, A. Q.; Landers, J. P., Multiplexed Centrifugal Microfluidic System for Dynamic Solid-Phase Purification of Polynucleic Acids Direct from Buccal Swabs. *Analytical Chemistry* **2021,** *93* (19), 7300-7309.

56. Homann, A. R.; Niebling, L.; Zehnle, S.; Beutler, M.; Delamotte, L.; Rothmund, M.-C.; Czurratis, D.; Beller, K. D.; Zengerle, R.; Hoffmann, H., A microfluidic cartridge for fast and accurate diagnosis of Mycobacterium tuberculosis infections on standard laboratory equipment. *Lab on a Chip* **2021,** *21* (8), 1540-1548.

57. Zourob, M.; Elwary, S.; Turner, A. P., Principles of bacterial detection: biosensors, recognition receptors and microsystems. Springer Science & Business Media: 2008.

58. Kim, J.; Jang, S. H.; Jia, G.; Zoval, J. V.; Da Silva, N. A.; Madou, M. J., Cell lysis on a microfluidic CD (compact disc). *Lab on a Chip* **2004,** *4* (5), 516-522.

59. Perebikovsky, A.; Liu, Y.; Hwu, A.; Kido, H.; Shamloo, E.; Song, D.; Monti, G.; Shoval, O.; Gussin, D.; Madou, M., Rapid sample preparation for detection of antibiotic resistance on a microfluidic disc platform. *Lab on a Chip* **2021,** *21* (3), 534-545.

60. Yin, J.; Suo, Y.; Zou, Z.; Sun, J.; Zhang, S.; Wang, B.; Xu, Y.; Darland, D.; Zhao, J. X.; Mu, Y., Integrated microfluidic systems with sample preparation and nucleic acid amplification. *Lab on a Chip* **2019,** *19* (17), 2769-2785.

61. Park, B. H.; Oh, S. J.; Jung, J. H.; Choi, G.; Seo, J. H.; Lee, E. Y.; Seo, T. S., An integrated rotary microfluidic system with DNA extraction, loop-mediated isothermal amplification, and lateral flow strip based detection for point-of-care pathogen diagnostics. *Biosensors and Bioelectronics* **2017,** *91*, 334-340.

62. Jackson, K.; Borba, J.; Meija, M.; Mills, D.; Haverstick, D.; Olson, K.; Aranda, R.; Garner, G.; Carrilho, E.; Landers, J., DNA purification using dynamic solid-phase extraction on a rotationally-driven polyethylene-terephthalate microdevice. *Analytica Chimica Acta* **2016,** *937*, 1-10.

63. Grumann, M.; Geipel, A.; Riegger, L.; Zengerle, R.; Ducrée, J., Batch-mode mixing on centrifugal microfluidic platforms. *Lab on a Chip* **2005,** *5* (5), 560-565.

64. Czilwik, G.; Messinger, T.; Strohmeier, O.; Wadle, S.; Von Stetten, F.; Paust, N.; Roth, G.; Zengerle, R.; Saarinen, P.; Niittymäki, J., Rapid and fully automated bacterial pathogen detection on a centrifugal-microfluidic LabDisk using highly sensitive nested PCR with integrated sample preparation. *Lab on a Chip* **2015,** *15* (18), 3749-3759.

65. Stumpf, F.; Schwemmer, F.; Hutzenlaub, T.; Baumann, D.; Strohmeier, O.; Dingemanns, G.; Simons, G.; Sager, C.; Plobner, L.; Von Stetten, F., LabDisk with complete reagent prestorage for sample-to-answer nucleic acid based detection of respiratory pathogens verified with influenza A H3N2 virus. *Lab on a Chip* **2016,** *16* (1), 199-207.

66. Rombach, M.; Hin, S.; Specht, M.; Johannsen, B.; Lüddecke, J.; Paust, N.; Zengerle, R.; Roux, L.; Sutcliffe, T.; Peham, J. R., RespiDisk: a point-of-care platform for fully automated detection of respiratory tract infection pathogens in clinical samples. *Analyst* **2020,** *145* (21), 7040-7047.

67. Garneret, P.; Coz, E.; Martin, E.; Manuguerra, J.-C.; Brient-Litzler, E.; Enouf, V.; González Obando, D. F.; Olivo-Marin, J. C.; Monti, F.; van der Werf, S., Performing point-of-care molecular testing for SARS-CoV-2 with RNA extraction and isothermal amplification. *PLoS One* **2021,** *16* (1), e0243712.

68. Kinahan, D. J.; Burger, R.; Lawlor, D.; Early, P. L.; Vembadi, A.; McArdle, N. A.; Kilcawley, N. A.; Glynn, M. T.; Ducrée, J., Centrifugally automated Solid-Phase Extraction of DNA by immiscible liquid valving and chemically powered centripetal pumping of peripherally stored reagents. *Biosensors and Bioelectronics: X* **2021,** 100085.

69. Cao, W.; Easley, C. J.; Ferrance, J. P.; Landers, J. P., Chitosan as a polymer for pH-induced DNA capture in a totally aqueous system. *Analytical Chemistry* **2006,** *78* (20), 7222-7228.

70. Turiello, R.; Dignan, L. M.; Thompson, B.; Poulter, M.; Hickey, J.; Chapman, J.; Landers, J. P., Centrifugal microfluidic method for enrichment and enzymatic extraction of Severe Acute Respiratory Syndrome Coronavirus 2 RNA. *Analytical Chemistry* **2022,** *94* (7), 3287-3295.

71. Kant, K.; Shahbazi, M.-A.; Dave, V. P.; Ngo, T. A.; Chidambara, V. A.; Than, L. Q.; Bang, D. D.; Wolff, A., Microfluidic devices for sample preparation and rapid detection of foodborne pathogens. *Biotechnology Advances* **2018,** *36* (4), 1003-1024.

72. Larremore, D. B.; Fosdick, B. K.; Bubar, K. M.; Zhang, S.; Kissler, S. M.; Metcalf, C. J. E.; Buckee, C. O.; Grad, Y. H., Estimating SARS-CoV-2 seroprevalence and epidemiological parameters with uncertainty from serological surveys. *eLife* **2021,** *10*, e64206.

73. Barclay, R.; Akhrymuk, I.; Patnaik, A.; Callahan, V.; Lehman, C.; Andersen, P.; Barbero, R.; Barksdale, S.; Dunlap, R.; Goldfarb, D., Hydrogel particles improve detection of SARS-CoV-2 RNA from multiple sample types. *Scientific Reports* **2020,** *10* (1), 1-11.

74. Corman, V. M.; Landt, O.; Kaiser, M.; Molenkamp, R.; Meijer, A.; Chu, D. K.; Bleicker, T.; Brünink, S.; Schneider, J.; Schmidt, M. L., Detection of 2019 novel coronavirus (2019-nCoV) by real-time RT-PCR. *Eurosurveillance* **2020,** *25* (3), 2000045.

75. van Oordt, T.; Barb, Y.; Smetana, J.; Zengerle, R.; von Stetten, F., Miniature stick-packaging–an industrial technology for pre-storage and release of reagents in lab-on-a-chip systems. *Lab on a Chip* **2013,** *13* (15), 2888-2892.

76. Zehnle, S.; Schwemmer, F.; Roth, G.; von Stetten, F.; Zengerle, R.; Paust, N., Centrifugo-dynamic inward pumping of liquids on a centrifugal microfluidic platform. *Lab on a Chip* **2012,** *12* (24), 5142-5145.

77. Ahmad, F.; Hashsham, S. A., Miniaturized nucleic acid amplification systems for rapid and point-of-care diagnostics: a review. *Analytica Chimica Acta* **2012,** *733*, 1-15.

78. El Wahed, A. A.; Patel, P.; Maier, M.; Pietsch, C.; Rüster, D.; Böhlken-Fascher, S.; Kissenkötter, J.; Behrmann, O.; Frimpong, M.; Diagne, M. M., Suitcase Lab for rapid detection of SARS-CoV-2 based on recombinase polymerase amplification assay. *Analytical Chemistry* **2021,** *93* (4), 2627-2634.

79. Tang, Y. W.; Schmitz, J. E.; Persing, D. H.; Stratton, C. W., Laboratory diagnosis of COVID-19: current issues and challenges. *Journal of Clinical Microbiology* **2020,** *58* (6), e00512-20.

80. Tang, M.; Wang, G.; Kong, S.-K.; Ho, H. P., A review of biomedical centrifugal microfluidic platforms. *Micromachines* **2016,** *7* (2), 26.

81. Dignan, L. M.; Turiello, R.; Layne, T. R.; O'Connell, K. C.; Hickey, J.; Chapman, J.; Poulter, M. D.; Landers, J. P., An ultrafast SARS-CoV-2 virus enrichment and extraction method compatible with multiple modalities for RNA detection. *Analytica Chimica Acta* **2021,** *1180*, 338846.

82. Li, Y. F.; Sun, Y. M.; Beier, R. C.; Lei, H. T.; Gee, S.; Hammock, B. D.; Wang, H.; Wang, Z.; Sun, X.; Shen, Y. D., Immunochemical techniques for multianalyte analysis of chemical residues in food and the environment: A review. *TrAC Trends in Analytical Chemistry* **2017,** *88*, 25-40.

83. Gan, S. D.; Patel, K. R., Enzyme immunoassay and enzyme-linked immunosorbent assay. *Journal of Investigative Dermatology* **2013,** *133* (9), e12.

84. Woolf, M. S.; Dignan, L. M.; Karas, S. M.; Lewis, H. M.; Hadley, K. C.; Nauman, A. Q.; Gates-Hollingsworth M. A.; AuCoin D. P.; Green H. R.; Geise G. M.; Landers J. P.; Characterization of a centrifugal microfluidic vertical flow platform. Micromachines 2021, 13 (3) 487.

85. Gong, M. M.; Sinton, D., Turning the page: advancing paper-based microfluidics for broad diagnostic application. *Chemical Reviews* **2017,** *117* (12), 8447-8480.

86. Gubala, V.; Harris, L. F.; Ricco, A. J.; Tan, M. X.; Williams, D. E., Point of care diagnostics: status and future. *Analytical Chemistry* **2012,** *84* (2), 487-515.

87. Dignan, L. M.; Woolf, M. S.; Ross, J. A.; Baehr, C.; Holstege, C. P.; Pravetoni, M.; Landers, J. P., A Membrane-Modulated Centrifugal Microdevice for Enzyme-Linked Immunosorbent Assay-Based Detection of Illicit and Misused Drugs. *Analytical Chemistry* **2021,** *93* (48), 16213-16221.

88. Lequin, R. M., Enzyme immunoassay (EIA)/enzyme-linked immunosorbent assay (ELISA). *Clinical Chemistry* **2005,** *51* (12), 2415-2418.

89. Noroozi, Z.; Kido, H.; Peytavi, R.; Nakajima-Sasaki, R.; Jasinskas, A.; Micic, M.; Felgner, P. L.; Madou, M. J., A multiplexed immunoassay system based upon reciprocating centrifugal microfluidics. *Review of Scientific Instruments* **2011,** *82* (6), 064303.

2. Centrifugal Microfluidic Dynamic Solid Phase Extraction

2.1. Introduction

Molecular genetic analysis, discussed in detail in **Chapter 1**, is a complex pipeline that requires a multiplicity of processing steps to obtain meaningful information from a sample. While direct amplification is possible for some applications,[1-4] most analyses rely on upstream nucleic acid extraction (NAE) as a critical, foundational step following cellular lysis to make liberated nucleic acids (NAs) amenable for downstream post-processing.[5-6] Numerous on-site nucleic acid amplification tests (NAATs) have emerged in response to an increased demand for point-of-need (PoN) NA testing, but most existing NAE techniques remain tethered to centralized laboratories.[7-10] Though commercial kits provide some relief for overburdened analysts, they suffer from operational constraints that preclude on-site use – namely limited throughput capabilities, propensities for contamination, and labor-intensive, time-consuming workflows (**Figure 2-1**).[6] However, as discussed in **Chapter 1**, increased attention and resources are being allocated to the development of effective, efficient, and fieldable NA preparation strategies, a traditionally underdeveloped research area.[9, 11]

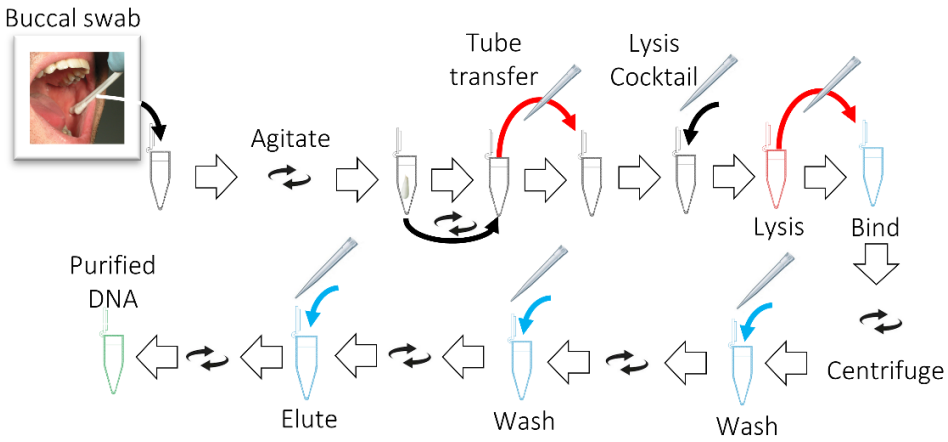

Figure 2-1. Stepwise schematic of conventional in-tube SPE workflow. After buccal swab collection, cells are eluted into solution via manual agitation. The supernatant is then collected and an aliquot is mixed with a lysis cocktail, then heated. An aliquot of the lysate is then passed through the extraction column via centrifugation. The column is then washed, potentially multiple times, via manual buffer application and centrifugation. Finally, an elution buffer is passed through the column to desorb purified NAs for collection.

Among these, centrifugal microfluidic 'lab-on-a-disc' (LoaD) platforms are especially promising as power ful, portable alternatives for convenient NA processing by nontechnical personnel.[10, 12] Rotationally-controlled fluidics offers an attractive format that obviates the need for bulky, complex external equipment, e.g., pneumatic pumps.[13-14] In addition to portability, LoaD systems offer additional advantages over traditional laboratory methods, including reduced sample/reagent consumption, total automation, self-contained formats, more rapid analysis, and decreased cost.[6, 10, 12] Adapting NA preparation to a LoaD system stands to make significant impact in comprehensively translating NA analysis on-site, eliminating laboratory dependence entirely. From a practical perspective, inclusion of not only NAE, but also lysis, is imperative to ensure capabilities for processing raw samples and effectively bridging the "world-to-chip" interface.[9, 11, 15] Ultimately, development of robust, efficient NA preparation methods opens the door to development of the optimal microfluidic solution for PoN use – fully-automated sample-to-answer miniaturized total analysis systems (μTAS)[16] that perform NA preparation, separation, and detection without user intervention.[5-6, 10-12]

Recall from the discussion of silica-based solid phase extraction (SPE) in **Chapter 1** that the preponderance of existing microfluidic NAE strategies utilize dynamic SPE (dSPE) due to ease of implementation at the microscale.[5-6] Here, the requirement for only minimal, inexpensive peripheral hardware for dSPE implementation dovetailed naturally with centrifugally-driven flow to permit the development of a cost-effective, portable, LoaD for complete NA preparation. Though magnetic dSPE is commonly achieved via silica particle transfer between numerous chambers,[17-19] the approach described here instead mirrors the traditional single-tube benchtop workflow; particles are retained in

single chamber and subjected to the sequential flowthrough of solutions to facilitate NA binding, washing, and eventual elution (**Figure 2-2**). The success of this on-disc dSPE strategy was directly contingent upon on-disc microvalves to provide spatiotemporal control over reagent delivery to, retention in, and removal from the extraction chamber.[18] To achieve this, valves must be compatible with a plethora of lysis and extraction reagents (e.g., buffers and detergents) which possess exceedingly variable fluidic properties.[20] Further, if PoN use is desired, valves must also behave reproducibly across a range of environmental conditions (e.g., temperature, humidity, etc.).

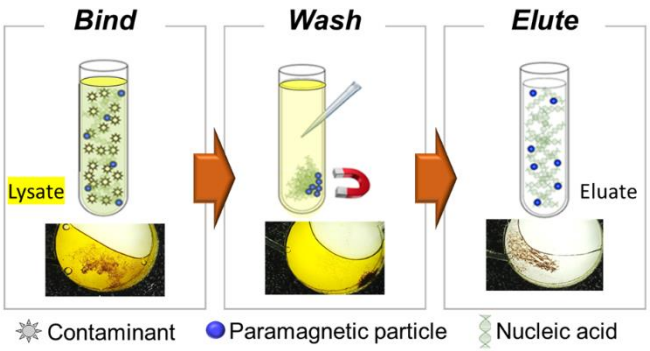

Figure 2-2. Depiction of in-tube and on-disc dSPE. Silica-coated particles are magnetically manipulated through a lysate sample (yellow) to facilitate NA capture via adsorption. Following particle collection (magnetically in tube or centrifugally on-disc), the supernatant was removed. The particles were then washed to remove sample contaminants and other PCR inhibitors prior to resuspension. Magnetically-driven mixing through an elution buffer (colorless) facilitated desorption of purified NAs from the silica-coated particles. Adapted from [17].

Previous efforts towards centrifugal microfluidic dSPE were hampered by unreliable, on-board passive fluidic control systems unable to meet these required metrics due to comprehensive reliance upon balancing centrifugal force with fluidic surface tension.[18, 21-22] These passive systems exhibited sensitivity to temperature fluctuations, changes in channel surface energy (quite variable in polymeric microdevices)[14] and fluid composition (e.g., viscosity, surface tension) contributed to a high frequency of valving failures.[18, 20] Fluidic control failure was further exacerbated by inconsistent burst pressures (± 0.5 Hz) of hydrophobic, xerographic toner valves in the system employed by Jackson et al. (first described by Ouyang et al.[23]); these valves exhibited a 10% failure rate under

temperature-controlled laboratory conditions due to variable toner deposition during printing.[18] Further, toner valves were irreversible, meaning that they could not be closed once actuated. Jackson et al. attempted to address these shortcomings by coupling passive valves with a manual tape valve strategy.[18] Unfortunately, regardless of this, the combined valving scheme produced a high incidence of fluidic control failures (23%)[18] and required incorporation of additional materials and fabrication steps that hindered the potential for translation to mass production and productization.[24-25]

Here, to address these shortcomings and realize reliable centrifugal NA preparation, passive valves were replaced by active, laser-actuated flow control modalities to provide robust fluidic control without increasing device complexity. In the valve opening method used here, first described by Zuchelli and van de Vyver, then adapted by Garcia-Cordero et al., irradiation of an optically-dense polymer separating two discrete fluidic layers induces localized heating and pinhole formation to allow flow between previously disconnected channels.[25-26] Though these valves are much more reliable than passive methods, opening only upon irradiation, these 'single shot' valves are also irreversible, remaining open after actuation.[25] To address this deficiency, a complimentary laser-based valve closure strategy, developed by Woolf et al., was implemented.[24] Irradiating microchannels just upstream from previously opened valves with insufficient incident energy to cause material ablation instead thermally deforms polymeric disc components, such that the channel is occluded and further flowthrough becomes impossible.[24] Both laser valve opening and closing are strictly timed, dependable, and can be easily automated using the same diode. Not only do these methods entirely supplant passive and manual valving methods (e.g., toner, tape, and siphon valves), the lack of requirement for specific

architectural features permits higher multiplexing – and, thus, increased throughput. Finally, since sacrificial laser valves are both pressure-resistant and vapor-tight, they also ease upstream microfluidic integration of thermally-aided, direct-from-swab enzymatic lysis. Thus, the LoaD is readily amenable for acceptance and processing of biological samples on solid substrates (e.g., buccal swab cuttings) to yield high-purity NAs.

For successful NA preparation, it is essential to control not only fluid flow, but also movement of paramagnetic silica particles within the microdevice. Here, application of a bidirectional rotating magnetic field (bRMF) drives back-and-forth bead sweeping within the extraction chamber to maximize NA capture, and eventually elution, from the solid phase. Since NAs were adsorbed to the beads' silica surfaces, retention of the nanoparticles within the extraction chamber is critical for NA recovery.[19] Together, careful architectural design of the extraction chamber and centrifugal bead pelleting prior to fluid transfer steps, were essential in mitigating such loss. The integrated lysis and dSPE NA preparation LoaD was initially characterized and optimized using aqueous dye solutions and a variety of empirical image analysis techniques. However, the purity and amplification-readiness of extracted NAs was probed using a panel of nucleic acid amplification tests (NAATs). Chiefly, methods based on the polymerase chain reaction (PCR) were used to assess assay performance during LoaD development and optimization.

Ultimately the described portable NAE platform incorporates on-board, upstream lysis to permit processing of raw samples and combines centrifugal microfluidics and dSPE, a logical pairing that is well-suited for field-forward use. To establish the spread and scope of potential applications for this centrifugal dSPE LoaD, DNA and RNA extracted on-disc was amplified via multiple downstream modalities.

2.2. Materials and Methods

2.2.1. Microdevice Fabrication

Multiplexed centrifugal microdevices contained 8 domains per disc for parallel NA preparation and were designed to permit integrated, automated enzymatic lysis and subsequent dSPE. LoaDs were fabricated via the well-characterized 'print-cut-laminate' method.[27] A CO_2 laser (VLS3.50, Universal® Laser Systems, Scottsdale, AZ) was used to ablate architectural features designed in AutoCAD software (2019, AutoDesk Inc., San Rafael, CA) into thermoplastic substrates. Specifically, the core device contained five polyethylene terephthalate (PeT) layers (101.6 µM, FilmSource Inc., Maryland Heights, MO). The outermost 'capping' layers (1 & 5) enclosed the microdevice. The PeT layers that housed the two fluidic layers (2 & 4) were coated in a heat-sensitive adhesive (HSA, 50.8 µM, Adhesives Research Inc., Glen Rock, PA) and separated by an intervening, optically dense black PeT layer (Lumirror* X30, Toray Industries, Inc., Chuo-ku, Tokyo, Japan) to permit laser-actuated valving.[24-25] Device layers were aligned and passed through an office laminator (UltraLam 250B, Alikes Products Inc., Mira Loma, CA). Channels cut into a single material layer were approximately 100 µm deep and 400-500 µm wide. Average chamber depth was 450 µm, except where augmented by laser-cut PMMA accessory pieces (1.5 mm thickness, McMaster Carr) affixed to the microdevice with pressure sensitive adhesive (PSA, 55.8 µm, Arcare 7876, Adhesives Research Inc.) to enable swab acceptance and recovery of the purified NA eluate solution following assay completion. The recovery chamber was capped with a polytetrafluoroethylene (PTFE) membrane (Sterlitech, Kent, WA) cutting via a pressure sensitive adhesive (Arcare 7876,

Adhesives Research Inc.) which could be punctured via pipette tip to facilitate sample retrieval for off-disc post-processing.

2.2.2. Reagent Preparation

Tris-EDTA (TE) buffer (1X, Molecular Biology Grade, pH = 8.0, Thermo Fisher Scientific) was used without modification. Guanidine hydrocholoride (GuHCl, Thermo Fisher Scientific) solutions were prepared in 1X TE at 3M and 6M; pH was adjusted to 6.1 using 2-(N-morpholino)ethanesulfonic acid (Thermo Fisher Scientific) and a Mettler Toledo MP 220 pH meter (MP Chemicals, Santa Ana, CA). The 3M GuHCl solution was then used to wash (3X) and resuspend Magnesil® paramagnetic particles (Promega, Madison, WI) with a final dilution factor of 3.3x. Isopropanol (IPA, Sigma Aldrich, St. Louis, MO) was prepared at 80% v/v in molecular biology grade water (Thermo Fisher Scientific). Proteinase K was used without modification (Qiagen, Valencia, CA).

2.2.3. Mechatronic Spin System Construction and Operation

The dSPE mechatronic system has capabilities for automated, rotationally-controlled fluidics, magnetic nanoparticle manipulation, and laser valve actuation via a program coded in-house in Propeller's native language, Spin. LoaD rotation, and therefore

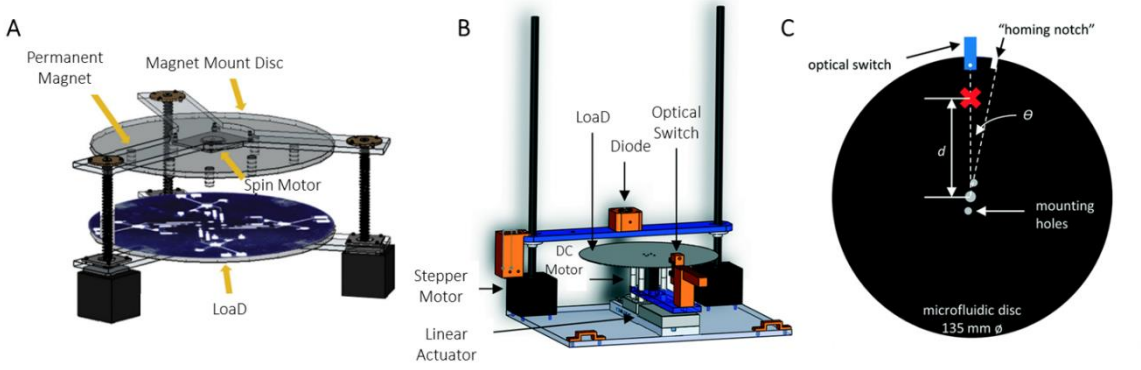

Figure 2-3. Schematic representations of mechatronic microfluidic platforms. (A) dSPE platform. In a newer iteration, a laser diode beneath the LoaD platform (not shown) permits laser valve opening. Adapted from [18]. (B) Power, Time, and Z-Height Adjustable Laser used for channel closures. Adapted from [24]. (C) Depiction of method for LoaD valve location. Valves are defined using two values: distance from the CoR (d) and the angle relative to a "homing notch" cut into the LoaD periphery. Adapted from [24].

centrifugal fluid flow, was driven by a DC brushless motor. Similarly, a stepper motor (Sanmotion Series, Sanyo denki, Moriguchi, Japan) controlled a PMMA disc featuring a pair of Neodymium permanent magnets affixed 7.50 mm above the sample disc platform on a 3-arm support structure similar to one described previously (**Figure 2-3A**).[18] Alternating the rotational direction of the magnet disc above the stationary microdevice created a bRMF, described previously, that drove back-and-forth nanoparticle sweeping.[17] Where necessary, the height of the magnets was adjusted using PMMA rings (1.5 mm thickness, McMaster Carr). Irradiation from a 700 mW 638 nm laser diode (L638P700M, Thorlabs, Inc. Newton, NJ) positioned 16.00 mm below the microdevice opened normally-closed valves (500 mW, 500 ms). Laser-actuated valve closures were controlled by the Power, Time, and Z-Height Adjustable Laser, described in detail elsewhere (**Figure 2-3B**).[24] A 700 mW 683 nm laser diode (L638P700M, ThorLabs, Inc., Newton, NJ) focused with a collimation tube containing a single aspherical lens element (LTN330-A, ThorLabs, Inc.) was positioned 26.00 mm above the microdevice platform using two stepper motors (Polulu Robotics and Electronics, Las Vegas, NV). Irradiating channels (700 mW, 2500 mS) facilitated their closure, and prevention of further flow.[24] Valving locations (opening and closing) were numerically defined in terms of two parameters – distance from the center of rotation (d) and the angle relative to a homing notch cut in the disc (θ) (**Figure 2-3C**). In each system, the diode's position relative to these features in the xy-plane was controlled by a motorized translational stage (MTS50-Z8, ThorLabs), a photointerrupting optical switch (TT Electronics/Optek Technology, Woking, UK), and a brushless DC motor. All functionalities in both systems were regulated via multi-processing microcontrollers (Propeller P8X32A-M44; Propeller Inc., Rocklin, CA).

2.2.4. Cellular Lysis

Epithelial cell lysates were prepared from cuttings taken from de-identified buccal swab samples collected via protocols approved by the University of Virginia Institutional Review Board and dried overnight. All lysates were used on the day of preparation.

In-Tube Workflow

A 28 µL aliquot of a lysis cocktail comprised of 6M GuHCl (18 µL) and Proteinase K (10 µL) was added to a 0.2 mL PCR tube along with a quarter swab cutting. Following a 10-minute incubation at 56 ˚C in a thermal cycler, the lysate was recovered via the 'piggyback' method, described elsewhere.[18] Briefly, the 0.2 mL PCR tube was punctured with a syringe needle, then nested in a 0.5 mL Eppendorf tube. The lysate was eluted into the outer tube via centrifugation.

On-disc Workflow

Within each domain, a quarter swab cutting was loaded into the PMMA swab chamber which was then sealed by applying a PeT coverlet. For epithelial cell lysis, no further treatment of the swabs was necessary. However, in instances of SARS-CoV-2 detection, the cuttings were spiked with armored SARS-CoV-2 RNA (40 µL, 100 copies/µL) (AccuPlexTM SARS-CoV-2 Reference Material, SeraCare, Milford, MA) then dried overnight. The swab chamber was filled with lysis cocktail (28 µL) then incubated at 56 ˚C (10 minutes) using a dual Peltier system. After heating, the laser valve beneath the swab chamber was opened.

2.2.5. Nucleic Acid Extraction

Traditional Extraction

To permit comparison of on-disc and in-tube lysis performance, liberated DNA was purified using the DNA Mini Kit (Qiagen) and amplified in triplicate using an ABI 7500 fast Real-Time PCR System (Thermo Fisher Scientific) by targeting the TPOX locus (primers and probe published previously[28]). Each 20 µL reaction contained 1X SensiFast Probe Lo-ROX One-Step Mix, 0.4 µM forward/reverse primers, 0.1 µM probe, and 4 µL extracted DNA. An initial denaturation step (95 ˚C, 3.5 minutes) was followed by 40 amplification cycles between 95 °C for 5 s and 60 °C for 30 s. Fluorescence was monitored in the FAM channel. The threshold cycle (C_t) was calculated automatically by 7500 software v2.3 (Thermo Fisher Scientific).

Microfluidic Extraction

The microdevice was prepared for the integrated workflow by loading the swab cutting and lysis cocktail (28 µL) to the swab chamber, bead suspension (3 µL) and GuHCl (3M, 2 µL) to the extraction chamber, and IPA (80%) and 1X TE to their respective chambers (8 µL each). After performing on-disc, direct-from-swab lysis as described above, the laser valve below the swab chamber was opened. Rapid device rotation (269 g, 120s) centrifugally pumped the lysate into the swab elution chamber. Following actuation of a second, downstream laser valve, a 2 µL aliquot was collected in a metering chamber, with excess flowing into the lysate overflow chamber (27 g, 30 s). The channel upstream of the metering chamber was laser-sealed prior to opening the valve below the metering chamber and pumping the 2 µL lysate into the extraction chamber. Here, an initial particle mixing step, driven by bRMF application was implemented for NA capture; the magnet disc was rotated above a stationary microdevice for 500 s total, alternating direction every

20 s. After mixing, the particles were centrifugally pelleted (-109 g, 5 s), the appropriate downstream laser valve was actuated, the supernatant lysate was driven into a waste chamber (109 g, 10 s), and the channel upstream of the newly opened laser valve was sealed. After IPA was introduced to the extraction chamber (laser valve actuated; 126 g, 10 s), a second magnetic mixing step was conducted. After centrifugally pelleting the particles (-109 g, 5 s), the second waste valve was opened, the IPA was removed (109 *g, 10 s), and the waste channel was closed. The 1X TE elution buffer was then introduced to the extraction chamber (laser valve actuated; 126 g, 10 s) prior to a final cycle of magnetic mixing and pelleting. Finally, a downstream laser valve was opened and the NA solution was driven into the NA recovery chamber (109 g, 10 s) from which it could be retrieved for off-disc analysis by puncturing the PTFE membrane with a pipette tip.

2.2.6. Nucleic Acid Post-Processing

Real-Time PCR

All amplification reactions were performed using an ABI 7500 fast Real-Time PCR System (Thermo Fisher Scientific). Fluorescence was monitored in the FAM channel and threshold cycle (Ct) values were calculated automatically by 7500 software v2.3 (Thermo Fisher Scientific). Relative DNA quantification was performed via real-time PCR amplification targeting the TPOX locus (primers/probe published previously[28]). Each reaction contained 1X PerfeCTa supermix low Rox (Quantabio, Beverly, MA), 0.3 µM forward/reverse primers, 0.4 µM probe, and 2 µL extracted DNA. Amplification conditions were analogous to those described for conventional DNA extraction (Section 2.2.5).

Pathogenic RNA detection was achieved using reverse transcription real-time PCR reaction. Specifically, each reaction targeting the SARS-CoV-2 N gene contained 5 µL

sample, 5 µL TaqPathTM 1-Step RT-qPCR Master Mix, CG (Thermo Fisher Scientific), 1.5 µL SARS CoV-2 (2019-nCoV) CDC RUO N1 primer-probe mix (Integrated DNA Technologies, Coralville, IA), and 8.5 µL PCR-grade water (Molecular Biologicals International, Inc.) by heating at 50 °C for 15 minutes, 95 ˚C for 3 minutes and 45 cycles of 95 °C for 3 s and 55 °C for 30 s.

Short Tandem Repeat (STR) Profiling

PCR amplification (18-plex) was performed using the PowerPlex® 18D system (Promega). Each 25 µL reaction was comprised of 1X master mix, 1X primers, and 2 µL unknown DNA. Amplicon electrophoresis and detection were achieved using an ABI® 3130 Genetic Analyzer (Applied Biosystems, Grand Island, NY). Resultant STR profiles were interpreted using GeneMarker HID software (SoftGenetics, State College, PA).

Loop-mediated isothermal amplification (LAMP)

Extracted DNA was amplified using the WarmStart® LAMP Kit (DNA&RNA) (New England Biolabs, Ipswitch, MA) and primers (sequences published previously[29]) targeting the TPOX locus. Each reaction contained 0.2 µM F3 and B3, 0.8 µM LF and LB, and 1.6 µM FIP and BIP and was incubated at 65°C for 60 minutes in a thermal cycler.

Microchip Electrophoresis

Where appropriate, electrophoretic detection and sizing of real-time PCR and LAMP was achieved using the DNA chip assay for the Bioanalyzer 2100 (Agilent Technologies, Santa Clara, CA) according to manufacturer's instructions.

2.2.7. Image Analysis

Device images were captured using an Epson Perfection V100 Photo desktop scanner (Seiko Epson Corporation, Suwa, Nagano Prefecture, Japan) and analyzed using the Fiji distribution of ImageJ freeware using techniques described elsewhere.[24, 30] Briefly, to calculate fluid volumes within microfluidic chambers, the pixels associated with the dye were 'masked' or selected through adjustment of color thresholds within ImageJ.[30] The pixels were then enumerated and compared to control conditions (e.g., 2 µL dye pipetted into the extraction chamber).[30] Other analyses that required simple measurement of individual image parameters leveraged the 'crop-and-go' method described by Woolf et al. in which circular or rectangular regions of interest (ROIs) were selected from raw images and converted to 3-slice hue-saturation-brightness (HSB) stacks. Individual hue and saturation values were measured directly from the relevant image slice.[24, 30]

2.3. Results and Discussion

Effective microscale dynamic solid phase NAE requires exquisite fluid flow control, optimized solid phase-sample interaction, performance of discrete, sequential fluidic steps without contamination, and isolation of amplification-ready NAs. Here, each of these functionalities have been integrated into a single centrifugal microfluidic lab-on-a-disc (LoaD) that combines enzymatic lysis directly from raw buccal swab cuttings and dynamic, chaotrope-driven binding to silica particles in a rotating magnetic field. Cellular contaminants were washed from the particles prior to elution of purified, amplification-ready NAs. This integrated process required a series of accurately executed fluid transfers (both temporally and spatially) promoted via optically-actuated valving methods. Resultant DNA purified on-disc was effectively amplified, not only by traditional polymerase chain

reaction (PCR) methods, but also via isothermal loop-mediated amplification (LAMP). Further, successful RNA isolation was demonstrated for the first time via downstream reverse transcriptase PCR (RT-PCR) targeting viral genetic material.

2.3.1. Microdevice Fabrication and Operational Principles

LoaDs were fabricated via the 'print-cut-laminate' (PCL) method to permit rapid device prototyping and optimization.[27] Use of commercial-off-the-shelf thermoplastic substrates and office equipment obviates reliance on hazardous chemicals (e.g., hydrofluoric acid), specialized expensive equipment (e.g., milling machines), or designated cleanroom space. Further, prototyping in this manor enables facile testing of iterative architectural designs. Despite extremely cost-effective fabrication (<$1 each), these devices are capable of performing complex bioanalytical processes including immunoassays,[31] genotyping,[32] PCR amplification,[33] and NAE.[17, 34] This large bandwidth of applications highlights the versatility of PCL microdevice fabrication. Though PCL devices generally are fabricated from five thermoplastic components and contain two distinct fluidic layers (**Figure 2-4**), LoaD functionality is ultimately determined via the microfluidic architecture.

Here, the multiplexed dSPE LoaD was designed with a view towards increased NA preparation throughput. The optimized device contained eight distinct, identical iterations of the architecture radially distributed around the center of rotation (CoR), each able to accept a single swab cutting for parallel, simultaneous on-disc processing (**Figure 2-5**). Architectural features to facilitate both enzymatic (Proteinase K) lysis (gold text) and dSPE (black text) interfaced seamlessly at the central extraction chamber, which housed the NAE silica solid phase. After NA capture, sequential introduction and removal of isopropanol

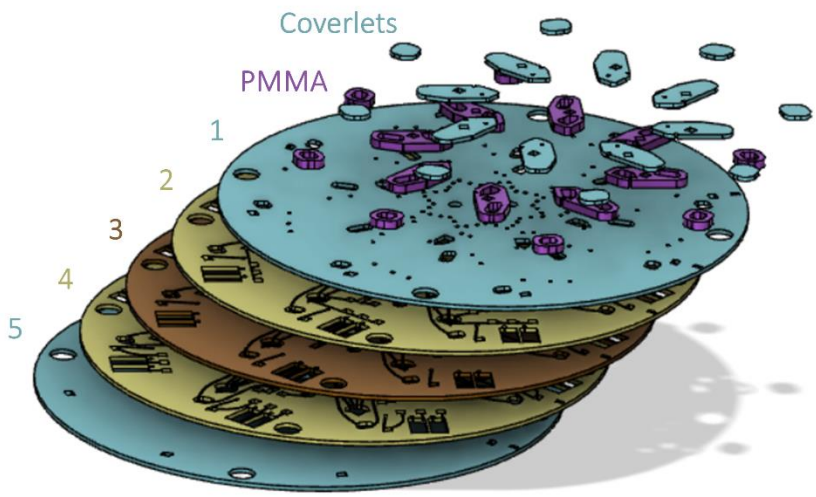

Figure 2-4. Isometric view of PCL microdevice fabrication. (A) Isometric exploded view of a conventional 5-layer PCL microdevice. Material layers 2 and 4 (yellow), comprised of polyethylene terephthalate (PeT) coated with a heat-sensitive adhesive, serve as the primary fluidic layers and are separated by an intervening, optically-dense black PeT layer to enable laser valving (amber, 3). Clear PeT capping layers (cyan, 1 and 4) enclose internal device architecture to provide a self-contained microdevice. After alignment, passage through an office laminator heat-bonds layers together to yield a finished microdevice. Where necessary, PMMA accessory pieces (purple) with PeT coverlets (cyan) are adhered to layer 1 for enhanced chamber volume and buccal swab acceptance.

(IPA) and 1X Tris-EDTA (1X TE), preloaded into the chambers above the extraction chamber, facilitated washing of the NA-bound beads, then elution of purified NAs. In addition to assuring that lysate, wash, and elution solutions are 'valved' for movement in the correct sequence, fluid reten tion with the beads in the extraction chamber for the requisite time for NA capture/elution is critical. To enable repeated sequences of fluid delivery, retention, and emptying of the extraction chamber, a robust valving strategy that alternated between permitting and preventing fluid flow was required. Jackson et al. incorporated siphon and manually-actuated tape valves for this purpose which, while good for proof of principle, led to periodic failures that contributed to a sub-adequate overall assay success rate.[18]

To enhance spatiotemporal fluidic control through our architecture while simplifying device fabrication, we supplanted the original tape and passive valves with laser-based methods (**Fig. 2 -6**). Optically-actuated sacrificial valves (**Fig. 2-5B**, red boxes) were opened simply and rapidly with short laser pulses to provide precise control over fluid

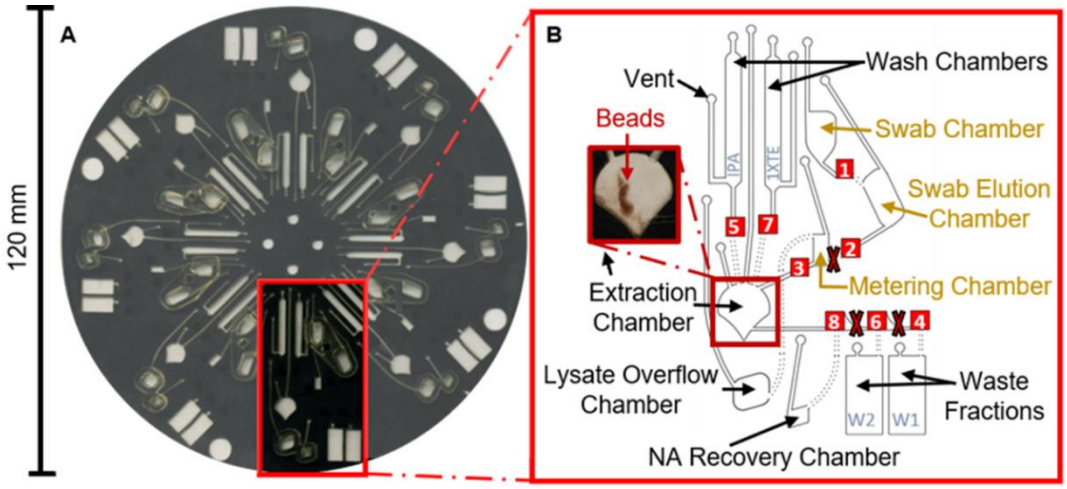

Figure 2-5. LoaD for lysis and dSPE of nucleic acids from buccal swabs. (A) Multiplexed microdevice for simultaneous preparation of nucleic acids from 8 samples. (B) Labeled schematic of the microfluidic architecture of one domain. Laser-actuated valve openings and closures are shown as red boxes and crosses, respectively. Channels depicted with solid and dashed borders are contained in the top and bottom fluidic layers, correspondingly. Adapted from [17].

flow between channels in formerly disconnected fluidic layers (**Fig. 2-6A**).[25-26] A complimentary optically-controlled valve closure strategy described by Woolf et al.[24] was implemented in conjunction with this irreversible technique to effectively 'close' previously opened valves. For channel closure, laser-induced thermal deformation of polymeric materials occluded microchannels to preclude further flow with a demonstrated success rate of >99% at relevant rotational frequencies (**Figure 2-6B**).[24] In conjunction, these strategies permitted the successive introduction, removal, and fractionation required to mirror the traditional "bind-wash-elute" benchtop workflow.

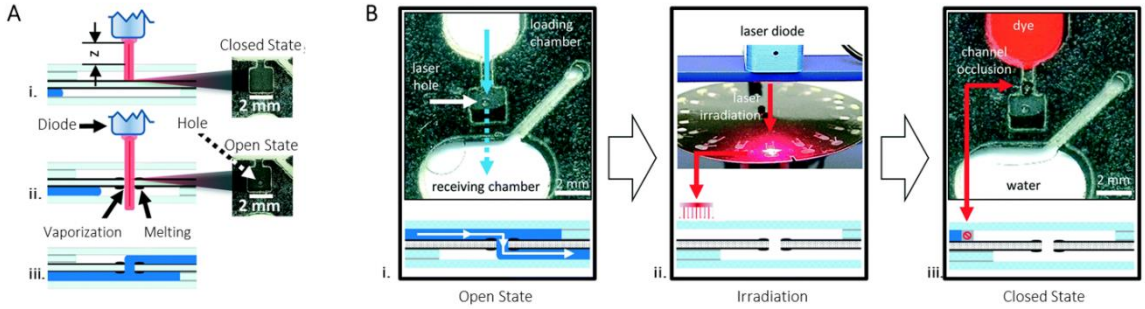

Figure 2-6. Laser-based microvalving strategies. (A) To open laser-actuated valves, (i.) an optically-dense material separating two distinct fluidic layers is irradiated. A hole is formed via material ablation to (iii.) permit flow between previously disconnected channels. (B) Using the same diode, (i.) a previously opened valve can be effectively closed via (ii.) irradiation of the upstream channel which causes material deformation that (iii.) prevents further flowthrough. Adapted from [24].

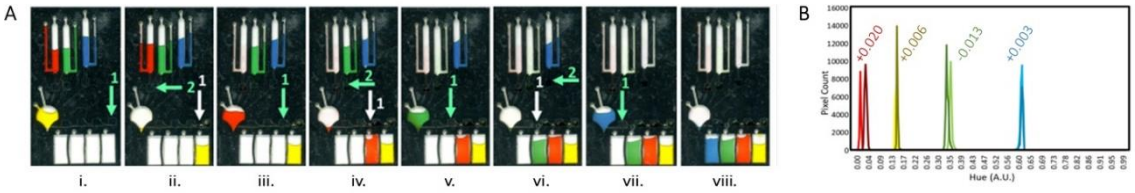

Figure 2-7. Dye simulation of dSPE workflow for valve closure evaluation. (A) Images of microdevice depicting stepwise fluidic protocol with green and white arrows representing valve openings and closures, respectively. Dyes were used to visually represent assay reagents to permit visual analysis. (i.) After opening the rightmost laser valve, the lysate (yellow) was spun to waste. (ii.) The channel upstream of the opened valve was closed and the IPA wash (red) was delivered to the extraction chamber. (iii.) The red dye was centrifugally pumped to waste after valve opening. (iv.) After the TE wash valve (green) was opened, the fluid was driven into the extraction chamber. (v.) The valve to the third waste chamber was opened and the green dye was driven therein. (vi.) After closing the waste valve, the TE elution buffer (blue) is released to the extraction chamber, then isolated in a downstream elution chamber. (B) Pixel distributions measure against normalized hue values (0 to 1) measured from the four dye solutions, with lighter traces representing initial values and darker traces corresponding to the dye hue values after the on-disc dSPE fluidic protocol. For each dye, the net hue value change is inset. Adapted from [24].

Visual, empirical demonstration of the success of this valving scheme was achieved by passing four differently colored dye solutions through the extraction chamber in isolation (**Figure 2-7**). Yellow, red, green, and blue dyes were sequentially introduced into the extraction chamber, then removed to one of four discrete, valved waste chambers for discarded fractions connected to a single downstream channel. To facilitate removal of each solution, the laser valve associated with the most distal unfilled chamber was opened, dye was centrifugally pumped in, and the channel upstream of the newly opened valve was laser-sealed. If the channels were effectively closed, upon introduction of the next dye solution, it would be retained in the extraction chamber. The success of this fluid fractionation strategy was clearly evident upon inspection of the four resultant fractions (**Figure 2-7A**). Visually, four distinct fractions were isolated with colors matching the initial dye solutions prior to conducting the on-disc fluidic protocol. Empirical confirmation of these visual results was obtained via analysis of hue, a circular variable which uniquely represents a color within the visible portion of the electromagnetic spectrum.[30] Hue shifts in the dye fractions after assay completion (relative to starting hue values) were used as metrics for successful sequential reagent delivery and removal, as

well as effective valving. Final fractions exhibiting minimal hue changes indicated a lack of premature reagent release, undesired mixing between fractions, and incomplete valve closures. If valve closures had failed, much larger hue shifts would have been observed due to mixing between multiple dyes. The exceedingly minor changes measured between initial and final hue values confirmed that fluid fractions could be successively passed through the extraction chamber with near-negligible crossover (**Figure 2-7B**). More broadly, this study demonstrated the robust reliability of our combined laser valving scheme as capable of providing the spatiotemporal fluidic control needed for implementation of lysis and extraction.

2.3.2. Direct-from-Swab Enzymatic Lysis

As discussed in **Chapter 1**, lysis from a wholly unprocessed sample is essential for practical application of LoaDs for NA analysis. To this end, an on-disc direct-from-swab method was developed to accept buccal swab cuttings, perform lysis, and deliver lysate to the extraction chamber for dSPE (**Figure 2-8**). Proteinase K (ProK), a broad-spectrum serine protease used ubiquitously in NA preparation schemes, was coupled with guanidine

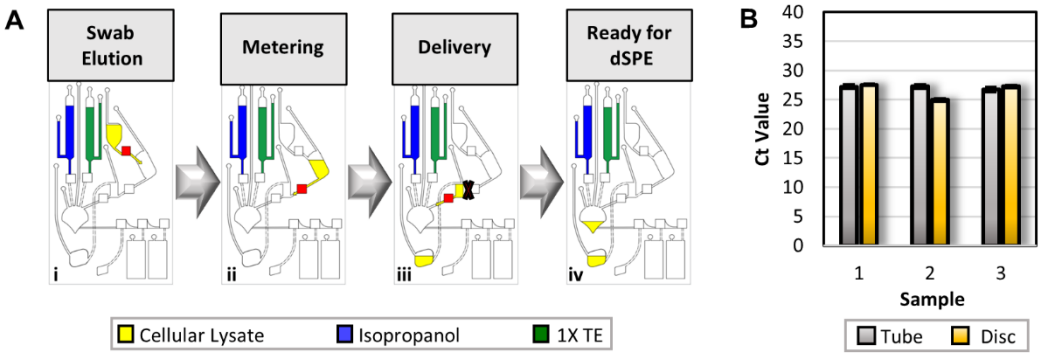

Figure 2-8. Integrated fluidic workflow and performance of on-disc lysis. (A) Schematic depicting sequential unit operations. (i) After enzymatic lysis, the valve beneath the swab chamber was actuated and the lysate was centrifugally eluted from the cutting. (ii) The downstream valve was opened, (iii) a 2 µL aliquot of lysate was metered out, the channel upstream of the metering chamber was closed, the subsequent laser valve was opened, and (iv.) the metered lysate was centrifugally pumped into the extraction chamber. (B) qPCR C_t values from amplification of the TPOX locus were similar between dSPE extracts following parallel on-disc and in-tube lysis of cells contained on three donor swabs, indicating successful on-disc lysis. Adapted from [17].

hydrochloride (GuHCl) to denature cellu lar proteins, including nucleases that would otherwise degrade NAs.[5, 7] Enzymatic lysis was expedited via heating at 56 ˚C for 10 minutes; reaching this temperature using our in-house mechatronic system, required ~30 seconds from room temperature and remained stable over the duration of incubation (data not shown). Leveraging pressure-resistant, vapor-tight sacrificial laser valves effectively contained the lysate within the swab chamber during heating.

After opening the valve beneath the swab chamber, the lysate was centrifugally-eluted from the substrate. As a result of centrifugally-generated pressure scaling with angular frequency, the LoaD was rotated at maximal rate permitted by the dSPE spin stand (3000 rpm) to maximize fluid recovery from the swab.[22] Notably, unlike passive valving, which is prone to failure when such high-speed spin steps are required early in the assay workflow,[21-22] laser valve actuation is entirely independent from fluidic pressure. Thus, the probability of premature release of the lysate or preloaded NAE reagents even during this high-speed spin step was effectively zero. To ensure consistent performance of downstream dSPE, the same, measured volume of lysate should be reproducibly introduced to the extraction chamber. A downstream metering chamber designed to accommodate and deliver a 2 µL lysate aliquot to the extraction chamber was characterized using aqueous dye. Briefly, pixels associated with the dye inside the extraction chamber were “masked” by adjusting color thresholds within ImageJ freeware.[30] Comparison of the number of pixels selected from the metered lysate aliquot to those of known dye volumes within the extraction chamber permitted determination that 2.17±0.60 µL lysate to the extraction chamber (**Figure 2-9**). After metering, the appropriate channel was closed to prevent any crude lysate, which contained PCR inhibitors, remaining in the swab from entering the

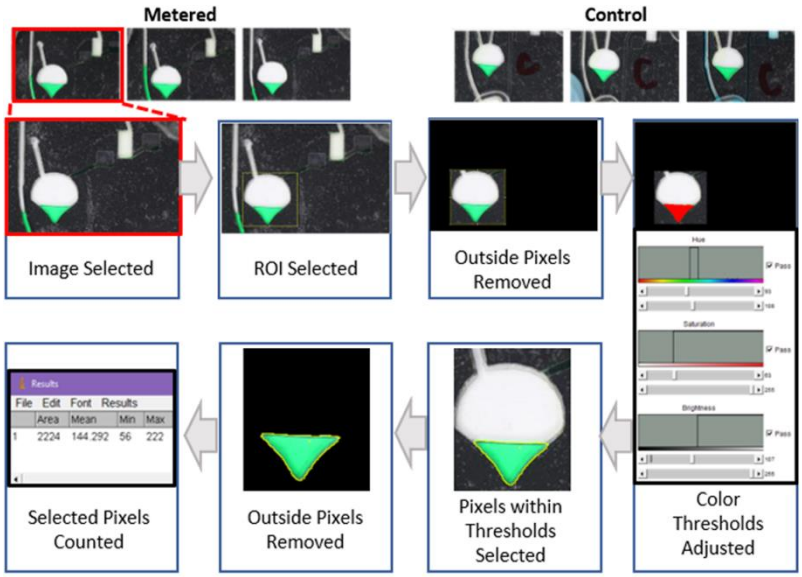

Figure 2-9. Visual quantification of metered lysate volume. The on-disc spin and valving protocol for lysis was performed using an aqueous green dye (28 µL) to visually represent the cellular lysate. To measure the volume of the dye aliquot delivered to the extraction chamber, a surrounding rectangular region of interest was selected using ImageJ freeware; all pixels outside of the bounds were cleared. Image color thresholds were adjusted such that only the pixels associated with the green dye were selected. The same color threshold adjustment values were applied uniformly across images. Comparison of the number of masked pixels in metered and control aliquots of known volume permitted volume discernment. Adapted from [17].

extraction chamber during downstream spin steps. The remaining bulk lysate was routed to an overflow chamber from which it could be collected for off-disc processing where necessary.

In one such instance, DNA from lysates obtained from duplicate swab cuttings prepared on-disc and in-tube were purified using a commercial method prior to qPCR amplification. Since Ct values are inversely related to target concentration, more effective cellular lysis would result in higher concentrations of DNA in solution and, therefore, more rapid amplification (e.g., lower Ct values). Since comparable Ct values were obtained across methods (**Figure 2-8B**), it was concluded that microfluidic lysis performed similarly to traditional, in-tube reactions. Although the small volume lysis chemistry used was described previously, this work represents the first integration of on-disc direct-from-swab lysis, directly interfaced with actively-valved centrifugal dSPE.[18, 35-36]

2.3.3. On-Disc Extraction

After lysate delivery to the extraction chamber, the on-disc dSPE protocol was initiated (**Figure 2-10**). First, NAs were captured by paramagnetic silica particles, as they were swept back-and-forth by the application of an external bidirectional rotating magnetic field (bRMF). Following centrifugal bead pelleting, the rightmost downstream laser valve was opened. After the supernatant lysate was driven to the associated waste chamber, the channel immediately upstream of the newly opened valve was laser-sealed, precluding further flow. IPA was introduced to the extraction chamber and retained for magnetic mixing, pending subsequent laser valve actuation and release of fluid to the next waste chamber. After closing the upstream channel, the TE elution buffer was delivered to the extraction chamber and retained for magnetically-assisted desorption of purified NAs. Finally, purified NAs were transferred to the recovery chamber following actuation of the appropriate laser valve for eluate retrieval. In addition to providing the high-level fluidic control needed for sequential washes, laser-valving strategies required no additional fabrication steps or materials, were easily automated, and required substantially less microfluidic 'real estate' to permit increased multiplexing from 4 (Jackson et al.) to 8,

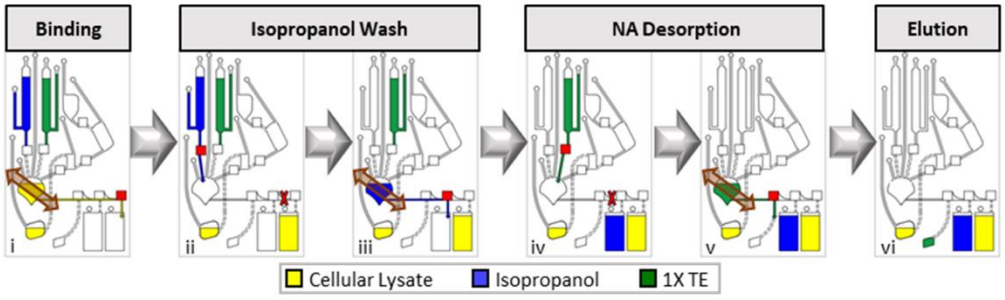

Figure 2-10. Stepwise on-disc dSPE fluidic protocol. Valve openings and closures are represented by red boxes and crosses, respectively; magnetic mixing steps are depicted by orange bidirectional arrows. (i) After NA capture ('binding') via magnetic mixing, beads are pelleted, and the lysate is driven to the first waste chamber following actuation of the appropriate valve. (ii) After sealing the channel upstream of the opened valve, the IPA wash is introduced to the extraction chamber. (iii) Following bead mixing, pelleting, and valving, IPA is pumped into the second waste chamber. (iv) After waste channel closure, TE is flowed into the extraction chamber where (v) magnetic mixing facilitates NA elution from the beads. (vi) The purified NA solution is driven into the elution chamber following bead pelleting and valve actuation. Adapted from [17].

doubling throughput.[18] The practical success of on-disc dSPE was largely contingent on optimization of three key parameters, namely magnetic solid phase manipulation, extraction chamber geometry, and the washing protocol. Each of these factors are discussed in detail below.

2.3.3.1. Optimization of Magnetic Solid Phase Manipulation

Magnetic actuation via bRMF application has been previously described for use in label-free DNA detection and quantification; paramagnetic particles formed visually-detectable aggregates upon entanglement by DNA.[37-38] Here, similar manipulation of paramagnetic particles was applied to NA purification. Following magnetic resuspension, repeated reversal of the bRMF direction induced back-and-forth bead 'sweeping' across the extraction chamber and collection on the opposing wall (**Figure 2-11**). Though bead mixing is commonly achieved through reliance on inertial forces during LoaD spin,[39] rotating the magnets instead eliminated adverse effects on the beads (i.e., pelleting) generated by centrifugal forces, which would ultimately preclude effective NA capture.[39]

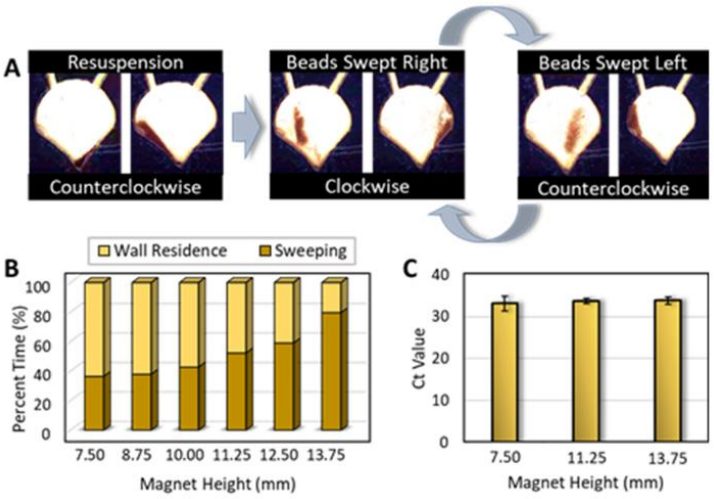

Figure 2-11. Characterization of magnetically-driven bead mixing. (A) Beads are resuspended from the bottom of the chamber using a rotating magnetic field (RMF). Reversing the direction of the RMF induces bead migration across the extraction chamber; beads reside against the chamber wall until the RMF again changes direction to drive the beads in the reverse direction. Repeated alterations of RMF orientation drives back-and-forth bead sweeping. (B) Percent distribution of bead sweeping and wall residence in each 20 s RMF step at 6 different magnet z-heights. Each bar represents the grand mean of 3 sets of 14 measurements. Here, sweeping speed was inversely related to z-height. (C) RT-PCR results from DNA obtained from parallel extractions with 7.50 mm, 11.25 mm, and 13.75 mm z-heights (each n = 4) produced similar Ct values, indicating similar DNA yields. Adapted from [17].

During initial assay evaluation, the distance

between the microfluidic and magnetic discs (z-height) was 7.50 mm. However, it was observed that under these conditions, during a given bRMF step, the beads swept across the chamber very rapidly, and spent the majority of time against the chamber wall, instead of interacting with NAs in solution (**Figure 2-11B**). Thus, it was anticipated that slower bead migration would promote more thorough bead-DNA interaction and, hence, improved yield. To test this hypothesis, the relationship between magnetically-driven 'sweeping' speed and NA yield was explored. Distance and magnetic field strength are inversely proportional, such that increasing the magnet z-height should diminish the magnetic force experienced by the beads, thereby slowing their movement. Indeed, a percent distribution of the time beads spent 'sweeping' through solution or against the chamber wall as a function of z-height demonstrated that the beads traversed the chamber most rapidly at the minimal z-height (7.50 mm), where the magnetic field strength was highest; time required for the beads to reach the opposing wall increased proportionally with height (**Figure 2-11B**). At z-heights greater than 13.75 mm, beads failed to reach the opposing wall within a single 20 s bRMF step. These studies demonstrated precise temporal control over bead migration enabled by untethering mixing from microdevice rotation.

To assess any effect of sweeping speed on NAE performance, DNA was extracted from lysates from swab cuttings spiked with a known mass (10 ng) of commercial human genomic DNA at z-heights of 7.50, 11.25, and 13.75 mm (**Figure 2-11C**). A classical one-way ANOVA of Ct values obtained via real-time PCR amplification (TPOX) of extracted DNA indicated statistically similar values across z-heights between 7.50 and 13.75 mm (p-value = 0.24, $\alpha = 0.05$). Residual analysis (Shapiro-Wilk's normality test and Levene's and Bartlett's test) indicated that all assumptions for the classical ANOVA were met; there

were no extreme outliers, residuals were normally distributed, and there was homogeneity of variances ($p > 0.05$). In the absence of evidence suggesting that slower bead migration improves NA recovery, all further experiments continued to use the z-height used during initial assay characterization (7.50 mm).

2.3.3.2. Extraction Chamber Geometry

Successful on-disc dSPE required not only effective manipulation of the silica beads, but also their retention in the extraction chamber for the entire assay duration. Since NAs are adsorbed to their silica surfaces, any undesired bead movement to waste during fluidic transfer steps would pose detriment to NA yield. To aid retention, beads were centrifugal pelleted, or collected, at the most radial edge of the extraction chamber prior to fluid removal. Despite this, it was immediately clear that substantial (near total) bead loss occurred during the first fluid removal step using the initial circular extraction chamber, (**Figure 2-12A**). Thus, thoughtful design of the extraction chamber geometry was essential to mitigate bead loss. Various geometries were evaluated, but it was determined that a pointed convex-shaped extraction chamber more successfully retained beads by effectively trapping them within the outer vertex via centrifugal pelleting (**Figure 2-12B**).[18]

A second advantage of the modified extraction chamber geometry was centered on the provision of highly pure, amplification-ready NAs in the final eluate fraction. As discussed in Chapter 1, reagents commonly used in chemical lysis methods (e.g.,

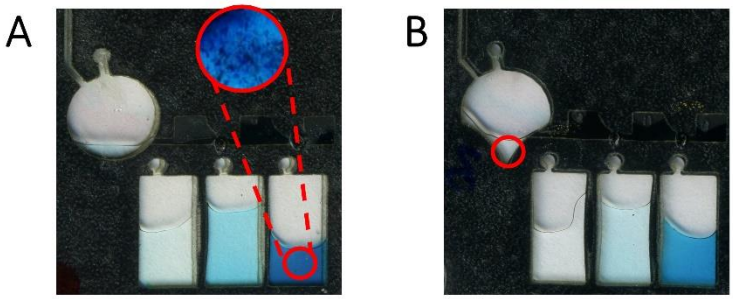

Figure 2-12. Effect of chamber geometry on bead retention. (A) During early architectural optimization, it was evident that using a circular extraction chamber led to immediate loss of beads to waste in the initial lysate fraction. (B) Adopting a chamber geometry with a convex vertex on the radially outer edge exhibited improved bead retention.

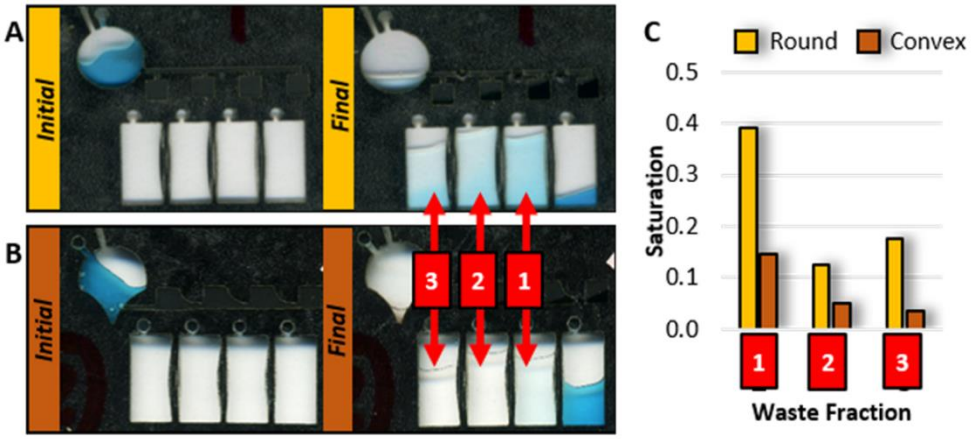

Figure 2-13. Evaluation of eluate purity with varied extraction chamber geometries. Empirical saturation analysis permitted characterization of removal of lysate, represented by blue dye, from the eluate. Images of dSPE LoaD with (A) round and (B) convex pointed extraction chambers. It was visually apparent that all three fractions (1-3) eluted from the round extraction chamber contained blue dye, whereas fractions 2-3 downstream of the convex pointed chamber appear colorless. (C) Using a round chamber shape, all waste fractions exhibited elevated saturation values relative to parallel tests using convex pointed chambers. Adapted from [17].

GuHCl) are, unfortunately, potent inhibitors of downstream NAATs.[21, 40] Thus, minimizing lysate carryover into the eluate was essential. Initial assessment of eluate purity was achieved by using an aqueous blue dye to simulate a cellular lysate, with repeated addition and removal of deionized water representing remaining NAE reagents (**Figure 2-13**). More effective removal of the blue color from subsequent fractions represented more complete washing away of the lysate. After completing the on-disc fluidic protocol, each of the waste fractions obtained via washing the round extraction chamber visually appeared blue in color, indicating the presence of residual dye (lysate). Conversely, the second and third waste fractions downstream of the convex, pointed extraction chamber were seemingly colorless, suggesting more minimal lysate carryover. Empirical analysis of saturation, or color intensity, was performed to more quantitatively inform on lysate prevalence in each fraction (**Figure 2-13**). Briefly, a larger constituency of dye within a sample produces an increased saturation value, whereas the presence of less dye will yield a lower saturation value, closer to the value associated with pure water (colorless). Saturation was selected for this analysis given its known utility for evaluation of such

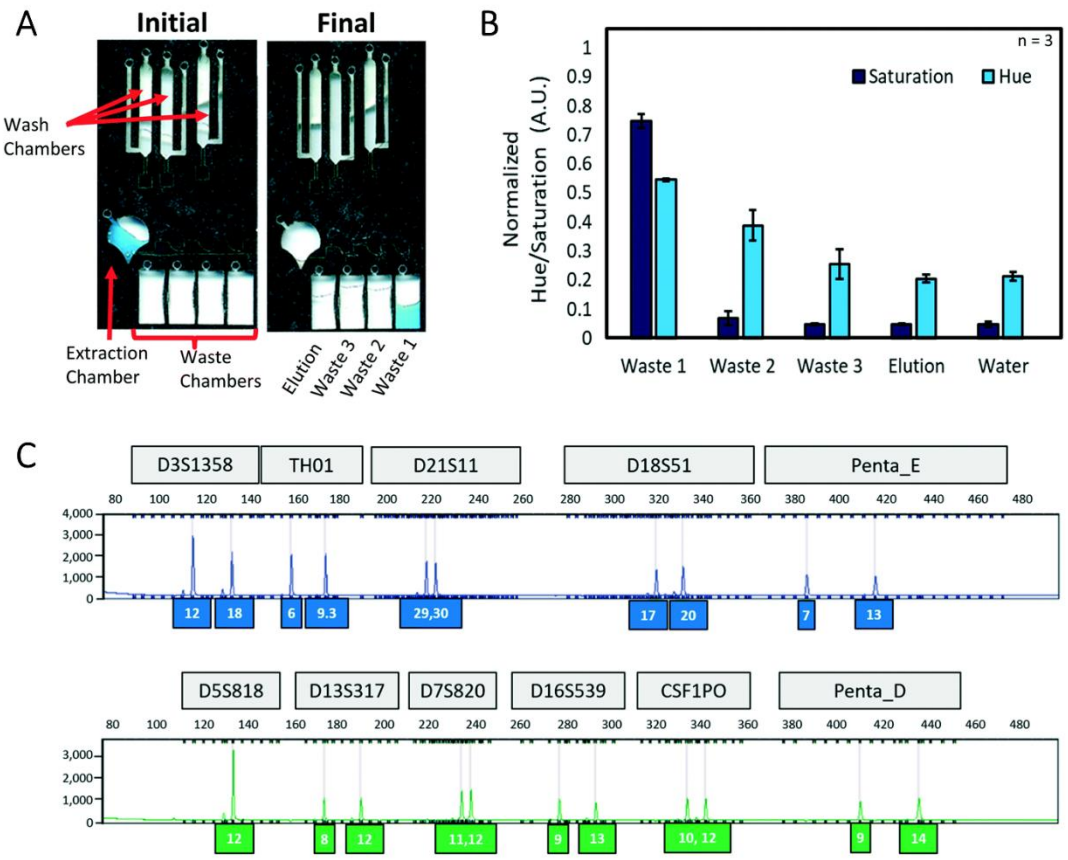

Figure 2-14. LoaD for dSPE of PCR-ready DNA reliant on laser-based valve closures. (A) Image PCL LoaD for dSPE before and after the washing protocol using blue dye to simulate the cellular lysate. (B) Empirical image analysis of each recovered fraction. Hue and saturation both decrease with continued washing; image parameters measured from the final eluate have returned to those of pure water, indicating thorough dye removal. (C) Two channels of an STR profile generated from DNA extracted on-disc, demonstrating successful purification and biocompatibility of the technique. Adapted from [24]

colorless-to-colored transitions.[30, 41-45] As expected, saturation measurements tracked with visual results; saturation of fractions downstream of the round extraction chamber were consistently higher than parallel measurements taken from architecture with a pointed, convex extraction chamber.

More thorough characterization of lysate removal was conducted by completing the on-disc assay in its entirety using blue dye to represent the lysate and water to simulate all other reagents (**Figure 2-14**). Following centrifugal pumping of the dye from the extraction chamber to the first waste chamber (1), sequential water fractions were spun into the central chamber from the wash chambers, and then to the remaining downstream chambers from

right to left to simulate the two wash steps, followed by elution. Though each fraction appeared visually colorless, analysis of both hue and saturation was performed (**Figure 2-14B**). Comparison of measured values with those taken from pure water permitted empirical estimation of dye (lysate) removal. The first waste chamber contained the pure blue dye representative of the lysate, and had the highest measured values for both hue and saturation. It was logical that each subsequent fraction had diminished hue and saturation values, as any dye initially remaining in the extraction chamber was diluted and removed with continued washing. Hue and saturation measured from waste chamber 2 remained slightly elevated, indicative of some dye carryover. This was not unexpected; the extraction chamber was specifically designed to trap nanoparticles in its vertex, so some fluid retention was unavoidable. However, the measured hue and saturation values in the third waste chamber approached those of pure water. Ultimately, a Welch's two sample t-test indicated statistical similarity between the mean hue (p-value = 0.3055) and saturation (p-value = 0.3706) values of the final elution fraction and deionized water (**Figure 2-14B**). It was anticipated that such effective removal of potential PCR inhibitors from on-disc eluates would allow for unimpeded amplification. In fact, full 18-plex STR profiles were generated from DNA purified from buccal swab cuttings via automated, on-disc dSPE. No indication of inhibition, such as allelic drop out or peak height imbalances, were observed (**Figure 2-14C**). These findings were essential in establishing the viability of the dSPE LoaD approach, as well as demonstrating that any combustion or ablation products formed as result of laser-based channel closures pose no appreciable detriment to downstream delicate PCR-based assays.

2.3.3.3. Wash Protocol Optimization

In early work demonstrating on-disc dSPE, an intermediate 1X TE wash was performed immediately prior to NA elution to ensure efficient removal of assay reagents (e.g., GuHCl, IPA) known to inhibit PCR. However, since TE is traditionally used to elute adsorbed NAs from silica, inclusion of this step introduced potential for NA loss and lower extraction efficiency.[5] To determine if this wash could be eliminated without PCR inhibition, parallel in-tube extractions were performed with and without the TE wash. Electropherograms obtained following multiplexed PCR amplification of numerous loci within the DNA extracted without the TE wash showed no signs of inhibition; peak heights were similar across methods (**Figure 2-15**). These preliminary in-tube results suggested that the intermediate TE wash could be eliminated, but further testing was required to determine if this was also true within the LoaD system.

Again, initial characterization was performed using aqueous dye solutions. Specifically, tartrazine, a yellow dye, was used to represent either IPA or GuHCl in two different dye studies designed to probe their prevalence in the final on-disc eluate (Figure

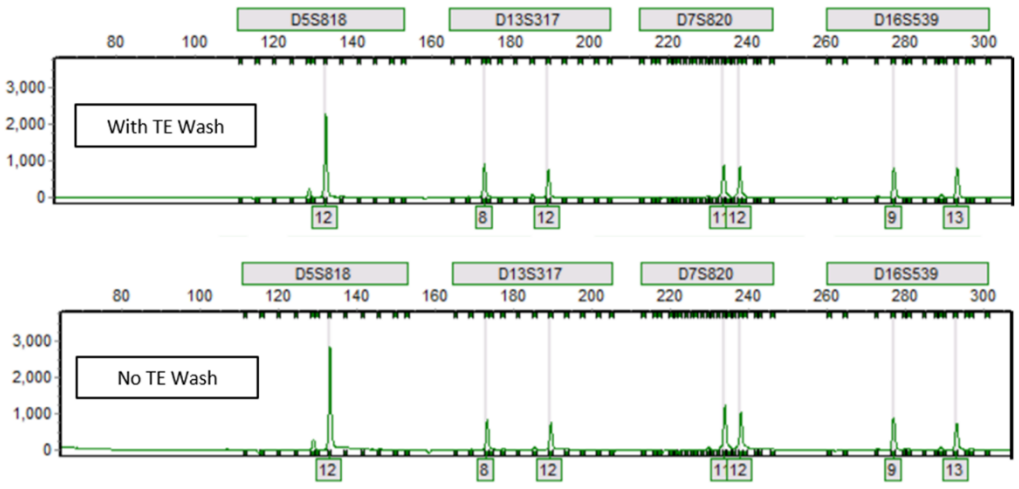

Figure 2-15. Evaluation of intermediate TE wash necessity. STR profiles from DNA obtained via in-tube dSPE with and without the intermediate TE wash. Peak heights were higher without the intermediate TE wash with no observed signs of inhibition. The intermediate TE wash was deemed to be unnecessary. Adapted from [17].

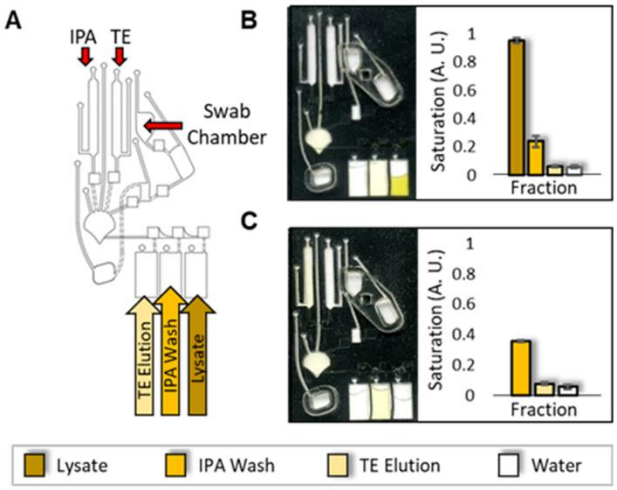

Figure 2-16. Optical assessment of eluate purity via dye-based visualization studies. (A) Modified architecture for dye studies, with chambers labeled with representative fractions. Image analysis following on-disc dSPE with tartrazine-spiked simulants of (B) lysate, and (C) IPA, produced colorless eluates; empirical analysis produced eluate saturation values to be comparable to pure water, indicating minimal GuHCl and IPA presence. Adapted from [17].

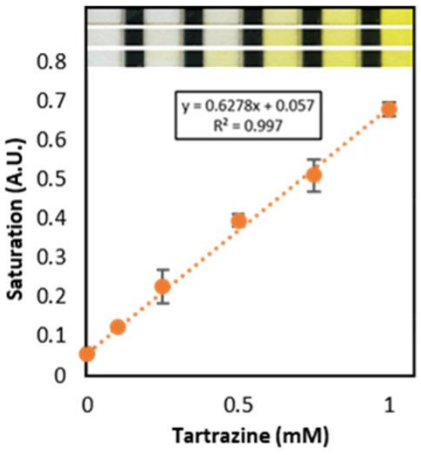

Figure 2-17. Tartrazine standard curve used in eluate purity assessment. Calibration curve relating measured saturation and aqueous tartrazine concentration measured in microfluidic chambers (images inset). Each point represents the mean of triplicate measurements with error bars depicted as one standard deviation in both directions. The excellent linear correlation ($R^2 = 0.997$) permitted quantification of eluate impurities. Adapted from [17].

2-16). Here, similarly to the study in the previous section, dye, and therefore inhibitor, prevalence in solution was optically quantified by measuring eluate saturation.

Dye Study I: Cellular Lysate.

The on-disc fluidic protocol was first completed with aqueous tartrazine representing the cellular lysate (**Figure 2-16A**). Though a slight yellow color was visually apparent in the IPA waste fraction, tartrazine carryover at this point was neither unexpected or problematic as the IPA wash is intended to remove lysate contaminants. Importantly, the eluate appeared colorless; the lack of perceivable tartrazine present was empirically confirmed by comparing its 'saturation' with that of pure water. A paired t-test for means (p-value = 0.17, $\alpha = 0.05$) indicated that the null hypothesis (equality of means) could not be rejected, so the saturation values of the final eluate and pure water were statistically similar. Therefore, there would be negligible presence of GuHCl or other lysate-derived contaminants in the purified NA solution.

Dye Study II: Isopropanol.

Similarly, in a separate study, dSPE was performed with a tartrazine-spiked IPA solution (**Figure 2-16B**). Though the eluate appeared colorless, analogous statistical treatment to that performed in Dye Study I indicated a statistical difference between the saturation values of the eluate and water (p-value = 6.0x10-4, $\alpha = 0.05$). However, the saturation of the eluate was below the calculated LoD for tartrazine (0.04 mM) (**Figure 2-17**). The IPA prevalence at the LoD was calculated as 3.0%. Thus, each subsequent 25 µL PCR reaction would contain only 0.24% IPA, below the reported inhibitory concentration of 1.0%.[46]

Taken together, the results of these two colorimetric studies, led to the conclusion that even without an intermediate TE wash, eluted NAs were highly pure and PCR inhibition was not expected.

2.3.4. Evaluation of Integrated Microfluidic NA Preparation

2.3.4.1. Short Tandem Repeat Profiling

With encouraging results from the dye studies, the 'PCR-readiness' of disc dSPE-purified DNA was truly challenged through multiplexed PCR and downstream short

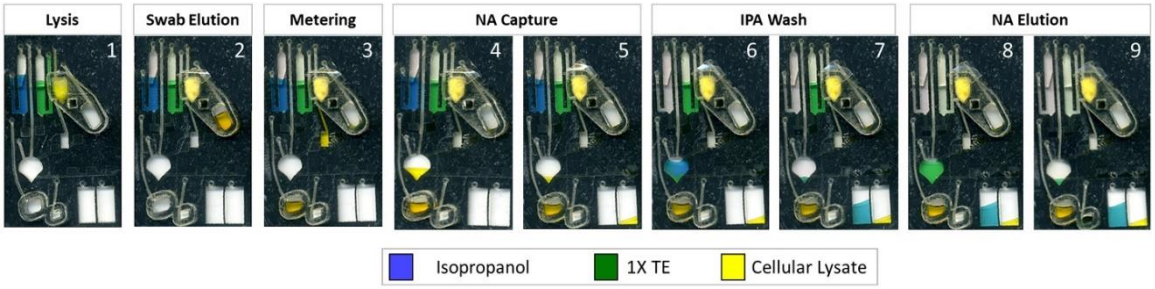

Figure 2-18. Images of the integrated fluidic control protocol for on-disc lysis and dSPE. Aqueous dyes representing the lysate (yellow), isopropanol (blue), and TE elution buffer (green) were used to visually depict the on-disc NAE preparation workflow. After incubation, (1) the lysate (yellow) is centrifugally eluted from the swab cutting, and (2) collected in the swab elution chamber. (3) A 2 uL lysate aliquot is metered, with the excess driven to an overflow chamber. (4) The metered lysate aliquot is delivered to the extraction chamber where purification proceeds using preloaded reagents. After NA capture, (5) the supernatant lysate is driven to waste and (6) isopropanol is delivered to the extraction chamber. (7) After washing the beads, the supernatant isopropanol is spun out of the extraction chamber. (8) Finally, the TE elution buffer is introduced to the extraction chamber to facilitate NA desorption from the beads and, (9) the purified eluate is transferred to the NA recovery chamber. Adapted from [17].

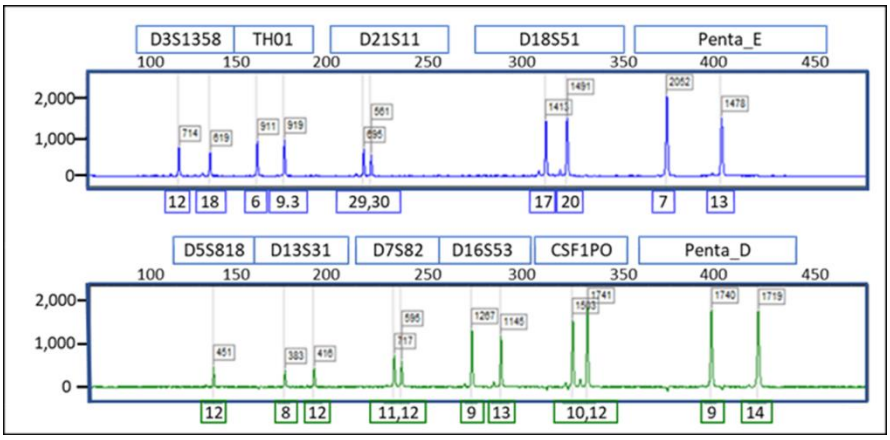

Figure 2-19. Extract compatibility with STR profiling. Electropherograms from an 18-plex STR profile generated following multiplexed PCR amplification of DNA prepared on-disc. No signs of inhibition, such as peak imbalances within a given locus, were observed, demonstrating the high purity and direct PCR compatibility of dSPE eluates. Adapted from [17].

tandem repeat (STR) analysis. STR analysis, pervasive in forensic human identification and familial testing, leverages multiple primer sets to simultaneously probe numerous genomic loci known to contain polymorphic STRs, or nucleotide sequences (e.g., 3 to 7 bases) replicated a variable number of times.[47] Individuals have two distinct copies (alleles) of each locus, and therefore up to two polymorphism lengths – one from each biological parent. An individual's STR profile can be constructed via the PCR-based amplification of these regions and the subsequent electrophoretic separation and sizing of the resultant amplicons. Notably, STR analysis provides a sensitive metric for evaluating amplification-readiness of DNA since multiplexed PCRs are especially sensitive to inhibiton.[48] To evaluate this method's capacity for integration with this workflow, DNA for amplification was prepared via the fully-integrated lysis and dSPE method (**Figure 2-18**). Full 18-plex profiles were reliably generated from on-disc dSPE eluates (**Figure 2-19**). Two channels of one such electropherogram show 11 of the 18 loci probed; amplicons at the remaining seven loci were also successfully detected but not depicted here. As seen previously, no signs of inhibition, such as peak dropout or imbalance, were noted despite omission of the intermediate TE wash.[49] All expected peaks were detected with similar heights between

allele pairs, decisively demonstrating the high purity of dSPE-extracted DNA and its direct PCR compatibility.

2.3.4.2. Demonstration of RNA Extraction

Up to this point, all dSPE efforts in our lab have centered on DNA purification.[18, 35-36] However, RNA binding to silica under chaotropic conditions occurs in a manner indistinguishable from that of DNA.[5] To evaluate if on-disc dSPE was amenable to preparation high-purity RNA from dried buccal swabs, cuttings were spiked with SARS-CoV-2 'armored' RNA. The use of armored RNA offers multiple advantages over viral samples (e.g., stability, homogeneity, and non- infectivity) and is commonly used as a full process control in the development and verification of viral detection assays.[50] The full SARS-CoV-2 genome is enveloped in a coded viral protein coat, which protects the genetic material and necessitates its extraction prior to amplification and detection. Following on-disc dSPE, with no changes to assay workflow or chemistry, SARS-CoV-2 RNA was successfully detected in all samples via real-time RT-PCR amplification with resultant C_t values below the CDC-defined cut-off (C_t = 40) (**Figure 2-20**). Although co-extracted human genomic DNA from epithelial cells collected on swabs can promote non-specific amplification, and ultimately false positive results, none

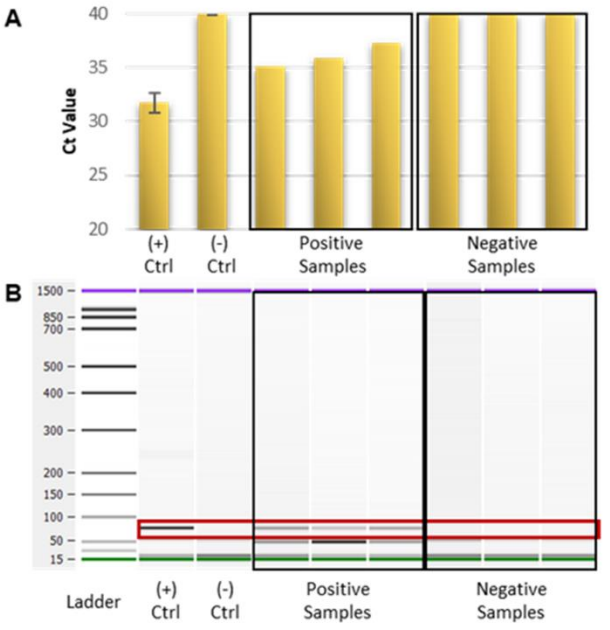

Figure 2-20. Detection of pathogenic RNA. (A) RT-qPCR amplification of the SARS-CoV-2 N1 RNA target was achieved from on-disc extracts from spiked buccal swab cuttings. (B) Gel-image rendering of electropherograms obtained from following RT-PCR showed amplicons that matched the intended product size (~72 bp) only in positive control and positive extracted samples. Adapted from [17].

was observed in post-processing of buccal swabs not spiked with armored SARS-CoV-2 RNA.[51] Though not conventionally performed, endpoint electrophoretic sizing of qPCR amplicons was included to assure amplification specificity. Following conversion of three positive and three negative electropherograms to a computer-generated 'gel' rendering, in which dark bands represent electropherogram peaks, amplicons corresponding to the intended SARS-CoV-2 N1 gene target size (~72 base pairs) were detected only in the positive control and three positive extracts from spiked swabs. This observation, coupled with the absence of amplification in the no-template control permitted conclusion that the observed amplification was specific to the intended viral target; DNase treatment was deemed unnecessary, as there would be increased cost and complexity (architectural and procedural) with little, if any, benefit.

2.3.4.3. Compatibility with Isothermal Amplification

As discussed in **Chapter 1**, PCR-based assays remain the 'gold standard' and constitute the majority of NA amplification tests (NAATs). However, the practicality of their use outside of conventional laboratory settings is limited, largely by extensive instrumentation requirements for thermal cycling and fluorescence detection that limit portability. Conversely, due to complete circumnavigation of thermal cycling requirements, isothermal NAATs are more suited to field use. For instance, loop-mediated isothermal amplification (LAMP), developed by Notomi et al., has been touted as a cost-effective, fieldable alternative to PCR with increased amenability to simple, point of need instrumentation.[6, 52-53] Instead of traditional PCR primer pairs, LAMP uses 4-6 primers that bind sequentially to NA targets, making this assay highly specific.[52-53] Consequently, step-wise LAMP primer annealing/extension generates multiple, polydisperse amplicons, which

appear as numerous distinct peaks when evaluated electrophoretically, significantly different from single length PCR amplicons.[53]

DNA prepared on-disc from buccal swab cuttings was isothermally amplified by targeting the TPOX locus. Electrophoretic separation and fluorescence detection of amplicons resulted in the characteristic peak pattern associated with LAMP amplicons, discussed above (**Figure 2-21A**). As done previously during SARS-CoV-2 detection (Section 2.3.4.2), electropherograms of LAMP products from four different buccal swab extracts were compiled and converted to a single gel-image rendering (**Figure 2-21B**). No product bands were observed in analysis of the no template control and reagent blank, demonstrating the absence of non-specific amplification. Conversely, the 'gel' lanes associated with all buccal swab samples contained numerous bands of differing lengths, consistent with characteristic LAMP product composition. Thus, all amplification observed from buccal swab extracts was determined to be specific for th e TPOX target. Further, triplicate cuttings from the same swab (Samples 4.1-4.3) produced identical peak patterns, demonstrating reproducibility of LAMP-based amplification of DNA extracted using on-disc dSPE across donors and replicates.

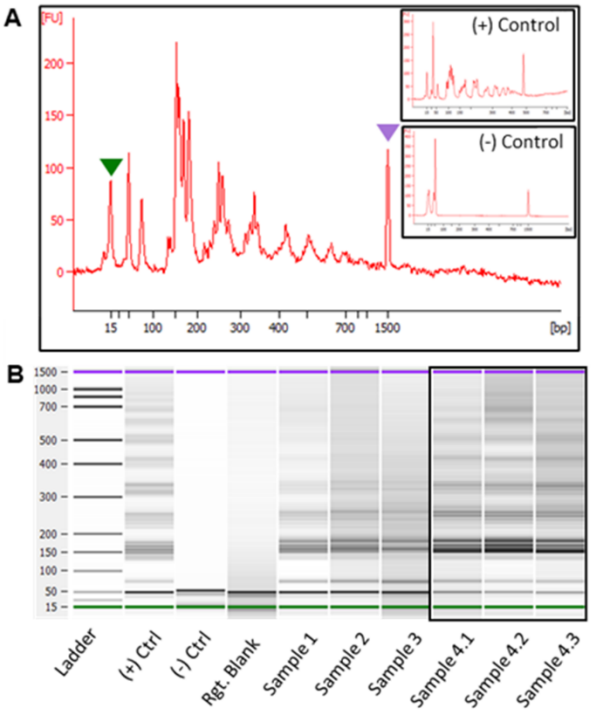

Figure 2-21. LAMP amplification of dSPE extracts. (A) Representative electropherogram of LAMP products depicting the distinct peak pattern indicative of successful amplification of DNA prepared on-disc. (B) Gel image rendering of LAMP electropherograms from extracts obtained across donors and replicates, demonstrating reproducibility of LAMP downstream of LoaD preparation. Adapted from [17].

2.4. Conclusions

The optimized dSPE LoaD described here performs fully-integrated, automatable, and multiplexed preparation of amplification-ready nucleic acids (NAs) directly from unprocessed buccal swab samples. Explicitly, up to eight samples may be processed in parallel in under 30 minutes, permitting increased throughput relative to conventional, manual methods. Further, this work represents the first reported example of incorporating on-disc, direct-from-swab enzymatic lysis upstream of dSPE in a centrifugal microdevice. Integrated lysis is essential for processing human samples, but lysis is frequently omitted from on-disc workflows, mandating in-tube pre-processing that precludes fully automated NA preparation.[9, 54-61] Here, the robust fluidic control required to integrate these two processes was enabled by two exceedingly reliable complementary laser-valving strategies.[24-25] Optically-controlled valve closures permitted the fluid fractionation required for the cascade of reagent introduction, retention, and removal required for completion of the 'bind-wash-elute' workflow in a single microfluidic chamber.[24] This work also represents the first demonstration that laser valve closures may be performed upstream of NAATs with no observed inhibition resulting from combustion or ablation products.[24] The success of these closures was unquestionably demonstrated through optical analysis of four distinct dye fractions sequentially flowed through the extraction chamber and sequestered in individual downstream chambers. Further dye studies were implemented to optimize lysis and dSPE microarchitectures and visually demonstrate high eluate purity, with minimal carryover of sample and assay components that may inhibit post-processing.

Ultimately, the amplification-readiness of NAs prepared on-disc was demonstrated using a panel of NAATs. Extracted DNA was directly compatible with not only real-time PCR, but also multiplexed PCR amplification – known to possess increased inhibitor susceptibility. STR profiles generated subsequently demonstrated that DNA targets at 18 different human genomic loci were simultaneously amplified with no observed inhibition. Successful isolation of detectable levels of DNA was reliably achieved from swab cuttings across donors. This highlights the robustness of on-disc NA preparation, since original concentrations of cells, and therefore quantities of genetic material, present are variable and unknown. Though PCR-based assays remain the 'gold standard' in many arenas, a rapidly expanding portfolio of isothermal NA amplification strategies are garnering attention as simpler, more portable alternatives. To ensure that the dSPE LoaD produced DNA of sufficient quantity and quality for use in isothermal amplification, DNA extracted on-disc was amplified via LAMP. This finding has important implications since LAMP is especially well-suited for portable microfluidic diagnostics due to simplified hardware requirements and compatibility with visual, colorimetric detection.

For the first time, RNA was extracted from a buccal swab sample; SARS-CoV-2 armored RNA was lysed enzymatically and the liberated pathogenic material was extracted with no modifications to assay workflow or chemistry. Therefore, both the lysis and extraction methodologies used here have wide bandwidths and are amenable to extracting both DNA and RNA from numerous sample types, namely human epithelial cells and virions. The successful analysis of viral samples prepared with this portable system demonstrates its potential for integration with analytical tools in diverse arenas (e.g., clinical diagnostics), especially in resource-limited settings.[9-10] Further, because a DNase

treatment was not needed to obtain amplification-ready RNA, coelution of both DNA and RNA is possible, increasing the volume of information that may be procured from a single extract via multiple detection modalities.[7, 11]

Historically, development of microfluidic NA preparation techniques has lagged behind amplification and detection for point of need use, including diagnostics.[5-6, 11] Thus, our strategy for producing high-purity NAs, effectively free from PCR inhibitors, stands to make significant impact in facilitating NA testing outside of traditional laboratory settings. To enable such portability, ongoing work involves the design and construction of a single mechatronic platform for comprehensive automation of lysis and NAE (**Figure 2-22**). This single system combines the functionalities of dSPE and the Power, Time, and Z-Height Adjustable Laser spin stands (discussed in section 2.2.3) to permit total automation of the NA preparation workflow with no required analyst intervention.

A fully-automated, multiplexed NA preparation LoaD stands to make significant impact by eliminating the variability associated with manual sample processing, increasing throughput, and decreasing the analytical interval and contamination risks inherent to traditional open-tube methods. Further, this custom spin stand possesses all required functionalities for eventual integration of on-disc downstream LAMP to yield a fully-integrated sample-to-answer LoaD akin to those described in **Chapter 1**.

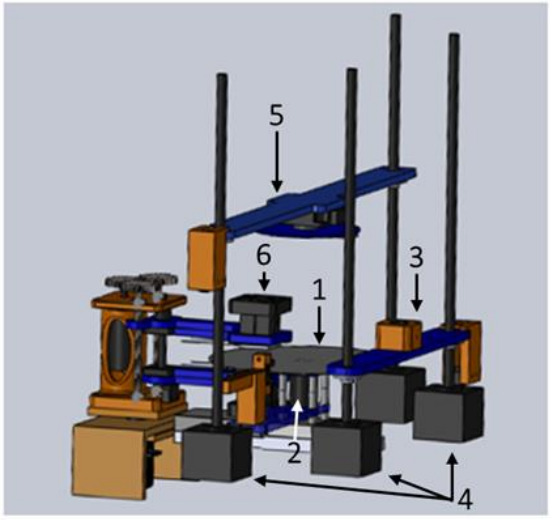

Figure 2-22. Integrated mechatronic spin stand for assay automation. After inserting the LoaD (1), flow is driven via rotation of a brushless DC motor (2). To enable valving, the laser diode (3) was positioned the appropriate distance above the LoaD using stepper motors (4). Similarly, magnets (5) can be positioned directly above the LoaD and rotated to facilitate on-disc bead manipulation. Finally, Peltiers (6) may be clamped onto the disc to enable heating where necessary.

2.5. References

1. Choi, G.; Jung, J. H.; Park, B. H.; Oh, S. J.; Seo, J. H.; Choi, J. S.; Seo, T. S., A centrifugal direct recombinase polymerase amplification (direct-RPA) microdevice for multiplex and real-time identification of food poisoning bacteria. *Lab on a Chip* **2016,** *16* (12), 2309-2316.

2. Chen, J.; Xu, Y.; Yan, H.; Zhu, Y.; Wang, L.; Zhang, Y.; Lu, Y.; Xing, W., Sensitive and rapid detection of pathogenic bacteria from urine samples using multiplex recombinase polymerase amplification. *Lab on a Chip* **2018,** *18* (16), 2441-2452.

3. Liu, D.; Zhu, Y.; Li, N.; Lu, Y.; Cheng, J.; Xu, Y., A portable microfluidic analyzer for integrated bacterial detection using visible loop-mediated amplification. *Sensors and Actuators B: Chemical* **2020,** *310*, 127834.

4. Tian, F.; Liu, C.; Deng, J.; Han, Z.; Zhang, L.; Chen, Q.; Sun, J., A fully automated centrifugal microfluidic system for sample-to-answer viral nucleic acid testing. *Science China Chemistry* **2020,** *63* (10), 1498-1506.

5. Ali, N.; Rampazzo, R. C. P.; Costa, A. D. T.; Krieger, M. A., Current nucleic acid extraction methods and their implications to point-of-care diagnostics. *BioMed Research International* **2017,** 2017.

6. Wu, J.; Kodzius, R.; Cao, W.; Wen, W., Extraction, amplification and detection of DNA in microfluidic chip-based assays. *Microchimica Acta* **2014,** *181* (13-14), 1611-1631.

7. Tan, S. C.; Yiap, B. C., DNA, RNA, and protein extraction: the past and the present. *Journal of Biomedicine and Biotechnology* **2009,** 2009.

8. Price, C. W.; Leslie, D. C.; Landers, J. P., Nucleic acid extraction techniques and application to the microchip. *Lab on a Chip* **2009,** *9* (17), 2484-2494.

9. Kim, J.; Johnson, M.; Hill, P.; Gale, B. K., Microfluidic sample preparation: cell lysis and nucleic acid purification. *Integrative Biology* **2009,** *1* (10), 574-586.

10. Jung, W.; Han, J.; Choi, J.-W.; Ahn, C. H., Point-of-care testing (POCT) diagnostic systems using microfluidic lab-on-a-chip technologies. *Microelectronic Engineering* **2015,** *132*, 46-57.

11. Dineva, M. A.; Mahilum-Tapay, L.; Lee, H., Sample preparation: a challenge in the development of point-of-care nucleic acid-based assays for resource-limited settings. *Analyst* **2007,** *132* (12), 1193-1199.

12. Yang, J.; Hurth, C.; Nordquist, A.; Smith, S.; Zenhausern, F., Integrated Microfluidic System for Rapid DNA Fingerprint Analysis: A Miniaturized Integrated DNA Analysis System (MiDAS)—Swab Sample-In to DNA Profile-Out. In Microfluidic Electrophoresis, Springer: 2019; pp 207-224.

13. Mark, D.; Haeberle, S.; Roth, G.; Von Stetten, F.; Zengerle, R., Microfluidic lab-on-a-chip platforms: requirements, characteristics and applications. In Microfluidics based microsystems, Springer: 2010; pp 305-376.

14. Gorkin, R.; Park, J.; Siegrist, J.; Amasia, M.; Lee, B. S.; Park, J. M.; Kim, J.; Kim, H.; Madou, M.; Cho, Y. K., Centrifugal microfluidics for biomedical applications. *Lab on a Chip* **2010,** *10* (14), 1758-1773.

15. Ramsey, J. M., The burgeoning power of the shrinking laboratory. *Nature Biotechnology* **1999,** *17* (11), 1061-1062.

16. Manz, A.; Graber, N.; Widmer, H. M., Miniaturized total chemical analysis systems: a novel concept for chemical sensing. *Sensors and Actuators B: Chemical* **1990,** *1* (1-6), 244-248.

17. Dignan, L. M.; Woolf, M. S.; Tomley, C. J.; Nauman, A. Q.; Landers, J. P., Multiplexed Centrifugal Microfluidic System for Dynamic Solid-Phase Purification of Polynucleic Acids Direct from Buccal Swabs. *Analytical Chemistry* **2021,** *93* (19), 7300-7309.

18. Jackson, K.; Borba, J.; Meija, M.; Mills, D.; Haverstick, D.; Olson, K.; Aranda, R.; Garner, G.; Carrilho, E.; Landers, J. P., DNA purification using dynamic solid-phase extraction on a rotationally-driven polyethylene-terephthalate microdevice. *Analytica Chimica Acta* **2016,** *937*, 1-10.

19. Li, L.; Miao, B.; Li, Z.; Sun, Z.; Peng, N., Sample-to-answer hepatitis B virus DNA detection from whole blood on a centrifugal microfluidic platform with double rotation axes. *ACS Sensors* **2019,** *4* (10), 2738-2745.

20. Loo, J.; Kwok, H.; Leung, C.; Wu, S.; Law, I.; Cheung, Y.; Cheung, Y.; Chin, M.; Kwan, P.; Hui, M., Sample-to-answer on molecular diagnosis of bacterial infection using integrated lab-on-a-disc. *Biosensors and Bioelectronics* **2017,** *93*, 212-219.

21. Gorkin, R.; Park, J.; Siegrist, J.; Amasia, M.; Lee, B. S.; Park, J. M.; Kim, J.; Kim, H.; Madou, M.; Cho, Y. K., Centrifugal microfluidics for biomedical applications. *Lab on a Chip* **2010,** *10* (14), 1758-1773.

22. Thio, T. H. G.; Soroori, S.; Ibrahim, F.; Al-Faqheri, W.; Soin, N.; Kulinsky, L.; Madou, M., Theoretical development and critical analysis of burst frequency equations for passive valves on centrifugal microfluidic platforms. *Medical & Biological Engineering & Computing* **2013,** *51* (5), 525-535.

23. Ouyang, Y.; Wang, S.; Li, J.; Riehl, P. S.; Begley, M.; Landers, J. P., Rapid patterning of 'tunable' hydrophobic valves on disposable microchips by laser printer lithography. *Lab on a Chip* **2013,** *13* (9), 1762-1771.

24. Woolf, M. S.; Dignan, L. M.; Lewis, H. M.; Nauman, A. Q.; Tomley, C. J.; Landers, J., Optically-Controlled Closable Microvalves for Polymeric Centrifugal Microfluidic Devices. *Lab on a Chip* **2020,** *20* (8), 1426-1440.

25. Garcia-Cordero, J. L.; Kurzbuch, D.; Benito-Lopez, F.; Diamond, D.; Lee, L. P.; Ricco, A. J., Optically addressable single-use microfluidic valves by laser printer lithography. *Lab on a Chip* **2010,** *10* (20), 2680-2687.

26. Zucchelli, P.; Van de Vyver, B. Devices and methods for programmable microscale manipulation of fluids. U.S. Patent US7152616, 2006.

27. Thompson, B. L.; Ouyang, Y.; Duarte, G. R.; Carrilho, E.; Krauss, S. T.; Landers, J. P., Inexpensive, rapid prototyping of microfluidic devices using overhead transparencies and a laser print, cut and laminate fabrication method. *Nature Protocols* **2015,** *10* (6), 875-886.

28. Horsman, K. M.; Hickey, J. A.; Cotton, R. W.; Landers, J. P.; Maddox, L. O., Development of a human-specific real-time PCR assay for the simultaneous quantitation of total genomic and male DNA. *Journal of Forensic Sciences* **2006,** *51* (4), 758-765.

29. DuVall, J. A.; Borba, J. C.; Shafagati, N.; Luzader, D.; Shukla, N.; Li, J.; Kehn-Hall, K.; Kendall, M. M.; Feldman, S. H.; Landers, J. P., Optical imaging of

paramagnetic bead-DNA aggregation inhibition allows for low copy number detection of infectious pathogens. *PLoS One* **2015,** *10* (6), e0129830.

30. Woolf, M. S.; Dignan, L. M.; Scott, A. T.; Landers, J. P., Digital postprocessing and image segmentation for objective analysis of colorimetric reactions. *Nature Protocols* **2020,** *16* (1), 218-238.

31. Dignan, L. M.; Woolf, M. S.; Ross, J. A.; Baehr, C.; Holstege, C. P.; Pravetoni, M.; Landers, J. P., A Membrane-Modulated Centrifugal Microdevice for Enzyme-Linked Immunosorbent Assay-Based Detection of Illicit and Misused Drugs. *Analytical Chemistry* **2021,** *98* (48), 16213-16221.

32. Sloane, H. S.; Carter, M. B.; Cecil, A. E.; Le Roux, D.; Mills, D. L.; Landers, J. P., Warfarin genotyping with hybridization-induced aggregation on a poly (ethylene terephthalate) microdevice. *Analyst* **2017,** *142* (2), 366-374.

33. DuVall, J. A.; Le Roux, D.; Thompson, B. L.; Birch, C.; Nelson, D. A.; Li, J.; Mills, D. L.; Tsuei, A.; Ensenberger, M. G.; Sprecher, C., Rapid multiplex DNA amplification on an inexpensive microdevice for human identification via short tandem repeat analysis. *Analytica Chimica Acta* **2017,** *980*, 41-49.

34. Turiello, R.; Dignan, L. M.; Thompson, B.; Poulter, M.; Hickey, J.; Chapman, J.; Landers, J. P., Centrifugal Microfluidic Method for Enrichment and Enzymatic Extraction of Severe Acute Respiratory Syndrome Coronavirus 2 RNA. *Analytical Chemistry* **2022,** *94* (7), 3287-3295.

35. Duarte, G. R.; Price, C. W.; Augustine, B. H.; Carrilho, E.; Landers, J. P., Dynamic solid phase DNA extraction and PCR amplification in polyester-toner based microchip. *Analytical Chemistry* **2011,** *83* (13), 5182-5189.

36. Duarte, G. R.; Price, C. W.; Littlewood, J. L.; Haverstick, D. M.; Ferrance, J. P.; Carrilho, E.; Landers, J. P., Characterization of dynamic solid phase DNA extraction from blood with magnetically controlled silica beads. *Analyst* **2010,** *135* (3), 531-537.

37. Ouyang, Y.; Li, J.; Haverstick, D. M.; Landers, J. P., Rotation-driven microfluidic disc for white blood cell enumeration using magnetic bead aggregation. *Analytical Chemistry* **2016,** *88* (22), 11046-11054.

38. DuVall, J. A.; Cabaniss, S. T.; Angotti, M. L.; Moore, J. H.; Abhyankar, M.; Shukla, N.; Mills, D. L.; Kessel, B. G.; Garner, G. T.; Swami, N. S., Rapid detection of Clostridium difficile via magnetic bead aggregation in cost-effective polyester microdevices with cell phone image analysis. *Analyst* **2016,** *141* (19), 5637-5645.

39. Grumann, M.; Geipel, A.; Riegger, L.; Zengerle, R.; Ducrée, J., Batch-mode mixing on centrifugal microfluidic platforms. *Lab on a Chip* **2005,** *5* (5), 560-565.

40. Homann, A. R.; Niebling, L.; Zehnle, S.; Beutler, M.; Delamotte, L.; Rothmund, M.-C.; Czurratis, D.; Beller, K.-D.; Zengerle, R.; Hoffmann, H., A microfluidic cartridge for fast and accurate diagnosis of Mycobacterium tuberculosis infections on standard laboratory equipment. *Lab on a Chip* **2021,** *21* (8), 1540-1548.

41. Krauss, S. T.; Nauman, A. Q.; Garner, G. T.; Landers, J. P., Color manipulation through microchip tinting for colorimetric detection using hue image analysis. *Lab on a Chip* **2017,** *17* (23), 4089-4096.

42. Cantrell, K.; Erenas, M.; de Orbe-Payá, I.; Capitán-Vallvey, L., Use of the hue parameter of the hue, saturation, value color space as a quantitative analytical parameter for bitonal optical sensors. *Analytical Chemistry* **2010,** *82* (2), 531-542.

43. Capitán-Vallvey, L. F.; Lopez-Ruiz, N.; Martinez-Olmos, A.; Erenas, M. M.; Palma, A. J., Recent developments in computer vision-based analytical chemistry: A tutorial review. *Analytica Chimica Acta* **2015,** *899*, 23-56.

44. Cao, S.; Huang, D.; Wang, Y.; Li, G., Phenolphthalein Alkalinity Testing Research Based on Computer Vision Technology and Electronic Technology. In Advances in Mechanical and Electronic Engineering, Springer: 2012; pp 381-386.

45. Krauss, S. T.; Holt, V. C.; Landers, J. P., Simple reagent storage in polyester-paper hybrid microdevices for colorimetric detection. *Sensors and Actuators B: Chemical* **2017,** *246*, 740-747.

46. Rossen, L.; Nørskov, P.; Holmstrøm, K.; Rasmussen, O. F., Inhibition of PCR by components of food samples, microbial diagnostic assays and DNA-extraction solutions. *International Journal of Food Microbiology* **1992,** *17* (1), 37-45.

47. Butler, J. M., Short tandem repeat typing technologies used in human identity testing. *Biotechniques* **2007,** *43* (4), Sii-Sv.

48. Huang, M. L.; Nguy, L.; Ferrenberg, J.; Boeckh, M.; Cent, A.; Corey, L., Development of multiplexed real-time quantitative polymerase chain reaction assay for detecting human adenoviruses. *Diagnostic Microbiology and Infectious Disease* **2008,** *62* (3), 263-271.

49. McCord, B.; Pionzio, A.; Thompson, R., Analysis of the effect of a variety of PCR inhibitors on the amplification of DNA using real time PCR, melt curves and STR analysis. US Department of Justice 2015, 317.

50. Pasloske, B. L.; Walkerpeach, C. R.; Obermoeller, R. D.; Winkler, M.; DuBois, D. B., Armored RNA technology for production of ribonuclease-resistant viral RNA controls and standards. *Journal of Clinical Microbiology* **1998,** *36* (12), 3590-3594.

51. Laurell, H.; Iacovoni, J. S.; Abot, A.; Svec, D.; Maoret, J.-J.; Arnal, J.-F.; Kubista, M., Correction of RT–qPCR data for genomic DNA-derived signals with ValidPrime. *Nucleic Acids Research* **2012,** *40* (7), e51-e51.

52. Ahmad, F.; Hashsham, S. A., Miniaturized nucleic acid amplification systems for rapid and point-of-care diagnostics: a review. *Analytica Chimica Acta* **2012,** *733*, 1-15.

53. Notomi, T.; Okayama, H.; Masubuchi, H.; Yonekawa, T.; Watanabe, K.; Amino, N.; Hase, T., Loop-mediated isothermal amplification of DNA. *Nucleic Acids Research* **2000,** *28* (12), e63.

54. Obino, D.; Vassalli, M.; Franceschi, A.; Alessandrini, A.; Facci, P.; Viti, F., An Overview on Microfluidic Systems for Nucleic Acids Extraction from Human Raw Samples. *Sensors* **2021,** *21* (9), 3058.

55. Choi, G.; Prince, T.; Miao, J.; Cui, L.; Guan, W., Sample-to-answer palm-sized nucleic acid testing device towards low-cost malaria mass screening. *Biosensors and Bioelectronics* **2018,** *115*, 83-90.

56. Wang, G.; Tan, J.; Tang, M.; Zhang, C.; Zhang, D.; Ji, W.; Chen, J.; Ho, H.-P.; Zhang, X., Binary centrifugal microfluidics enabling novel, digital addressable functions for valving and routing. *Lab on a Chip* **2018,** *18* (8), 1197-1206.

57. Van Nguyen, H.; Seo, T. S., High-throughput human DNA purification on a centrifugal microfluidic device for rapid forensic sex-typing. *Biosensors and Bioelectronics* **2021,** *181*, 113161.

58. Van Nguyen, H.; Phan, V. M.; Seo, T. S., A portable centrifugal genetic analyzer for multiplex detection of feline upper respiratory tract disease pathogens. *Biosensors and Bioelectronics* **2021,** *193*, 113546.

59. Zhang, L.; Tian, F.; Liu, C.; Feng, Q.; Ma, T.; Zhao, Z.; Li, T.; Jiang, X.; Sun, J., Hand-powered centrifugal microfluidic platform inspired by the spinning top for sample-to-answer diagnostics of nucleic acids. *Lab on a Chip* **2018,** *18* (4), 610-619.

60. Yuan, D.; Kong, J.; Li, X.; Fang, X.; Chen, Q., Colorimetric LAMP microfluidic chip for detecting three allergens: peanut, sesame and soybean. *Scientific Reports* **2018,** *8* (1), 1-8.

61. Oh, S. J.; Seo, T. S., Combination of a centrifugal microfluidic device with a solution-loading cartridge for fully automatic molecular diagnostics. *Analyst* **2019,** *144* (19), 5766-5774.

3. Microscale nanoparticle-based enrichment and RNA extraction

3.1. Introduction

The global SARS-CoV-2 outbreak that caused the COVID-19 pandemic exposed critical shortcomings in existing nucleic acid analysis workflows. SARS-CoV-2, a positive-sense RNA virus, exhibits high transmission rates and pathogenicity due, in part, to surface spike proteins that facilitate facile host cell entry through homology with angiotensin-converting enzyme (ACE2) receptors.[1] In an effort to combat worldwide infections, widespread testing was implemented but imposed massive analytical burdens that many clinical laboratories were unable to meet.[2-4] Delays created by already time- and labor-intensive diagnostic workflows were exacerbated by supply chain limits as demand for materials and reagents, such as nucleic acid extraction (NAE) kits, outpaced production.[2-4] Most 'gold standard' NAE kits rely on lytic enzymes (e.g., proteases) to initially disrupt viral envelopes. The resultant lysate is then passed through a packed silica column to capture liberated pathogenetic RNA.[5] These solid phase extraction (SPE) methods require extensive manual intervention and possess an open-tube format, which both limits analytical throughput and risks analyst exposure to infectious agents. Though both of these issues were effectively ameliorated via SARS-CoV-2 RNA extraction using the lab-on-a-disc (LoaD) format for silica-based dynamic SPE (dSPE), as described in **Chapter 2**. However, this microfluidic device and workflow were not specifically tailored to diagnostics, and therefore, may not be suitable for all relevant samples. For instance, to conserve NAE supplies and improve testing throughput, especially in asymptomatic or low disease prevalence populations, the United States Department of Human Health and Safety recommended pooling samples from up to 20 individuals in a single test.[6] Pertinent

concerns lingered regarding whether existing NAE methods were capable of providing detectable levels of pathogenic RNA for successful viral detection in such low-titer, pooled samples.[4, 7] Preconcentration of the target virions prior to lysis, not performed in conventional SPE, could make the difference between successful detection and a false negative result.[8] Here, a second magnetically-controlled nanoparticle-based method for NA preparation, specifically designed to include virion preconcentration, or enrichment, prior to extraction of SARS-CoV-2 RNA from clinical samples, is described.[9]

Specifically, hydrogel nanoparticles were leveraged for SARS-CoV-2 enrichment as they have previously been demonstrated to improve downstream detection sensitivity, including in pooled sample mimics.[8, 10] These nanoparticles are decorated with both affinity baits to capture virions via spike protein interaction and paramagnetic materials to allow for facile manipulation.[8, 10] Enrichment also allows for removal of the sample matrix, which often contains substances (e.g., electrolytes, mucins, enzymes) known to inhibit downstream nucleic acid amplification tests (NAATs), widely recognized as the most reliable, ubiquitous methods for patient diagnosis of SARS-CoV-2 infection.[11-12] Upstream nanoparticle-based enrichment was coupled with rapid, one-step enzymatic extraction of amplification-ready RNA from clinically relevant matrices. Specifically, following enrichment, nanoparticles were resuspended in a rnaGEM extraction cocktail containing a thermophilic proteinase[13] that simultaneously digested viral envelopes and stabilized liberated RNA through RNase hydrolysis.[14] Through adaptation of this so-called ‘enriched rnaGEM’ chemistry to commercial PDQeX technology, RNA isolation and sequestration of nanoparticles from the eluate were achieved in a single, hands-free step. No further purification was required prior to RNA amplification, entirely circumventing the

requirement for conventional SPE. Implementation of enriched rnaGEM extraction augments throughput, avoids the reliance on supply-chain limited kits, and reduces the analytical interval to permit more timely diagnosis.

Enriched rnaGEM extractions performed using the PDQeX system represented a significant decrease in the time, labor, and material requirements relative to conventional methods. However, further streamlining the workflow could allow for total assay automation. To achieve this, the enriched rnaGEM chemistry was adapted to a microfluidic LoaD platform, which have garnered substantial attention as powerful, portable alternatives for convenient NA processing by non-technical personnel.[15-16] When compared with traditional laboratory-based techniques, microfluidic strategies offer appeal in terms of decreased sample/reagent consumption, ease of automation, enclosed formats, rapid analysis, and decreased cost.[15, 17] Among these, rotationally-controlled, centrifugal LoaDs constitute an especially attractive format by obviating the need for bulky, complex external equipment, e.g., pneumatic systems.[18-19] Here, one such self-contained centrifugal microdevice was developed for enriched rnaGEM extraction of purified, amplification-ready SARS-CoV-2 RNA from patient samples.

The success of enriched rnaGEM extraction performances of both platforms (PDQeX and LoaD) were thoroughly characterized through comparison with a ‘gold standard’ commercial SPE kit. Though real-time reverse transcription polymerase chain reaction (real-time RT-PCR) is best known as the “gold standard” NAAT for clinical diagnosis,[20] it may also be used as an analytical tool to evaluate the success of upstream nucleic acid preparation. This principle is harnessed here to compare RNA extraction from clinically-positive SARS-CoV-2 samples in parallel using the proposed technique and a

conventional, commercial method. Though this robust technique is specific and sensitive,[20] real-time RT-PCR requires complex instrumentation for precisely timed and controlled temperature cycling and fluorescence detection. Consequently, relatively long analytical intervals and extensive hardware requirements leave conventional RT-PCR methods tethered to centralized laboratories.[21] Consequently, numerous alternative isothermal NAATs for more fieldable, rapid viral detection have emerged. For instance, loop-mediated isothermal amplification (LAMP)[22] has been used in conjunction with colorimetric indicators, such as hydroxy naphthol blue (HNB),[23] to provide instrument-free, visual SARS-CoV-2 detection with limits of detection as low as 10 genetic copies per reaction.[24-28] Similarly, recombinase polymerase amplification (RPA)[29-30] can provide optical detection of the viral target in as little as seven minutes.[7] These portable, isothermal techniques demonstrated the potential to alleviate analytical burdens placed on existing laboratory testing infrastructure by allowing for use outside of the laboratory (e.g., at home).[28, 31-33] Thus, the compatibility of enriched rnaGEM extracts with isothermal NAATs, namely LAMP and RPA, was also explored to demonstrate applicability with more fieldable portative amplification methods.

Since effective epidemiological control requires prioritization and diversification of methods, this work stands to make a significant impact in RNA preparation that would be independent of benchtop instrumentation. Ultimately, this would enable widespread in situ clinical testing, especially when used in conjunction with portable amplification methods for simple, rapid, and sensitive on-site diagnostics.[2, 34]

3.2. Materials and Methods

3.2.1. Clinical SARS-CoV-2 Sample Preparation and Analysis

Standard of care analysis was performed according to manufacturer instructions using either the Abbot Alinity-m SARS-CoV-2 assay, the Abbot M2000 Real-Time SARS-CoV-2 Assay, or the Xpert Xpress SARS-CoV-2 assay, each of which was granted emergency use authorization (EUA) from the Food and Drug Administration. After analysis, clinical samples were stored in viral transport medium (VTM) and de-identified according to protocols approved by the University of Virginia Institutional Review Board. An aliquot (600 – 1000 µL) was transferred to a 2 mL microcentrifuge tube and heat-inactivated via incubation at 65 ˚C for 30 minutes. All samples were stored at -20 ˚C until analysis. Here, any patient sample with a cycle threshold (Ct) value assigned via these standard of care tests was considered clinically positive. Clinical Ct values were also used to infer relative viral titers.

In-Tube RNA Extraction.

Conventional Column-Based Extraction. In each extraction, viral RNA was isolated from a 250 µL aliquot of a heat-inactivated clinical VTM sample using the RNeasy Mini Kit (Qiagen, Valencia, CA, USA) with an upstream DNase I treatment (New England Biolabs, Ipswitch, MA, USA) according to manufacturers' instructions.

Viral Enrichment and rnaGEM Extraction. An initial in-tube preconcentration step was performed by adding NanoTrap Magnetic virus particles (25 µL) (CERES Nanosciences, Inc., Manassas, VA, USA) to sample VTM (250 µL), mixing, and incubating briefly at room temperature prior to magnetic pelleting of the nanoparticles. The supernatant was then removed and replaced with a lysis cocktail (50 µL total volume)

comprised of 1 µL rnaGEM enzyme in 1X BLUE buffer (MicroGEM International, PLC., Charlottesville, VA, USA). After heating (75 ˚C for 10 minutes, 95 ˚C for 5 minutes) in a thermal cycler, the nanoparticles were again collected magnetically such that the supernatant RNA lysate could be collected.

RNA Extraction using the PDQeX System.

VTM. A 25 µL aliquot of the hydrogel nanoparticles was added to sample VTM (250 µL) and incubated briefly at room temperature prior to magnetic pelleting. The nanoparticles were then resuspended in a lysis buffer comprised of 1% rnaGEM enzyme in 1X BLUE buffer (MicroGEM International, PLC.) with a total volume of either 50 µL or 100 µL. In instances where a DNase treatment was incorporated, the lysis cocktail also included 1X dsDNase buffer and 1 µL HL-sdDNase enzyme (ArcticZymes Technologies ASA, Tromsoe, Norway). The suspension was then transferred to PDQeX tubes, inserted into the associated instrument (MicroGEM International, PLC.) and heated at 95 ˚C for 5 minutes.

Saliva. Saliva was diluted at a 1:3 ratio in a dilution buffer comprised of 400 µL BLUE buffer (MicroGEM International, PLC.) in 1X phosphate-buffered saline (PBS). PBS was prepared by dissolving sodium chloride (3.2073 g), potassium chloride (0.0807 g), sodium phosphate dibasic (0.5678 g), and potassium phosphate monobasic (0.0978 g) in molecular biology grade water (40 mL) (Thermo Fisher Scientific, Waltham, MA, USA) prior to pH adjustment to 7.35 with sodium hydroxide. Prior to PDQeX extraction, VTM was serially diluted in the saliva mixture.

All RNA isolates were stored at -80 ˚C until RNA amplification was performed.

3.2.2. Conventional Real-Time RT-PCR Analysis

Extracted SARS-CoV-2 RNA was amplified using the real-time RT-PCR assay developed under EUA by the Centers of Disease Control and Prevention (CDC).[35] The resultant C_t values were used to assess the relative success of upstream RNA extraction performance across methods. Each 20 µL reaction was comprised of 5 µL TaqPathTM 1-Step RT-qPCR Master Mix, CG (Thermo Fisher Scientific), 1.5 µL SARS-CoV-2 (2019-nCoV) CDC RUO N1 primer-probe mix (Integrated DNA Technologies, Coralville, IA, USA), 8.5 µL PCR-grade water (Molecular Biologicals International, Inc.), and 5 µL RNA extract. Amplification positive controls contained the 2019-nCoV_N_Positive Control Plasmid (Integrated DNA Technologies) and no template controls (NTCs) were included. Samples were amplified in duplicate using a MyGo Pro real-time PCR instrument (IT-IS Life Science, Ltd., Dublin, Ireland); fluorescence was monitored in the FAM channel. Reverse transcription (50˚C, 900 s) was followed by denaturation (95 ˚C, 180 s) and 40 amplification cycles (denaturation: 95 ˚C, 3 s and annealing/extension: 55 ˚C). Ramp up and down rates were programmed as 5 ˚C/s and 4 ˚C/s, respectively. In subsequent optimization, reverse transcription was shortened to 60 s and the cycle annealing temperature was elevated to 60 ˚C. All samples with Ct values less than the cut-off cycle given by the assay manufacturer (40) were considered indicative of SARS-CoV-2 detection.

3.2.3. Alternative Amplification Methods

Loop-mediated Isothermal Amplification (LAMP)

Each LAMP reaction was comprised of 3.25 µL PCR-grade water, 6.25 µL 2x WarmStart master mix (New England Biolabs), 1.25 µL primer mix (sequences published

previously24), 120 µM hydroxynaphthol blue (HNB) to enable colorimetric detection, and 1.25 µL sample. The primer mix contained 2 µM F3 and B3 primers, 8 µM LF and LB primers, and 16 µM FIP and BIP primers. Samples, along with NTCs and positive controls (2019-nCoV_N_Positive Control plasmid (Integrated DNA Technologies)), were amplified in triplicate via a 60-minute incubation at 63 ˚C prior to polymerase denaturation (95 ˚C, 60 s). Images of the tubes were captured prior to heating (0 minutes), after 30 minutes, and upon assay completion (60 minutes) using a Huawei smartphone (Huawei Technologies Co., Ltd., Shenzhen, China). The hue of a circular region of interest in each reaction tube (diameter = 15 pixels) was measured in ImageJ software and averaged across replicates.36-37 A threshold was established three standard deviations below the mean hue value of all reactions prior to amplification; samples above (purple) and below (blue) this threshold were considered colorimetrically negative and positive for SARS-CoV-2, respectively.

Recombinase Polymerase Amplification (RPA)

Reverse transcription and RPA were performed in a single step using lyophilized RPA reagents from the TwistAmp© Exo Kit (TwistDxTM Ltd. San Diego, CA, USA). The reagents were rehydrated in a mixture of 29.5 µL TwistAmp Primer Free Rehydration buffer, 0.13 µM Exo-IQ probe (Eurofins Genomics LLC., Louisville, KY, USA), 10 U/µL ProtoScript II reverse transcriptase (Invitrogen, Carlsbad, CA, USA), 0.25 U/µL thermostable RNase H (New England Biolabs), 0.44 µM each SARS_RPA_F1 and SARS_RPA_R1 primers[38] (Eurofins Genomics LLC.), and 6.2 µL PCR-grade water. Individual reaction tubes each contained 21.25 µL of the mixture described above, with 14 nM magnesium acetate (TwistDxTM) and 2.5 µL RNA extract placed on the inside of the

tube lid. Reactions were initiated by centrifugation immediately prior to tube insertion into a TS16-ISO instrument (Axxin, Fairfield, Victoria, Australia), preheated to 42 °C. Fluorescence monitoring (20% LED) was performed throughout the incubation (1920 s total), which included a brief mixing step after 300 s. An amplification threshold was established three standard deviations above the mean fluorescence readings taken from NTCs over the assay duration.

3.2.4. Microdevice Fabrication

Centrifugal microdevices designed to permit integrated, automated, and multiplexed SARS-CoV-2 enrichment as well as enzymatic viral RNA extraction were fabricated using the well-characterized 'print-cut-laminate' method.[38] A CO_2 laser (VLS3.50, Universal® Laser Systems, Scottsdale, AZ, USA) was used to ablate architectural features designed in AutoCAD software (2019, AutoDesk Inc., San Rafael, CA, USA) into thermoplastic substrates. Specifically, the core device contained five polyethylene terephthalate (PeT) layers (101.6 µm, FilmSource Inc., Maryland Heights, MO, USA). The outermost layers (1 & 5) served as 'capping layers' to enclose the microdevice. The PeT layers that housed the two fluidic layers (2 & 4) were coated in a heat-sensitive adhesive (HSA, 50.8 µm, Adhesives Research Inc., Glen Rock, PA, USA) and separated by an intervening, optically dense black PeT layer (Lumirror* X30, Toray Industries, Inc., Chuo-ku, Tokyo, Japan) to permit laser-actuated valving.[39-40] The device layers were aligned and passed through an office laminator (UltraLam 250B, Alikes Products Inc., Mira Loma, CA, USA). Laser-cut polymethyl methacrylate (PMMA, McMaster Carr, Elmhurst, IL, USA) accessory pieces (1.5 mm thickness) were affixed to

the microdevice using pressure sensitive adhesive (PSA, 55.8 µm, Arcare 7876, Adhesives Research Inc.) to augment chamber depth, and thereby volume, where appropriate.

3.2.5. Mechatronic Spin System Construction and Operation

Rotationally-controlled fluidics and laser-actuated valving were controlled by the Power, Time, and Adjustable z-Height Laser, described in detail elsewhere.[40] A 700 mW 683 nm laser diode (L638P700M, ThorLabs, Inc., Newton, NJ, USA) focused with a collimation tube containing a single aspherical lens element (LTN330-A, ThorLabs, Inc.) was positioned above the stage onto which the microdevice was mounted. The diode's position relative to architectural features (valves, channels) in the xy-plane was controlled by a motorized translational stage (MTS50-Z8, ThorLabs) a photointerrupting optical switch (TT Electronics/Optek Technology, Woking, UK), and a brushless DC motor. The z-height of the laser relative to the microdevice was adjusted using two stepper motors (Polulu Robotics and Electronics, Las Vegas, NV, USA). Normally-closed valves were opened via irradiation (500 mW, 500 mS) at 15.00 mm.[39] Conversely, positioning the diode 26.00 mm above the device and irradiating channels (700 mW, 2500 mS) facilitated their closure, and prevention of further flow.[40] A separate system was used to promote manipulation of the Nanotrap hydrogel particles within the microdevice. Briefly, a pair of Neodynium permanent magnets affixed to a PMMA disc oriented 7.50 mm above the sample disc platform on a 3-arm support structure similar to one described previously.[41] By alternating the direction of spin of the magnet disc using a stepper above the stationary microdevice via a stepper motor (Sanmotion Series, Sanyo Denki, Moriguchi, Japan), a bidirectional rotating magnetic field (bRMF) was generated that drove back-and-forth

nanoparticle sweeping.[42] All functionalities in both systems were regulated via multi-processing microcontrollers (Propeller P8X32A-M44; Propeller Inc., Rocklin, CA, USA).

3.2.6. Optical Characterization of On-Disc Enrichment and Extraction

Initial characterization and optimization of microdevice architecture were performed via on-disc fluidic studies that leveraged aqueous dye solutions for visualization. All images were captured using an Epson Perfection V100 Photo desktop scanner (Seiko Epson Corporation, Suwa, Nagano Prefecture, Japan) and analyzed using the Fiji distribution of ImageJ software. Specifically, rectangular regions of interest (ROIs) within each microdevice chamber were selected using the 'crop-and-go' method described elsewhere.[37] ROI raw images were then converted to 3-slice hue-saturation-brightness (HSB) stacks to permit hue measurement. The sample and extraction cocktail solutions (50 µL each), represented by blue and yellow dye solutions, respectively, were loaded into their individual chambers positioned radially inward relative to the magnetic manipulation chamber which, in practice, would house the Nanotrap particles. To simulate the in-tube workflow, the blue solution (sample) was first introduced to the magnetic manipulation chamber after opening the corresponding laser valve (1500 g, 30 s). The most distal downstream laser valve was then actuated, the bulk blue dye solution was centrifugally pumped to waste (1500 g, 30 s), and the channel upstream of the most recently opened valve was laser-sealed. The yellow dye solution (extraction cocktail) was then analogously introduced to and removed from the magnetic manipulation chamber, then transferred to the recovery chamber. The hue of both eluted fractions was measured (n = 6 each) and compared with parallel measurements taken from serially diluted (1:2) blue dye in yellow dye from 10% to 0% (n = 3 each).

3.2.7. On-Disc RNA Preparation

Aliquots of sample (50 µL), Nanotrap particles (10 µL), and the rnaGEM extraction cocktail prepared without a DNase as described above (50 µL) were added to their respective chambers within the microdevice. Specifically, the Nanotrap particles were added to the central magnetic manipulation chamber, whereas the other two fluids were added as described in the previous section. Irradiation of the appropriate laser valve, followed by device rotation (1500 g, 30 s), introduced the liquid sample into the magnetic manipulation chamber. Here, bRMF application (300 s total, 20s cycles in each direction) drove back-and-forth sweeping of the Nanotrap particles across the width of the chamber, which allowed for virion capture. After centrifugally pelleting the particles (2000 g, 60 s), a downstream laser valve was opened, and the sample supernatant was driven into a waste chamber (1500 g, 30 s). The channel upstream of the newly opened valve was closed via laser irradiation, and the rnaGEM extraction cocktail was introduced to the magnetic manipulation chamber (1500 g, 30 s) following actuation of the appropriate laser valve. After a second bRMF mixing step, the nanoparticle suspension in the extraction cocktail was incubated at 95 ˚C for 60 s. After centrifugally pelleting the nanoparticles (2000 g, 60 s) and opening a downstream laser valve, the supernatant RNA extract was centrifugally pumped into a downstream recovery chamber from which it could be recovered by pipette for off-disc RT-PCR amplification, performed as described above in a QuantStudio 5 Real-Time PCR System (Thermo Fisher Scientific).

3.3. Results and Discussion

NAAT-based viral detection in biological matrices is essential for effective epidemiological control, yet directly contingent on effective upstream isolation of purified

genetic material. This work details the development and characterization of a novel, orthogonal approach to preparation of amplification-ready SARS-CoV-2 RNA from patient samples. Virion enrichment using commercial Nanotrap® particles was coupled with single-step rnaGEM chemistry for RNA isolation to decrease time, required manual intervention, and reliance on supply-chain-limited conventional solid phase extraction (SPE) kits. Virion enrichment prior to lysis imparted the sensitivity required for analysis of low-titer samples. Adaptation of this workflow to the PDQeX system permitted rapid pathogen enrichment from clinically relevant matrices (e.g., viral transport media (VTM) and saliva) followed by a single-step, hands-free virion lysis, DNA isolation, and nanoparticle removal. The performance of enriched rnaGEM extraction was evaluated through comparison with conventional, 'gold standard' SPE kits via real-time reverse transcription polymerase chain reaction (RT-PCR) amplification. Subsequent efforts involved the design of a multiplexed LoaD that mirrored this workflow to provide comprehensive, automatable SARS-CoV-2 RNA preparation with higher throughput.

3.3.1. Enrichment and Extraction Assay Design

The enzymatic rnaGEM extraction method leveraged here is unique among existing NAE approaches due to its homogenous format. The overwhelming majority of such techniques are biphasic – partitioning the desired genetic material into one phase while removing sample impurities, such as cellular debris or other inhibitory exogeneous compounds (e.g., VTM[43]), into the other. Most commonly, NAE involves genetic material capture on a solid phase, which is then washed extensively to remove contaminants prior to NA elution. Despite widespread acceptance, SPE methods are extremely time-consuming and require extensive manual manipulation (e.g., washing, centrifugation) by

trained analysts in an open-tube format that offers gratuitous opportunity for contamination.[13] Alternatively, rnaGEM chemistry leverages a neutral, thermophilic protease from the thermophilic Bacillus species EA1 to provide amplification-ready genetic material in a single, closed-tube step.[14] Simple thermal reaction control obviates the need for solvent extraction or column purification, effectively eliminating the need for manual intervention altogether.[14] Though SARS-CoV-2 was successfully detected from patient samples following direct RNA amplification from neat rnaGEM lysates (data not shown), this workflow was augmented by upstream virion enrichment using NanoTrap® hydrogel particles due to previously published data demonstrating associated improvements to post-processing performance.[3] Paramagnetic components embedded within the particles' hydrogel network allow for facile magnetic retention during removal of the supernatant sample (**Figure 3-1A**). Upon nanoparticle resuspension in rnaGEM extraction with applied heat, captured virions are rapidly lysed to provide SARS-CoV-2 RNA (**Figure 3-1B**) that is directly compatible with downstream amplification methods, including real-time RT-PCR.

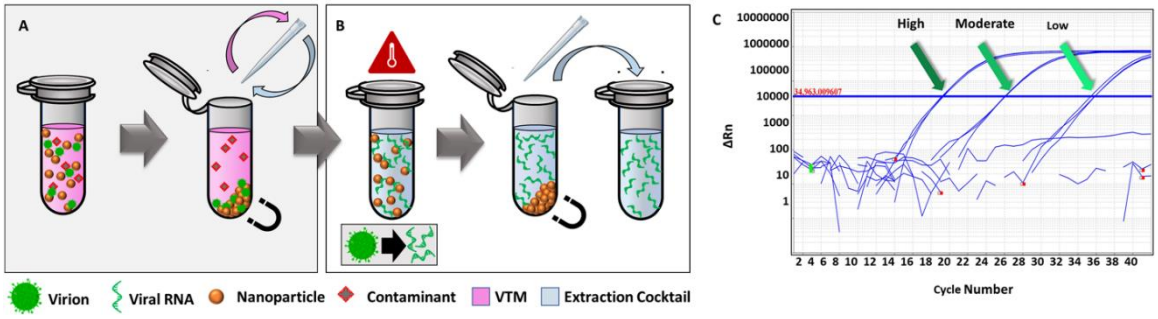

Figure 3-1: Workflow for in-tube viral preconcentration and RNA extraction. (A) SARS-CoV-2 virions were preconcentrated from viral transport medium (VTM) using paramagnetic capture particles. Following adsorption of the virion to the capture particles, they were collected magnetically and the supernatant VTM was removed. (B) The capture particles were re-suspended in rnaGEM extraction cocktail and heated to liberate viral RNA. Following a second magnetic immobilization step, the purified RNA supernatant was transferred to a second tube. (C) A representative amplification plot from RT-PCR amplification of extracted RNA. Such amplification techniques were used to characterize extraction and ultimately detect SARS-CoV-2. Adapted from [9].

In addition to the benefits derived from significantly streamlining the NAE workflow relative to column-based SPE discussed above, this approach circumnavigates more nuanced issues exposed during the pandemic. Practically, as COVID-19 lingered and more research groups endeavored to develop diagnostic and treatment technologies, commercial NAE kits became difficult to obtain and even pipette tips became exceedingly scarce. The enriched rnaGEM method avoids these limitations by reducing reliance on both pipetting steps and the highly specific commercial equipment needed for conventional SPE. Thus, this method provides an alternative NAE approach with increased independence from supply chains. In a clinical sense, enriched rnaGEM extraction is advantageous over column-based methods with regard to accurate characterization of patient infectivity. Naked RNA is known to persist in sample matrices well beyond the period of infection transmissibility.[44] However, in conventional SPE virions are lysed prior to RNA capture, rendering it impossible to distinguish RNA obtained from recently lysed, transmissible virions versus persistent free RNA. This inability to determine RNA source confounds diagnostic efforts by public health officials attempting to determine key metrics, such as an appropriate quarantine duration.[44] Conversely, nanoparticle-based enrichment facilitates sequestration of active, intact virions while naked RNA in the supernatant is removed prior to extraction. Thus, enriched rnaGEM extraction may provide more accurate information regarding patient infectivity via downstream post-processing.

3.3.2. Characterization of Enriched rnaGEM Extraction

Clinical laboratories ubiquitously use ‘gold standard’ real-time RT-PCR to provide patient diagnoses. In practice, diagnostic laboratories provide clinicians with only a qualitative diagnosis (e.g., pathogen detected or not detected), despite capabilities of real-

time RT-PCR to produce a vastly greater depth of information. The output of real-time RT-PCR is given in cycle threshold (C_t) values, defined as the cycle at which the fluorescence signal generated from a sample exceeds a threshold indicative of amplification having occurred. C_t values are measured relative to target concentration; lower C_t values indicate more starting genetic material. Thus, though Ct values are not typically reported to physicians, they do possess clinical significance. Patients who provide samples with C_t values above 24 are likely not infectious and do not need to abide by strict transmission control measures, such as quarantining.[44] Alternatively, real-time RT-PCR can be used as an analytical tool to evaluate the relative success of upstream nucleic acid preparation methods. Explicitly, more successful nucleic acid extraction yields higher levels of liberated RNA, thus promoting more rapid, sensitive amplification. Thus, it follows that more successful extraction procedures would result in higher concentrations of RNA in solution, which, in turn, yields lower C_t values via real-time RT-PCR.

This principle was used to determine that the performance of enriched rnaGEM RNA preparation was comparable with a ubiquitous, commercial 'gold standard' SPE kit, given the similar Ct values obtained across methods. To ensure enriched rnaGEM

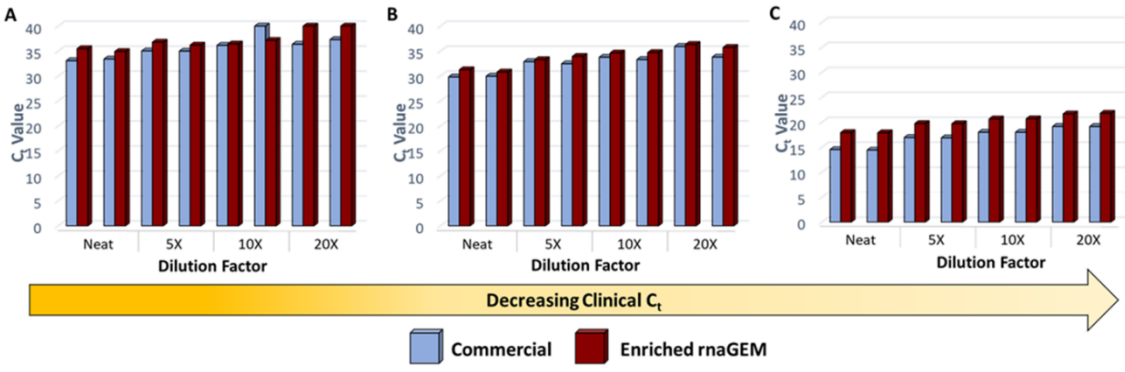

Figure 3-2: Comparison of enriched rnaGEM extraction with a commercial kit. SARS-CoV-2 RNA was extracted from known clinical positives in parallel using two methods - a commercial SPE kit, and enriched rnaGEM extraction. Three samples with comparatively (A) high, (B) moderate, and (C) low Ct values were selected for comparison. Extracts were analyzed neat and serially diluted at factors of 5X, 10X, and 20X, each in duplicate. Ct values obtained from the enriched rnaGEM extracts were only slightly higher than extracts obtained using the commercial kit. Adapted from [9].

extraction was robust across viral loads, samples with comparatively low, moderate, and high viral titers (estimated using clinically-reported C_t values) were evaluated (**Figure 3-2**). Each sample, both neat and serially-diluted, showed excellent concordance in C_t values obtained between the 'gold standard' commercial and enriched rnaGEM methods. As mentioned, numerical C_t values themselves have negligible import for diagnosis in current clinical workflows, as long as RNA was definitively detected prior to the designated cut-off cycle. Here, amplification was indeed observed regardless of viral titer or dilution factor, with only minor differences (1-2 cycles) between the proposed and gold standard methods. The most pronounced difference across methods was observed in the lowest C_t, or highest relative titer, sample. It was suspected that this disparity in performance stemmed from viral saturation of the nanoparticles, suggested by Barclay et al.[3] In such instances, if nanoparticles effectively became encapsulated by electrostatically-bound virions, pathogens remaining in solution would be sterically prevented from nanoparticle interaction, thus remaining in solution until being discarded along with the supernatant sample. This phenomenon likely contributed to C_t values obtained from commercial kit extracts being approximately three units lower than parallel enriched rnaGEM isolates. However, such nanoparticle saturation does not affect the utility of enrichment-aided extractions, nor does it prevent qualitative SARS-CoV-2 identification.[3] In this evaluation, SARS-CoV-2 was readily detected in all enriched rnaGEM dilutions with Ct values of 20±2 units, well below the CDC-recommended cut-off cycle (40).

SARS-CoV-2 RNA was also detected successfully in each dilution of the moderate and high titer extracts, down to 20X. Similar differences in performance were observed in analysis of the lowest titer sample evaluated, with the exception of some discrepancies in

the highest-factor dilutions. Here, all replicates of the 10X enriched rnaGEM extracts successfully amplified, while one of the 'gold standard' commercial samples did not. Conversely, while SARS-CoV-2 RNA was not detected in the 20X enriched rnaGEM extracts, commercial extracts produced C_t values below the cut-off cycle – though only just. In fact, the C_t values measured from the low titer neat extracts also approached the cut-off cycle. Therefore, it was presumed that RNA concentrations in subsequent dilutions fell within the stochastic regime, where inhomogeneous RNA distribution led to inconsistent trends in amplification. Thus, it was concluded that the enriched rnaGEM extraction method performed comparably to the commercial approach.

3.3.3. Adaptation to the PDQeX System

Though the in-tube enriched rnaGEM method already exhibited a streamlined workflow relative to conventional methods, further expedition was sought via adaptation to the commercial PDQeX system (**Figure 3-3**).

3.3.3.1. Platform Description

Dual-layer PDQeX tubes are comprised of a rigid outer layer encasing an inner thermally-reactive layer. Upon heating the tube in a commercial PDQeX system, the inner layer shrinks with simultaneous actuation of the heat-burst valve below the sample reservoir. These two steps together force the sample fluid through an on-board filter into a collection tube. Suspensions of nanoparticles with adsorbed virions were exposed to a single-temperature heating step that simultaneously induced hands-free enzymatic virion lysis, RNA extraction, RNase elimination, and physical separation of the capture particles from the eluate (**Figure 3-3A, B**).

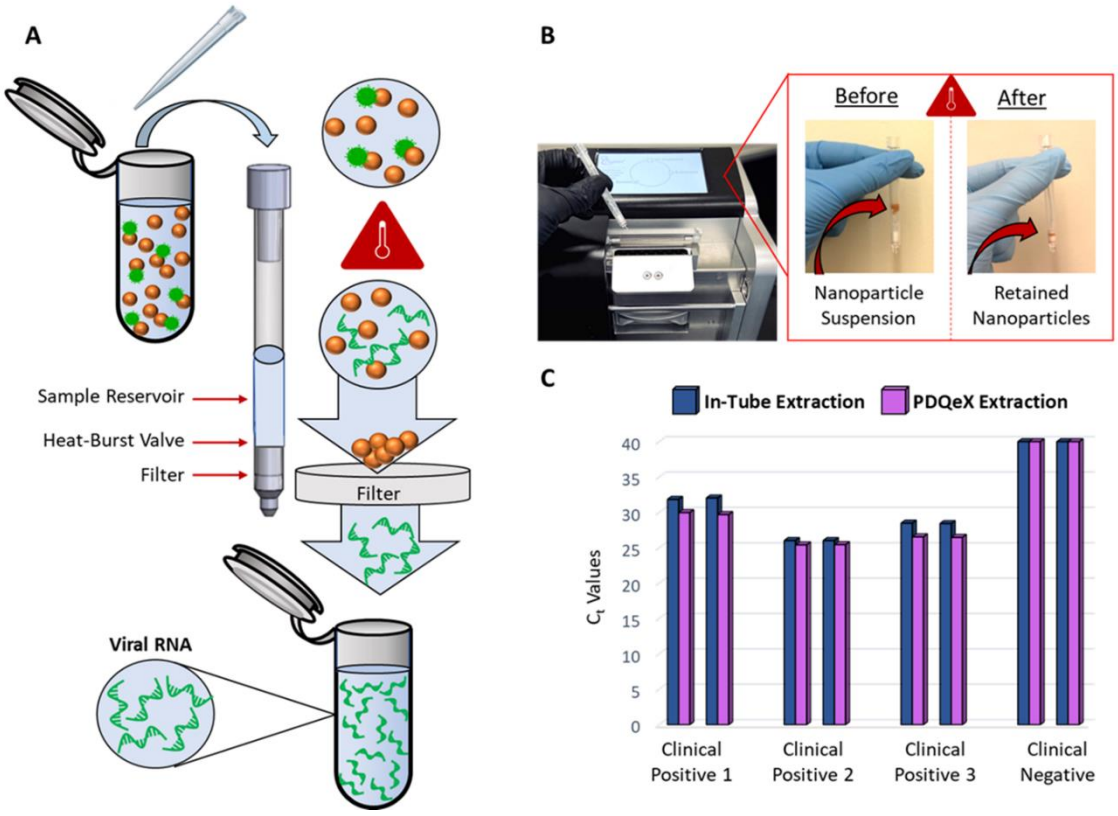

Figure 3-3: Adaptation of enriched rnaGEM extraction to the PDQeX system. (A) Following in-tube viral preconcentration, the nanoparticle suspension in rnaGEM cocktail was transferred to a PDQeX tube. Incubation induced the inner walls of the tube to shrink and the heat-burst valve below the sample reservoir to be actuated, forcing the purified RNA solution through an on-board filter and into a final collection tube. (B) PDQeX instrument with inset images depicting the PDQeX tube before and after incubation showing nanoparticles were retained by the on-board filter. (C) Comparison of the Ct values obtained from duplicate RT-PCR reactions following parallel enriched rnaGEM extractions from four clinical samples (three positive and one negative) in-tube versus the PDQeX. Across all samples, RNA amplification occurred ~1-2 cycles sooner using the PDQeX system. Adapted from [9].

3.3.3.2. Performance Evaluation

To assess the effect of this platform on extraction performance relative to the in-tube (thermal cycler) methods, RNA was isolated from parallel aliquots of 3 clinical positives using both platforms. Subsequent real-time RT-PCR analysis indicated comparable amplification across platforms, with C_t values consistently 1-2 cycles lower following PDQeX extraction (**Figure 3-3C).** Although the limited sample size in these proof-of-concept studies prevented a statistically-informed conclusion of superior PDQeX performance, it was definitively true that the methods are comparable. However, the

PDQeX was more attractive due to supplanting the several sequential manual steps required in-tube with a single automated process, thereby decreasing variability and required analyst time.

3.3.4. Extraction Chemistry Optimization

Following demonstration of the validity of the PDQeX for SARS-CoV-2 RNA extraction, the chemistry was optimized. From a practical perspective, increasing the elution volume was advantageous in allowing for more extensive testing from a single extract. Surprisingly, doubling the elution volumes from 50 to 100 µL for RNA extracted in parallel from 3 clinical positives changed downstream real-time RT-PCR performance very little. All three neat extracts, as well as dilutions down to 20X, exhibited differences of only approximately one C_t unit (**Figure 3-4**). Despite RNA dilution, the detriment to downstream detection was minimal. The increased bandwidth for testing outweighed the minor loss in sensitivity. Therefore, all further RNA extracts were prepared in 100 µL.

Although no false positives were observed in NTCs, this was a concern since genomic DNA (gDNA) present in the sample increases background fluorescence and facilitates non-specific amplification during PCR.[45-46] Accordingly, DNase treatment

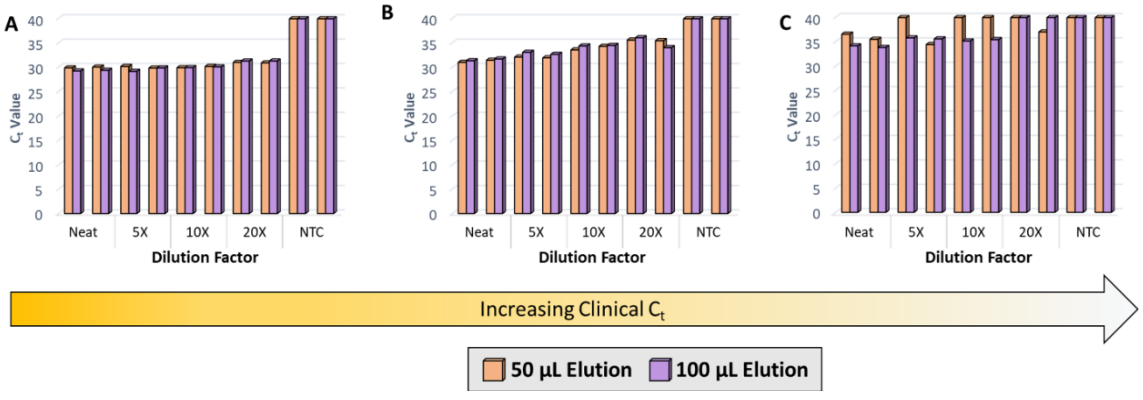

Figure 3-4 Comparative RNA yield with varied elution volumes. Parallel extractions performed from serially diluted (5X, 10X, and 20X) clinical positives with comparatively (A) low, (B) moderate, and (C) high clinical Ct values, using either 50 µL or 100 µL final volumes were analyzed by RT-PCR amplification (in duplicate). Ct values for samples and dilutions were comparable across methods. Adapted from [9].

reagents were easily incorporated into the rnaGEM extraction cocktail, avoiding any complication of the assay workflow. The resulting C_t values remained concordant across parallel samples, prepared with and without this inclusion, which was surprising as DNase treatments generally decrease RNA yield (**Figure 3-5**).[47-48] Taken together, these results indicated that the optimal enriched rnaGEM PDQeX method, used in all further experiments, used 100 µL rnaGEM extraction cocktail including a DNase.

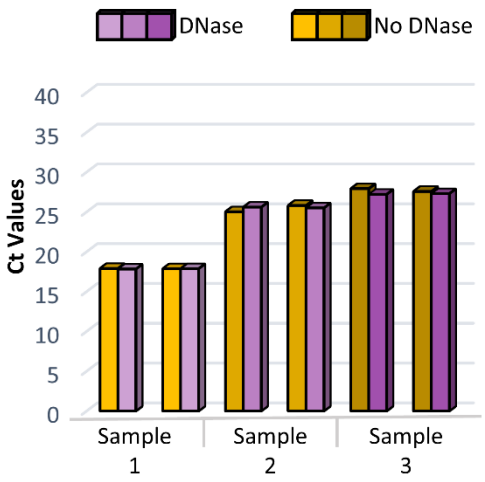

Figure 3-5. Effect of DNase inclusion on extraction and downstream detection. Parallel RNA extractions from three clinical positives were conducted with and without DNase treatment. For all samples, Ct values obtained from RT-PCR amplification (in duplicate) were within 1 unit across methods; DNase incorporation was not harmful to extraction efficiency. Adapted from [9].

3.3.5. Saliva Compatibility

Though SARS-CoV-2 detection is commonly performed from nasopharyngeal swab samples, it has been demonstrated that respiratory pathogens, including endemic coronaviruses, may be detected in saliva with comparable sensitivity.[49] Saliva is much more amenable for at-home diagnostics due to simple, non-invasive sampling that minimizes nosocomial transmission risk, lessens the demand for consumables (e.g., swabs and personal protective equipment), decreases cost, shortens turnaround time, and allows for facile repeat testing.[49] Unfortunately, practical limitations arise from saliva's high protein content and viscosity, resulting in low analytical efficiency.[50] To circumnavigate this issue, as well as prevent clogging of the on-board PDQeX filter, saliva was mixed with a dilution buffer prior to virion enrichment.

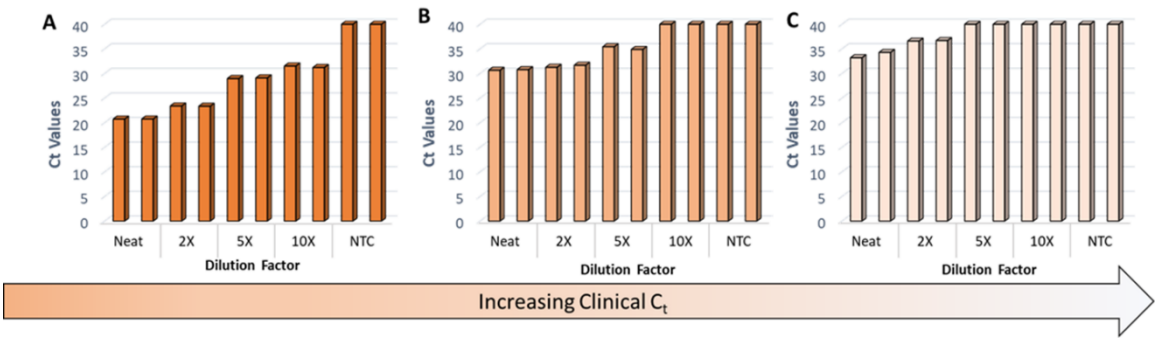

Figure 3-6. Compatibility of extraction from saliva matrices. The enriched rnaGEM method was used to extract SARS-CoV-2 RNA from three known clinically positive VTM samples serially diluted in a saliva matrix. Three samples with comparatively (A) low, (B) moderate, and (C) high clinical Ct values were selected to allow for comparison of extraction efficacy across a broad range of samples. Extracts were analyzed by RT-PCR, each in duplicate. For all three samples, SARS-CoV-2 was detected in at least one saliva extract. Adapted from [9].

To demonstrate the compatibility of the enriched rnaGEM PDQeX extractions with saliva testing, three clinical VTM samples with different titers were evaluated neat and diluted 2X, 5X, and 10X in the prepared saliva solution (**Figure 3-6**). In all samples, viral detection was successful in at least one saliva dilution. For the highest titer (lowest C_t) clinical sample, SARS-CoV-2 was detected in all dilutions, including the 10X dilution comprised of 90% saliva solution. Admittedly, these samples are not explicitly representative of true patient samples. Nonetheless, these results provide conclusive evidence that enriched rnaGEM PDQeX extraction was capable of providing detectable levels of amplification-ready RNA from saliva.

3.3.6. Optimization of Amplification Conditions

Enriched rnaGEM extraction represents significantly decreased time and labor requirements relative to traditional methods. However, downstream real-time RT-PCR remains time-consuming and contributes to lengthy analytical intervals. This delay, on the order of 24-48 hours, negatively impacts success of transmission control measures implemented.[51-52] To address this, efforts were made to shorten real-time RT-PCR amplification by both truncating hold durations and increasing the temperature ramping

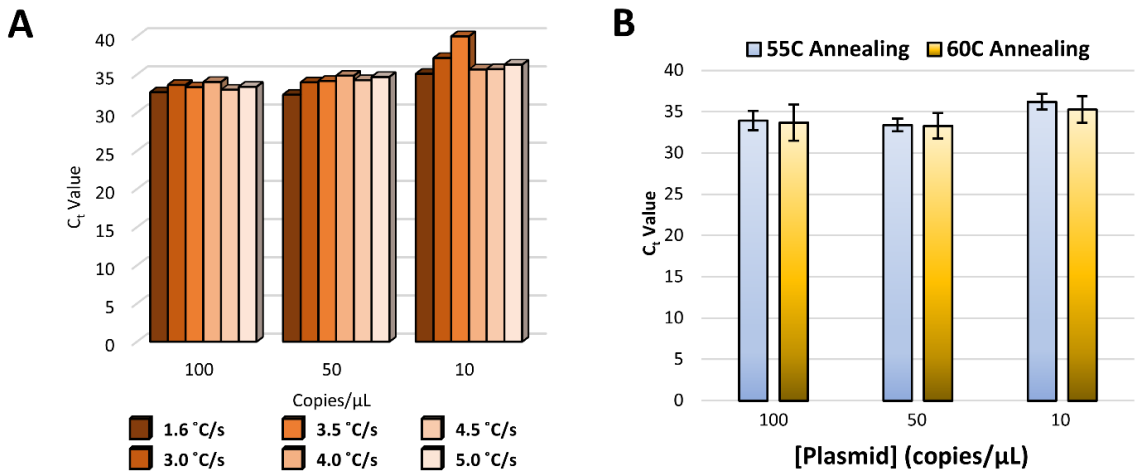

Figure 3-7. Optimization of rapid RT-PCR cycling conditions. All optimization was performed using the 2019-nCoV_N_Positive Control plasmid diluted to 100, 50, and 10 copies/µL amplified in duplicate. (A) Temperature ramp rates were incrementally increased from the kit manufacturer's recommended conditions (1.6 ˚C/s) to the fastest rate allowed by the real-time RT-PCR instrument (5 ˚C/s) with minimal impact on resultant Ct values. (B) Amplification was performed with cycle annealing temperatures of both 55°C and 60°C, each in triplicate. Averaged Ct values indicated that increasing the annealing temperature to 60°C is not detrimental to RT-PCR performance. Adapted from [9].

rate between cycle annealing and denaturation steps. Upon stepwise manipulation of individual variables, C_t values were compared between the initial and altered conditions to characterize the effect of each change on amplification performance.

Optimization of thermal cycling parameters was performed using the CDC positive control plasmid, as concentration could be more easily defined and reproducibly controlled than possible using real patient samples, in which RNA concentrations remain largely unknown. Initial efforts centered on decreasing cycle time and involved evaluation of six different ramp rates, ranging from the manufacturer's recommended conditions of 1.6 ˚C/s to the maximal values permitted by the instrument software of 5 ˚C/s in approximately 0.5 ˚C/s increments. Resultant C_t values were concordant between ramp rates across all three plasmid concentrations tested, which indicated that increasing the ramp rate to even the maximal value had minimal effect on assay performance (**Figure 3-7A**). Using the fastest ramp rates possible (5 ˚C/s up and 4 ˚C/s down) led to a 64% decrease in required cycling

time relative to the manufacturer's recommended conditions. Changing solely this parameter equated to a 36% reduction in overall time for real-time RT-PCR, from approximately 57 minutes to 36 minutes, with no observed performance detriment (**Figure 3-7B**). Finally, to further minimize amplification time, the temperature differential between the cycle annealing and denaturation steps was decreased. By changing the cycle annealing temperature from 55 ˚C to 60 ˚C, the amplification interval decreased by two minutes with a negligible impact on C_t values (**Figure 3-7C**).

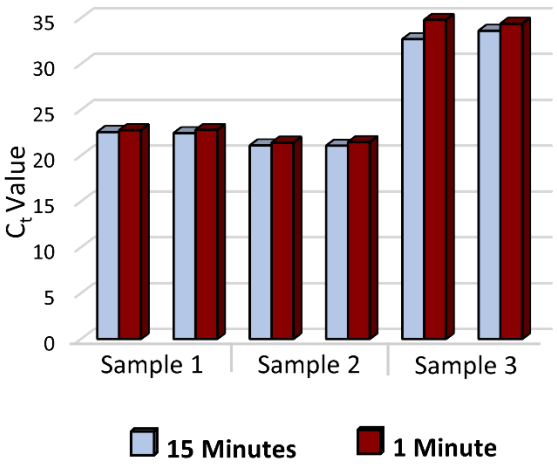

Figure 3-8. Effect of decreased reverse transcription time on detection. Viral RNA was obtained from three clinical positives using the enriched PDQeX rnaGEM extraction and amplified in duplicate following reverse transcription for either 1 or 15 minutes. Direct comparison of the resultant Ct values showed only a minor increase (~1-2 units) with the shortened reverse transcription step. Adapted from [9].

Though the positive control DNA plasmid could be used for amplification optimization (**Figure 3-7**), it was unsuitable for reverse transcription (RT) characterization, which requires an RNA template. Therefore, parallel extracts of patient samples were leveraged to explore the effect of truncating the RT hold step from 15 minutes (manufacturer's recommendation) to 1 minute. Comparable C_t values obtained across both conditions indicated that shortening the RT step to only 1 minute had minimal effect on RNA detection (**Figure 3-8**).

In conjunction, all of the above-described alterations to the real-time RT-PCR protocol equated to a decrease of approximately 37 minutes, or 63% reduction in time, for SARS-CoV-2 detection. Pairing this modified temperature profile for amplification with

the ultra-fast extraction method described here demonstrates great potential for expanding laboratory throughput and testing capabilities, as well as expediting diagnoses and enhancing surveillance effectiveness.

3.3.7. Double-Blind Study

To objectively demonstrate the reliable applicability of enriched rnaGEM extraction and amplification methods, a double-blind study was performed using neat VTM from ten de-identified patient samples. Removal of information regarding clinical diagnosis eliminated the possibility of confirmational bias. Ten samples were randomly selected from a pool of clinical negatives and positives with C_t values below 32. This cut-off value was selected with the objective of surveillance and transmission control in mind since the likelihood of infectivity above this threshold is low.[44] Following enriched rnaGEM extractions using the PDQeX system, five of the ten deidentified samples (B, C, F, H, and I) exhibited amplification via real-time RT-PCR and five did not (A, D, E, G, and J) (**Figure 3-9**). These results exhibited complete concordance with clinical diagnoses,

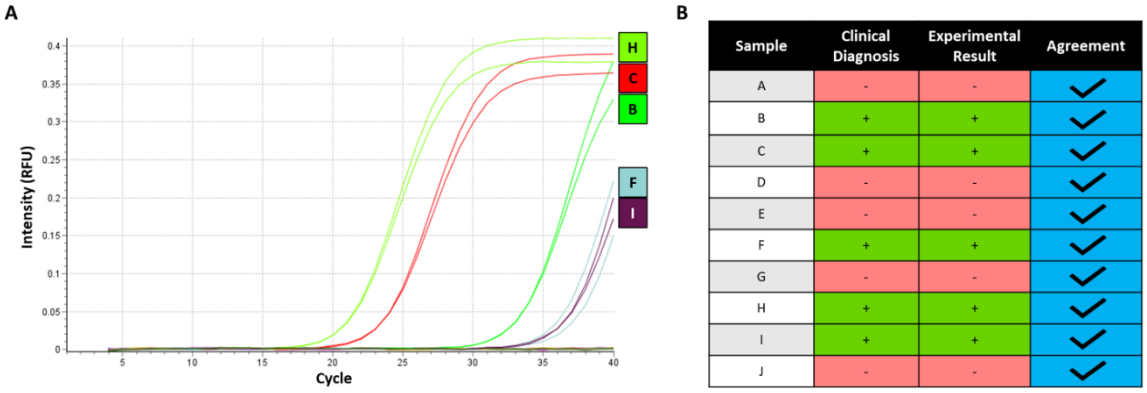

Figure 3-9. Qualitative double-blind study. (A) RT-PCR amplification plot depicting enriched rnaGEM extracts from de-identified clinical samples. SARS-CoV-2 RNA was detected in five of the ten samples analyzed (B, C, F, H, and I). The positive control (data not shown) had Ct values of 29.56 and 29.66, and the NTCs did not exhibit amplification. (B) A graphical representation of concordance between experimental results and clinical designations. These results demonstrate 100% agreement of experimental results with clinical diagnoses of all ten patient samples, amplified in duplicate. Adapted from [9].

demonstrating that enriched rnaGEM extraction reliably isolates SARS-CoV-2 RNA from patient samples to provide accurate downstream real-time RT-PCR results.

3.3.8. Alternative Amplification Methods

PCR-based NAATs remain the gold standard for clinical diagnosis, though promising alternative techniques are emerging for use both in the laboratory and at the point-of-need (PoN). Such diversification of methods for SARS-CoV-2 detection will continue to elicit rapid, simple, and portable systems for on-site testing. Here, compatibility of enriched rnaGEM extracts with two isothermal amplification assays was evaluated.

3.3.8.1. Recombinase Polymerase Amplification

In RPA, thermal denaturation of template genetic material is unnecessary; instead, double-stranded DNA (dsDNA) is interrogated by recombinase-primer complexes for

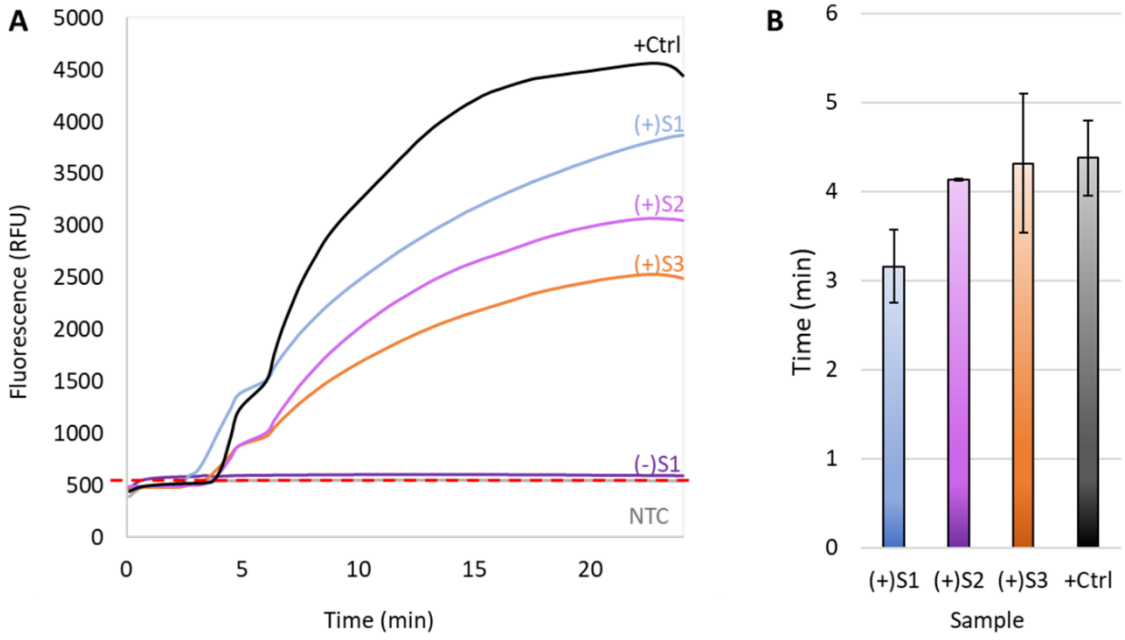

Figure 3-10. RT-RPA of enriched rnaGEM SARS-CoV-2 RNA extracts. (A) Amplification plot depicting mean fluorescence of three clinical positives and one clinical negative, along with no template and positive (2019-nCoV_N_Positive Control plasmid, 1000 copies/µL) controls (n = 3). An amplification threshold (618.6187 RFU, dotted red line) was established 3 standard deviations above the mean NTC fluorescence. SARS-CoV-2 RNA was detected in all three clinical positives, but not in the clinical negative or NTCs. (B) Mean time to amplification for each sample. Error bars represent one standard deviation in each direction. Clinical positives amplified in the same or less time than the positive control plasmid. Adapted from [9].

complementary regions. Upon sequence recognition, these regions are unwound to facilitate primer annealing and extension via a strand-displacing polymerase.[29] Though RPA necessarily amplifies dsDNA, one-pot reverse transcription RPA (RT-RPA) can be achieved simply through inclusion of the appropriate enzyme. Despite operational differences, both real-time RT-PCR and RT-RPA leverage fluorescence detection to produce sigmoidal curves indicative of exponential amplification. Amplification was observed in all three clinical positives, as well as the positive control (CDC plasmid), but not the clinical negative or negative control (**Figure 3-10A**). Usage of probe-based detection, as opposed to an intercalator, and the lack of observed amplification in negatives led to the conclusion that observed amplification was specific to the SARS-CoV-2 target. However, unlike real-time RT-PCR, RPA does not involve cycles, so samples are not assigned C_t values. Results are instead reported as a time until a given sample's fluorescence crosses an empirical threshold. Here, all three clinical positives had similar times to amplification as the cDNA plasmid positive control. Since RPA amplifies only dsDNA, it was clear that reverse transcription occurred very quickly in the RT-RPA reactions; the allotted one-minute incubation upstream of amplification was sufficient (**Figure 3-10B**). In fact, the fluorescence measured from all positive solutions crossed the amplification threshold in less than five minutes, which represented a significant decrease relative to even the expedited RT-PCR protocol's duration of more than 30 minutes.

3.3.8.2. Loop-Mediated Isothermal Amplification

As discussed in **Chapters 1 and 2**, LAMP is especially promising for point-of-need (PoN) use; unlike PCR and RPA, LAMP is compatible with colorimetric detection – a more cost-effective and portable technique compared to fluorescence detection. HNB

was selected from among the numerous colorimetric LAMP indicators available due to readily apparent visual differences between positive and negative results. HNB changed from a purple to blue color with nucleic acid amplification, providing a binary metric for the presence of SARS-CoV-2. Visually, all four enriched rnaGEM extracts prepared from clinical positives, in addition to dilutions of the plasmid positive control, appeared blue which indicated successful amplification (**Figure 3-11A**). Conversely, the negative extract and the no template control (NTC) became increasingly purple, indicating assay specificity for the SARS-CoV-2 target. Though amplification status was readily apparent via the 'naked eye', subjectivity and variability in human color interpretation, as well as changing ambient conditions, can cause erroneous result reporting.[53] To ameliorate this, empirical colorimetric analysis based on cellphone image capture and ImageJ freeware was incorporated.[36, 54] Specifically, hue were measured, where each discrete value represents a unique color within the visible portion of the electromagnetic spectrum.[37] This value was measured over time to quantify the bitonal change and provide semi real-time reaction monitoring.[37, 55] A threshold was established three standard deviations below the mean hue of all samples at 0 minutes; samples with measured hue values above and below this

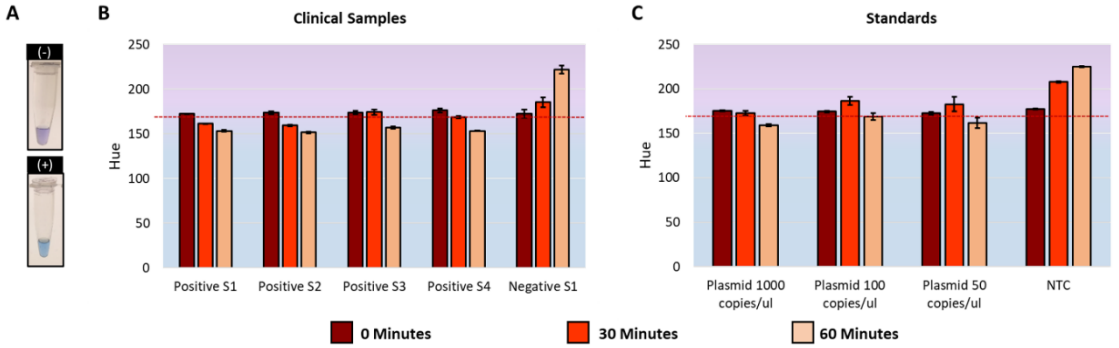

Figure 3-11. Colorimetric LAMP of enriched rnaGEM extracted RNA. (A) Images of positive and negative LAMP reactions, which were visually blue and purple, respectively. (B) Four clinical positive extracts and one clinical negative were amplified in triplicate with images captured at 0, 30, and 60 minutes. Samples with hue values above the threshold were negative (purple), whereas values below the threshold (blue) were positive. By 60 minutes, all four clinical positives exhibited colorimetrically positive hue values, but the clinical negative remained purple (no amplification). (C) Serial dilutions of the 2019-nCoV_N_Positive Control plasmid were also determined to be positive by 60 minutes, while NTCs remained negative. Adapted from [9].

demarcation were considered negative and positive, respectively. Empirical analysis confirmed the visual observations discussed above: by 60 minutes, the hue of all four clinical positives fell below the threshold, indicating amplification had occurred (**Figure 3-11B**). Similar patterns were observed after analysis of the positive control plasmid at 1000, 100, and 50 copies/µL (**Figure 3-11C**). Conversely, the average hue values for all NTCs and clinical negatives increased during incubation, moving further into the purple (negative) range. These findings demonstrate that sufficient RNA is liberated via enriched rnaGEM extraction to enable colorimetric RT-LAMP detection.

3.3.9. Enriched rnaGEM Extraction LoaD

As described above, effective virion enrichment and enzymatic extraction of amplification-ready SARS-CoV-2 RNA required optimized nanoparticle-sample interaction, effective virion lysis, and sequential spatiotemporally distinct fluidic manipulation steps. To this point, one such rapid, reliable method was demonstrated using

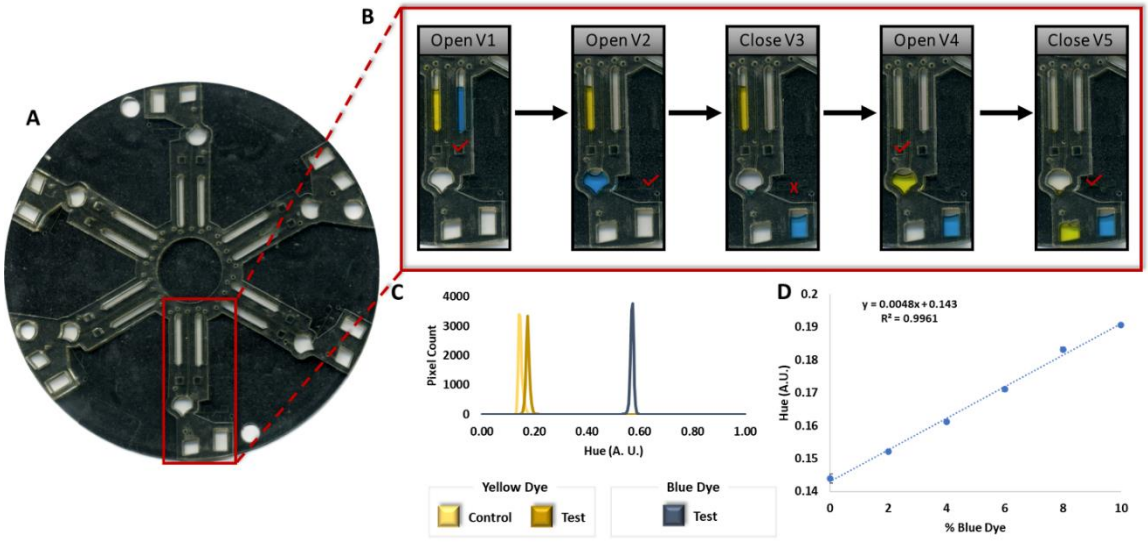

Figure 3-12. LoaD for multiplexed enriched rnaGEM extraction. (A) Image of a 6-plex centrifugal microdevice. (B) Depiction of enriched rnaGEM extraction using aqueous solutions of blue and yellow dye, which represent the sample and extraction cocktail, respectively. (C) Line graph depicting the hue values of dyes following on-disc assay completion, and a control yellow dye solution. The increased hue measured from the test yellow dye relative to the control represents the carryover of the blue dye. (D) Calibration curve between hue and the percentage of blue dye mixed into yellow solution. The resultant linear relationship was used to calculate the prevalence of sample carryover into the final on-disc eluate. Adapted from [56].

hydrogel nanoparticles and rnaGEM chemistry in conjunction with commercial PDQeX technology.[9] Though the PDQeX enriched rnaGEM extraction method described here represents significant progress over existing 'gold standard' extraction kits in terms of labor, it ultimately remained an open-tube assay that required manual intervention, albeit to a greatly diminished extent. In an effort to fully ameliorate these shortcomings, a centrifugally-driven "print-cut-laminate" LoaD[38] was developed with an architecture adapted from the one described in Chapter 2 to enable on-board integration of the complete enriched rnaGEM sample preparation workflow (**Figure 3-12**).[42, 56]

Successful microscale adaptation of on-disc enriched rnaGEM SARS-CoV-2 RNA extraction required successive 1) virion capture, 2) removal of the supernatant sample matrix, 3) extraction cocktail introduction, 4) one-step lysis and RNA isolation, and 5) collection of the purified genetic material. Because these essential unit operations closely mirror those required for the dSPE LoaD, described in **Chapter 2**, analogous fluidic and magnetic control mechanisms were implemented.[42] Fluids (e.g., sample and extraction cocktail) were introduced to the extraction chamber via rotationally-controlled flow following laser valve actuation.[39] During both initial virion capture and extraction, back-and-forth sweeping of hydrogel nanoparticles was driven via application of a bidirectional rotating magnetic field (bRMF) to ensure comprehensive sample-solid phase interaction. After each of these steps, the nanoparticles were centrifugally pelleted into the vertex of the central extraction chamber designed to prevent their loss during fluidic transfer steps.[42] To facilitate supernatant removal, a downstream valve to a waste chamber was actuated via laser radiation prior to centrifugal pumping of liquid therein. Additional undesired flow into the waste chamber was prevented via laser-based closure of the upstream channel.[40]

The integrity of this channel closure was essential for subsequent collection of the purified NA rnaGEM isolate.

These laser-based channel closures have been demonstrated to be compatible with NA processing (**Chapter 2**) as well as exceedingly reliable, with successful closure rates above 99% at relevant rotational frequencies.[40, 42] However, all previous implementations of this microvalving strategy have been applied to relatively small volumes (≤10 µL) housed in chambers within the 5 core material layers that comprise a "print-cut-laminate" microdevice. Here, successful laser-based microchannel closures were demonstrated with much larger fluid volumes (50-60 µL) contained in PMMA chambers applied to the microdevice to augment capacity. Initial characterization of assay performance, including valving, was performed using aqueous dye solutions, with blue and yellow representing the sample and rnaGEM cocktail, respectively (**Figure 3-12B**). To mimic virion capture, the blue dye was added to, then removed from, the extraction chamber via actuation of a series of laser valves. The success of the channel closure upstream of the waste chamber was evident by the successful retention of yellow dye (rnaGEM cocktail) in the extraction chamber after opening the appropriate laser valve prior to device rotation. Ultimately, the yellow dye was collected in a separate elution chamber on-disc, demonstrating the feasibility of enriched rnaGEM extraction in this LoaD system.

However, since the extraction chamber was designed to retain nanoparticles in its vertex,42 there was inevitably some carryover of blue dye (lysate) into the eluate. In practice, this equates to carryover of sample matrix (e.g., VTM) into the RNA eluate, which may result in inhibition of downstream real-time RT-PCR.[43] Again, hue was used for empirical characterization, this time to evaluate the magnitude of carryover and determine

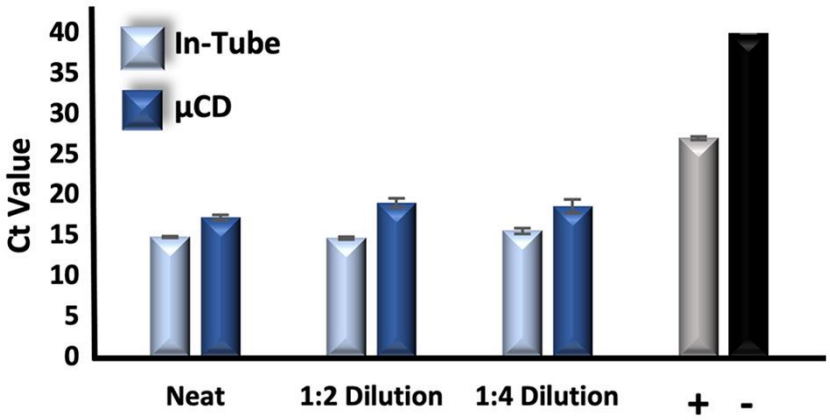

Figure 3-13. Assessment of on-disc enriched rnaGEM extraction performance. Comparison of RT-PCR Ct values obtained following in-tube and on-disc RNA preparation. Using both methods, SARS-CoV-2 was successfully detected in neat samples and dilutions (1:2, 1:4), though on-disc Ct values were marginally (~ 3 units) higher. Adapted from [56].

if it was likely to interfere with downstream post-processing. Images of dye solutions following the on-disc assay were captured and compared with control chambers containing pure dye solutions. Unsurprisingly, the hue of the yellow dye in the eluate chamber following completion of the on-disc enriched rnaGEM workflow (0.175±0.003) was significantly higher than pure yellow dye (0.147±0.004), according to an unpaired t-test for means ($\alpha = 0.05$, two-tailed p-value <0.0001) (**Figure 3-12C**). This upward shift in hue was attributed to contamination with blue dye (hue = 0.571±0.002). To characterize the extent of blue dye (matrix) carryover, hue measurements taken from the on-disc eluate were compared with serially diluted dye standards (blue in yellow) (**Figure 3-12D**). The resultant strong linear correlation between increases in hue and the prevalence of blue dye ($R^2 = 0.996$) was used to calculate that the final eluate contains 6.58±0.72% blue dye (matrix) in the absence of nanoparticles. However, in practice, nanoparticles would occupy the chamber vertex during sample transfer to waste, sterically excluding fluid. Therefore, on-disc eluates would contain a diminished matrix prevalence, unlikely to inhibit PCR.

Ultimately, the success of this enriched rnaGEM LoaD for isolation of amplification-ready SARS-CoV-2 RNA was demonstrated by Turiello et al. via comparison of RT-PCR performance following parallel in-tube and on-disc preparations (**Figure 3-13**).[56] Although a minimal increase in on-disc C_t values was observed, and attributed directly to matrix carryover, this minor detriment to post-processing performance has minimal practical import. This holds true especially considering complete assay integration within a self-contained, automatable LoaD that could reasonably be used at the PoN without manual intervention.

3.4. Conclusions

Here, novel methods for simple, rapid (<10 minutes) SARS-CoV-2 preconcentration and enzymatic RNA extraction from clinically relevant matrices were described. These approaches leveraged rnaGEM extraction chemistry, centered on the heat-activated lytic activity of the thermophilic proteinase EA1.[13-14] Amplification-ready nucleic acids were obtained in a single step via simple temperature modulation, which was easily automated with complete freedom from manual intervention, unlike the numerous wash steps required by conventional SPE strategies. For comparison, a commonly used commercial NAE method requires approximately 6X more time for completion (1 hour).[57] RnaGEM extraction chemistry was augmented with upstream affinity-based virion preconcentration, or enrichment, using magnetically-actuated Nanotrap® hydrogel nanoparticles to improve sensitivity of downstream-post processing. Enrichment permitted removal of the sample matrix, and any inhibitors therein, prior to RNA extraction and amplification. The already simple enriched rnaGEM extraction method was then further streamlined through adaptation to the commercially-available PDQeX system to permit

single-step, automatable hands-free virion lysis, nanoparticle removal, and production of amplification-ready SARS-CoV-2 RNA from both nasopharyngeal swab VTM and saliva.

Real-time RT-PCR amplification indicated that enriched rnaGEM extraction provided similar performance to 'gold standard' commercial SPE kits, but with significantly reduced time, labor, and specialized equipment. Amplification of extracts from VTM-based samples, including both neat patient diagnostic remnants and dilutions reminiscent of surveillance samples, exhibited concordant C_t values using both methods and, thus, comparable RNA yields. In a double-blind RT-PCR study, detection of SARS-CoV-2 following enriched rnaGEM extractions exhibited 100% concordance with clinical results, highlighting the reliability of this RNA preparation for diagnostic use. Potential applicability to pooled sampling, essential for transmission control and consumables conservation,[25] was also demonstrated via successful viral detection in extract dilutions up to 20X. SARS-CoV-2 RNA extraction from saliva samples was illustrated as well, which has important implications for PoN diagnostics; saliva collection is preferable over nasopharyngeal sampling due to its simple, non-invasive nature amenable for use by non-medical personnel. Despite the propensity for low analytical efficiency in saliva extractions due to complexity and viscosity,[50] detectable levels of viral RNA were extracted from even low-titer samples comprised of up to 90% saliva.

The compatibility of enriched rnaGEM PDQeX extractions with two isothermal amplification techniques was also established. These modalities are increasingly used within emerging portable diagnostic tools, including LoaDs, due to significantly reduced requirements for peripheral hardware and expedited analysis relative to PCR-based assays.[58-60] For example, using RPA, all enriched rnaGEM extracts from clinically positive

VTM amplified in ~5 minutes, achieving NA preparation in significantly less time than even the fastest RT-PCR achieved here (~37 minutes). Using this method, the total analytical turnaround time, including sample preparation, was only 15 minutes – orders of magnitude below the 24–48-hour interval for conventional laboratory testing. However, RPA still relied on fluorescence detection. Conversely, LAMP permitted colorimetric readout, and therefore simplified optical interpretation – either by eye or with empirical smartphone-based image capture. Such visual detection is exceedingly well-suited for PoN use by nontechnical personnel due to facile interpretation and implementation. The combination of either of these isothermal NAATs with upstream enriched rnaGEM extraction could provide a powerful, orthogonal approach to SARS-CoV-2 diagnosis outside of traditional laboratory settings. In fact, the initial publication of this method stated that the reported assay and workflow could be easily modified for microscale integration; subsequent work on this project was centered on exactly that.[9, 56]

Specifically, the enriched rnaGEM chemistry and workflow was adapted to a multiplexed LoaD56 that leveraged architectural features, microvalving patterns, and the magnetic manipulation strategy adapted from the microfluidic system described in **Chapter 2** for dynamic solid phase NAE.[42] Again, beyond manual addition of clinical sample and reagents, all fluidic steps were automated to minimize user intervention and ease implementation. Further, the self-contained microdevice format limited the risk for analyst exposure to any pathogens present relative to the open-tube formats discussed above. On-board hydrogel nanoparticles were controlled on-disc via multiple previously described modalities.[42] Specifically, application of a bRMF drove back-and-forth nanoparticle sweeping to facilitate virion capture and eventual lysis. Additionally,

centrifugal pelleting enabled nanoparticle retention within the extraction chamber during fluidic transfer steps (e.g., sample matrix removal). Device architecture and associated on-disc workflow were initially optimized via dye studies. It was especially crucial to ensure integrity of the laser-based valve closure that facilitated fractionation of waste and subsequent eluate.[40] Though this microvalving method has already been demonstrated as both robust and compatible with NAATs (**Chapter 2**),[40, 42] this device was the first demonstration of its amenability to large volumes (≥ 50 μL) housed in PMMA accessory pieces used to augment chamber depth and capacity in PCL microdevices.[56] Due largely to this valving success, only a small amount of residual matrix remains (≤6.58±0.72%) in the eluate, determined via empirical hue analysis. Despite this small volume carryover, downstream real-time RT-PCR amplification of on-disc extracts from clinically-relevant matrices (VTM and saliva) resulted in comparable C_t values to extracts prepared via a 'gold-standard' commercial SPE kit.

In this work, detection was accomplished off-disc. However, numerous methods for on-disc NA amplification and detection have been recently described.[60-61] Coupling on-disc enriched rnaGEM extractions with such techniques would permit fully automated sample-to-answer LoaD analysis for in situ viral detection, entirely untethered from a centralized laboratory. The same is true for the dSPE LoaD described in **Chapter 2** as, in both cases, purified NA eluates are located at the disc periphery upon extraction completion. As discussed in the introductory **Chapter 1**, rotationally-controlled fluid processing can no longer be implemented at this point, given that centrifugal force acts radially outward relative to the center of rotation.[62] Though this operation principal represents a key roadblock for sample-to-answer NA LoaDs,[58] it can be overcome via

implementation of novel unit operations, especially those that induce radially-inward on-disc flow.[58, 63] The following **Chapter 4** describes the development and characterization of a simple, automatable method for inward fluid displacement intended for application to these NA preparation LoaDs to enable downstream, on-disc amplification and permit comprehensive integration of molecular diagnostics in a single microfluidic device, or micro-total analysis system (μTAS).[64-65]

3.5. References

1. Chen, N.; Zhou, M.; Dong, X.; Qu, J.; Gong, F.; Han, Y.; Qiu, Y.; Wang, J.; Liu, Y.; Wei, Y., Epidemiological and clinical characteristics of 99 cases of 2019 novel coronavirus pneumonia in Wuhan, China: a descriptive study. *The Lancet* **2020,** *395* (10223), 507-513.

2. Esbin, M. N.; Whitney, O. N.; Chong, S.; Maurer, A.; Darzacq, X.; Tjian, R., Overcoming the bottleneck to widespread testing: a rapid review of nucleic acid testing approaches for COVID-19 detection. *Rna* **2020,** *26* (7), 771-783.

3. Barclay, R.; Akhrymuk, I.; Patnaik, A.; Callahan, V.; Lehman, C.; Andersen, P.; Barbero, R.; Barksdale, S.; Dunlap, R.; Goldfarb, D., Hydrogel particles improve detection of SARS-CoV-2 RNA from multiple sample types. *Scientific Reports* **2020,** *10* (1), 1-11.

4. Corman, V. M.; Landt, O.; Kaiser, M.; Molenkamp, R.; Meijer, A.; Chu, D. K.; Bleicker, T.; Brünink, S.; Schneider, J.; Schmidt, M. L., Detection of 2019 novel coronavirus (2019-nCoV) by real-time RT-PCR. *Eurosurveillance* **2020,** *25* (3), 2000045.

5. Ali, N.; Rampazzo, R. C. P.; Costa, A. D. T.; Krieger, M. A., Current nucleic acid extraction methods and their implications to point-of-care diagnostics. *BioMed Research International* **2017,** 2017.

6. Department of Health and Human Services Report to Congress: COVID-19 Strategic Testing Plan. 2020. (Accessed 25 January 2021).

7. Lohse, S.; Pfuhl, T.; Berkó-Göttel, B.; Rissland, J.; Geißler, T.; Gärtner, B.; Becker, S. L.; Schneitler, S.; Smola, S., Pooling of samples for testing for SARS-CoV-2 in asymptomatic people. *The Lancet Infectious Diseases* **2020,** *20* (11), 1231-1232.

8. Barclay, R. A.; Akhrymuk, I.; Patnaik, A.; Callahan, V.; Lehman, C.; Andersen, P.; Barbero, R.; Barksdale, S.; Dunlap, R.; Goldfarb, D., Nanotrap® particles improve detection of SARS-CoV-2 for pooled sample methods, extraction-free saliva methods, and extraction-free medium methods. *BioRxiv* **2020**.

9. Dignan, L. M.; Turiello, R.; Layne, T. R.; O'Connell, K. C.; Hickey, J.; Chapman, J.; Poulter, M. D.; Landers, J. P., An ultrafast SARS-CoV-2 virus enrichment and extraction method compatible with multiple modalities for RNA detection. *Analytica Chimica Acta* **2021,** *1180*, 338846.

10. Luchini, A.; Geho, D. H.; Bishop, B.; Tran, D.; Xia, C.; Dufour, R. L.; Jones, C. D.; Espina, V.; Patanarut, A.; Zhou, W., Smart hydrogel particles: biomarker harvesting: one-step affinity purification, size exclusion, and protection against degradation. *Nano Letters* **2008,** *8* (1), 350-361.

11. Maddu, N., Functions of saliva. In Saliva and Salivary Diagnostics, IntechOpen: 2019.

12. Schrader, C.; Schielke, A.; Ellerbroek, L.; Johne, R., PCR inhibitors–occurrence, properties and removal. *Journal of Applied Microbiology* **2012,** *113* (5), 1014-1026.

13. Lounsbury, J. A.; Coult, N.; Miranian, D. C.; Cronk, S. M.; Haverstick, D. M.; Kinnon, P.; Saul, D. J.; Landers, J. P., An enzyme-based DNA preparation method for application to forensic biological samples and degraded stains. *Forensic Science International: Genetics* **2012,** *6* (5), 607-615.

14. Moss, D.; Harbison, S. A.; Saul, D., An easily automated, closed-tube forensic DNA extraction procedure using a thermostable proteinase. *International Journal of Legal Medicine* **2003,** *117* (6), 340-349.

15. Jung, W.; Han, J.; Choi, J. W.; Ahn, C. H., Point-of-care testing (POCT) diagnostic systems using microfluidic lab-on-a-chip technologies. *Microelectronic Engineering* **2015,** 132, 46-57.

16. Yang, J.; Hurth, C.; Nordquist, A.; Smith, S.; Zenhausern, F., Integrated Microfluidic System for Rapid DNA Fingerprint Analysis: A Miniaturized Integrated DNA Analysis System (MiDAS)—Swab Sample-In to DNA Profile-Out. In Microfluidic Electrophoresis, Springer: 2019; pp 207-224.

17. Wu, J.; Kodzius, R.; Cao, W.; Wen, W., Extraction, amplification and detection of DNA in microfluidic chip-based assays. *Microchimica Acta* **2014,** *181* (13-14), 1611-1631.

18. Mark, D.; Haeberle, S.; Roth, G.; Von Stetten, F.; Zengerle, R., Microfluidic lab-on-a-chip platforms: requirements, characteristics and applications. In Microfluidics based microsystems, Springer: 2010; pp 305-376.

19. Gorkin, R.; Park, J.; Siegrist, J.; Amasia, M.; Lee, B. S.; Park, J. M.; Kim, J.; Kim, H.; Madou, M.; Cho, Y. K., Centrifugal microfluidics for biomedical applications. *Lab on a Chip* 2010, 10 (14), 1758-1773.

20. Uhteg, K.; Jarrett, J.; Richards, M.; Howard, C.; Morehead, E.; Geahr, M.; Gluck, L.; Hanlon, A.; Ellis, B.; Kaur, H., Comparing the analytical performance of three SARS-CoV-2 molecular diagnostic assays. *Journal of Clinical Virology* **2020,** *127*, 104384.

21. Fraga, D.; Meulia, T.; Fenster, S., Real-time PCR. *Current Protocols Essential Laboratory Techniques* 2014, 8 (1), 10.3. 1-10.3. 40.

22. Notomi, T.; Okayama, H.; Masubuchi, H.; Yonekawa, T.; Watanabe, K.; Amino, N.; Hase, T., Loop-mediated isothermal amplification of DNA. *Nucleic Acids Research* **2000,** *28* (12), e63.

23. Goto, M.; Honda, E.; Ogura, A.; Nomoto, A.; Hanaki, K. I., Colorimetric detection of loop-mediated isothermal amplification reaction by using hydroxy naphthol blue. *Biotechniques* **2009,** *46* (3), 167-172.

24. Zhang, Y.; Odiwuor, N.; Xiong, J.; Sun, L.; Nyaruaba, R. O.; Wei, H.; Tanner, N. A., Rapid molecular detection of SARS-CoV-2 (COVID-19) virus RNA using colorimetric LAMP. *MedRxiv* **2020**.

25. Huang, W. E.; Lim, B.; Hsu, C. C.; Xiong, D.; Wu, W.; Yu, Y.; Jia, H.; Wang, Y.; Zeng, Y.; Ji, M., RT-LAMP for rapid diagnosis of coronavirus SARS-CoV-2. *Microbial Biotechnology* **2020,** *13* (4), 950-961.

26. Park, G. S.; Ku, K.; Baek, S.-H.; Kim, S.-J.; Kim, S. I.; Kim, B.-T.; Maeng, J.-S., Development of reverse transcription loop-mediated isothermal amplification assays targeting severe acute respiratory syndrome coronavirus 2 (SARS-CoV-2). *The Journal of Molecular Diagnostics* **2020,** *22* (6), 729-735.

27. Thi, V. L. D.; Herbst, K.; Boerner, K.; Meurer, M.; Kremer, L. P.; Kirrmaier, D.; Freistaedter, A.; Papagiannidis, D.; Galmozzi, C.; Stanifer, M. L., A colorimetric RT-LAMP assay and LAMP-sequencing for detecting SARS-CoV-2 RNA in clinical samples. *Science Translational Medicine* **2020,** *12* (556).

28. Kellner, M. J.; Ross, J. J.; Schnabl, J.; Dekens, M. P.; Heinen, R.; Grishkovskaya, I.; Bauer, B.; Stadlmann, J.; Menéndez-Arias, L.; Fritsche-Polanz, R., A rapid, highly sensitive and open-access SARS-CoV-2 detection assay for laboratory and home testing. *Frontiers in Molecular Biosciences* **2022,** *9*, 801309.

29. Piepenburg, O.; Williams, C. H.; Stemple, D. L.; Armes, N. A., DNA detection using recombination proteins. *PLoS Biology* **2006,** *4* (7), e204.

30. Lobato, I. M.; O'Sullivan, C. K., Recombinase polymerase amplification: Basics, applications and recent advances. *Trac Trends in Analytical Chemistry* **2018,** *98*, 19-35.

31. Ahmad, F.; Hashsham, S. A., Miniaturized nucleic acid amplification systems for rapid and point-of-care diagnostics: a review. *Analytica Chimica Acta* **2012,** *733*, 1-15.

32. El Wahed, A. A.; Patel, P.; Maier, M.; Pietsch, C.; Rüster, D.; Böhlken-Fascher, S.; Kissenkötter, J.; Behrmann, O.; Frimpong, M.; Diagne, M. M., Suitcase Lab for rapid detection of SARS-CoV-2 based on recombinase polymerase amplification assay. *Analytical Chemistry* **2021,** *93* (4), 2627-2634.

33. Tang, Y. W.; Schmitz, J. E.; Persing, D. H.; Stratton, C. W., Laboratory diagnosis of COVID-19: current issues and challenges. *Journal of Clinical Microbiology* **2020,** *58* (6), e00512-20.

34. Larremore, D. B.; Fosdick, B. K.; Bubar, K. M.; Zhang, S.; Kissler, S. M.; Metcalf, C. J. E.; Buckee, C. O.; Grad, Y. H., Estimating SARS-CoV-2 seroprevalence and epidemiological parameters with uncertainty from serological surveys. *eLife* **2021,** *10*, e64206.

35. Hadaya, J.; Schumm, M.; Livingston, E. H., Testing individuals for coronavirus disease 2019 (COVID-19). Journal of the *American Medical Association* **2020,** *323* (19), 1981.

36. Jackson, K. R.; Layne, T.; Dent, D. A.; Tsuei, A.; Li, J.; Haverstick, D. M.; Landers, J. P., A novel loop-mediated isothermal amplification method for identification of four body fluids with smartphone detection. *Forensic Science International: Genetics* **2020,** *45*, 102195.

37. Woolf, M. S.; Dignan, L. M.; Scott, A. T.; Landers, J. P., Digital postprocessing and image segmentation for objective analysis of colorimetric reactions. *Nature Protocols* **2020,** *16* (1), 218-238.

38. Thompson, B. L.; Ouyang, Y.; Duarte, G. R.; Carrilho, E.; Krauss, S. T.; Landers, J. P., Inexpensive, rapid prototyping of microfluidic devices using overhead transparencies and a laser print, cut and laminate fabrication method. *Nature Protocols* **2015,** *10* (6), 875-886.

39. Garcia-Cordero, J. L.; Kurzbuch, D.; Benito-Lopez, F.; Diamond, D.; Lee, L. P.; Ricco, A. J., Optically addressable single-use microfluidic valves by laser printer lithography. *Lab on a Chip* **2010,** *10* (20), 2680-2687.

40. Woolf, M. S.; Dignan, L. M.; Lewis, H. M.; Nauman, A. Q.; Tomley, C. J.; Landers, J., Optically-Controlled Closable Microvalves for Polymeric Centrifugal Microfluidic Devices. *Lab on a Chip* **2020,** *20* (8), 1426-1440.

41. Jackson, K.; Borba, J.; Meija, M.; Mills, D.; Haverstick, D.; Olson, K.; Aranda, R.; Garner, G.; Carrilho, E.; Landers, J., DNA purification using dynamic solid-phase extraction on a rotationally-driven polyethylene-terephthalate microdevice. *Analytica Chimica Acta* **2016,** *937*, 1-10.

42. Dignan, L. M.; Woolf, M. S.; Tomley, C. J.; Nauman, A. Q.; Landers, J. P., Multiplexed Centrifugal Microfluidic System for Dynamic Solid-Phase Purification of Polynucleic Acids Direct from Buccal Swabs. *Analytical Chemistry* **2021,** *93* (19), 7300-7309.

43. Kirkland, P.; Frost, M., The impact of viral transport media on PCR assay results for the detection of nucleic acid from SARS-CoV-2. *Pathology* **2020,** *52* (7), 811-814.

44. Bullard, J.; Dust, K.; Funk, D.; Strong, J. E.; Alexander, D.; Garnett, L.; Boodman, C.; Bello, A.; Hedley, A.; Schiffman, Z., Predicting infectious severe acute respiratory syndrome coronavirus 2 from diagnostic samples. *Clinical Infectious Diseases* **2020,** *71* (10), 2663-2666.

45. RNA Isolation for qRT-PCR. https://www.thermofisher.com/us/en/home/references/ambion-tech-support/rtpcr-analysis/general-articles/rna-isolation-for-qrt-pcr.html (Accessed 15 October 2020).

46. Laurell, H.; Iacovoni, J. S.; Abot, A.; Svec, D.; Maoret, J.-J.; Arnal, J.-F.; Kubista, M., Correction of RT–qPCR data for genomic DNA-derived signals with ValidPrime. *Nucleic Acids Research* **2012,** *40* (7), e51.

47. Gadkar, V. J.; Filion, M., Development of a versatile TaqMan™ real-time quantitative PCR (RT-qPCR) compliant anchor sequence to quantify bacterial gene transcripts from RNA samples containing carryover genomic DNA. *BMC Biotechnology* **2013,** *13* (1), 7.

48. Norhazlin, J.; Nor-Ashikin, M.; Hoh, B.; Kadir, S. S. A.; Norita, S.; Mohd-Fazirul, M.; Wan-Hafizah, W.; Razif, D.; Rajikin, M.; Abdullah, B., Effect of DNase treatment on RNA extraction from preimplantation murine embryos. *Genetics and Molecular Research* **2015,** *14* (3), 10172-10184.

49. Wyllie, A. L.; Fournier, J.; Casanovas-Massana, A.; Campbell, M.; Tokuyama, M.; Vijayakumar, P.; Geng, B.; Muenker, M. C.; Moore, A. J.; Vogels, C. B., Saliva is more sensitive for SARS-CoV-2 detection in COVID-19 patients than nasopharyngeal swabs. *MedRxiv* **2020**.

50. Wei, F.; Wong, D., Point-of-care platforms for salivary diagnostics. *The Chinese journal of Dental Research: The Official Journal of the Scientific Section of the Chinese Stomatological Association (CSA)* **2012,** *15* (1), 7-15.

51. Larremore, D. B.; Wilder, B.; Lester, E.; Shehata, S.; Burke, J. M.; Hay, J. A.; Tambe, M.; Mina, M. J.; Parker, R., Test sensitivity is secondary to frequency and turnaround time for COVID-19 surveillance. *MedRxiv* **2020**.

52. Mina, M. J.; Parker, R.; Larremore, D. B., Rethinking Covid-19 Test Sensitivity—A Strategy for Containment. *New England Journal of Medicine* **2020,** *383* (22), e120.

53. Krauss, S. T.; Remcho, T. P.; Lipes, S. M.; Aranda IV, R.; Maynard III, H. P.; Shukla, N.; Li, J.; Tontarski Jr, R. E.; Landers, J. P., Objective method for presumptive field-testing of illicit drug possession using centrifugal microdevices and smartphone analysis. *Analytical Chemistry* **2016,** *88* (17), 8689-8697.

54. Scott, A.; Jackson, K.; Carter, M.; Comeau, R.; Layne, T.; Landers, J., Rapid sperm lysis and novel screening approach for human male DNA via colorimetric loop-mediated isothermal amplification. *Forensic Science International: Genetics* **2019,** *43*, 102139.

55. Cantrell, K.; Erenas, M.; de Orbe-Payá, I.; Capitán-Vallvey, L., Use of the hue parameter of the hue, saturation, value color space as a quantitative analytical parameter for bitonal optical sensors. *Analytical Chemistry* **2010,** *82* (2), 531-542.

56. Turiello, R.; Dignan, L. M.; Thompson, B.; Poulter, M.; Hickey, J.; Chapman, J.; Landers, J. P., Centrifugal Microfluidic Method for Enrichment and Enzymatic Extraction of Severe Acute Respiratory Syndrome Coronavirus 2 RNA. *Analytical Chemistry* **2022,** *94* (7), 3287-3295.

57. Van Nguyen, H.; Seo, T. S., High-throughput human DNA purification on a centrifugal microfluidic device for rapid forensic sex-typing. *Biosensors and Bioelectronics* **2021,** *181*, 113161.

58. Strohmeier, O.; Keller, M.; Schwemmer, F.; Zehnle, S.; Mark, D.; von Stetten, F.; Zengerle, R.; Paust, N., Centrifugal microfluidic platforms: advanced unit operations and applications. *Chemical Society Reviews* **2015,** *44* (17), 6187-6229.

59. Oh, S. J.; Seo, T. S., Combination of a centrifugal microfluidic device with a solution-loading cartridge for fully automatic molecular diagnostics. *Analyst* **2019,** *144* (19), 5766-5774.

60. Sunkara, V.; Kumar, S.; Sabaté Del Río, J.; Kim, I.; Cho, Y.-K., Lab-on-a-Disc for Point-of-Care Infection Diagnostics. *Accounts of Chemical Research* **2021,** *54* (19), 3643-3655.

61. Zhang, L.; Tian, F.; Liu, C.; Feng, Q.; Ma, T.; Zhao, Z.; Li, T.; Jiang, X.; Sun, J., Hand-powered centrifugal microfluidic platform inspired by the spinning top for sample-to-answer diagnostics of nucleic acids. *Lab on a Chip* **2018,** *18* (4), 610-619.

62. Madou, M.; Zoval, J.; Jia, G.; Kido, H.; Kim, J.; Kim, N., Lab on a CD. *Annual Review of Biomedical Engineering* **2006,** *8*, 601-628.

63. Zehnle, S.; Schwemmer, F.; Roth, G.; von Stetten, F.; Zengerle, R.; Paust, N., Centrifugo-dynamic inward pumping of liquids on a centrifugal microfluidic platform. *Lab on a Chip* **2012,** *12* (24), 5142-5145.

64. Reyes, D. R.; Iossifidis, D.; Auroux, P.-A.; Manz, A., Micro total analysis systems. 1. Introduction, theory, and technology. *Analytical Chemistry* **2002,** *74* (12), 2623-2636.

65. Manz, A.; Graber, N.; Widmer, H. M., Miniaturized total chemical analysis systems: a novel concept for chemical sensing. *Sensors and Actuators B: Chemical* **1990,** *1* (1-6), 244-248.

4. Inward Fluid Displacement in LoaDs for Nucleic Acid Processing

4.1. Introduction

Demand for sample-to-answer point-of-need (PoN) nucleic acid (NA) analysis platforms has increased dramatically, as discussed in **Chapters 1-3**.[1-2] To reiterate briefly, LoaDs are ideal candidates for the miniaturization and automation of biological, clinical, forensic, and analytical processes at the PoN.[3-5] Rotationally-driven flow directly addresses many limitations associated with traditional benchtop laboratory methods by reducing sample and reagent volumes, manual intervention, cross-contamination, processing time, hardware requirements, and risk for analyst exposure to dangerous samples. However, despite these numerous advantages, a key operational limitation resulting from the comprehensive reliance on rotational forces is the necessitation of unidirectional, radially outward flow relative to the center of rotation (CoR). Since no further on-board processing is possible upon fluid arrival at the disc periphery, integration of complex assays, such as sample-to-answer NA testing, are made difficult due to device size constraints.[3, 6-7] For instance, NAs prepared using the LoaDs described in **Chapters 2 and 3** were located adjacent to the disc edge, such that on-disc amplification and detection was effectively impossible through centrifugal processing alone (**Figure 4-1**).

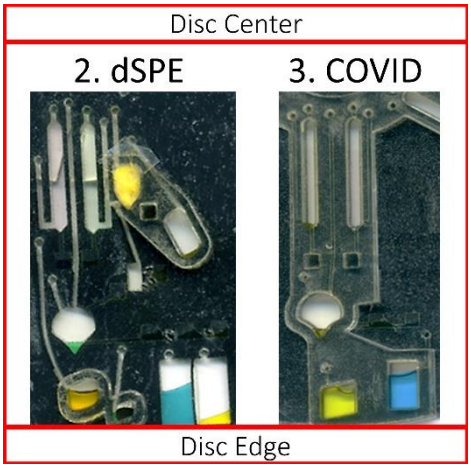

Figure 4-1. Motivation for centrifugal microfluidic IFD. Following NAE via both dSPE and enriched rnaGEM extraction, eluates were located at the disc edge such that no further on-disc processing was possible. Returning these fluids to the CoR would allow for integration of additional process chains, such as NA amplification and detection.

Radially inward fluid displacement (IFD) from the edge of the disc to the CoR would address this limitation by increasing the number of

sequential unit operations possible, thereby enabling added assay complexity and, for instance, lowering the barrier towards sample-to-answer LoaDs.[3, 8-9] Broadly, existing strategies for IFD in polymeric LoaDs leverage capillary action and hydraulic or pneumatic pressure changes to drive fluid towards the CoR. Arguably, the simplest strategies for IFD exploit the interplay between on-board capillary and centrifugal forces and requires no peripheral reagents or equipment.[10] However, spontaneous capillary refill relies on the hydrophilic character and surface energy of the polymeric disc materials, which is known to be variable.[11] Another strategy centered on relatively simple operational principles involved introducing dry compressed air into a microfluidic vent to force fluid radially inward;[12] key drawbacks of this approach include the need for bulky air tanks and supporting peripheral hardware that hinder portability, potential for contamination, and a pulsatile nature.[8]

Most remaining published IFD strategies in LoaDs rely upon internal hydraulic or pneumatic pressure changes that exceed outwardly oriented centrifugally-generated pressure. Some approaches affect IFD by increasing the thermal energy, and therefore the pressure, of trapped air volumes. However, the requirement for external hardware (e.g., halogen lamp, IR thermometer, etc.) limits portability and heating may damage sensitive reagents and assay components in neighboring chambers/channels. Alternatively, physical (not thermal) compression or expansion of trapped air volumes can also drive IFD, as seen in some examples of sample-to-answer LoaDs discussed in **Chapter 1**.[13-14] Here, careful design of unique architectural features permits on-disc storage and release of pneumatic energy.[15] For instance, centrifugally-driven compression of air trapped between a sample solution and a large volume of an immiscible displacer fluid creates pneumatic pressure

that drives IFD.[16] Displacer fluids may also directly interface with sample solutions to exert hydrostatic pressure that forces flow radially inward.[16-17] Although this approach does not necessitate increased peripheral hardware or fabrication complexity, Kong et al. substantial working fluid volume (90 µL) was required and resulted in incomplete sample displacement (55%).[16] The capabilities of this approach have been expanded upon through inclusion of event-triggered dissolvable films to enable multiple sequential displacements with excellent temporal control, though this approach required specialized materials and fabrication.[17] Unfortunately, each of the approaches discussed here were slow (≥ 90 s) required large architectural features, particularly chambers to contain large volumes of working fluids and/or air, which consume significant microfluidic 'real estate.'[8, 16, 18]

Such architectural features are not required in IFD techniques that harness positive pressure generated from on-board gas evolution to return fluid to the CoR.[17, 19-21] For instance, Noroozi et al. generated carbon dioxide (CO_2) gas within a microsystem electrolytically, but delivering the required current to the electrodes demanded complex engineering and additional peripheral equipment.[21] Alternatively, other previously described self-contained LoaDs for gas-driven IFD leveraged on-board acid-base reactions.[17, 19-20] While these techniques are effective and attractive due to instrumental simplicity, existing strategies possess operational limitations that preclude practical, widespread use, including requirements for concentrated strong acid, and custom fabrication or integration of additional device components/reagents (e.g., miniature ampoules,19 dissolvable films,[17, 20] or ancillary working liquids[17, 20]). Further, each of these methods require some degree of manual intervention for neutralization initiation and/or for chamber sealing, ultimately precluding total automation.[17, 19-20] For instance, since gas-

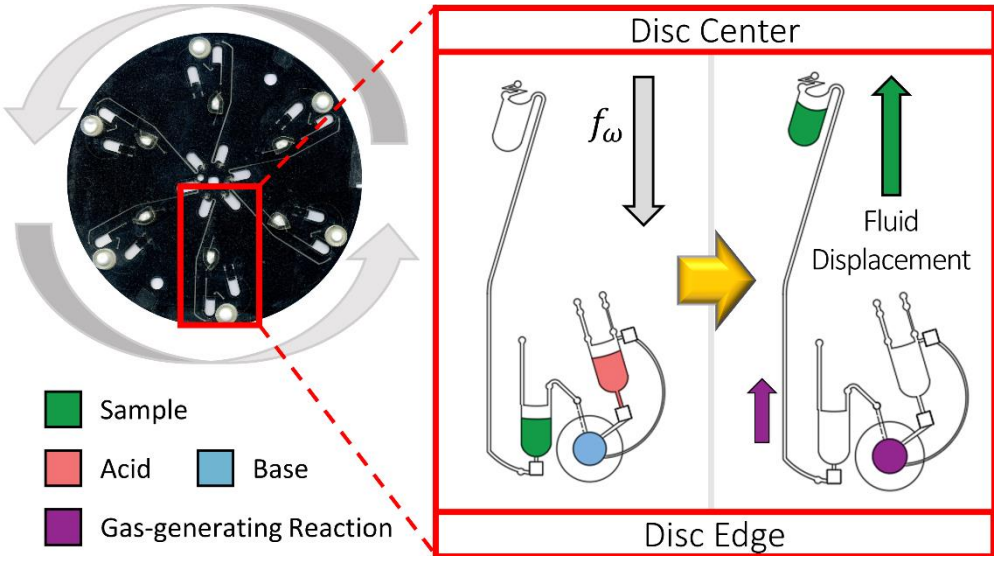

Figure 4-2. Graphical overview of gas-driven IFD. Sample displacement towards the CoR (against centrifugal force) was affected by harnessing the gas generated from on-board acid-base neutralization. Adapted from [22].

driven IFD relies on effective containment and direction of an evolving pressure head, all vents except those in the intended IFD flow path needed to be sealed; this was primarily achieved in existing publications via tape application. Additionally, manual breakage of custom-built ampoules was required prior to gas generation.[19] Regardless, none of these methods have been demonstrated for use in conjunction with NA amplification tests. It must be demonstrated that sample acidification resulting from CO_2 dissolution during IFD does not hinder downstream post-processing. Here, a simple, easy-to-implement gas-driven IFD technique is described that directly addresses the limitations of these existing methods (**Figure 4-2**).[22]

This novel, automatable method for IFD exploits recently described active valving strategies for fluid delivery, neutralization reaction activation, and leak-free vent and inlet sealing independent of manual intervention. Further, the reagents used to drive IFD were easily incorporated during device fabrication and may be stored stably on-disc for at least six months, highlighting both the robust nature of the method and its potential for field-

forward use. Crucially, compatibility with both ‘gold standard’ polymerase chain reaction (PCR)-based methods and loop-mediated isothermal amplification (LAMP) was clearly characterized. Thus, this improved approach is directly compatible with NAATs, which stands to make significant impact in expanding sample-to-answer LoaD capabilities by easing integration of both NA preparation and post-processing within a single microfluidic device. In fact, one such putative LoaD using this IFD strategy was designed to enable comprehensive performance of all process chains needed for direct-from swab NA isolation and downstream LAMP from four samples in parallel. Continued development and optimization of this and other devices will contribute to increased translation of traditional laboratory-based genetic analysis from the benchtop to the PoN.

4.2. Materials and Methods

4.2.1. Microdevice Fabrication

As described in detail within the previous two chapters, IFD LoaDs were fabricated according to the ‘print-cut-laminate’ method.[20, 23] Following alignment of the five core layers, circular laser-cut PeT-supported polytetrafluoroethylene (PTFE) membranes (10.00 mm radius) were nested into cutouts in the central black PeT layer (3) (Lumirror* X30, Toray Industries, Inc., Chuo-ku, Tokyo, Japan) that separated the two internal fluidic layers and enabled laser-actuated valving.[24-25] These membranes were fabricated via a two-step laser cutting process (**Figure 4-3**). First, an array of circular cutouts was made in PeT. After wetting the PeT with methanol, a commercial PTFE film was overlaid and allowed to dry at room temperature, effectively solvent bonding the two substrates together. A second ablation step was performed to create a larger, concentric circle around each of the previous cutouts to yield circular PTFE membranes with PeT supports lining their periphery. After

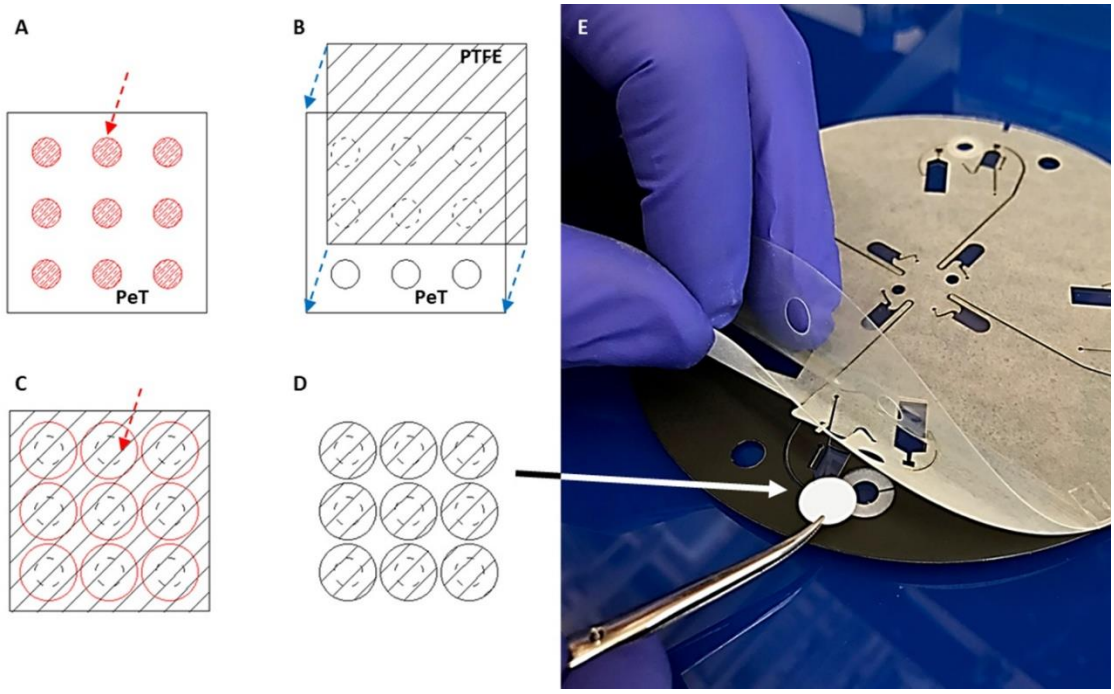

Figure 4-3. Preparation of PeT-supported PTFE inserts. (A) Circular holes (2.5 mm radius) were laser-cut into a PeT film and the internal circular areas were removed (denoted by red arrow and red hatched fill). (B) A PTFE membrane was applied on top of the pre-cut PeT, wetted with methanol, and allowed to dry at room temperature to solvent bond the two substrates together. (C) Larger circular holes (5 mm radius) were cut into the bonded PTFE-PeT assembly concentrically around the previously removed PeT (red arrow and red outline). (D) Excess material outside these new cuts was removed, revealing the PeT supported inserts. (E) Prior to lamination, the PTFE inserts were nested into cutouts within the central layer of the disc with the PeT support facing down. Adapted from [22].

placement into the LoaD, PTFE membranes were anchored in place via heat-sensitive adhesive (HSA, EL-7970-39, Adhesives Research, Inc., Maryland Heights, MO) on either adjacent device layer during lamination (UltraLam, 250B, Akiles Products, Inc., Mira Loma, CA).[26] In addition to the traditional five layers per device, which housed the majority of the architecture, two 'reinforcing layers' (R1, R2) were applied via a second lamination step to improve valving performance.[25]

4.2.2. On-Disc Reagent Storage

Dry reagents were loaded into polymethyl methacrylate (PMMA) (1.5 mm thickness, McMaster Carr, Elmhurst, IL) for on-board storage using a custom 3-D printed press (Form 3 printer and RS-F2-GPCL-04 resin, FormLabs, Somerville, MA). Up to 18

cups were prepared in parallel; following placement into wells in the bottom half of the press, the cups were filled and covered with sodium bicarbonate (Thermo Fisher Scientific, Waltham, MA) and excess was scraped away using the edge of the top half of the press. Where appropriate, citric acid (Sigma-Aldrich, Inc. St. Louis, MO) was mixed with the sodium bicarbonate prior to cup loading such that each contained, on average, 3 mg citric acid and 527 mg sodium bicarbonate. The top component of the press was then aligned with the bottom component such that its 'teeth' are aligned with the cup and applied pressure compressed the reagents within each cup. PMMA reagent cups and accessory pieces for swab acceptance (0.5 mm thickness, Astra Products, Copiague, NY) were affixed to the device using pressure sensitive adhesive (PSA, Arcare 7876, Adhesives Research Inc.) and cured under weight (~10 pounds) overnight. To enable recovery and off-disc post-processing of displaced lysates, sample recovery chambers were augmented by PMMA (McMaster Carr) capped with PTFE membranes.

4.2.3. Mechatronic Spin System Construction and Operation

Rotationally-driven fluidics were controlled using the custom-built Power, Time, and Adjustable Z-Height Laser (PrTZAL) system, described elsewhere.[25] Device rotation was driven by a brushless DC motor to promote flow. A photointerrupting optical switch (TT Electronics/Optek Technology, Woking, UK) and a motorized translational stage (MTS50-Z8, Thorlabs, Inc.) were used to position a 700 mW 638 nm laser diode (L638P700M, ThorLabs, Inc., Newton, NJ) at the appropriate location for laser valving. Diode z-height relative to the LoaD surface was adjusted to 15.00 mm for valve opening (500 mW, 500 ms) and 27.00 mm for channel closures (700 mW, 2500 ms) using two stepper motors (Polulu Robotics and Electronics, Las Vegas, NV). All PrTZAL

functionalities were controlled using a 32-bit multi-processing microcontroller (Propeller P8X32A-M44, Propeller, Inc., Rocklin, CA).

4.2.4. Sample Collection and Processing

Deidentified buccal swabs were collected from anonymous, consenting donors. To isolate epithelial cells, the swab was rolled against the walls of a 0.5 mL Eppendorf tube containing 300 µL 1X Tris-EDTA (Thermo Fisher Scientific). Epithelial cells were stained with Syto-11 (0.2 µL) (Thermo Fisher Scientific) for visualization and quantification by hemocytometry using a Zeiss Axio microscope. One-eighth cotton swab cuttings (Puritan Medical Products, Guilford, ME) were spiked with 1,500 cells and placed in on-disc swab chambers. A 14 µL aliquot of a lysis cocktail comprised of 12.46 µL water, 1.4 µL 10X blue buffer, and 0.14 µL prepGEM enzyme (MicroGEM International, PLC., Charlottesville, VA) was added to the swab chamber and incubated (75 ˚C, 300 s; 95 ˚C, 60 s) using a clamped dual-Peltier system. For in-tube comparison, swab cuttings spiked in the same way were heated on a thermal cycler with the same temperature profile. In-tube lysis was performed in 0.2 mL PCR tubes using this reduced (14 µL) volume chemistry described for on-disc implementation and the manufacturer recommended lysis cocktail volume of 100 µL (88 µL water, 10 µL 10X blue buffer, 1 µL prepGEM enzyme (MicroGEM International, PLC.)). In-tube lysates were recovered via the ‘piggyback method’.[27] Briefly, the bottom of the PCR tube containing the swab cutting was punctured with a syringe needle. After nesting this PCR tube inside of a 0.5 mL Eppendorf tube, centrifugation facilitated lysate elution from the swab and transfer into the outer tube. In on-disc dye studies used to assess the functionality of the fluidic architecture, aqueous green dye (14 µL) was used to visually represent the cellular lysate.

4.2.5. On-Disc IFD Workflow

After adding the swab cutting and sample solution (dye or lysis cocktail) to the LoaD, the liquid reagent chamber was loaded with 10 µL of either sulfuric acid, phosphoric acid (both Thermo Fisher Scientific), or deionized water. The water was used to rehydrate the citric acid-sodium bicarbonate dry mixture within reagent cups to initiate neutralization. Regardless of acid type, 1.63×10^{-5} moles were used in each reaction. Actuation of the laser valve beneath the swab chamber permitted centrifugal elution of the lysate from the swab and transfer into the sample chamber (398.5 g, 120s). All vents and inlets associated with the liquid reagent and swab chambers were laser sealed. After opening laser valves beneath the sample and liquid reagent chambers, device rotation (257.1 g, 2 s) permitted mixing of liquid and dry reagents stored on-board to initiate acid-base neutralization. Gas evolved during the neutralization reaction passed through the PTFE membrane, into the sample chamber, and finally out of the vent of the sample recovery chamber after pumping the sample fluid radially inward. Successful inward displacement was characterized by liquid transfer from the sample chamber into the sample recovery chamber. Displaced lysates were collected for off-disc post-processing by puncturing the PTFE membrane capping the recovery chamber with a pipette tip. All device images were captured by an Epson Perfection V100 Photo desktop scanner (Seiko Epson Corporation, Suwa, Nagano Prefecture, Japan).

4.2.6. Recovery Analysis

Dye volumes were calculated by “masking” the relevant pixels from optical measurements using ImageJ freeware (Fiji distribution), as described elsewhere.[28] Briefly, the pixels associated with the dye solution were selected through application of optimized

color thresholds (hue: 80-255, saturation: 89-255, brightness: 60-191), then counted. Experimentally measured pixel counts were compared with controlled calibration volumes (1-10 µL, n = 3 each) (R^2 = 0.992) to extrapolate recovered volumes. Hue analysis was performed from a circular region of interest (ROI) taken from the relevant chamber after conversion of the native image to a 3-slice hue-saturation-brightness stack. Recovery of BLUE buffer (MicroGEM International, PLC.) was characterized by mass. A calibration curve of mass vs. volume was constructed by measuring the mass of known buffer volumes in pre-weighed 0.2 mL PCR tubes (3-10 µL, n = 3 each, R^2 = 0.995).

4.2.7. DNA Post-Processing

4.2.7.1. Relative DNA Quantification

Relative DNA quantification was achieved by targeting the TPOX locus via real-time PCR with the primer and probes used in **Chapter 2**;[29] sequences were published previously.[30] Each 20 µL reaction was comprised of 1X SensiFast Probe Lo-ROX One-Step Master Mix (Meridian Bioscience, Memphis, TN), 0.4 µM each forward and reverse primers, 0.1 µM probe, and 4 µL diluted lysate (1:4 in water). Triplicate amplification reactions performed using a QuantStudio 5 (Thermo Fisher) involved an initial denaturation step (95 ˚C, 210 s), followed by 40 cycles of denaturation (95 ˚C, 5 s) and annealing (60 ˚C, 30 s) prior to a final 4 ˚C hold step. Fluorescence monitored in the FAM channel permitted calculation of C_t values using the threshold generated automatically by the QuantStudioTM Design & Analysis software (v1.5.0).

4.2.7.2. Multiplexed PCR

Multiplexed PCR amplification of DNA from neat on-disc lysates was performed using the PowerPlex 18D system (Promega, Madison, WI) according to manufacturer's

instructions using 28 cycles. Resultant amplicons were electrophoretically separated and fluorescently detected using an ABI 3130 Genetic Analyzer (Applied Biosystems, Grand Island, NY) prior to short tandem repeat (STR) profiling using Gene Marker HID software (v2.7.6) (SoftGenetics, State College, PA).

4.2.7.3. Loop-Mediated Isothermal Amplification

Amplification targeted the TPOX locus using primer sequences published elsewhere.[31] Each in-tube reaction contained 0.2 µM F3 and B3, 0.8 µM LF and LB, and 0.6 µM FIP and BIP primers, 120 µM hydroxy napththol blue (HNB), and 1.25 µL sample in 1X WarmStart (DNA and RNA) Master Mix (New England Biolabs, Ipswitch, MA). During isothermal heating at 65 ˚C, images were captured at 30, 45, and 75 minutes using a smartphone (Huawei Technologies Co., Ltd. Shenzhen, China). In ImageJ, hue values of 60-pixel diameter circular ROIs from each tube at each timepoint were measured. Endpoint electrophoretic amplicon separation and detection was performed using the DNA chip assay for the Bioanalyzer 2100 (Agilent Technologies, Santa Clara, CA). On-disc LAMP was performed with the same primer concentrations but 2 µL sample and was heated using free-standing clamped dual-Peltiers. A 40 µL aliquot of master mix was loaded into the reagent chamber. After opening the downstream laser valve, reaction aliquots were centrifugally metered (27.2 g, 30 s), then delivered to LAMP reaction chambers (496.0 g, 90 s). Prior to heating, microchannels upstream of the reaction chambers were laser-sealed. Temperature control was provided by a program written in Propeller.

4.2.8. Fluidic Workflow for Sample-to-Answer On-Disc Analysis

In the fully-integrated LoaD, swab lysis and IFD were performed as described previously (Sections 4.2.4 and 4.2.5, respectively). After IFD, the laser valve beneath the

sample recovery chamber was opened, and a lysate aliquot of approximately 2 µL was metered out via device rotation (27.2 g, 30 s), with excess driven to an overflow chamber. Following laser actuation of the downstream valve, the metered lysate was delivered to the central LAMP reaction chamber through a channel that was laser-sealed after use. On-disc LAMP was then conducted as described in Section 4.2.7.3.

4.3. Results and Discussion

Portable LoaDs represent a powerful set of tools for automating, expediting, and translating NA analysis to the PoN.[11, 32] However, as discussed previously, the unidirectional, outward flow restricts the number of possible sequential on-board process chains, often limiting assay complexity and precluding total microfluidic sample-to-answer processing.[8-9, 32] As discussed in **Chapter 1**, this limitation has contributed to the existence of very few relevant micro total analysis systems (µTAS); many LoaDs automate NA amplification and detection, but upstream cell lysis and NA extraction (NAE) remain tethered to traditional, manual methods. The work detailed in this chapter aimed to ease integration of more extensive NA analysis process chains on-disc by describing both a simple, easy-to-implement NA isolation method and IFD of the sample towards the CoR to allow continued microfluidic processing. First, single-step, on-disc, direct-from-swab isolation of amplification-ready NAs was enabled by a thermophilic protease (EA1, discussed in **Chapter 3**). The resultant lysate was returned to the CoR via automatable, self-contained, gas-driven IFD that leveraged on-board acid-base neutralization for CO2 evolution. Though other CO_2-based IFD modalities have been described, this work is the first demonstration of its compatibility with NA amplification tests (NAATs), which is crucial for future development of sample-to-answer LoaDs. Further, this work directly

addresses the limitations of previous gas-driven IFD strategies by eliminating 1) required manual intervention, 2) complex, custom fabrication, 3) highly corrosive, dangerous reagents, and 4) large volumes of displacer fluids.[17, 19, 33] Further, reagents stored on-board maintain their reactivity for at least six months under ambient conditions, which is promising in terms of potential commercialization and use at the PoN.

4.3.1. Microdevice Fabrication and Operational Principles

4.3.1.1. Microfluidic Design

Gas generation, containment, and direction were the essential functionalities taken into consideration during architectural design of the IFD LoaD device (**Figure 4-4**). Since IFD relies on harnessing an evolving pressure head on-disc, it was essential that the LoaD could achieve the tight seals required for effective gas containment. This importance cannot be overstated, given that 'leaky' systems are known to result in unreliable IFD performance.[19, 33] Laser-based valving is more robust than other approaches that exhibit frequent failure (leaking) within pressurized systems or in the presence of alcohol-based

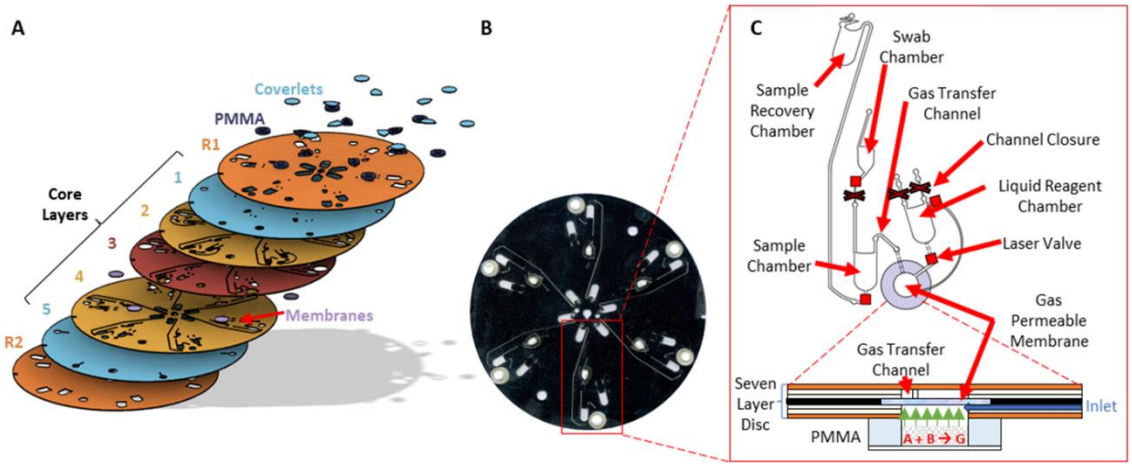

Figure 4-4. Design and fabrication of a LoaD for IFD demonstration. (A) Isometric schematic rendering of a 7-layer microdevice. The primary fluidic architecture is housed within the 5 core layers. The primary fluidic layers (2 and 4) are separated by an intervening valving layer (3). Re-enforcing layers (R1 and R2) were added on either side of the core layers to improve channel closure success. PMMA accessory pieces are added where necessary to enhance chamber volume and enable on-board reagent storage. The PTFE gas-permeable membrane is inserted into layer 3 prior to lamination (B) Image of a fully assembled microdevice accommodating on-board direct-from-swab lysis and subsequent inward displacement of the lysate. (C) AutoCAD rendering of the microfluidic architecture in which laser valve openings and closures are designated by red squares and crosses, respectively. Adapted from [22].

solvents.[19, 27] Here, laser-actuated channel closures, leveraged for liquid flow control in **Chapters 2 and 3**, is applied to gas containment for the first time. Explicitly, irradiation of channel vents and inlets permitted hermetic sealing, and therefore unidirectional gas flow within the microarchitecture. While PCL LoaDs typically contain five material layers,[23, 26] it has previously been shown that additional bulk material in the form of reinforcing layers improved the success rate of laser-based channel closures to over 99% at the relevant rotational frequencies.[25] Consequently, two additional reinforcing layers, one on either side of the device, were incorporated to yield 7-layer proof-of-concept IFD LoaDs with reliable laser-actuated channel closures. Coupling laser-based channel sealing with a complementary valve opening strategy permitted leak-free sealing of the LoaD system and precise spatiotemporal control over on-board fluidics.

4.3.1.2. On-Disc Reagent Storge and Reaction

CO_2 evolution from on-board acid-base neutralization is a critical feature of this self-contained IFD approach. In each domain, this reaction occurs within a PMMA reagent cup positioned directly above the embedded hydrophobic, gas-permeable PTFE membrane (**Figure 4-4C**). Solid and liquid reagents were sequestered on one side of the membrane, which precluded their direct contact with and contamination of the sample solution. Conversely, CO_2 gas generated as a byproduct of neutralization freely passed through the membrane, through the gas transfer channel, and ultimately affected IFD.

Simple, reproducible on-board storage was critical for consistent IFD performance. To simplify reagent loading, a custom 3D-printed press was developed (**Figure 4-5**) to allow simultaneous preparation of up to eighteen cups. Previously, Krauss et al. described a vastly different method centered on manually adding sequential aliquots of a sodium bicarbonate ($NaHCO_3$) slurry prepared in methanol into individual cups with intermittent drying steps.[19] Comparatively, the iterative, manual workflow for slurry addition was much more time and labor than the single-step, higher-throughout press-based method. Further, the press-based method involved addition of a larger, more consistent average reagent mass per cup (0.039 ± 0.002 g (coefficient of variation (CV) = 5.92%)) than the slurry technique (0.030 ± 0.003 g (CV = 10.8%)) (n = 15 each). This additional reagent mass increased the potential for gas evolution while simultaneously minimizing the dead air volume within the reaction chambers, both of which stand to enhance IFD performance. Moreover, reagent loading using the press permitted storage of acid-base mixtures ($NaHCO_3$ and citric acid) without rehydration, which would initiate the neutralization reaction. This reagent storage approach could also be applied to other dry mixtures for on-disc gas generation, such as baking powder.[20, 33]

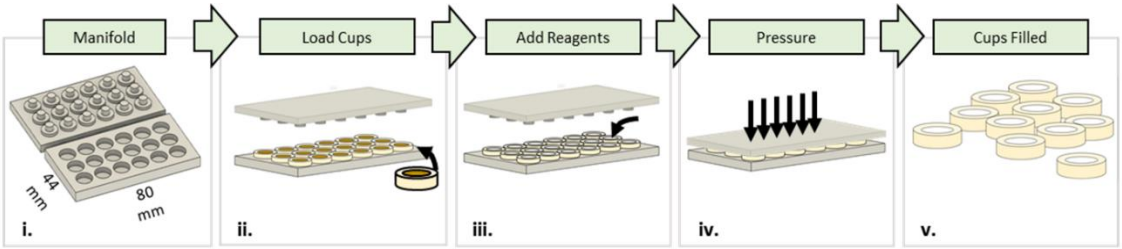

Figure 4-5. Method for reproducible dry reagent loading. (i.) Fusion360 schematic of the 3D-printed reagent press used to facilitate uniform loading of PMMA cups. (ii.) First, empty PMMA cups were nested into recessed wells in the bottom plate, then (iii.) covered entirely with solid reagent prior to scraping away excess with the flat edge of the top half of the press, such that each cup was filled evenly to its brim. (iv.) The top plate was aligned with its cylindrical 'teeth' above the cup openings prior to pressure application. (v.) Completed PMMA cups contained compressed dry reagents ready for LoaD attachment. Adapted from [22].

To demonstrate the feasibility of IFD performance and NAAT compatibility, each of the six identical domains contained features that enabled on-board direct-from-swab enzymatic lysis and subsequent displacement of the recovered lysate back towards the CoR.

4.3.2. On-Disc IFD Evaluation

4.3.2.1. Optimization of Architecture for Swab Integration

In this direct-from-swab approach, successful fluid recovery from absorbent substrates is crucial, and is directly related to swab position within the LoaD. Initially, it may seem that positioning the swab adjacent to the CoR would be best in terms of conserving available LoaD area for downstream sample processing. However, since the magnitude of centrifugal force an object experiences directly depends on its radial distance from the CoR (rotor length), this approach is impractical. Positioning the swab closer to the LoaD periphery increases the centrifugal force experienced, which, in turn, increases fluid recovery. Visual demonstration was achieved via optical quantification of recovered dye volumes obtained from parallel sets of swab cuttings near the LoaD CoR and periphery (n = 4 each). After loading aqueous dye into each swab chamber (14 µL), downstream laser valves were opened and LoaD rotation was sustained for 120 s at 3,000 rpm, which is the upper limit of many spin systems.[25] Fluid volumes transferred to the chambers beneath the swab chambers were quantified via ‘masking’ as described in **Chapter 2** (**Figure 4-6**). No detectable volume of dye was eluted from the cuttings adjacent to the CoR (14.2 mm, 142.9 g). However, approximately 10 µL were recovered from swabs positioned 39.60 mm (398.5 g) from the CoR of the same LoaD; this distance was used in all subsequent IFD experiments. Thus, maximizing sample recovery from a solid substrate

necessitates its positioning near the LoaD edge, such that significant continued on-disc processing requires eluate transfer radially inward.

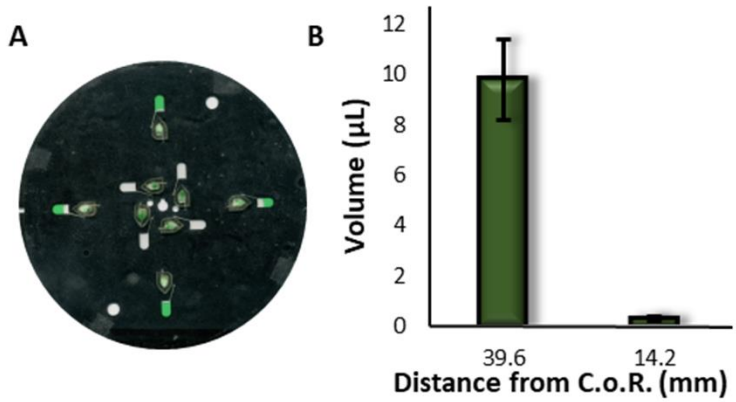

Figure 4-6. Fluid recovery from swabs at different radial positions (A) Image of microdevice showing dye elution from swab cuttings placed at 14.2 and 39.6 mm from the center of rotation. (B) Calculated recovered volume from each condition (each n = 4). Adapted from [22].

4.3.2.2. Gas-Driven IFD

Accordingly, the gas-driven IFD workflow (**Figure 4-7**) was demonstrated following on-disc direct-from-swab enzymatic cellular lysis. Centrifugally-controlled lysate retrieval from the substrate involved actuation of a normally-closed laser valve below the swab chamber, followed by centrifugally transfer of the eluate into the sample chamber (**Figure 4-7ii**). After lysate recovery from the swab, all vent and inlet channels associated with the sample and liquid reagent chambers were laser-sealed such that the only remaining point of gas exchange between the LoaD and environment was the vent of the sample recovery chamber adjacent to the CoR (**Figure 4-7iii**). Mixing the liquid and dry reagents on-disc initiated acid-base neutralization, which produced CO_2 as a byproduct. This evolved gas passed through the embedded PTFE membrane and flowed into the sample chamber, placing pneumatic pressure on the sample therein (**Figure 4-7v**). Functionally, this pressure application directly on the sample is similar to that provided by working 'displacer' fluids,[16-17] but was advantageous in terms of architectural requirements. As discussed in the introduction of this chapter, displacer fluid volumes must greatly exceed that of the sample, necessitating large chambers that consume significant microfluidic 'real estate' near the CoR, whe

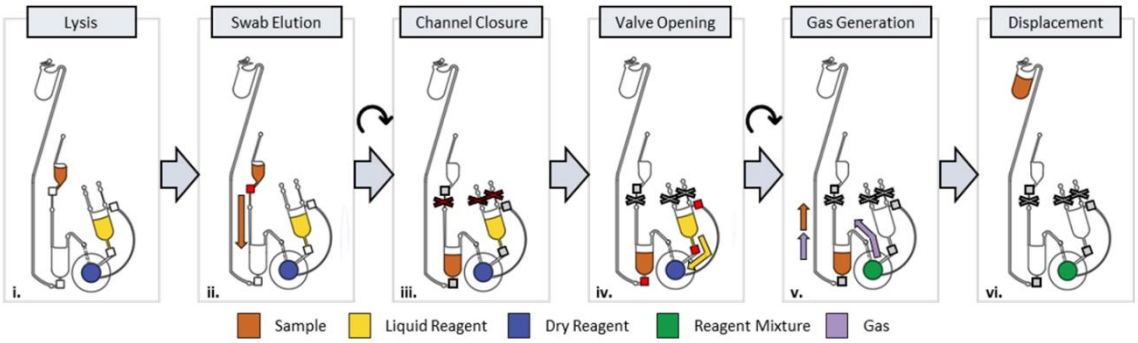

4-7. Diagrammatic depiction of on-disc IFD workflow. (i.) Direct-from-swab enzymatic cellular lysis was performed on-disc prior to (ii.) the laser valve beneath the swab chamber being opened. The lysate was centrifugally eluted from the swab into the sample chamber. (iii.) To ensure that the only remaining port for gas exchange was the sample recovery chamber vent, all inlets and vents associated with sample and liquid reagent chambers were laser-sealed. (iv). After opening the laser valves beneath the sample and liquid reagent chambers, (v.) device rotation drove transfer of the liquid reagent into the chamber containing the dry reagent. The subsequent acid-base neutralization reaction generated carbon dioxide gas that (vi.) drove the bulk sample solution radially inward into the sample recovery chamber. Adapted from [22].

re device surface area is most scarce. Here, the liquid reagent volume required is less than that of the sample, and all displacement reagents (liquid and dry) were located near the disc edge, where surface area is most abundant. The importance of these differences can be empirically understood through consideration of a 12 cm diameter LoaD, in which >30% of microfluidic surface area is located within the 1 cm ring along the periphery, whereas the innermost ring of the same width contains <8.5%.[17] Hence, the IFD approach described here consumes less, and less valuable, device real estate than methods based on displacer fluids since IFD reagents here are stored at the edge of the device. When sufficient pressure had accumulated, the sample fluid was pumped radially inward into the sample recovery chamber as the CO_2 escaped its open vent (**Figure 4-7vi**).

Effective, leak-free containment and unidirectional focus of this evolving gaseous pressure head was essential for successful IFD. In early pilot studies, two failure modes were noted. First, incomplete channel closures occurred due to misalignment of the diode with the relevant architectural features. In these cases, gas was able to flow backwards and escape from sample and/or liquid reagent chamber vents such that the gas pressure inside

the LoaD was insufficient to drive IFD. Fortunately, this issue was corrected easily via automated alignment using the PrTZAL system, described in **Chapter 2**.[25] In fact, when properly performed, these channel closures were strong enough to contain gas within fully sealed, pressurized reagent cups. Here, neutralization was performed on-disc without actuating the valve beneath the sample chamber such that evolved gas was trapped within the cup. While the channel closures maintained their integrity, the adhesive bond (PSA) between the PMMA reagent cups and the PeT microdevice surface did not (data not shown). However, this mechanical failure mode was not observed under normal operational conditions (e.g., valve opened as normal) and after curing LoaDs under constant weight and pressure (~10 lbs.) overnight prior to use.

4.3.3. Recovery Characterization

Early pilot studies probing IFD and fluid recovery leveraged aqueous dye solutions to facilitate optical image analysis (**Figure 4-8**). Regions of interest (ROIs) encompassing the sample and sample recovery chambers were selected from images captured following swab elution and IFD, respectively (**Figure 4-8B**). Within each cropped image, pixels attributable to the dye solution were specifically selected via 'masking', a method described in detail elsewhere.[28] Briefly, adjustment of color thresholds within the ImageJ

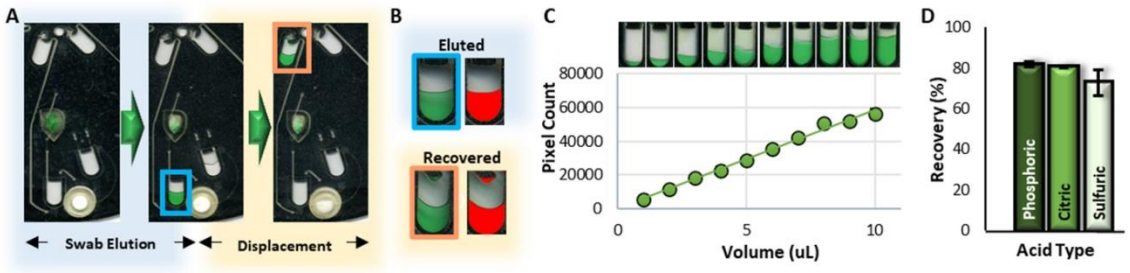

Figure 4-8. Visual characterization of IFD recovery. (A) Device images after swab elution, and IFD with green dye representing a cellular lysate. (B) Image masking in which specific pixels corresponding to dye eluted from the swab before and after displacement were selected. (C) The calibration curve between dye volume vs. pixel count exhibited an excellent linear correlation (R^2= 0.992). (D) Recovery calculations following dye displacement using equimolar concentrations of phosphoric, citric, and sulfuric acid (each n = 6). Adapted from [22].

freeware permitted selection of pixels containing dye, while excluding those associated with the image background and microdevice surfaces. A calibration curve constructed by measuring the number of pixels associated with dye solutions of known volumes on-disc exhibited excellent linear correlation (R^2 = 0.992) (**Figure 4-8C**) and was used to determine the volumes of dye eluted from swab cuttings and dye present in the sample recovery chamber following IFD. Notably, the percentage of dye eluted from the swab and successfully displaced into the sample recovery chamber was comparable using equimolar concentrations of sulfuric, phosphoric, and citric acids (**Figure 4-8D**). Weak acids (citric and phosphoric) are advantageous for practical implementation due to increased compatibility with device materials and obviation of the need for custom fabrication strategies, such as the miniaturized ampoules used by Krauss et al.[19] due to the highly corrosive nature of concentrated sulfuric acid, employed for IFD by Krauss et al. (**Figure 4-9A**).

Fortunately, the recoveries (approximately 80%) obtained following IFD driven by weak acids were statistically similar to the strong acid (unpaired t-test, $\alpha = 0.05$, p- value = 0.58). Both citric and phosphoric acids could be used with no detriment to performance.

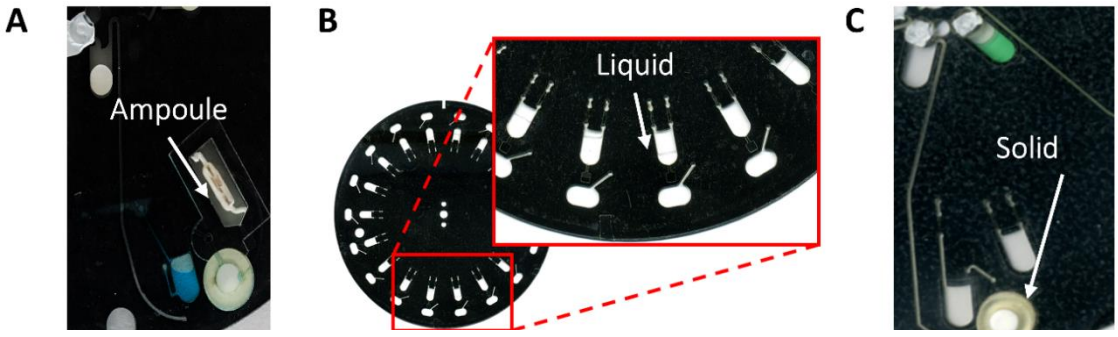

Figure 4-9. On-disc acid storage methods. (A) Previously, *Krauss et al.* used custom, microfabricated ampoules to store concentrated acid solutions on-disc. (B) Less concentrated acids could be added directly into PCL chambers, then laser-sealing vents/inlets, but issues were apparent with long-term on-disc liquid storage. (C) Acidic and basic reagents could be stored together as a dry mixture such that simple rehydration with water would initiate the neutralization reaction.

Thus, on-disc storage of liquid phosphoric acid in PCL chambers (**Figure 4-9B**) could reasonably be explored, but it was expected that such efforts would be confounded by evaporative loss, infiltration of the semi-porous HSA between device material layers, and the potential for LoaD degradation. Conversely, citric acid could be easily stored dry on-disc as a mixture with $NaHCO_3$ such that simple rehydration with water affected neutralization initiation, and therefore gas generation (**Figure 4-9C**). When using this dry, on-board citric acid-$NaHCO_3$ mixture, the user need not handle an acid directly and no liquid reagents must be stored within the LoaD. This simplicity of use led to implementation of citric acid in all subsequent IFD reactions.

4.3.4. Long-Term Reagent Storage Evaluation

Characterization of the on-disc stability of the citric acid-$NaHCO_3$ mixture on-disc over time was essential in evaluating the practicality of this IFD approach. Following LoaD fabrication, dye studies were performed at one-month intervals (0-6 months) with storage under ambient conditions (n = 4 each). After performing IFD of aqueous green dye (starting volume = 10 µL), recovered volumes were calculated via masking dye pixels and comparison with the standard curve as done in initial assay characterization (**Figure 4-10**). According to a single factor ANOVA, resultant volumes were statistically similar across all time points ($\alpha = 0.05$, $p = 0.69$), which indicated that

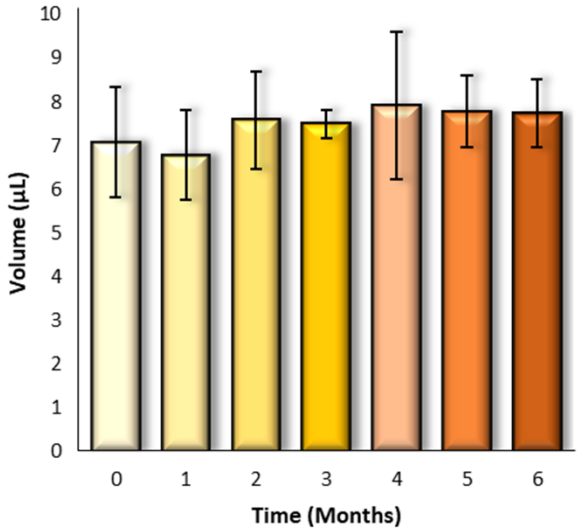

Figure 4-10. Evaluation of long-term on-board reagent storage. Volumes recovered following IFD at one-month intervals were statistically similar up to six months storage under ambient conditions (n = 4 each). Adapted from [22].

displacement can be achieved using reagents stored dry on-disc for at least 6 months with no loss in performance (**Figure 4-10**). This demonstrated stability of reagents stored on-board is paramount to practical implementation and potential future integration in commercialized microdevices.

4.3.5. Fluid Loss Attribution

During both acid selection and long-term reagent storage characterization, it was apparent that fluid volume was lost during IFD. Despite recovery rates below 100%, the sample chambers at the disc periphery were visually empty, suggesting that sufficient pneumatic pressure was generated to fully drive fluid out of the sample chamber. To more thoroughly characterize this fluid loss and understand its origin, we performed IFD with a range of aqueous dye volumes (**Figure 4-11**). Optical determination of chamber volumes (masking) indicated the presence of a strong, positive linear correlation between recovery and starting volume (R^2 = 0.992) (**Fig. 4-11**, yellow). Calculations of volume lost in each condition showed that 1.5-2 µL were reproducibly lost, regardless of starting volume (**Figure 4-11**, blue). In fact, according to a single factor ANOVA, all mean volumes of fluid loss were statistically similar (α = 0.05, p-value = 0.51). This reproducible volume loss led to the conclusion that detriments to recovery had not resulted from

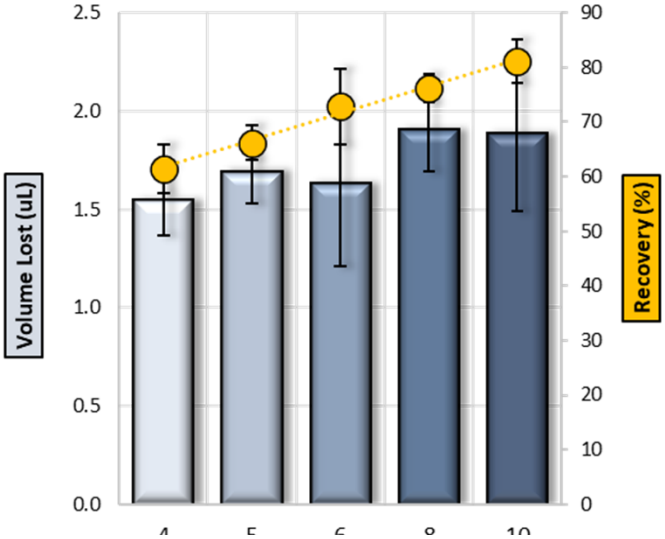

Figure 4-11. Volume loss characterization. Calculated recoveries (%) following displacement of various volumes of aqueous dye are shown as yellow points in a scatterplot. The blue histogram bars correspond to calculated volumes lost under each condition (each n = 3). The % recovery scaled linearly directly with the starting volume (R^2 = 0.9915), whereas the volume lost remained consistent across conditions. Adapted from [22].

incomplete or failed IFD, but rather were consequences of the laser valving and PCL fabrication strategies employed. For example, normally-closed laser valves are known to retain small volumes of fluid (0.5 - 2 μL) in the valving "patch", or rectangular cutout in the top fluidic layer. The manufactured roughness of channel walls resulting from laser ablation was also hypothesized to contribute to fluid loss; such microscopic crevices are known to collect fluid.[34] These two mechanisms, in combination, were presumed to cause fluid losses within the PCL IFD system described. Although these factors cannot be eliminated from our LoaD system without significantly changing its operational principles, these phenomena are reproducible and predictable, so they may be accounted for experimentally.

4.3.6. Characterization of On-Disc Direct-from-Swab Lysis

Following thorough characterization of IFD performance via dye studies, on-disc direct-from-swab enzymatic lysis was implemented. This work leveraged the same EA1 chemistry used in **Chapter 3** for single-step, hands-free cell lysis and isolation of liberated nucleic acids. However, to simplify on-disc architecture, it was desirable to decrease the lysis reaction volume such that no downstream unit operations (e.g., metering) were required prior to displacement. Since dye studies primarily used starting volumes of 10 μL, this was the target volume for lysate swab elution. By adding variable dye volumes to on-disc swab cuttings and optically quantifying centrifugally eluted volumes, it was determined that spiking cuttings with 14 μL resulted in recovery of approximately 10 μL (data not shown). However, the manufacturer recommends a lysis reaction volume of 100 μL, so it was essential to ensure the smaller volume reaction proceeded as expected. As in previous chapters, real-time PCR was employed as an analytical tool to characterize DNA

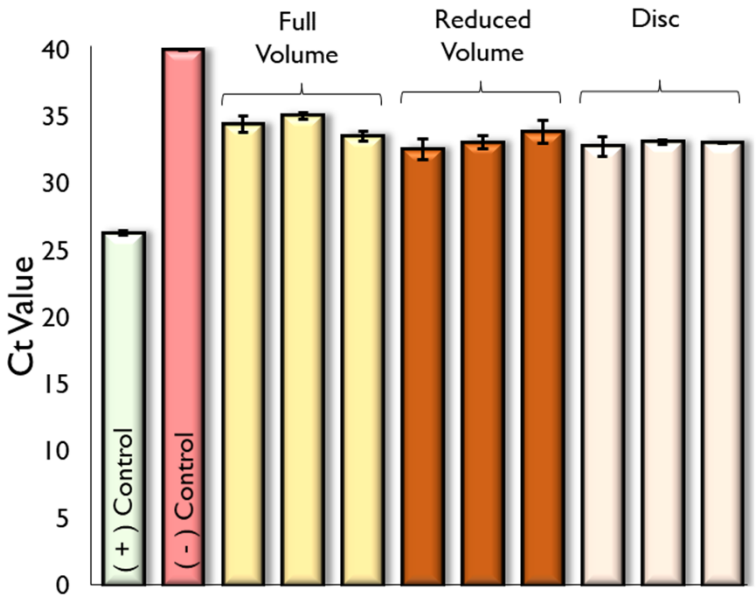

Figure 4-12. Characterization of DNA extraction at the microscale. Parallel triplicate extractions were performed from cotton swab cuttings spiked with buccal epithelial cells in-tube at full (100 µL) and reduced (14 µL) volumes and on-disc (14 µL). Real-time PCR amplification (triplicate) of all extracts resulted in similar C_t values.

yield. Triplicate 'full' (100 µL) and 'reduced' (14 µL) volume in-tube lysis reactions produced similar C_t values (**Figure 4-12**). In fact, a t-test for means indicated no statistical difference in the grand means across volumes ($\alpha = 0.05$, $p = 0.241$); therefore, comparable DNA concentrations were produced. Importantly, comparison of the reduced volume lysis in-tube and on-disc also resulted in statistically similar C_t values ($\alpha = 0.05$, $p = 0.806$), which indicated that microfluidic lysis was successful with no detriment to performance and could feasible be used in conjunction with downstream IFD.

4.3.7. Architectural Changes for Bioanalysis

Initial pilot studies to characterize displacement performance using blue buffer instead of aqueous dye resulted in significant fluid loss from the LoaD following IFD. To mitigate this, LoaD architecture, specifically that of the sample recovery chamber, was modified (**Figure 4-13**). In the original device, this chamber was cut into the core PCL layers and was vented conventionally. However, the `buffer was reproducibly observed to

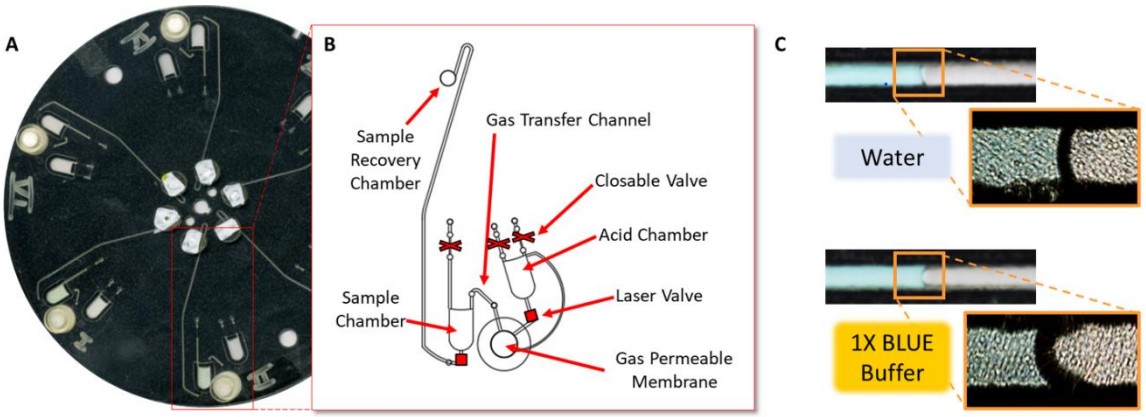

Figure 4-13. Modified IFD LoaD for lysate displacement. (A) Image of a fully-assembled modified LoaD for on-board direct-from-swab lysis and subsequent IFD. Adapted from [22]. (B) LoaD architecture (AutoCAD rendering) where laser valve openings and closures are represented by red squares and crosses, respectively. No vent is required on the sample recovery chamber due to inclusion of a PTFE capping layer. Adapted from [22]. (C) Microscopic images of dyed water (top) and BLUE buffer (bottom) demonstrating the decreased surface tension of the latter.

have exited the sample recovery vent along with the gas during displacement. It was hypothesized that the buffer was not retained as the aqueous solution had been due to compositional differences. Though the exact makeup of the blue buffer is proprietary, empirical microscopic observation of dyed water and blue buffer hinted at a possible explanation. Images captured of both fluids in microchannels showed that the meniscus of the blue buffer was much more pronounced than that of the water, indicative of reduced surface tension (**Figure 4-13C**). To prevent fluid loss, the sample recovery chamber was augmented with PMMA, and capped with PTFE – the same membrane embedded within the LoaD for neutralization reagent containment during gas flowthrough. This gas-permeable PTFE cap permitted removal of the vent channel altogether, since the CO_2 could pass directly through the membrane. However, since the membrane is hydrophobic, the displaced buffer was reliably contained. Additionally, this architecture eased recovery of displaced lysates for off-disc post-processing, which was achieved simply by puncturing the membrane with a pipette.

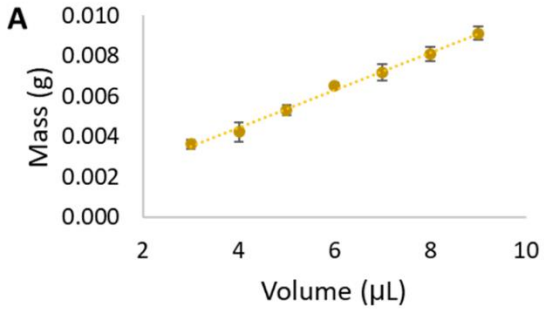

B	Recovered Mass (g)	Calculated Volume (µL)
Replicate1	0.0070	6.7465
Replicate 2	0.0062	5.8872
Replicate 3	0.0057	5.3502
Average		**5.9946**
Stdev		**0.7043**

Figure 4-14. Determination of IFD recovery by mass. (A) Calibration curve relating mass and volume of prepGEM BLUE buffer measured in triplicate exhibited an excellent linear correlation ($R^2 = 0.995$). (B) Calculated recovery following IFD of blue buffer retrieved from sample recovery chambers was determined to be 5.99±0.70.

Unfortunately, increased chamber depth and membrane flexibility precluded use of the previously implemented optical recovery analysis strategy. Instead, displaced buffer samples were retrieved from the sample recovery chambers by pipette and transferred to pre-weighed PCR tubes. An established linear calibration curve ($R^2 = 0.995$) relating blue buffer mass and volume was used to calculate an average recovered volume of 5.99±0.70 µL (**Figure 4-14**). The reduction in recovered volume relative to that calculated for aqueous solutions likely resulted from incomplete manual recovery from the LoaD prior to measuring mass. Regardless, this volume is more than adequate for most amplification-based post-processing modalities, some of which were explored in the following section.

4.3.8. Nucleic Acid Amplification Test Compatibility

4.3.8.1. Polymerase Chain Reaction-Based Techniques

As discussed in previous chapters, real-time PCR may be employed as a powerful analytical tool to evaluate the success of upstream nucleic acid preparation, for instance in characterization of EA1 lysis volume scaling (Section 4.3.6).[35] Here, according to an unpaired t-test for means, real-time PCR amplification of DNA from parallel on-disc, direct-from-swab cellular lysates with and without IFD produced statistically similar C_t values (H_0 = mean difference across conditions is zero, $\alpha = 0.05$, $p = 0.62$) (**Figure 4-15A**).

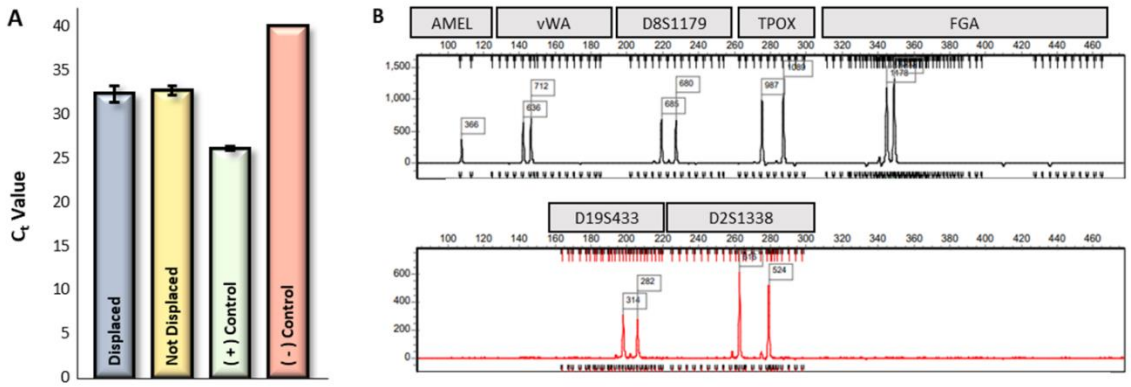

Figure 4-15. IFD compatibility with PCR amplification. Amplification of DNA prepared on-disc from one-quarter buccal swab cuttings. (A) Real-time PCR C_t values obtained via amplification of triplicate displaced and not displaced samples were statistically similar. (B) Two channels of a representative full 18-plex STR profile obtained from DNA prepared using the IFD LoaD. Adapted from [22].

This finding was crucial since it demonstrated that no observable inhibition of PCR amplification resulted from exposure to CO_2 during IFD. If resultant sample acidification, or even mechanical DNA damage, had occurred, higher C_t values would have been observed from amplification of displaced lysates relative to the non-displaced samples.

Further, compatibility with multiplexed PCR, and subsequent short tandem repeat (STR) profiling, was explored. Recall from **Chapter 2** that STR analysis involves numerous primer pairs that target multiple distinct DNA loci that contain repeating nucleotide sequences; humans possess up to two differently sized alleles at a given locus, one inherited from each biological parent, though these polymorphic regions may, coincidently, be the same length.[36] Here, we show two channels of a representative STR profile generated from a sample lysed and displaced on-disc which showed no amplification inhibition (**Figure 4-15B**). All expected peaks in the 18 loci probed were present with good peak height balance within allele pairs (e.g. no 'ski sloping' or dropout).[37] This observation was important since multiplexed PCR is more sensitive to inhibitors than real-time PCR.[38]

4.3.8.2. Loop-Mediated Isothermal Amplification

LAMP offers an alternative to PCR that leverages a strand-displacing polymerase to facilitate exponential target amplification at a single temperature via repeated, sequential annealing and extension of 4-6 primers to yield polydisperse amplicons.[39] Instead of the single peak observed following PCR amplification, electrophoretic separation of LAMP amplicons creates a repeating peak pattern that spans a substantial molecular range.[39] Such peak patterns were apparent in the electropherograms obtained from on-disc lysates with and without IFD, as well as the positive control (commercial human genomic DNA), indicating successful, on-target amplification (**Figure 4-16**). No peaks were observed in the no template control, which demonstrated the absence of non-specific amplification. For ease of pattern recognition, triplicate electropherograms (displaced and not displaced) were converted to a 'gel' image rendering; bands in each lane visually represent patterns

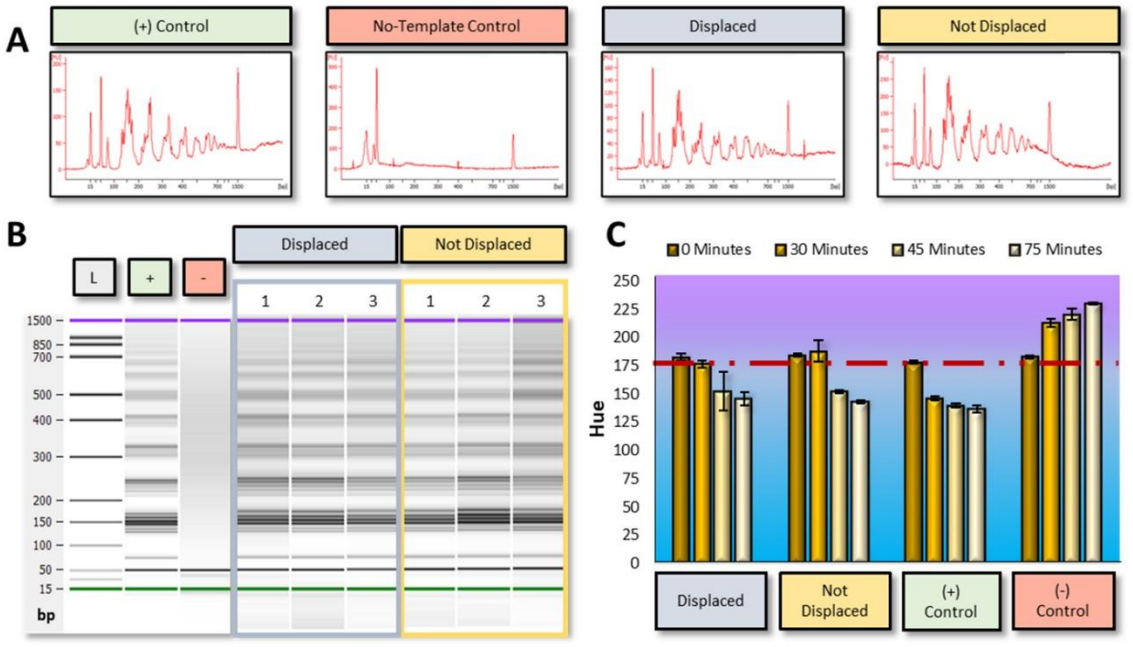

Figure 4-16. Characterization of LAMP performance following IFD. (A) Representative endpoint electropherograms of controls and samples with and without IFD. (B) Gel image rendering of triplicate displaced and not displaced samples showing reproducible amplification. (C) Semi real-time colorimetric LAMP detection showed amplification in all samples in less than 45 minutes. Adapted from [22].

resulting from successful LAMP, indicating reproducible amplification of DNA prepared on-disc with no detriment resulting from on-disc, gas-driven IFD.

Though microchip electrophoresis provided valuable endpoint detection, it could not provide temporal insight regarding amplification speed. Semi-real-time reaction monitoring was achieved via measuring optical readout over the course of amplification. Compatibility with visually-apparent, colorimetric detection makes LAMP especially attractive for PoN use. As done previously in **Chapters 2 and 3**, inclusion of the indicator HNB provided binary, semi-quantitative visual indication regarding whether a target has been detected (blue) or not (purple) at discrete time points (0, 30, 45, and 75 minutes). By 45 minutes, all samples appeared visibly blue (positive), while the no template control remained purple (negative). However, such naked eye interpretation is possible, but not advisable given inter-user variation in color perception and variable environmental lighting conditions.[40-41] Accordingly, we analyzed the hue of each reaction and established a threshold for differentiating positive and negative results three standard deviations below the mean initial hue (0 minutes) across all samples (175.16 A.U.).[28, 42] Hue readings above (purple) and below (blue) this delineation colorimetrically indicated negative and positive results, respectively (**Figure 16C**). Results from hue analysis were concordant with simple visual observations; all samples were empirically positive by 45 minutes, with measured hue values below the threshold.

Taken together, the colorimetric and electrophoretic results detailed in this section indicated that on-disc lysis provided amplification-ready DNA and IFD did not hinder downstream LAMP or PCR-based NAATs.

4.3.9. Microfluidic LAMP Adaptation

Ultimately, on-disc incorporation of one of these amplification and detection modalities was desired to yield a sample-to-answer LoaD. From a practical perspective, integration of microfluidic LAMP is more facile than PCR-based methods due to simplified hardware requirements for isothermal heating and colorimetric detection that ease portability for PoN use.[39, 43] Prior to developing a fully integrated architecture, however, it was essential to demonstrate successful fluidic performance of the microfluidic LAMP process chain. To achieve this, an architecture for two-step metering was implemented (**Figure 4-17**) to split the LAMP master mix bulk fluid into three identical, defined sub-volumes which could then be delivered to amplification chambers.[44-45] Two-step metering is well-suited to such applications where further processing of aliquots (e.g., LAMP) is required.[46] Each aliquot chamber was designed to hold 10 uL, and was filled during low-speed LoaD rotation, with overflow routed to a waste chamber. A subsequent high-speed spin actuated capillary burst valves at the bottom of each aliquoting chamber to deliver the

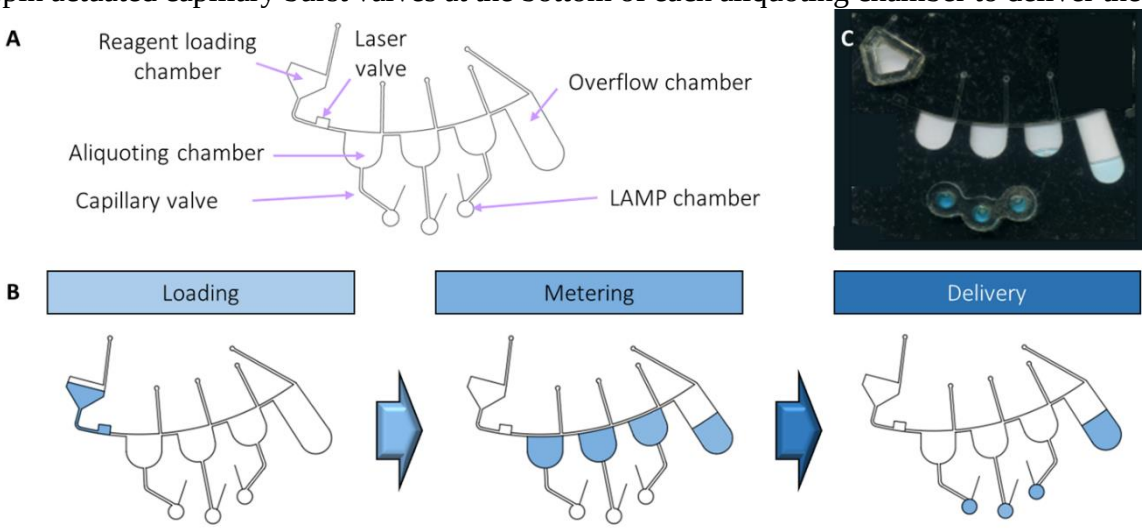

Figure 4-17. Microfluidic on-disc LAMP protocol. (A) Labelled schematic of LAMP architecture for parallel amplification of three samples. (B) (i.) After loading LAMP master mix onto the disc, a downstream laser valve was actuated and (ii.) low-speed disc rotation drove metering of three equal volume aliquots, each of which are (iii.) delivered to individual LAMP reaction chambers for simultaneous amplification. A no template control, a positive control, and the sample may be heated simultaneously. (C) Image of successful metering and delivery of aqueous dye to each LAMP chamber.

metered volumes to fluidically separated chambers for parallel amplification of NA samples therein. Explicitly, the LAMP architecture was designed with three amplification chambers expressly so positive and no template controls could be amplified in parallel with each sample. This entire metering and delivery process was rotationally controlled, and therefore easily automated. After demonstrating the fluidic success of this architecture, the next step involved its integration with on-disc direct-from-swab lysis and IFD.

4.3.10. Integrated Sample-to-Answer Architecture

The fully-integrated LoaD developed was capable of sample-to-answer processing of four samples in parallel (**Figure 4-18**). The LAMP architecture discussed in the previous section was incorporated downstream of the microfeatures for on-disc direct-from-swab lysis and IFD described in previous sections. After lysate preparation and displacement proceeded as normal, the unit operations for on-disc LAMP were performed (**Figure 4-19**). Initially, a 2 µL aliquot of the displaced lysate was metered out for subsequent

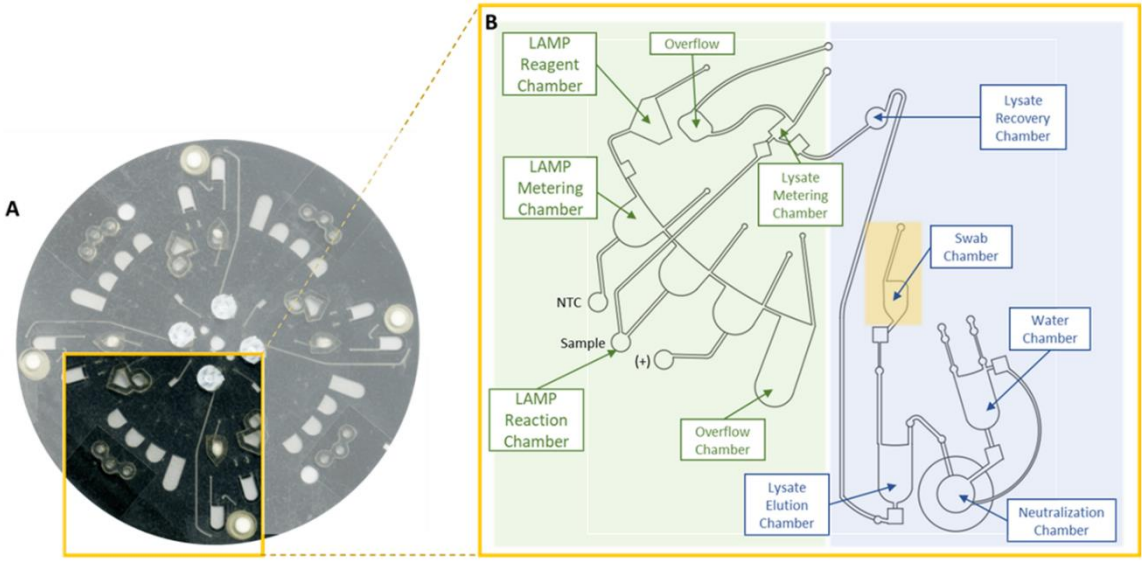

Figure 4-18. Sample-to-answer LoaD for nucleic acid detection. (A) Image of a fully-assembled 4-plex LoaD for sample-to-answer NA analysis. (B) Schematic (AutoCAD) rendering of architectural features accommodating on-board direct-from-swab lysis (yellow), subsequent inward displacement of the lysate (blue), and, finally, nucleic acid amplification (green).

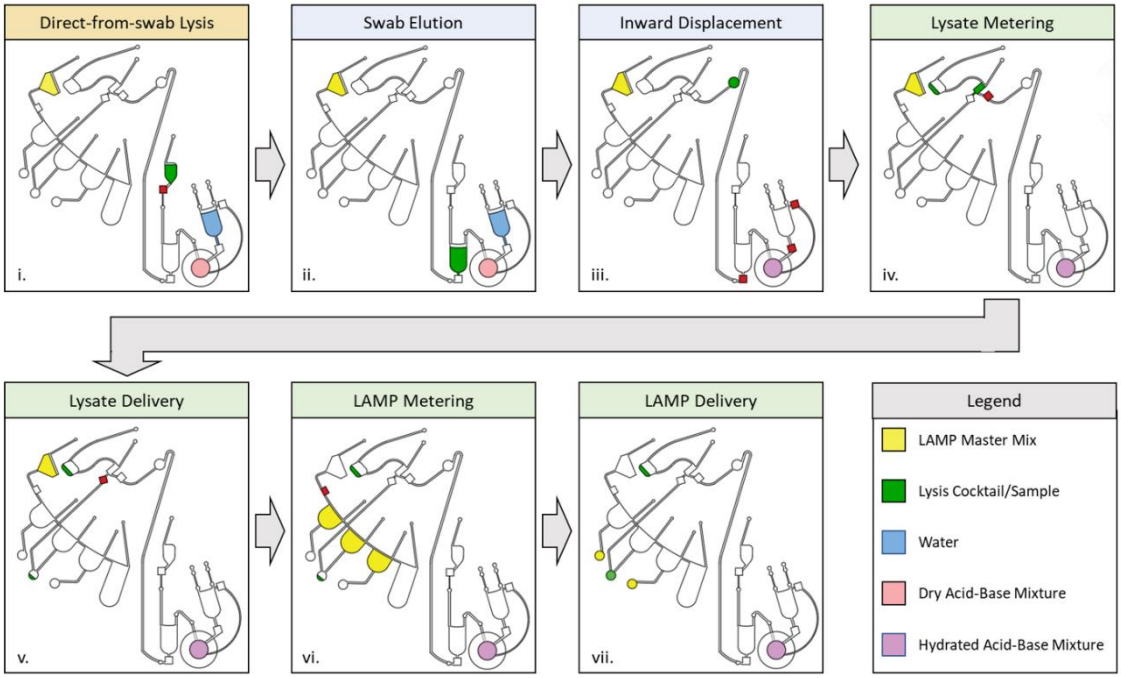

Figure 4-19. Stepwise workflow for sample-to-answer nucleic acid processing. Following (i.) loading of the LAMP master mix, sample, lysis cocktail, and water into the device, on-disc lysis occurs. After actuation of the laser valve beneath the swab chamber, (ii.) the sample was centrifugally eluted from the substrate. (iii.) The acid-base mixture stored on-board was rehydrated and generates gas for IFD. (iv.) A 2 µL lysate aliquot is metered out, then (v.) delivered to the central LAMP chamber. (vi.) Three equivalent aliquots of master mix were metered, then delivered to three separate LAMP reaction chambers. Here, single-temperature incubation permits parallel amplification of the sample, a positive control, and a no-template control.

amplification. Precise input volumes to each on-board LAMP reaction were needed to ensure quantitatively reproducible result with high accuracy. Fortunately, the volume needed matched the sample input for on-disc dSPE (**Chapter 2**), so the same lysate metering architecture, known to deliver 2.17±0.60 µL, was employed here. The principal challenge in development of this architecture involved delivery of this aliquot of the displaced lysate directly to the appropriate amplification chamber. The lysate delivery channel was laser-sealed prior to lysate metering to ensure the capillary valve beneath the aliquot chamber functioned properly during LAMP master mix metering. Explicitly, capillary burst valves could not be actuated until all three aliquot chambers were filled, which requires trapping of air within the LAMP receiving chambers. If the lysate delivery channel were not closed, the sample LAMP chamber would effectively be vented via the

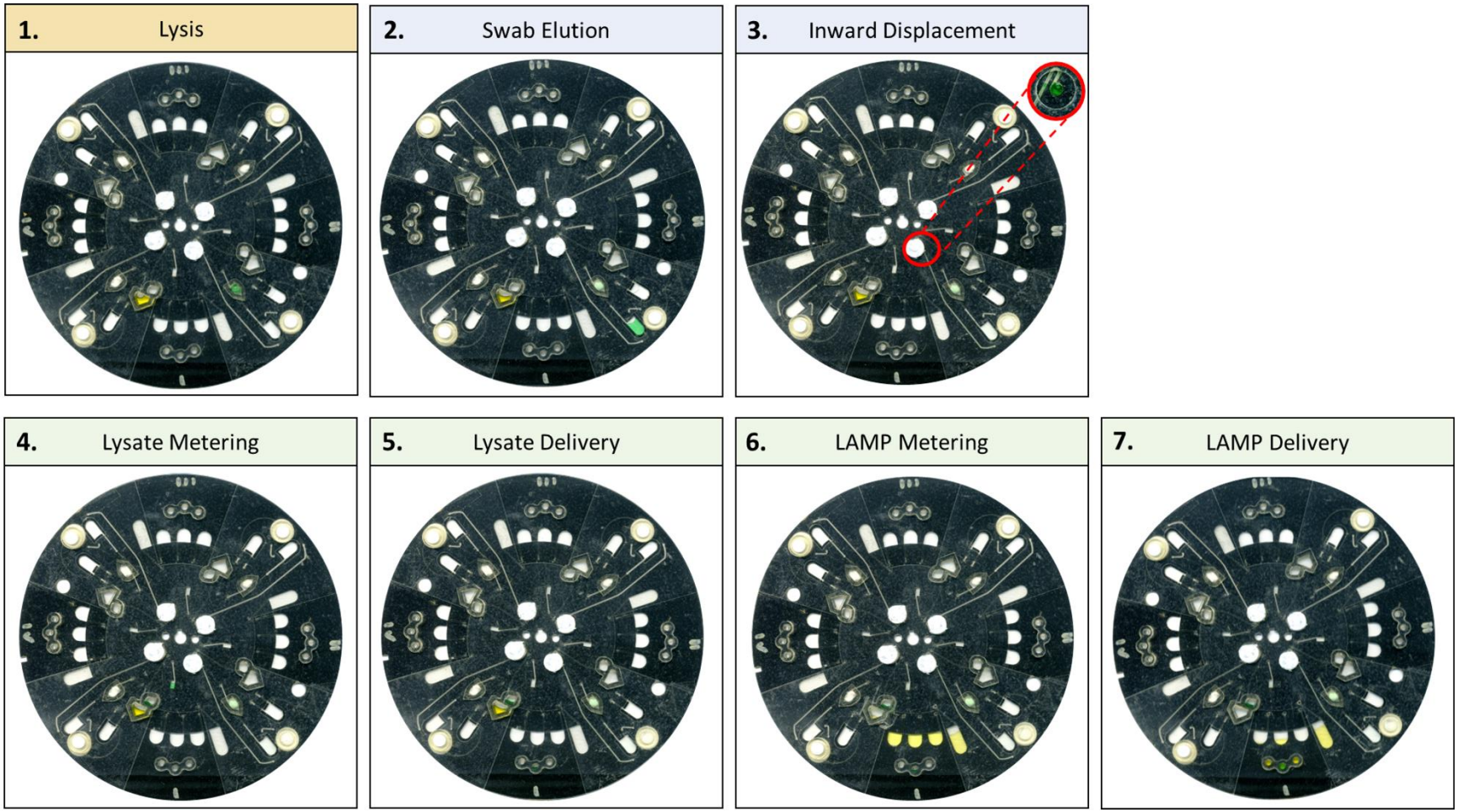

Figure 4-20. Integrated workflow images in a single domain of a 4-plex LoaD. Images depict successive post-lysis (2) swab elution, (3) IFD, (4) lysate metering, (5) lysate delivery to the central LAMP chamber, then (6) metering and (7) delivery of these aliquots to the LAMP reaction chambers where amplification occurs.

upstream metering architecture, fill prematurely, and preclude effective downstream metering. Successful delivery of displaced lysate to the relevant chamber, as well as on-board LAMP master mix and metering, was visually demonstrated using aqueous dye solutions (**Figure 4-20**).

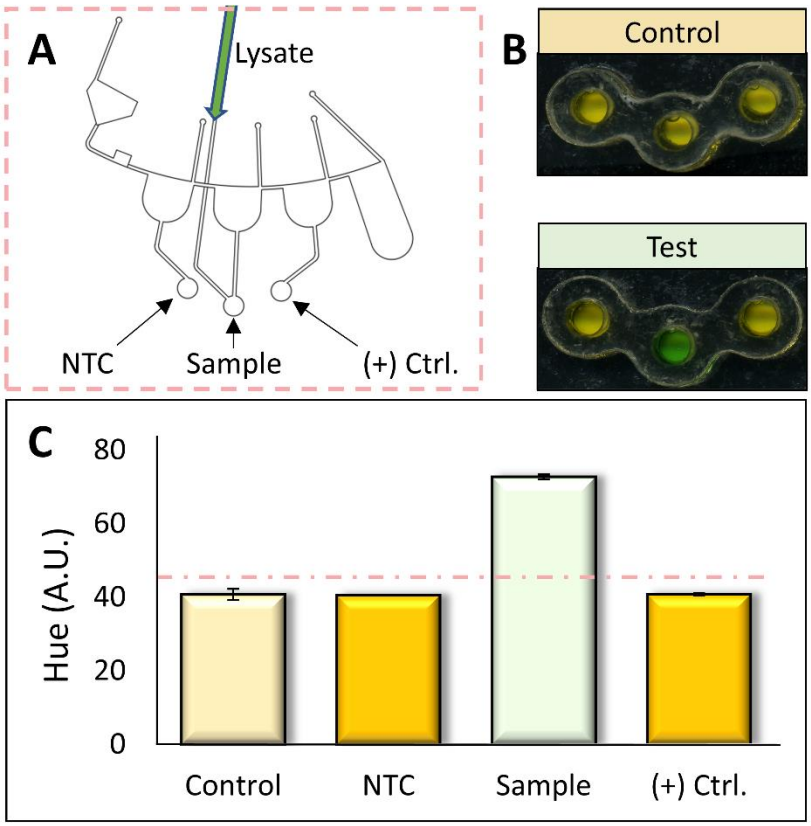

Figure 4-21. Visual characterization of lysate delivery. Selective delivery of lysate into the central LAMP chamber was characterized using dye solutions. (A) Sample was delivered to the LAMP chamber via a microchannel cut into the bottom fluidic layer. (B) Image of LAMP chambers after displaced green dye (sample) was delivered to the central sample chamber and yellow dye (master mix) was delivered. Image of controls comprised of pure yellow dye. (D) Hue comparison indicated that only the hue from the sample chamber was statistically different than the controls; no green dye was detected in the NTC and (+) Ctrl chambers.

Since the ultimate goal of this device is to amplify the sample in parallel with controls, it was essential to demonstrate that the delivered sample did not contaminate the two adjacent LAMP chambers. Generally, two-step metering mitigates the risk for cross-contamination by spatially separating metered aliquots from the samples or reagents in downstream chambers.[47] Nonetheless, a dye study was conducted where sample (green dye) was delivered to the central amplification chamber prior to delivery of yellow dye to each chamber, which represented LAMP master mix (**Figure 4-21**). The hue of fluid contained in each chamber was measured and compared with on-disc control solutions (pure yellow

dye). A threshold was established three standard deviations above the mean control hue (n = 3). As expected, only the hue measured from the sample chamber was above this threshold, indicating the presence of green dye. Hue values of the solutions in the two adjacent chambers, which represent the NTC and positive control reactions, were statistically similar to the control (Single factor ANOVA, $\alpha = 0.05$, $p = 0.96$), which suggests no green dye was present. To eliminate the risk of cross-contamination during heating as a result of thermal fluid pumping, for instance, the channels upstream of each LAMP chamber (capillary burst valves) were laser sealed to ensure that fluid remained in chambers for the duration of incubation. In summation, the architecture developed here can reliably accommodate the fluidics for the entire genetic analysis workflow.

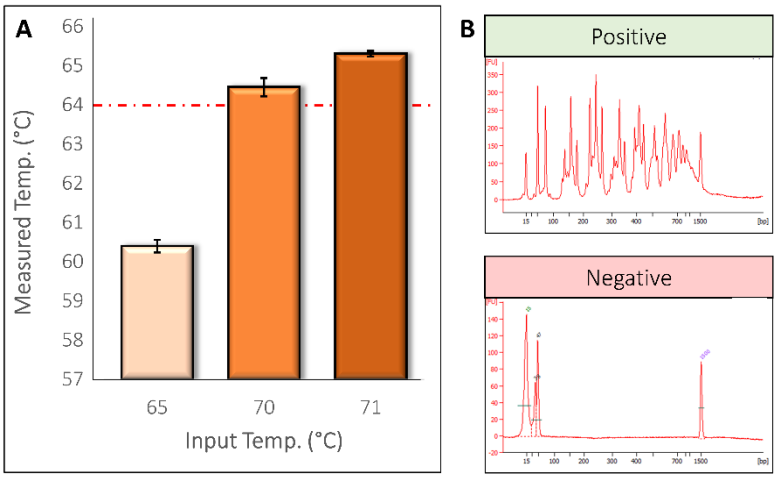

Figure 4-22. Electrophoretic analysis of on-disc LAMP amplicons. (A) Temperature studies indicated that an input temperature of 70° C was required to achieve the desired input temperature of 64 °C. (B) In negative samples, no amplification was observed. However, in positive samples, the repeating peak pattern characteristic of LAMP was clearly present.

Preliminary pilot studies moving beyond dye-based visualizations have shown that LAMP may be successfully performed on-disc (**Figure 4-22**). Temperature studies indicated that, to achieve the desired reaction temperature of 65 °C in solution, an input value of 70 °C must be given to the clamped dual-Peltier system used for heating. Using these conditions and the same chemistry in the in-tube studies above (Section 4.3.8.2), the successful microfluidic amplification of the TPOX locus was demonstrated, though off-

disc microchip electrophoresis was required for detection (**Figure 4-22B**). However, much work remains in reliably adapting this chemistry to the LoaD system. A detailed discussion regarding remaining obstacles will be presented in Chapter Six. Briefly, non-specific amplification occured sporadically in no template controls on-disc, but not in parallel in-tube reactions performed on a 'gold standard' instrument. Therefore, continued optimization of the microfluidic amplification, for instance through adjusting primer and polymerase concentrations or incubation duration, is required. Further, to eliminate dependence on benchtop instruments, an appropriate colorimetric indicator must be incorporated.

4.4. Conclusions

Here, a novel, easy-to-implement method for radially-inward fluid displacement (IFD) was described for use in development of highly-integrated polymeric NA processing LoaDs. Fluid return to the CoR allows for augmented LoaD functionalities, including fluid recovery from absorbent substrates (e.g., swabs), and increased the number of stepwise unit operations possible. This IFD approach leverages well-characterized disc fabrication[23] and valving methods,[24-25] as well as safe-to-handle reagents stored on-board without the need for complex, custom ampoules.[19] Displacement within the self-contained LoaDs was driven by CO_2 generated from the reaction between sodium bicarbonate and citric acid stored on-board as dry solids; simple rehydration initiated the acid-base neutralization. Statistically similar recoveries of aqueous dyes (approximately 80%) were obtained following IFD using this approach and an equimolar amount of liquid sulfuric and phosphoric acids. IFD occurred rapidly (~ 2 seconds) during device rotation. The on-disc acid-base mixture retained its reactivity for six months, with statistically similar IFD

recovery percentages throughout that interval when stored under ambient conditions. Thus, this robust reagent storage method is amenable for use in commercial or field-forward devices with broad applicability. Though the majority of data involves displacement of relatively small volumes to chambers adjacent to the CoR, fluid can also be pumped completely across the disc, and even larger volumes (~25 µL) contained in PMMA reagent chambers can be displaced (**Figure 4-23**).

Following initial characterization of IFD performance, the compatibility with a panel of NAATs was explored. To achieve this, IFD was coupled with upstream on-disc, direct-from-swab enzymatic lysis that leveraged single-step prepGEM DNA isolation chemistry to yield PCR-compatible lysates that did not require further purification. No practical detriment to amplification performance occurred as a result of IFD. Statistically similar real-time PCR C_t values were obtained from displaced and non-displaced DNA isolates. Further, generation of full 18-plex STR profiles was successful following multiplexed PCR amplification with no apparent signs of inhibition; all expected peaks were present with good peak height balance at each allele pair. Finally, LAMP, one of several isothermal techniques that constitute a burgeoning class of field deployable NAATs, performed comparably on displaced and non-displaced samples. This work represents the first demonstration of

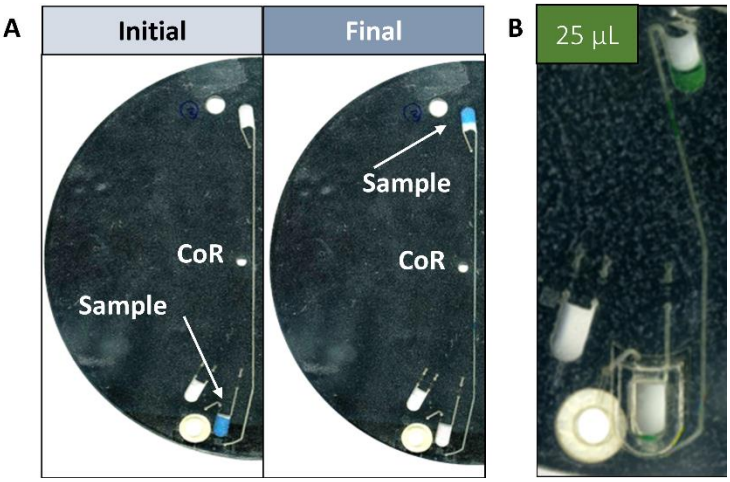

Figure 4-23. Expansion of IFD capabilities. (A) Images of LoaD before (left) and after (right) demonstrating IFD of aqueous blue dye from the disc edge orthogonally inward past the CoR to the opposing disc periphery. (B) Image of successfully displaced fluid from a PMMA chamber that originally held 25 µL.

compatibility of NAs displaced via CO_2 with downstream amplification and definitively showed that inhibition via sample acidification or mechanical NA damage was not observed. Thus, the novel method for on-disc fluidic re-routing described herein shows tremendous potential in enabling comprehensive NA analysis (e.g., lysis, NAE, amplification, and detection) in LoaDs, which has been traditionally difficult.[3]

For instance, though post-processing was performed off-disc during initial IFD characterization, architecture for on-disc LAMP was eventually integrated. This architectural inclusion of amplification downstream of sample preparation and IFD was enabled directly via circumnavigation of inherently unidirectional flow in the centrifugal LoaD. Further, the ability to amplify samples and controls in parallel on-disc was demonstrated using dye studies. The feasibility for on-disc amplification was demonstrated in proof-of-principle LAMP tests, but further amplification optimization and indicator selection is required prior to comprehensive, reliable demonstration of entirely integrated workflow. Regardless, this easily implemented IFD approach stands to make a significant impact in developing highly complex microdevices for use across numerous fields, including clinical diagnostics and forensics.

4.5 References

1. Larremore, D. B.; Fosdick, B. K.; Bubar, K. M.; Zhang, S.; Kissler, S. M.; Metcalf, C. J. E.; Buckee, C. O.; Grad, Y. H., Estimating SARS-CoV-2 seroprevalence and epidemiological parameters with uncertainty from serological surveys. *eLife* **2021,** *10*, e64206.

2. Li, Z.; Bai, Y.; You, M.; Hu, J.; Yao, C.; Cao, L.; Xu, F., Fully integrated microfluidic devices for qualitative, quantitative and digital nucleic acids testing at point of care. *Biosensors and Bioelectronics* **2021,** *177*, 112952.

3. Strohmeier, O.; Keller, M.; Schwemmer, F.; Zehnle, S.; Mark, D.; von Stetten, F.; Zengerle, R.; Paust, N., Centrifugal microfluidic platforms: advanced unit operations and applications. *Chemical Society Reviews* **2015,** *44* (17), 6187-6229.

4. Liu, Q.; Zhang, X.; Chen, L.; Yao, Y.; Ke, S.; Zhao, W.; Yang, Z.; Sui, G., A sample-to-answer labdisc platform integrated novel membrane-resistance valves for detection of highly pathogenic avian influenza viruses. *Sensors and Actuators B: Chemical* **2018,** 270, 371-381.

5. Van Nguyen, H.; Phan, V. M.; Seo, T. S., A portable centrifugal genetic analyzer for multiplex detection of feline upper respiratory tract disease pathogens. *Biosensors and Bioelectronics* **2021,** *193*, 113546.

6. Tang, M.; Wang, G.; Kong, S.-K.; Ho, H.-P., A review of biomedical centrifugal microfluidic platforms. *Micromachines* **2016,** *7* (2), 26.

7. Sunkara, V.; Kumar, S.; Sabaté Del Río, J.; Kim, I.; Cho, Y.-K., Lab-on-a-Disc for Point-of-Care Infection Diagnostics. *Accounts of Chemical Research* **2021,** *54* (19), 3643-3655.

8. Abi-Samra, K.; Clime, L.; Kong, L.; Gorkin, R.; Kim, T.-H.; Cho, Y. K.; Madou, M., Thermo-pneumatic pumping in centrifugal microfluidic platforms. *Microfluidics and Nanofluidics* **2011,** *11* (5), 643-652.

9. Soroori, S.; Kulinsky, L.; Kido, H.; Madou, M., Design and implementation of fluidic micro-pulleys for flow control on centrifugal microfluidic platforms. *Microfluidics and Nanofluidics* **2014,** *16* (6), 1117-1129.

10. Ouyang, Y.; Li, J.; Phaneuf, C.; Riehl, P. S.; Forest, C.; Begley, M.; Haverstick, D. M.; Landers, J. P., Multilevel fluidic flow control in a rotationally-driven polyester film microdevice created using laser print, cut and laminate. *Lab on a Chip* **2016,** *16* (2), 377-87.

11. Gorkin, R.; Park, J.; Siegrist, J.; Amasia, M.; Lee, B. S.; Park, J.-M.; Kim, J.; Kim, H.; Madou, M.; Cho, Y. K., Centrifugal microfluidics for biomedical applications. *Lab on a Chip* **2010,** *10* (14), 1758-1773.

12. Kong, M. C.; Salin, E. D., Pneumatically pumping fluids radially inward on centrifugal microfluidic platforms in motion. *Analytical Chemistry* **2010,** *82* (19), 8039-8041.

13. Stumpf, F.; Schwemmer, F.; Hutzenlaub, T.; Baumann, D.; Strohmeier, O.; Dingemanns, G.; Simons, G.; Sager, C.; Plobner, L.; Von Stetten, F., LabDisk with complete reagent prestorage for sample-to-answer nucleic acid based detection of respiratory pathogens verified with influenza A H3N2 virus. *Lab on a Chip* **2016,** *16* (1), 199-207.

14. Rombach, M.; Hin, S.; Specht, M.; Johannsen, B.; Lüddecke, J.; Paust, N.; Zengerle, R.; Roux, L.; Sutcliffe, T.; Peham, J. R., RespiDisk: a point-of-care platform for fully automated detection of respiratory tract infection pathogens in clinical samples. *Analyst* **2020,** *145* (21), 7040-7047.

15. Zehnle, S.; Schwemmer, F.; Roth, G.; von Stetten, F.; Zengerle, R.; Paust, N., Centrifugo-dynamic inward pumping of liquids on a centrifugal microfluidic platform. *Lab on a Chip* **2012,** *12* (24), 5142-5145.

16. Kong, M. C.; Bouchard, A. P.; Salin, E. D., Displacement pumping of liquids radially inward on centrifugal microfluidic platforms in motion. *Micromachines* **2012,** *3* (1), 1-9.

17. Kinahan, D. J.; Burger, R.; Lawlor, D.; Early, P. L.; Vembadi, A.; McArdle, N. A.; Kilcawley, N. A.; Glynn, M. T.; Ducrée, J., Centrifugally automated solid-phase extraction of DNA by immiscible liquid valving and chemically powered centripetal pumping of peripherally stored reagents. *Biosensors and Bioelectronics: X* **2021,** 100085.

18. Thio, T. H. G.; Ibrahim, F.; Al-Faqheri, W.; Moebius, J.; Khalid, N. S.; Soin, N.; Kahar, M. K. B. A.; Madou, M., Push pull microfluidics on a multi-level 3D CD. *Lab on a Chip* **2013,** *13* (16), 3199-3209.

19. Krauss, S. T.; Woolf, M. S.; Hadley, K. C.; Collins, N. M.; Nauman, A. Q.; Landers, J. P., Centrifugal microfluidic devices using low-volume reagent storage and inward fluid displacement for presumptive drug detection. *Sensors and Actuators B: Chemical* **2019,** *284*, 704-710.

20. Kinahan, D. J.; Burger, R.; Vembadi, A.; Kilcawley, N. A.; Lawlor, D.; Glynn, M. T.; Ducrée, J. In Baking-powder driven centripetal pumping controlled by event-triggering of functional liquids, 28th IEEE International Conference on Micro Electro Mechanical Systems (MEMS) 2015; pp 504-507.

21. Noroozi, Z.; Kido, H.; Madou, M. J., Electrolysis-induced pneumatic pressure for control of liquids in a centrifugal system. *Journal of The Electrochemical Society* **2011,** *158* (11), 130.

22. Dignan, L. M.; Karas, S. M.; Mighell, I. K.; Treene, W. R.; Landers, J. P.; Woolf, M. S., A Novel Method for Inward Fluid Displacement in Centrifugal Microdevices for Highly Integrated Nucleic Acid Processing with Long-Term Reagent Storage. *Analytica Chimica Acta* **2022,** In Press.

23. Thompson, B. L.; Ouyang, Y.; Duarte, G. R.; Carrilho, E.; Krauss, S. T.; Landers, J. P., Inexpensive, rapid prototyping of microfluidic devices using overhead transparencies and a laser print, cut and laminate fabrication method. *Nature Protocols* **2015,** *10* (6), 875-886.

24. Garcia-Cordero, J. L.; Kurzbuch, D.; Benito-Lopez, F.; Diamond, D.; Lee, L. P.; Ricco, A. J., Optically addressable single-use microfluidic valves by laser printer lithography. *Lab on a Chip* **2010,** *10* (20), 2680-2687.

25. Woolf, M. S.; Dignan, L. M.; Lewis, H. M.; Nauman, A. Q.; Tomley, C. J.; Landers, J., Optically-Controlled Closable Microvalves for Polymeric Centrifugal Microfluidic Devices. *Lab on a Chip* **2020,** *20* (8), 1426-1440.

26. Birch, C.; DuVall, J. A.; Le Roux, D.; Thompson, B. L.; Tsuei, A.-C.; Li, J.; Nelson, D. A.; Mills, D. L.; Landers, J. P.; Root, B. E., Rapid Fabrication of Electrophoretic Microfluidic Devices from Polyester, Adhesives and Gold Leaf. *Micromachines* **2017,** *8* (1), 17.

27. Jackson, K.; Borba, J.; Meija, M.; Mills, D.; Haverstick, D.; Olson, K.; Aranda, R.; Garner, G.; Carrilho, E.; Landers, J., DNA purification using dynamic solid-phase extraction on a rotationally-driven polyethylene-terephthalate microdevice. *Analytica Chimica Acta* **2016,** *937*, 1-10.

28. Woolf, M. S.; Dignan, L. M.; Scott, A. T.; Landers, J. P., Digital postprocessing and image segmentation for objective analysis of colorimetric reactions. *Nature Protocols* **2020,** *16* (1), 218-238.

29. Dignan, L. M.; Woolf, M. S.; Tomley, C. J.; Nauman, A. Q.; Landers, J. P., Multiplexed Centrifugal Microfluidic System for Dynamic Solid-Phase

Purification of Polynucleic Acids Direct from Buccal Swabs. *Analytical Chemistry* **2021,** *93* (19), 7300-7309.

30. Horsman, K. M.; Hickey, J. A.; Cotton, R. W.; Landers, J. P.; Maddox, L. O., Development of a human-specific real-time PCR assay for the simultaneous quantitation of total genomic and male DNA. *Journal of Forensic Sciences* **2006,** *51* (4), 758-765.

31. DuVall, J. A.; Borba, J. C.; Shafagati, N.; Luzader, D.; Shukla, N.; Li, J.; Kehn-Hall, K.; Kendall, M. M.; Feldman, S. H.; Landers, J. P., Optical imaging of paramagnetic bead-DNA aggregation inhibition allows for low copy number detection of infectious pathogens. *PLoS One* **2015,** *10* (6), e0129830.

32. Ducrée, J.; Haeberle, S.; Lutz, S.; Pausch, S.; Von Stetten, F.; Zengerle, R., The centrifugal microfluidic Bio-Disk platform. *Journal of Micromechanics and Microengineering* **2007,** *17* (7), S103.

33. Kinahan, D. J.; Renou, M.; Kurzbuch, D.; Kilcawley, N. A.; Bailey, É.; Glynn, M. T.; McDonagh, C.; Ducrée, J., Baking powder actuated centrifugo-pneumatic valving for automation of multi-step bioassays. *Micromachines* 2016, 7 (10), 175.

34. Pereiro, I.; Khartchenko, A. F.; Petrini, L.; Kaigala, G. V., Nip the bubble in the bud: a guide to avoid gas nucleation in microfluidics. *Lab on a Chip* **2019,** *19* (14), 2296-2314.

35. Dignan, L. M.; Turiello, R.; Layne, T. R.; O'Connell, K. C.; Hickey, J.; Chapman, J.; Poulter, M. D.; Landers, J. P., An ultrafast SARS-CoV-2 virus enrichment and extraction method compatible with multiple modalities for RNA detection. *Analytica Chimica Acta* **2021,** 1180, 338846.

36. Butler, J. M., Short tandem repeat typing technologies used in human identity testing. *Biotechniques* **2007,** *43* (4), Sii-Sv.

37. McCord, B.; Pionzio, A.; Thompson, R., Analysis of the effect of a variety of PCR inhibitors on the amplification of DNA using real time PCR, melt curves and STR analysis. US Department of Justice **2015,** 317.

38. Huang, M. L.; Nguy, L.; Ferrenberg, J.; Boeckh, M.; Cent, A.; Corey, L., Development of multiplexed real-time quantitative polymerase chain reaction assay

for detecting human adenoviruses. *Diagnostic Microbiology and Infectious Disease* **2008,** *62* (3), 263-271.

39. Notomi, T.; Okayama, H.; Masubuchi, H.; Yonekawa, T.; Watanabe, K.; Amino, N.; Hase, T., Loop-mediated isothermal amplification of DNA. *Nucleic Acids Research* **2000,** *28* (12), e63.

40. Liu, J.; Shao, Z.; Cheng, Q., Color constancy enhancement under poor illumination. *Optics Letters* **2011,** *36* (24), 4821-4823.

41. Krauss, S. T.; Remcho, T. P.; Lipes, S. M.; Aranda IV, R.; Maynard III, H. P.; Shukla, N.; Li, J.; Tontarski Jr, R. E.; Landers, J. P., Objective method for presumptive field-testing of illicit drug possession using centrifugal microdevices and smartphone analysis. *Analytical Chemistry* **2016,** *88* (17), 8689-8697.

42. Ibraheem, N. A.; Hasan, M. M.; Khan, R. Z.; Mishra, P. K., Understanding color models: a review. *ARPN Journal of Science and Technology* **2012,** *2* (3), 265-275.

43. Wu, J.; Kodzius, R.; Cao, W.; Wen, W., Extraction, amplification and detection of DNA in microfluidic chip-based assays. *Microchimica Acta* **2014,** *181* (13-14), 1611-1631.

44. Scott, A. T.; Layne, T. R.; O'Connell, K. C.; Tanner, N. A.; Landers, J. P., Comparative evaluation and quantitative analysis of loop-mediated isothermal amplification indicators. *Analytical Chemistry* **2020,** *92* (19), 13343-13353.

45. Mark, D.; Weber, P.; Lutz, S.; Focke, M.; Zengerle, R.; von Stetten, F., Aliquoting on the centrifugal microfluidic platform based on centrifugo-pneumatic valves. *Microfluidics and Nanofluidics* **2011,** *10* (6), 1279-1288.

46. Hwang, H.; Kim, Y.; Cho, J.; Lee, J.-y.; Choi, M. S.; Cho, Y. K., Lab-on-a-disc for simultaneous determination of nutrients in water. *Analytical Chemistry* **2013,** *85* (5), 2954-2960.

47. Focke, M.; Stumpf, F.; Roth, G.; Zengerle, R.; von Stetten, F., Centrifugal microfluidic system for primary amplification and secondary real-time PCR. *Lab on a Chip* **2010,** *10* (23), 3210-3212.

5. Microfluidic enzyme-linked immunosorbent assay-based opiate detection

5.1. Introduction

As the most widely consumed class of illicit or misused substances worldwide, with 57.8 million annual users, opioids cause the majority of overdose-related fatal intoxications.[1-2] Such widespread use imposes large analytical burdens on clinical and forensic laboratories alike for substance identification. Optimally, presumptive testing should be conducted at the point-of-need (PoN) to guide on-site decision making prior to confirmatory laboratory analysis. Colorimetric tests are especially attractive for in situ use by non-technical personnel (e.g., law enforcement officials) due to cost-effectiveness, speed, simplicity, and amenability to visual interpretation.[4] However, naked-eye interpretation of colorimetric tests permits only qualitative detection and subjectivity in color perception and/or variable environmental lighting conditions contribute to high error rates.[5-6] For these reasons, ampoule-based field tests – the most common presumptive field test used by law enforcement officials – possess high error rates that can contribute to wrongful arrests.[5-7] In light of these and other issues, many jurisdictions advise against the use of these devices.[8] Since no widely-accepted alternatives have emerged for reliable colorimetric PoN drug identification, analysis is primarily conducted by trained analysts in centralized facilities using expensive benchtop instrumentation and/or time-consuming, labor-intensive workflows.[5, 9] Thus, accurate and simple-to-use devices for on-site opioid identification stand to make a significant impact in both decreasing analytical burdens on laboratories as well as permitting generation of real-time, actionable information on-site.[4]

Previous efforts towards developing such PoN analytics have been made to adapt existing chromogenic chemistries to the microscale with inclusion of objective image

analysis for more reliable, semi-quantitative results.[5, 10-11] Still, detection performance is ultimately limited by the chemical nature of the test; the ampoule-based methods discussed above, and microfluidic adaptations thereof, leverage small-molecule reactions for chromogenesis, which generally exhibit limited discriminatory power, poor sensitivity, and low specificity.[6, 12] For instance, the Marquis reagent for colorimetric opiate detection has remained in use, essentially unchanged, since its original 1896 publication despite known false positive responses to innocuous, non-controlled, and ubiquitous substances (e.g., aspirin, sugar).[12-14] Clearly, there is an urgent need to supplant existing colorimetric PoN drug testing methods with more accurate, reliable, and semi-quantitative tools.[6]

Immunoassays coupled with a visual detection strategy have been widely adapted as rapid diagnostic tools for diverse clinical, military/defense, and PoN applications for cost-effective, on-site qualitative or semiquantitative detection of a broad range of targets, including nucleic acids, hormones, viruses, bacteria, food adulterants, and drugs.[15-20] These immunologic methods are reputed as powerful screening tools due to their excellent specificity, selectivity, and cost-effectiveness.[21-22] Among these, lateral-flow immunoassays (LFIs) have been widely commercialized as portable, simple, rapid, and cost-effective tools for PoN (e.g., home) use due to the absence of required user training and near-instantaneous provision of results.[20, 23-25] Generally, LFIs function via capillary action that drives sample flow through the device's cellulosic matrix after introduction at the sample pad (**Figure 5-1A**). During capillary flow, gold nanoparticle labelled detection antibodies (Abs) stored on-board are rehydrated and interact with target antigen (Ag) present in the sample; Ab-Ag complexes are formed as the solvent front approaches the detection zone. Upon specific binding between the nanoparticle-tagged antibodies and their

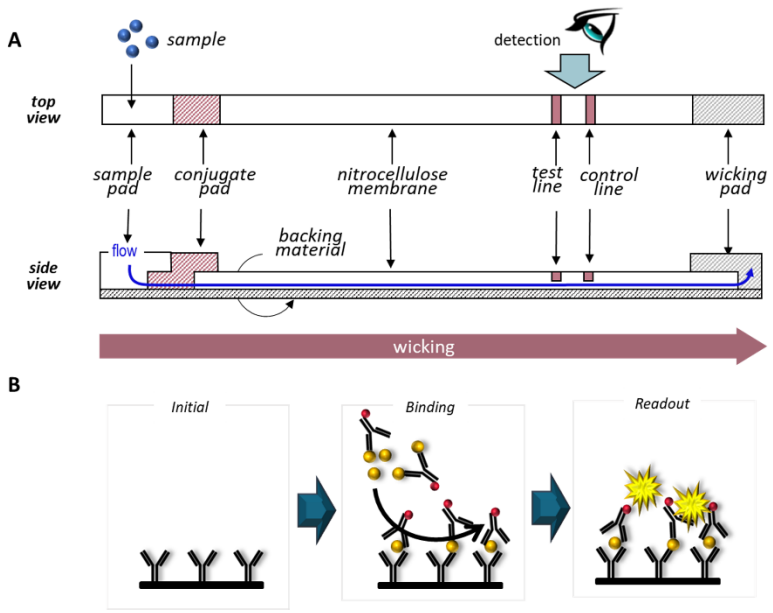

Figure 5-1. Lateral flow immunoassay (LFI) operational principles. (A) Top and side view schematics of a typical LFI device. A solution introduced to the sampling pad flows via capillary action through the conjugate pad towards the detection zone, comprised of test and control lines. Adapted from [36]. (B) Diagrammatic representation of the sandwich-style immunoassay that permits visual readout at the test and control lines. During LFI production, both the test and control lines are spotted with capture antibodies. During flow along the device, detection antibodies are rehydrated from the conjugate pad and mix with the sample. Target antigen molecules are then bound by the detection antibodies, which are tagged with gold nanoparticles. In the detection zone, antibody-antigen complexes are bound by anchored capture antibodies. Aggregation of the gold nanoparticle labels results in generation of an optically-detectable visual response.

corresponding antigens, the gold nanoparticle labels are brought into close proximity, resulting in visually apparent color generation (**Figure 5-1B**).[15, 26] This forms the basis for a common, sensitive, biocompatible, and reliable method for providing an optical readout.[19, 23, 26] While total reliance on capillary flow is advantageous in the provision of instrument-free assay performance, it also creates key operational limitations that limit practical LFI use, including poor control over flow rate, diffusion-limited mixing which makes particularly viscous biofluids (e.g., blood, saliva) incompatible, creates small/variable sampling volumes, and is unsuitable for total automation.[27-29] Furthermore, multiplexing detection of numerous targets within a single LFI device is not straightforward, effectively limiting throughput.[30]

Consequently, vertical flow immunoassays (VFIs), in which fluid flows orthogonally (not parallel) through a porous matrix, have been developed to address existing LFI shortcomings.[25] Although the simplest VFI analogs continue to rely primarily on capillary flow through stacked LFI substrates, recently described pressure-driven analogs provide more control and flexibility in sample type, volume, and flow rates.[25, 31] Our group has recently described and characterized one such approach using a lab-on-a-disc (LoaD) VFI system that relied on centrifugally-generated pressure to drive continuous flow through embedded cellulosic membranes.[29] As discussed in **Chapter 1**, membranes embedded within LoaDs are commonly used for filtration,[32-33] while silica membranes in particular are frequently used for nucleic acid capture during centrifugally-controlled flowthrough.[34-35] Here, we leverage a similar strategy and describe a LoaD for membrane-based capture of different targets (e.g., illicit or misused drugs and biowarfare agents) using a different class of bioanalytical techniques – namely immunoassays. Pilot studies demonstrating feasibility of this system were centered on sandwich-style pathogen immunodetection, used in LFIs (**Figure 5-1B**).[29, 36] Although this 'sandwich' format is readily compatible with relatively large (μm) targets, it is not particularly well-positioned for detection of small molecules (e.g., opioids), known collectively as 'haptens' In these cases, the small antigen size (nm) hinders the required simultaneous interaction with the detection and capture Abs. Though a few LFIs have been developed for drug screening in urine and oral fluid,[9] immunodetection of these compounds is much more commonly achieved using enzyme-linked immunosorbent assays (ELISAs).

Among the various ELISA formats available, indirect, competitive assays are especially suited for hapten (<1,000 Daltons) detection (**Figure 5-2**).[22, 37] Briefly, device

surfaces are coated with an Ag-protein (e.g. bovine serum albumin, BSA) conjugate, instead of Abs. The key event in these assays is centered on competition between Ag in the sample versus Ag coating device surfaces for a finite number of Ab binding sites.[22] After subsequent binding of secondary (2º) Abs to any 1º Abs bound to the coated Ag, chromogenic readout is catalyzed by enzymes linked to 2º Abs. Since Ags must interact with only one Ab for successful immunodetection, as opposed to two in sandwich style assays, this immunoassay type is commonly applied to hapten (e.g., opioid) detection.[22, 37]

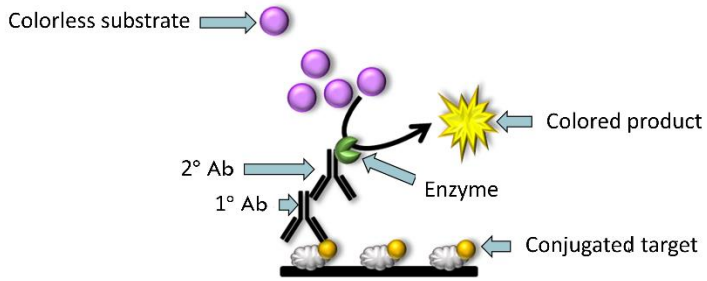

Figure 5-2. Indirect competitive ELISA format. Assay surfaces are coated with a conjugate-target compound, which is recognized by the primary antibody. A secondary antibody with affinity for the primary antibody's species of origin is added. The secondary antibody is labelled with an enzyme that catalyzes a chromogenic substrate to permit visual immunodetection.

Though ELISAs exhibit excellent specificity and selectivity, they traditionally remain tethered to centralized laboratories due to reliance on highly manual, time-intensive workflows (**Figure 5-3**), significant analyst expertise, and specialized benchtop

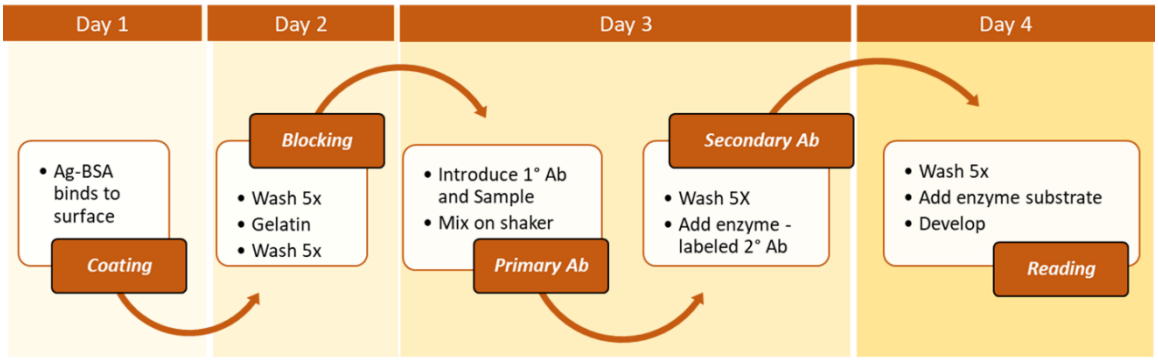

Figure 5-3. Typical competitive indirect ELISA workflow. The multi-day timeline begins by coating wells with a target-bovine serum albumin (BSA) conjugate. Following an overnight incubation, each well is washed multiple (e.g., 5) prior to gelatin introduction and incubation. After washing again (5X), the plate was incubated overnight. However, the section labeled 'Day 3' may be combined with Day 2 if desired. Aliquots of the test solution comprised of sample and primary antibody solutions were added to each well and incubated on the plate shaker prior to washing the wells (5X). After adding the enzyme-labelled secondary antibody, the plate was incubated overnight. Subsequently, after washing, an enzymatic substrate was added and incubated for 30 minutes in the dark to permit color development prior to reading. Following each overnight refrigerated incubation, the plate was equilibrated to room temperature for one hour prior to continued processing.

instrumentation (e.g., plate readers and washers).[38-39] Explicitly, conventional ELISAs require multi-day analysis with a multiplicity of manual washing steps and lengthy incubations that preclude generation of timely, actionable information. In order to streamline the performance of these steps, as well as provide semi-quantitative opioid detection, the capabilities of the original 'sandwich-style' VFI LoaD were expanded upon to allow on-disc ELISA adaptation.[40] Both assays leverage the unique advantages of centrifugal microfluidics to confer simple, rotationally-controlled flow, enabling the cascade of binding events required for immunodetection. This adaptation includes objective color interpretation strategies that facilitated sensitive, specific, and accurate microfluidic immunodetection with current, subjective fieldable color-based drug tests. Additionally, both approaches rely on incorporation of cellulosic matrices, but key functional differences between the sandwich-style and ELISA LoaDs were centered on how embedded membranes were utilized. In the original sandwich-style VFI, flowthrough was continuous, with the membrane used solely as structural support for immunodetection,[29] whereas in the ELISA LoaD, the embedded cellulosic matrices were used to augment control of centrifugally-generated flow.[40] As discussed in **Chapter 2** regarding on-disc dSPE, successful microfluidic ELISA performance requires spatiotemporal control over reagent delivery, incubation, and removal.[41-43] This was achieved here using embedded membranes that backed the ELISA chambers and acted as microvalves, permitting selective fluid retention and elution via carefully balancing rotational frequency with fluid surface tension in membrane pores. Membrane-modulated centrifugal flow permitted successful microfluidic adaptation of the ELISA workflow without the external fluidic triggers used in other approaches for actuation, such as magnets

or pneumatic pumps, that increase device size and cost.[41, 44] Since immunoassays are presently a key, validated tool in forensic and clinical analysis, future micro total analysis systems (μTAS) leveraging this technology could be easily integrated into existing workflows to enable rapid, on-site use.

5.2. Materials and Methods

5.2.1. Microdevice Fabrication

As in previous chapters, microdevices were fabricated according to the 'print-cut-laminate' method.[45] Architecture designed in AutoCAD® 2019 software (Autodesk Inc., San Rafael, CA) was ablated into five polyethylene terephthalate layers (PeT, 101.6 μm thickness, Film Source, Inc. Maryland Heights, MO) using a 50 W CO_2 laser (VLS3.50, Universal® Laser Systems, Scottsdale, AZ). Each device contained two discrete fluidic layers (2 and 4) containing microchannels (width = 0.6-1.1 mm) separated by an intervening 'via' layer (3). In this instance, the intervening layer was not used solely for laser valving. The via layer contained 'ports', or circular openings into which unbacked nitrocellulose membrane cutouts (7 mm diameter) (Whatman Protran® BA85 0.45 μm pore size, GE Healthcare, Little Chalfont, UK) were nested.[29] These membranes were effectively anchored in place by the heat-sensitive adhesive (HSA, 50.8 μm thickness, EL-7970-39, Adhesives Research, Inc. Glen Rock, PA) coating material layers 2 and 4 upon device lamination (UltraLam 250B, Akiles Products, Inc., Mira Loma, CA).[45-46] Where necessary, polymethyl methacrylate (PMMA, 1.5 mm, McMaster-Carr, Elmhurst, IL or 0.5 mm, Astra Products, Copiague, NY) accessory pieces added via pressure-sensitive adhesive (PSA, 55.8 μm thickness, ARcare 7876, Adhesives Research, Inc.) augmented chamber volume. Devices were cured under weights (~4.5 kg) overnight prior to use.

5.2.2. Antibody and Conjugate Synthesis

Anti-morphine monoclonal antibodies (mAbs) from murine hybridoma clone HY4-1F9,[47] were purified from hybridoma supernatant via Protein A Sepharose (GE Healthcare) chromatography, sterilized by 0.2 μm filtration, and stored in sterile phosphate-buffered saline (PBS) with no preservative. A morphine-based hapten with a tetraglycine linker was synthesized and conjugated to bovine serum albumin (BSA) by carbodiimide chemistry according to published procedures.[48-49] The resultant morphine-BSA conjugate (M-BSA) was dialyzed against PBS. Both antibodies and conjugates were stored at 4°C.

5.2.3. Reagent Preparation

Coating buffer (0.20 M) was made according to manufacturer's instructions by dissolving one capsule of BupHTM carbonate-bicarbonate powder (Fisher Scientific, Waltham, MA) in 100 mL deionized water, then diluting to 0.05 M. Phosphate buffered saline – Tween (PBS-T) was prepared at 1X by diluting 50 mL 20X concentrate (Fisher Scientific) to 1.0 L in deionized water. Blocking buffer was comprised of 1% gelatin (Fisher Scientific) in 1X PBS-T (Fisher Scientific). Lyophilized horseradish peroxidase (HRP)-labelled goat anti-mouse antibodies (2˚ Ab, Peroxidase AffiniPure Goat Anti-Mouse IgG (H+L), Jackson ImmunoResearch Laboratories, Wet Grove, PA) were reconstituted in 2 mL deionized water. Antibody stock solutions, drug standards (1 mg/mL, Cerilliant Corporation, Round Rock, TX), procaine hydrochloride (Millipore Sigma, Burlington, MA), caffeine (Millipore Sigma), and sucrose (Fisher Scientific) were diluted to desired concentrations in 1X PBS-T. In some instances, artificial urine was used as the diluent for drugs or adulterants instead. Specifically, artificial urine was constructed via dissolution of urea (1.254 g), sodium chloride (0.451 g), ammonium chloride (0.151 g),

creatinine (0.100 g), disodium phosphate (0.127 g), monopotassium phosphate (0.125 g), and sodium sulfite (0.152 g) in 50 mL deionized water.50 Artificial body fluids were stored at 4°C. Test solutions were comprised of 1:10 mixtures of a given drug and/or adulterant to 2 µg/mL primary anti-morphine mAb (1˚ mAb) by volume. For visualization, Sigmafast HRP substrate o-phenylenediamine dihydrochloride (OPD) (MilliporeSigma, St. Louis, MO) was prepared according to manufacturer's instructions. Stop solution was comprised of 20 mg/mL aqueous oxalic acid (Fisher Scientific).

5.2.4. High-Speed Videography

A custom high-speed video system (HSVS) built in-house was used to empirically characterize flow rates through embedded membranes. Video was recorded by a a MotionBLITZ EoSens® mini high-speed CMOS recording camera (Mikrotron-GmbH, Unterschleißheim, Germany), augmented with a TV ZOOM LENS G6X16 16–100 mm 1:1.9 1" macro (Mikrotron-GmbH), and controlled using MotionBLITZDirector software v.2 1.4.0.1 (Mikrotron-GmbH). Illumination of microdevice features was achieved by a Nova-Strobe PBL LED portable stroboscope (Monarch Instrument, Amherst, NH). Strobing and LoaD rotation were controlled by a mechatronic spin system comprised of a stepper motor (Sanmotion series, Sanyo denki, Moriguchi, Japan), stepper motor driver (drv8801), photo-interrupting optical switch (TT Electronics/Optek Technology, Woking, UK), and an 8-core microcontroller (Propeller P8X32A-M44; Propeller Inc., Rocklin, CA). Discs used for these tests contained embedded BioRad nitrocellulose membranes with 0.2 µm pore size (BioRad, Hercules, CA) and possessed linear gradations rastered into the PeT loading chamber coverlets at 1 mm increments. After a 200 µL aliquot of a given fluid (buffer, artificial urine, artificial blood plasma) was added to the loading chamber of a

single domain, the LoaD was rotated at a fixed, constant frequency. Tests were performed at frequencies beginning at 750 rpm and increasing by 250 rpm increments up to and including 2000 rpm. The time at which the fluid meniscus crossed each rastered demarcation was recorded. Subsequent data analysis and visualization were performed in R Studio (R v.3.5.1 and RStudio v.1.1.456).

5.2.5. ELISA Performance

5.2.5.1. Traditional ELISA Protocol

Individual wells in a 96-well plate were first coated with M-BSA (100 µL, 0.05 µg/mL in carbonate coating buffer) during overnight incubation at 4°C in a sealed box with damp paper towel. The plate was equilibrated to room temperature (1 hour), and each well was washed (1X PBS-T, 5 X 250 µL) by pipette, then filled with blocking buffer (300 µL). Following a 1-hour room temperature incubation, each well was washed five times with 450 µL aliquots of 1X PBS-T. After overnight incubation at 4°C, the plate was again equilibrated to room temperature, the wells emptied, then filled with test solutions (100 µL), mixed for 90 minutes on a plate shaker, and incubated for 30 minutes at room temperature. After washing with 5 sequential 250 µL aliquots of 1X PBS-T, the 2˚ Ab solution (100 µL, diluted 1:30,000 from stock) was added to each well and incubated at 4°C overnight. After equilibration to room temperature, each well was washed five times with 250 µL 1X PBS-T prior to addition of 100 µL OPD. After a final incubation at room temperature in the dark for 30 minutes, 100 µL stop solution was added to each well and device images were captured.

5.2.5.2. On-Disc ELISA Protocol

Device rotation was driven by a DC brushless motor regulated using a 32-bit multi-processing microcontroller (Propeller P8X32A-M44; Propeller, Inc.). Within each domain, sequential fluidic steps were achieved via solution addition to the loading chamber (6.2 mm W x 19.7 mm H), centrifugal pumping into the ELISA chamber (1.5 mm thickness PMMA, diameter = 3.6 mm) for incubation and/or mixing, and finally flow into the outflow chamber (approx. 34.1 mm W x 9.5 mm H). Following M-BSA introduction to the ELISA chambers (70 µL each, 0.20 µg/mL, 14.0 g, 5 s), the microdevice was incubated at 4 ˚C overnight in a sealed vapor barrier bag (Uline, Pleasant Prairie, WI) that also contained a damp (deionized H2O) paper towel. Next, the device was equilibrated to room temperature (1 hour), ELISA chambers were emptied (224.5 g, 120 s), and washed with a single 150 µL aliquot of 1X PBS-T (224.5 g, 120 s). Blocking buffer (70 µL) was added to each ELISA chamber (14.0 g, 5s) and incubated for 1 hour at room temperature to yield a ready-to-use device. Upon assay initiation, ELISA chambers were emptied (224.5 g, 120s), and each was washed with 150 µL 1X PBS-T (224.5 g, 120 s) then filled with test solution (40 µL, 14.0 g, 5 s) prior to batch mode mixing (1.3 g, 15 cycles, 20 s each direction). After emptying (224.5 g, 120 s) and washing (150 µL 1X PBS-T, 224.5 g, 120 s) ELISA chambers, 2˚ Ab was introduced (40 µL, diluted 1:28,600 from stock, 14.0 g, 5s) and incubated overnight at 4˚C. After equilibration to room temperature, ELISA chambers were emptied (224.5 g, 120 s), washed (150 µL 1X PBS-T, 224.5 g, 120s), filled with OPD (40 µL, 14.0 g, 5 s), and developed in the dark (30 min).

5.2.5.3. Rapid On-Disc ELISA Protocol

Each ELISA chamber (0.5 mm thickness PMMA, diameter = 3.6 mm) was coated with M-BSA (28.8 µL, 0.48 µg/mL; 14.0 g, 5 s) and incubated at 4 ˚C overnight as described above. Following equilibration to room temperature (1 hour), ELISA chambers were emptied (224.5 *g, 10 s) and each was washed with 61.8 µL 1X PBS-T (224.5 g, 10 s) prior to filling with blocking buffer (28.8 µL, 14.0 g, 5 s). After incubation at room temperature for 1 hour, ELISA chambers were emptied (224.5 g, 120 s) and washed (61.8 µL 1X PBS-T, 224.5 g, 120 s). Test solution (16.48 µL, [mAb=4.8 µg/mL]) was added to ELISA chambers (14.0 g, 5 s), then mixed (1.3 g, 15 cycles, 20 s each direction). ELISA chambers were emptied (224.5 g, 5 s), washed (61.8 µL 1X PBS-T, 224.5 g, 10 s), then filled with 2˚ Abs (diluted 1:11,800, 16.48 µL, 14.0 g, 5 s). After mixing (1.3 g, 15 cycles of 20 s each direction), ELISA chambers were emptied (224.5 g, 5 s), washed (61.8 µL 1X PBS-T, 224.5 g, 10s), filled with OPD (16.48 µL, 14.0 g, 5 s), then developed in the dark (30 min).

5.2.6. Colorimetric Interpretation and Analysis

All disc images were captured using an Epson Perfection V100 Photo desktop scanner (Seiko Epson Corporation, Suwa, Nagano Prefecture, Japan). Empirical image analysis was conducted via our previously published ‘crop and go’ technique in the Fiji distribution of ImageJ freeware.[51-53] Briefly, circular regions of interest (80-pixel diameter) from the center of the ELISA chamber were selected and converted to 3-slice image stacks (red-green-blue, hue-saturation-brightness). Mean values of individual parameters were measured individually.

5.3. Results and Discussion

Like the nucleic acid preparation methods described in **Chapters 2 and 3**, successful implementation of enzyme-linked immunosorbent assays (ELISAs) mandates on-disc performance of several sequential, temporally resolved fluidic steps in the requisite order. Traditionally, fluid introduction and removal from microtiter plate wells was achieved by pipette during highly manual, time-intensive workflows tethered to traditional laboratory equipment and facilities. To provide a portable alternative, a lab-on-a-disc (LoaD) was designed with embedded membranes that modulated centrifugally-driven fluidics during immunocapture events and colorimetric detection. Upon the application of sufficient centrifugal force, flowthrough occurred orthogonally through the membrane rather than perpendicularly, as in lateral flow immunoassays (LFIs). The so-called orthogonal flow immunoassay (OFI) method was originally developed to accommodate single-step sandwich-style immunodetection during continuous fluid passage through the membrane.[29] However, successful on-disc ELISA performance required intermittent flow for successive delivery, incubation, and removal of numerous different reagents. Balancing rotationally-controlled fluidics with the resistance provided by embedded membranes permitted their implementation as automatable, rotationally-controlled microvalves. Ultimately, this new on-disc functionality permitted the cascade of on-board affinity-based binding events that ultimately enable sensitive, specific colorimetric opioid detection both in buffer and mock clinical samples with minimal equipment requirements. Inclusion of a simple, cost-effective, and objective image analysis strategy eliminated the subjective, and therefore potentially erroneous, interpretation that plagues many colorimetric tests.[11]

5.3.1. Microfluidic Design

The multiplexed ELISA LoaD, designed with a view towards high throughput, is capable of processing 8 samples in parallel (**Figure 5-4**). PMMA accessory pieces augmented the depth of the ELISA chamber to permit retention of larger fluid volumes. Concurrently, this also served to increase the path length for monitoring colorimetric responses, therefore improving sensitivity according to Beer-Lambert's Law. Within each device, two distinct fluidic layers interfaced solely at ports containing embedded nitrocellulose membranes. As described in **Chapter 4**, circular membranes nested into the central device layer (3) were effectively anchored in place by the heat-sensitive adhesive (HSA) coating the adjacent material layers (2 and 4) during device lamination. Although the membrane incorporation strategy was analogous in both methods, the membrane composition differed greatly. For inward fluid displacement (**Chapter 4**), embedded polytetrafluoroethylene (PTFE) membranes served to permanently sequester liquid

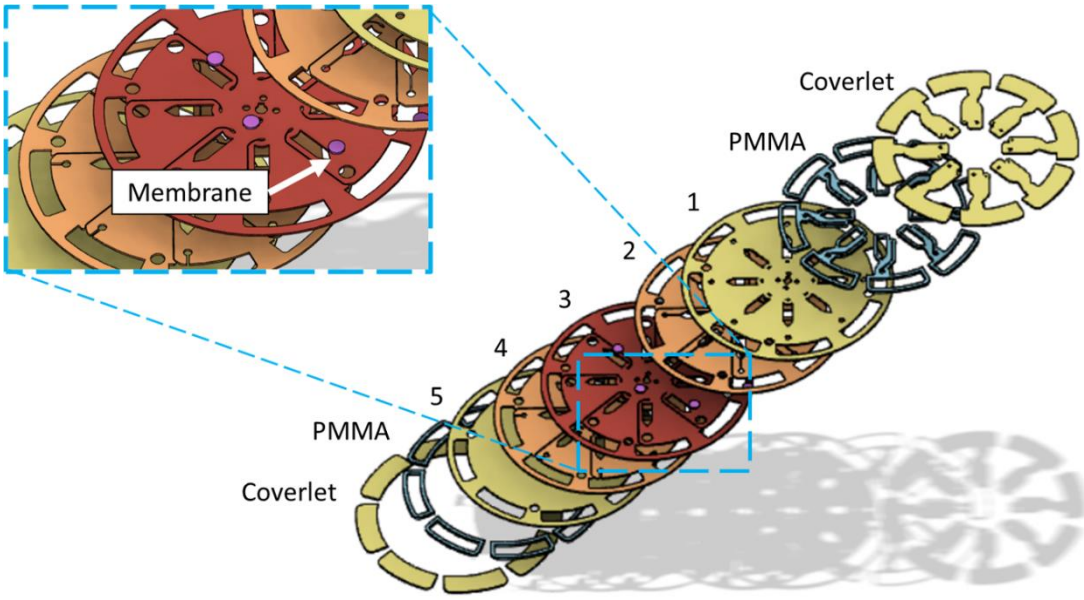

Figure 5-4. Isometric exploded view of an ELISA LoaD. The five core PCL device layers (1-5) were augmented on both sides with PMMA accessory pieces. Circular laser-cut nitrocellulose membranes were nested into cutouts in the central material layer (3) and became anchored in place by activation of the heat-sensitive adhesive on both adjacent layers (2 + 4) during device lamination. The two primary fluidic layers were contained in material layers 2 and 4.

reagents while freely permitting gas exchange. Conversely, a key function of the nitrocellulose membranes in microfluidic ELISA performance is centered on permitting liquid passage (**Figure 5-5**).

In each sequential assay step, discussed in detail in the next section, fluid added to the loading chamber was centrifugally pumped into the ELISA chamber through a microchannel in the top fluidic layer (dashed, white arrows). Continued centrifugation redirected fluid orthogonally through the membrane which backed the dead-end ELISA chamber (dashed, blue arrows). Upon entering the second fluidic layer, centrifugal flow was reinstated during solution transfer to the outflow chamber (**Figure 5-5A**). Proof-of-

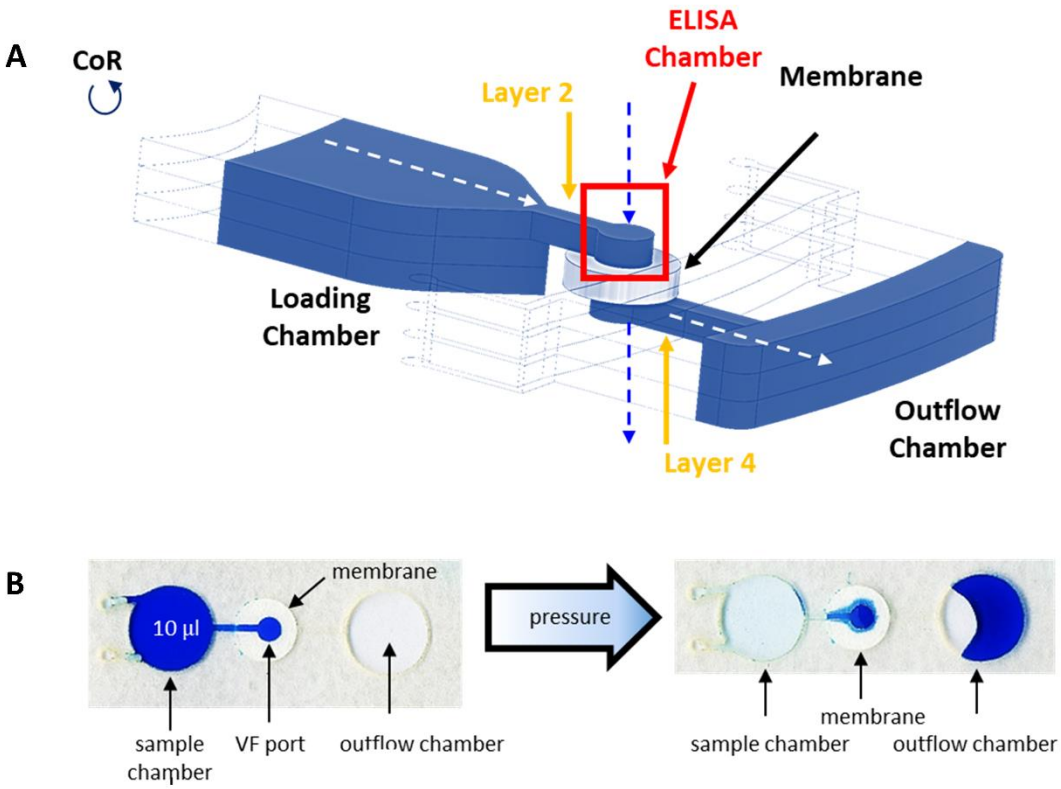

Figure 5-5. Fluid flow path through embedded membranes. (A) After fluid is added to the loading chamber, device rotation is driven radially outward from the CoR, depicted by white arrows. When fluid flows through a channel in material layer 2 (fluidic layer 1), it reaches the dead-end ELISA chamber (red box) backed by an embedded cellulosic membrane. Upon continued centrifugation at a sufficient frequency, flow is orthogonally redirected through the embedded membrane (blue arrows) prior to entering a channel cut into material layer 4 (fluidic layer 2) and to continue radially outward passage (white arrow) into the outflow chamber. Adapted from [40]. (B) Proof-of-principle on-disc orthogonal flow of aqueous dye solutions through embedded membranes within a LoaD driven by centrifugally-generated pressure. Adapted from [36].

principle membrane flowthrough via rotationally-generated pressure was visualized using an aqueous dye solution (**Figure 5-5B**). After centrifugation, dye retained in the membrane was concentrated solely around the inlet channel and orthogonal flow (OF) port. Thus, it was apparent that flow occurred through, not around, the membrane due to the tight, leak-free seal facilitated by HSA within the microdevice; bypass would have been visually obvious in the form of dye at the membrane periphery. However, these pilot studies involved continuous fluid flow through the membrane. While this was well-suited for the single-step sandwich-style immunoassay described by Woolf et al.,[29] ELISAs require a multiplicity of processing steps, including incubations and mixing, that require intermittent fluid retention. Consequently, to permit successful ELISA integration, utilizing the membranes as reversible microvalves for successive, repeated cycles of flow permission and prevention was explored.

5.3.2. On-Disc ELISA Principles and Demonstration

Achieving selective fluid retention relied on balancing rotationally-generated centrifugal force with the surface tension at membrane pores, or the liquid entry pressure (LEP).[54] Here, embedded membranes act as normally-closed valves, with LEP opposing centrifugal force to resist radially outward flow.[54-55] As centrifugal force, and the resultant pressure, scale with the square of rotational frequency, fluid penetration into the membrane could be controlled simply by tuning the rotational frequency.[56] In each fluidic assay step, flow was first directed into the ELISA chamber via a low-speed spin such that insufficient pressure was generated to drive flow through the membrane (f_ω<LEP), and the solution was retained (**Figure 5-6**). Low-frequency unit operations could then be conducted to promote affinity-based interactions, including stationary incubations and low-speed batch

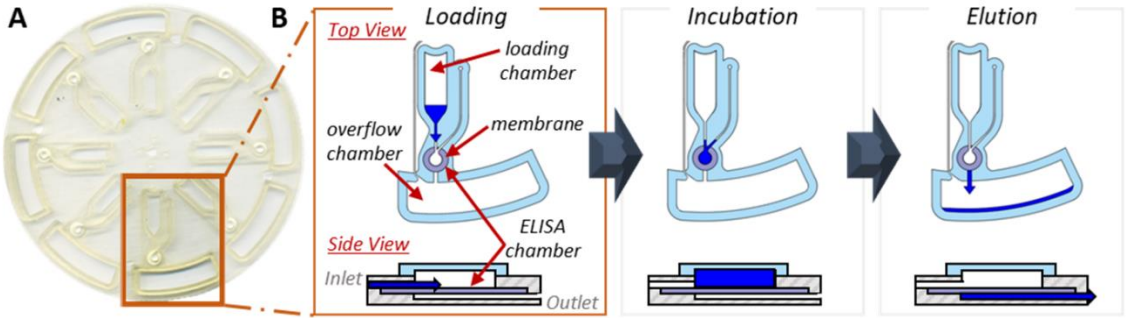

Figure 5-6. On-board membrane-based flow control. (A) Image of an 8-plex microdevice with a single domain boxed in red. (B) Labelled AutoCAD renderings of top and side views of a single domain architecture. In each fluidic step, a solution is added to the loading chamber, then pumped into the ELISA chamber via low-speed LoaD rotation. The fluid could be retained for incubation and/or mixing prior to high-speed LoaD rotation to pump the solution through the membrane to the outflow chamber. Adapted from [40].

mode mixing. Active mixing promoted affinity-based binding events by minimizing reliance on diffusion, which is common in traditional 96-well plate assays.[57] A subsequent high-frequency spin (f_ω>LEP) forced fluid orthogonally through the membrane and out of the ELISA chamber (**Figure 5-6**). Though membranes embedded within a LoaD have been used previously for flow control, these were single-use, sacrificial valves that acted analogously to conventional capillary valves to permit sequential reagent release at varied frequencies.[55] Here, through careful juxtaposition of f_ω with LEP, membranes instead provided reversible flow control for repeated addition and removal of numerous solutions to and from a single chamber. It was hypothesized that this microvalving strategy could permit performance of the numerous discrete fluidic steps required for on-board ELISAs.

Ultimately, both LoaD preparation and analysis were directly contingent upon this novel flow modulation strategy (**Figure 5-7**). For on-disc morphine detection, low-frequency centrifugation was first used to introduce and retain an M-BSA conjugate solution within the ELISA chamber. This step was followed by incubation, during which M-BSA adsorbed to, or "coated", internal device surfaces. After coating, a high-speed spin drove the supernatant through the membrane such that the chamber could be blocked with

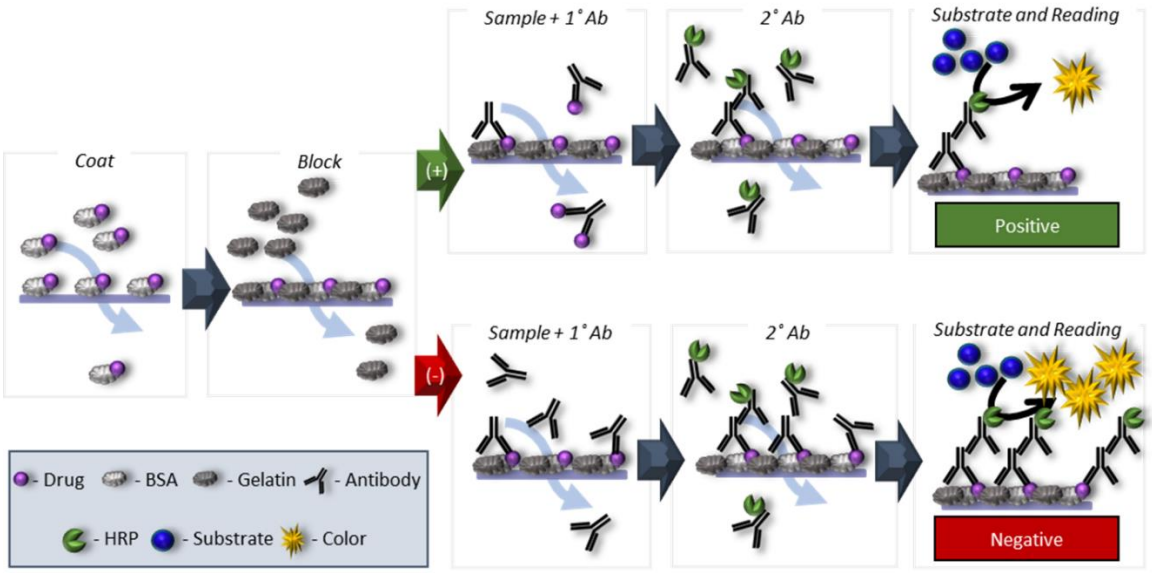

Figure 5-7. Diagrammatic molecular depiction of on-disc ELISA performance. On-disc workflow mirrored the traditional 96-well plate protocol. Device surfaces were first coated with a drug-BSA conjugate, then blocked. Differentiation of positive and negative ELISA results began with introduction of a test solution (sample and 1˚mAbs) into the ELISA chamber, 1˚ mAb binding sites. In positive samples (top lane), 1˚ mAb binding sites are occupied by Ag in the sample, precluding Ab interaction with conjugate drug coated on device surfaces. Conversely, in negative samples (bottom lane), no drug was present in the sample, so 1˚ mAbs binding sites were free to bind the drug conjugate on assay surfaces, effectively anchoring the 1˚ mAbs in place. Enzyme-labelled 2˚ Abs with affinity for the 1˚ Ab species were then introduced and bound surface-anchored 1˚ mAbs. Because fewer 1˚ Abs were retained in positive samples, fewer 2˚ Abs were subsequently retained in the ELISA chamber than in negative samples. Detection was enabled via introduction of a chromogenic substrate; enzymatic conversion of the colorless substrate to a yellow product provided colorimetric readout. Adapted from [40].

gelatin to prevent downstream non-specific Ab adsorption. To further minimize such off-target binding events, the ELISA chamber was washed prior to introduction of each successive fluid; buffer (1X PBS-T) was passed through the membrane to remove unbound components and mitigate downstream nonspecific chromogenesis. Following LoaD preparation, analysis could be conducted. First, a test solution containing both sample and 1˚ mouse anti-morphine monoclonal antibodies (mAbs) was introduced. For positive samples, morphine (Ag) present in the sample was bound by 1˚ Ab to yield Ab-Ag complexes. With their binding sites were occupied, 1˚ Abs were unable to interact with M-BSA coating device surfaces; unbound Ab-Ag complexes were eluted from the ELISA chamber through the membrane.[22] Conversely, if no Ag was present in negative samples, 1˚ Ab binding sites remained available to bind the coated M-BSA. In these instances, 1˚

Abs effectively become anchored to microdevice surfaces and remained in the ELISA chamber during centrifugal supernatant removal. Regardless of sample composition, batch mode mixing was performed during test solution retention in the ELISA chamber to facilitate and expedite any binding events. Next, secondary horseradish peroxidase (HRP)-labelled goat anti-mouse Ab (2˚ Ab) bound anchored 1˚ mAbs, then acted as transducer elements for signal output via enzymatic production of an optically-detectable (yellow) compound.[58] Due to the competitive assay format, fewer 1˚ Abs remained in the ELISA chamber in positive samples than in negative tests. Consequently, positive samples also exhibited diminished 2˚ Ab retention, and thus fewer enzymes remained for catalysis. Therefore, the magnitude of chromogenic response was inversely related to morphine concentration of the sample, with negative samples yielding a distinctly more intense color than positive counterparts.

Early on-disc pilot studies aligned with these theoretical results, both on-disc and using the traditional microtiter plate format (**Figure 5-8**). In both instances, pale yellow responses of positive samples (100 ng/µL morphine) were much less saturated, or intense, than the dark orange color produced via analysis of negatives (no morphine). Qualitatively, the magnitude of these colorimetric responses appeared visually comparable between plate assays and regions of interest (ROIs) cropped from microfluidic ELISA chambers. These high-concentration

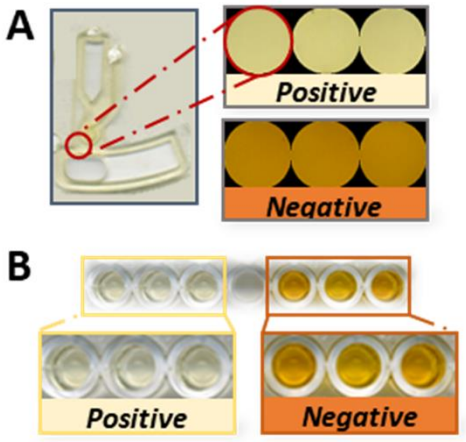

Figure 5-8. Proof-of-concept microfluidic ELISA. Images of parallel positive (100 ng/µL morphine) and negative (no morphine) colorimetric ELISA responses obtained using (A) LoaD, and (B) a microtiter plate. In both formats, experimental and theoretical results aligned, with negative responses exhibiting increased saturation relative to positives. Adapted from [40].

positives were readily distinguished from negatives by eye, but differences between negatives and lower concentration morphine samples were not as apparent. These observations, along with known variation and shortcomings of naked eye detection, necessitated incorporation of an empirical, objective image analysis method to ensure accurate, reliable results.[5-6, 51]

5.3.3. Semi-Quantitative Visual Analysis

To enable robust, semi-quantitative interpretation of colorimetric ELISA results, several distinct image parameters were explored. Colorimetric analytical chemical data is most commonly measured and reported using the hue-saturation-brightness (HSB) and red-green-blue (RGB) color spaces – abstract models that quantitatively define the range of colors perceived by human vision (**Figure 5-9**).[51] The RGB model served as a logical starting point since it is used in the majority of portable image capture platforms, including smartphones and the desktop scanner used here.[11] This additive tristimulus system numerically defines each color as a tuple containing three values which independently

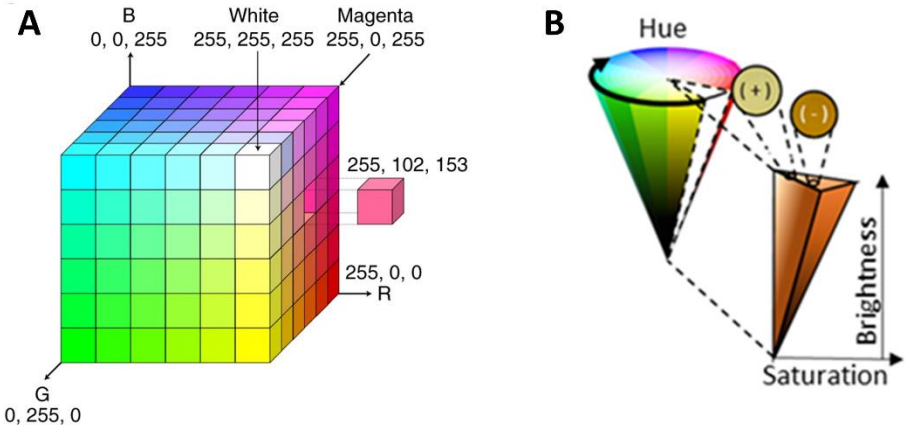

Figure 5-9. Visualizations of the RGB and HSB color spaces. (A) Tristimulus 8-bit RGB system in which each color is numerically represented as a tuple comprised of red, green, and blue components, whereas hue (H), saturation (S), and brightness (B) are represented as a value between 0 and 255. Adapted from [51] (B) In the conical representation of the HSB color space, hue is represented by the circular, top face and describes a unique color. Saturation and brightness reflect color intensity and/or richness. Inset Image crops taken from positive and negative ELISA responses were inserted in the appropriate area. Adapted from [40].

represent red, green, and blue primary contributions.[51, 59] However, the HSB color space has been reported to be more intuitive, and therefore easier to use, especially for inexperienced analysts.[11] Hue and saturation are especially useful in characterizing color changes. Hue can be thought of as continuous band of color analogous to the color wheel, where each color is defined by a single value; saturation represents a color's "purity" or intensity.[11, 51, 59]

Initial characterization of ELISA results in the traditional microtiter plate format was in both color spaces (**Figure 5-10**). All colorimetric analyses performed leveraged the "crop-and-go" approach described by Woolf et al.[51] Briefly, a circular ROI was selected from the chamber or well where immunodetection occurred. After clearing the pixels outside the ROI, the native 8-bit RGB image was converted to a 3-slice stack (either RGB or HSB) and each parameter was processed individually. Direct juxtaposition of results in each channel clearly demonstrated saturation and blue contributions as the most useful for semiquantitative detection. Red and green contributions exhibited only minor differences across conditions, but negative samples exhibited greatly diminished blue values relative to positives. These findings aligned with literature reports for such colorless-to-colored

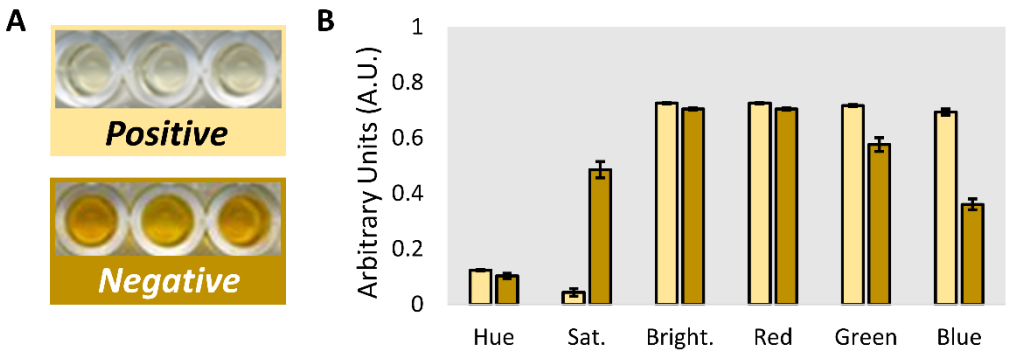

Figure 5-10. Morphine detection in a traditional, plate-based ELISA. (A) Images of endpoint ELISA results for proof-of-concept morphine detection. (B) Empirical analysis of individual image parameters within both the HSB and RGB color spaces (n = 3 each). Saturation and blue contributions provided the clearest differentiation between positive and negative samples.

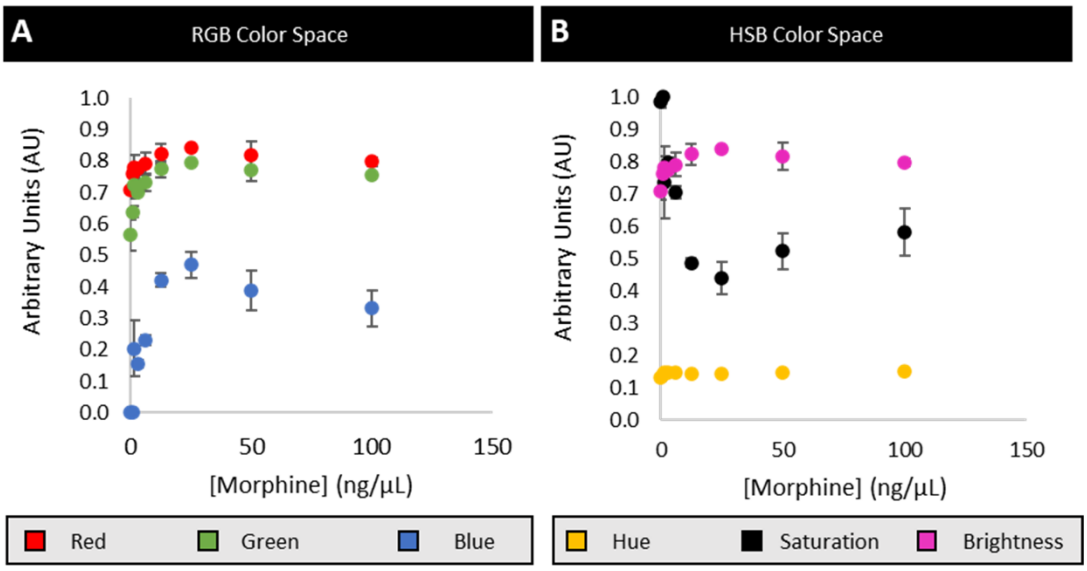

Figure 5-11. Empirical image analysis for semi-quantitative detection. Analysis of individual image parameters from serially diluted morphine (1:2, 100 - 0.8 ng/µL) was analyzed on-disc (n = 3). (A) Among RGB parameters, analysis of the blue contribution provided the most facile differentiation of color responses across samples with various concentrations of morphine. Similarly, (B) in the HSB color space, saturation scaled with concentration and provided the most sensitive morphine detection, with high discrimination between positive and negative responses. Adapted from [40].

monotonal transitions, wherein changes in only one channel are commonly reported.[51, 60] For example, the pH indicator phenolphthalein is colorless within neutral and acidic pH ranges, but the pink color generated with increasing basicity can be quantitatively monitored using the red channel alone.[60] Thus, it would be reasonable to leverage the blue contribution for semi-quantitative opioid detection. However, saturation measurements are more easily understood and known to be useful for colorless-to-colored responses such as those seen here and in Chapter 2.[51, 60-61] As expected given the visually apparent increased darkness in negative results, there was a large discrepancy between empirical saturation values measured from positive and negative tests. Hue is well-understood to be uninformative in characterizing monotonal color changes, so it was expected that measured hue values were effectively the same across conditions.[51] Because saturation provided the best combination of discriminatory power and intuitive interpretation, it showed the most promise for semi-quantitative morphine detection.

Although anticipated, it was essential to establish that these trends were mirrored during on-disc analyses. Here, the dependence of each color parameter on morphine concentration was also explored (**Figure 5-11**). As expected, the same trends emerged, with saturation and blue again providing the best discrimination between positives and negatives. Additionally, both parameters scaled with concentration between approximately 0 and 12.5 ng/µL (linear ranges) prior to plateauing at a constant value. As predicted from the data taken from traditional plate-based ELISAs, blue scaled directly with concentration, whereas saturation indicated an inverse relationship. Since saturation exhibited a more pronounced difference between negative (no morphine) and positive (25, 50, and 100 ng/µL morphine) samples at the plateau (0.419 > 0.332 A.U.), it was selected for further use.

Accordingly, saturation analysis was used in early on-disc assay optimization to streamline the washing protocol (**Figure 5-12**). Effective washing removes bound reagents, prevents nonspecific chromogenesis, and is imperative for successful ELISA

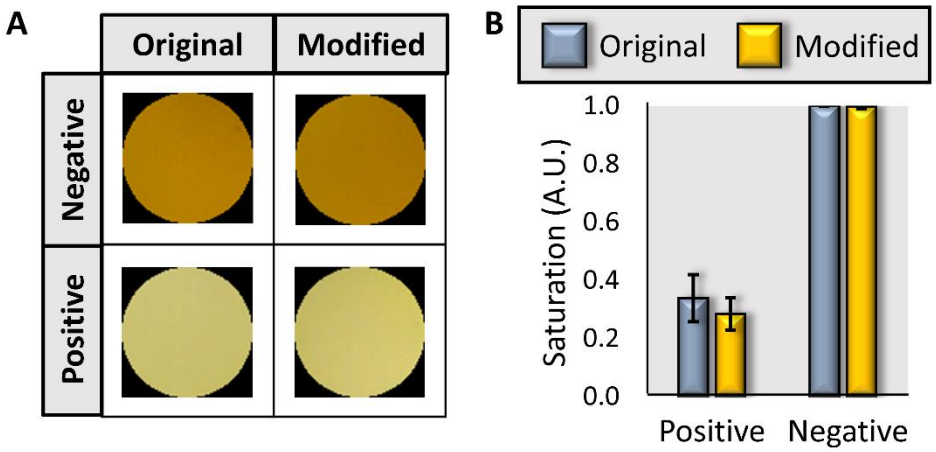

Figure 5-12. Characterization of the simplified washing method. The original wash protocol involved pumping 5 sequential, discrete 30 µL PBS-T washes through the membrane to remove unbound assay reagents. To simplify on-disc workflow, combining these aliquots into a single 150 µL wash was explored. (A) Representative images of both colorimetric positive (100 ng/µL morphine) and negative responses using each protocol. Visually, the results appear comparable across methods. (B) Saturation measurements taken from both positive and negative responses using both wash methods are statistically similar, indicating that a single wash aliquot could be implemented without detriment to assay performance (n = 3 each).

performance.[41-43] Traditionally, washing requires the addition, and subsequent removal, of numerous small volume buffer aliquots. Since complete fluid removal from microtiter wells is not practically feasible, this iterative washing repeatedly dilutes residual reagents, thereby facilitating their effectual removal. Initial pilot studies mirrored this workflow on-disc but it was not conducive to automation and remained laborious. However, it was hypothesized that the lack of dead volume within the membrane-backed, circular ELISA chambers would allow for more complete fluid removal, permitting a single-step fluidic wash procedure. Evaluation of positive sample saturation across methods informed on washing performance; elevated saturation would indicate unwanted retention of assay reagents and chromogenesis not attributable to on-target immunodetection. Fortunately, according to an unpaired t-test for means ($\alpha = 0.05$), the saturation values obtained on-disc using the original and modified washing protocols were statistically similar ($p = 0.456$). Therefore, a single large volume wash effectively removed assay components, and ultimately prevented non-specific chromogenesis. Detriment to analysis of the saturation values for negatives was not expected or observed; these saturation values were also found to be statistically similar across methods ($p = 0.423$). Therefore, this expedited and streamlined washing protocol did not negatively affect assay performance and was used in all subsequent testing.

5.3.4. Microfluidic ELISA Characterization

As mentioned in the introduction to this chapter, existing fieldable colorimetric drug tests possess key operational limitations that preclude reliable implementation. Thus far, the subjectivity inherent to many chromogenic tests has been eliminated through incorporation of impartial image analysis. This analytical method was used to empirically

determine whether the ELISA LoaD successfully addressed the other shortcomings of common color tests. First, the sensitivity of microfluidic immunodetection was explored. Assay discriminatory power was then probed to determine if class-based differentiation could be further refined. Finally, it was necessary to establish that false positive responses were avoided during analysis of innocuous, uncontrolled compounds.

4.3.4.1. Sensitivity

Saturation was used to semi-quantitatively detect serially-diluted (1:2) morphine, ranging in concentration from 0.8-100 ng/µL. An empirical threshold for detection was established as three standard deviations below the mean negative saturation value (0.89 A.U.) Measured saturation values above (red region) and below (green region) threshold were considered to be colorimetrically negative and positive, respectively (**Figure 5-13**). Notably, only the lowest concentration morphine samples (0.8 ng/µL) were determined to be negative, exhibiting a mean saturation value that fell above the threshold and was

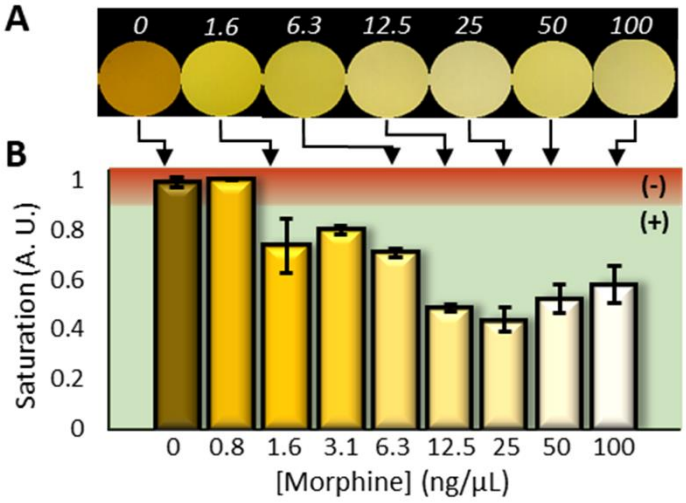

Figure 5-13. Optical on-disc sensitivity characterization. (A) Representative crops from serially-diluted morphine (1:2, 100 – 0.8 ng/µL, n=3) analyzed on-disc. (B) At each concentration, histogram bars represented the mean saturation value and error bars represented one standard deviation in each direction. A threshold for semiquantitative morphine detection was established three standard deviations below the mean saturation of the negative control. Saturation values in the above (red region) and below (green region) were determined as colorimetrically negative and positive, respectively. Of the samples tested, all those with morphine concentrations ≥1.6 ng/µL were experimentally positive. Adapted from [40].

statistically similar to the saturation of the negative control according to an unpaired t-test for means ($\alpha = 0.05$, $p = 0.424$). All other samples exhibited saturation values below the established threshold and were therefore colorimetrically positive. Morphine was successfully detected at the ng/µL level, well below capabilities of current ampoule methods, which have limits of detection on the order of micrograms.[6] Low sensitivity of ampoule-based drug tests equate to large sampling requirements (4-6 mg/mL), which are adequate to cause serious analyst intoxication.[5, 7] Here, improved assay sensitivity allows for smaller sample masses that minimize the potential for analyst exposure to dangerous substances.

Given the well-publicized issues concerning the high prevalence of false positive results in current colorimetric tests,[14] emerging alternatives must exhibit greatly enhanced specificity. Since Ab-Ag interactions are highly specific, it was anticipated that only morphine and closely related compounds would elicit positive responses. This was characterized here using two panels of compounds, other illicit/controlled substances and common adulterants.

4.3.4.2. Specificity

Illicit Substances

A panel of drugs spanning numerous classes was tested (50 ng/µL, n = 5 each) and the results were colorimetrically evaluated (**Figure 5-14**). In addition to the expected positive result obtained from morphine, three other compounds elicited statistically similar saturation values well below the threshold for detection (Single Factor ANOVA, $\alpha = 0.05$, $p = 0.310$), namely heroin, codeine, and morphine-6-glucuronide (M-6-G), a key opiate metabolite. Each of these substances belongs to a subclass of opioids known as opiates,

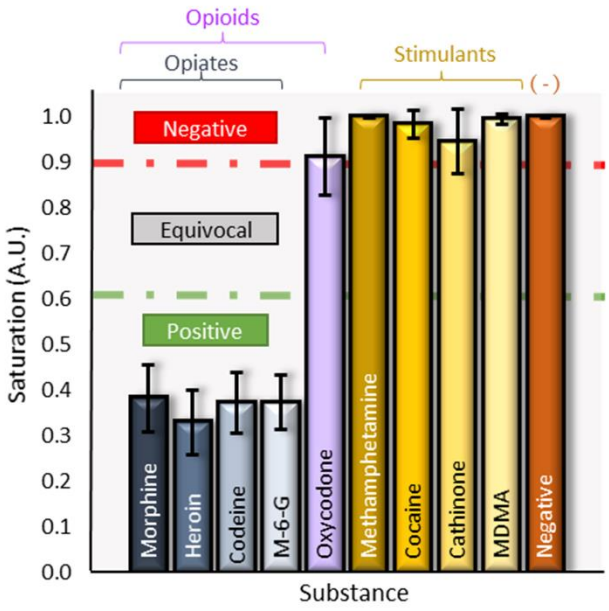

Figure 5-14. Assessment of a panel of illicit substances. A panel of controlled substances were evaluated. Only opiates (blue bars) exhibited measured positive saturation values, whereas stimulants (yellow) and a synthetic opioid (purple) were colorimetrically negative. All substances were evaluated with concentrations of 50 ng/µL (n = 5 each). Adapted from [40].

which are naturally occurring compounds. Interestingly, on-disc analysis of oxycodone, a synthetic opioid (e.g., not an opiate), failed to yield positive results. Thus, opiates could be differentiated from the broader category of opioids. Other non-opioid substances, including amphetamines (methamphetamine, 3,4-methylenedioxidemethamphetamine (MDMA)), cocaine, and a synthetic cathinone, were colorimetrically negative with saturation values statistically similar to negative controls (Single Factor ANOVA: $\alpha = 0.05$, $p = 0.133$). However, replicate tests for some substances exhibited variability such that standard deviations crossed the threshold for negativity. To address this, a second threshold (0.603 A.U.) was implemented three standard deviations above the mean morphine (50 ng/µL) saturation value. While all samples with saturation measurements below this second threshold were unquestionably positive, values that fell between the two thresholds were said to be inconclusive, or 'equivocal', and require reanalysis using confirmatory tests. This analytical strategy aligns with current clinical guidelines that dictate all positives and

any unexpected negatives undergo confirmatory testing to ensure accuracy.[62] Since the ELISA LoaD platform is intended for presumptive testing, downstream confirmatory testing of all samples not clearly within the negative range would be conducted regardless. In summation, better than class-based discrimination was possible using the ELISA LoaD, with essentially no cross-reactivity of the 1˚ mAb with the non-opiate substances evaluated. Therefore, this method displayed minimal risk for false positive results.

Common Adulterants

The effect of adulterants commonly found in seized illicit drug samples, namely caffeine, procaine, and sucrose, was also explored (**Figure 5-15**).[63] Though false negatives were not anticipated, this was confirmed experimentally. Analysis of mixtures of heroin and adulterants (50 ng/µL each) produced mean saturation values statistically similar with the positive (heroin only) control (Single Factor ANOVA, $\alpha = 0.05$, $p = 0.306$). False positive responses were of far more concern, given the known propensities of existing tests for this result. To determine if any of these substances would yield false positive ELISA responses, high-concentration (50 ng/µL) dilutions of each adulterant were evaluated. This

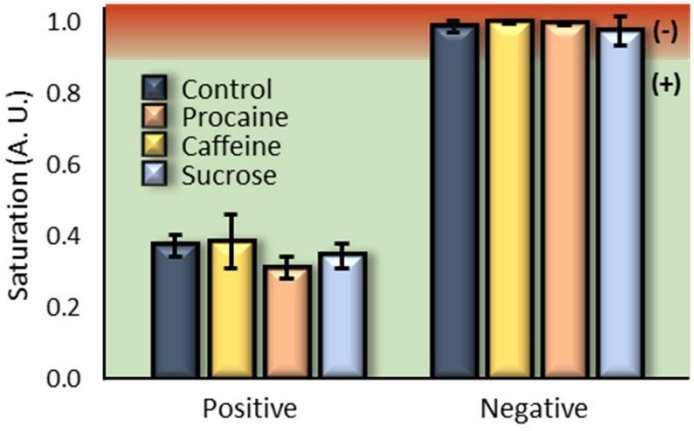

Figure 5-15. ELISA performance in the presence of common adulterants. Heroin standard dilutions (50 ng/µL) and negative samples (buffer only) were evaluated neat and spiked with equimolar amounts of either procaine, caffeine, or sucrose (n = 3). Regardless of adulterant presence, heroin was successfully detected with no detriment to detection, i.e., no false negatives were observed. Conversely, adulterant solutions without heroin were all colorimetrically negative, again indicating an absence of false negatives. Adapted from [40].

concentration was selected because it produced a visually apparent positive response in morphine analysis. Thus, false positive reactions would be easily detected. However, the highly intense, dark orange responses resulting from analysis of each adulterant solution were negative; measured saturation values were statistically similar to negative controls (Single-Factor ANOVA, $\alpha = 0.05$, $p = 0.580$). Thus, no false positive responses were observed, an important advantage of our approach over existing colorimetric field tests for opioids. For instance, the Marquis reagent, used in ampoule tests for law enforcement, incorrectly indicates the presence of opioids in analysis of compounds as innocuous as sugar (e.g., sucrose).[12]

Taken together, the results presented in this section clearly show that leveraging immunodetection instead of small-molecule chromogenesis confers the on-disc ELISA with accuracy and specificity beyond class-based differentiation, as well as high assay tolerance of common adulterants, for reliable opiate identification.

5.3.5. Toxicological Application to Mock Clinical Samples

To this point, the ELISA LoaD demonstrated applicability for detection of neat drug samples in buffer, this is adequate only for certain situations, such as forensic identification of 'unknown white powders'. However, immunodetection is also the foremost presumptive method for urinalysis drug screening.[3] As a result, the compatibility of our ELISA platform with mock clinical samples prepared in artificial urine was explored. The main potential obstacle anticipated involved performance disparities of on-disc membrane microvalves resulting from the changing sample composition, encountered in previous work (**Figure 5-16**).[29] Flowthrough rates of both fluids through embedded membranes was monitored during single-speed rotation, with the height of the remaining

fluid column plotted against elapsed time. Complete drainage of artificial urine occurred much more rapidly than buffer. It was posited that differences in ionic strength between these two fluids affected the spatial distribution of nitrocellulose fibers within the membrane, and therefore flowthrough.[29] Explicitly, the increased solute concentration, and therefore osmotic pressure, of artificial urine induced a corresponding decrease in the thermodynamic activity of the solvent. Resultant 'osmotic de-swelling' of membrane fibers caused interstitial membrane pores to become larger, which increased membrane permeability and, ultimately, flow rate.[64-68] Thus, the more rapid drainage of artificial urine through the membrane could be attributed to increased ionic strength relative to buffer alone. Though flow rate itself was not expected to impact microfluidic ELISA performance, membrane hydrodynamic resistance to flow (e.g., LEP) strongly depends on the size, number, and distribution of constituent fibers.[69] Thus, it was essential to determine

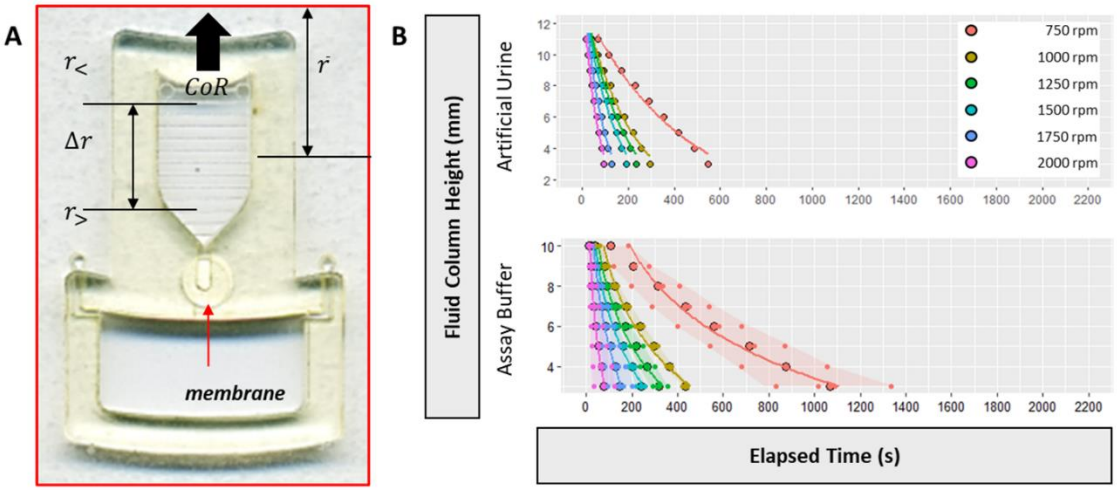

Figure 5-16. Sample composition effect on membrane behavior. (A) Labelled image of vertical flow immunoassay architecture with rastered lines in the PeT coverlet to permit visual measurement of fluid drainage through the embedded nitrocellulose (BioRAD 0.2 µm pore size) membrane. The remaining fluid column height in the loading chamber (Δr) could be calculated by subtracting the bottom height ($r_>$) of the fluid column from the top meniscus ($r_<$). Adapted from [29]. (B) To assess the sample composition on membrane flowthrough, aliquots of each 200 µL aliquots artificial urine and assay buffer were centrifugally pumped through embedded membranes at various rotational frequencies ranging from 750 to 2000 rpm (n = 4 each). The changing fluid column height over time was monitored via high speed, stroboscopic videography. Exponential decay curves depicting the remaining fluid column height in the sample chamber ($\Delta r\Delta r$) as a function of elapsed time. Scatterplots relating the remaining fluid column height in the sample chamber to the mean elapsed time were fitted with exponential decay curves. Generally, artificial urine drained more rapidly than the conventional assay buffer

if the hypothesized changes in membrane structure and behavior would affect the performance of on-disc ELISA by hindering membrane-based fluid retention.

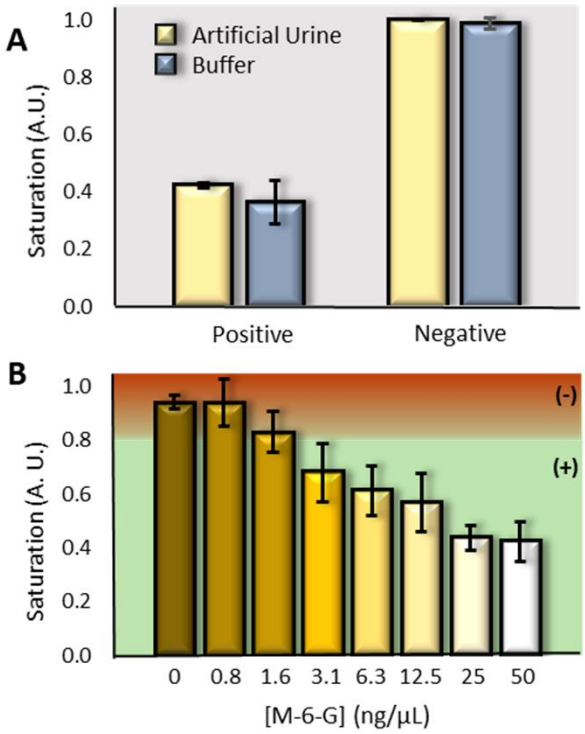

Figure 5-17. Microfluidic ELISA compatibility with mock biological samples. (A) Morphine-6-glucuronide (M-6-G, 50 ng/µL) diluted in parallel in both artificial urine and 1X PBS-T (n = 4) Saturation analysis indicated similar positive and negative saturation values across matrices. There was no observed effect on assay performance resulting from changing matrix composition. (B) Serially-diluted M-6-G (1:2, 50 – 0.08 ng/uL, n = 6) was detected in artificial urine in the ng/uL range, similar to morphine. Adapted from [40].

To assess this, parallel analysis of M-6-G (50 ng/µL) positive samples alongside negative controls in both buffer and artificial urine was performed (**Figure 5-17A**). As a key opioid metabolite, M-6-G was selected to mirror clinically-relevant urinalysis samples. According to an unpaired t-test for means, the saturation values for positive samples were statistically similar across matrices. However, this was not particularly informative since, even under normal conditions, no affinity-based binding events are necessary to achieve the anticipated unsaturated results (Section 5.3.2). It was much more telling that the saturation of negative controls (matrix only, no M-6-G) was statistically similar between buffer and artificial urine ($\alpha = 0.05$, $p = 0.142$). Since the highly saturated responses seen in these samples requires successful binding of all sequentially introduced assay reagents (e.g., M-BSA, 1° mAb, enzyme-labelled 2° Ab, and enzyme substrate), it was clear that on-disc ELISAs could be successfully performed from artificial urine samples, despite matrix-related changes to the membrane structure.

Having first demonstrated feasibility for urinalysis, pilot studies were performed to characterize the sensitivity of M-6-G detection in artificial urine (**Figure 5-17B**). As before, a threshold was established 3 standard deviations below the mean negative saturation; values above (red region) and below (green region) this threshold were considered negative and positive, respectively. As seen in morphine analysis, the 0.8 ng/µL M-6-G sample was colorimetrically negative. However, detection of M-6-G also failed at 1.6 ng/µL in artificial urine, whereas the same concentration of morphine had been detected in buffer. This minor sensitivity loss was attributed to the addition of the glucuronide moiety; it was suspected that the comparatively bulky modification made immunocapture of M-6-G more sterically challenging than unmodified morphine. Nonetheless, M-6-G was colorimetrically detected in artificial urine at 3.1 ng/µL, on the same order of magnitude as morphine in buffer. Therefore, little to no detriment in performance resulting from matrix effects was detected. The lowest reliably detected concentration (3.1 ng/µL) equates to 6.7 µM, well below the M-6-G concentration in the urine of patients prescribed morphine (11 µM) published by Lee et al.[70] These results highlight the potential applicability of the ELISA LoaD for urinalysis drug screening.

5.3.6. Enabling Rapid Analysis

While the proof-of-principle validity of microfluidic ELISA format had been established with considerable reduction in both time and labor relative to traditional methods, practical PoN use requires that analytical interval be decreased further still. The longest required step within the on-disc ELISA workflow remained the overnight 2˚ Ab incubation. Initially, this immunocapture step mirrored the traditional plate-based assay and relied entirely on passive, diffusive processes within the ELISA chamber, which are

known to be slow. Initial efforts to truncate this step incorporated active, batch-mode mixing (~10 minutes), which had successfully expedited upstream 1˚ mAb binding. Unfortunately, on-disc analysis of parallel sets of positive (50 ng/µL morphine) and negative controls (1X PBS-T only) using either the traditional, overnight and rapid 2˚ Ab incubation indicated unsuccessful ELISA performance (**Figure 5-18**). While the saturation of positive samples was comparable across methods, juxtaposition of negative results clearly indicated a disparity in performance. As anticipated, the saturation values of negative samples processed with traditional 2˚ Ab application were colorimetrically negative, but the 'rapid' negatives led to false positive results (**Figure 5-18B**). This outcome was likely derived from insufficient interaction between the 2˚ Ab and 1˚ Ab, such that fewer binding events occurred than would be anticipated. Consequently, the diminished HRP enzyme abundance in the ELISA chamber ultimately led to less intense chromogenesis.

To rectify this, the surface area-to-volume ratio of the ELISA chamber was increased to better encourage affinity-based Ab interactions on solid device substrates. Chamber depth was decreased by approximately 50% by fabricating device components from thinner PMMA than originally used (0.5 mm < 1.5 mm). However, this modification alone failed to produce the highly saturated response expected in negative tests (data not shown). These false positive responses were thought to be a consequence of the decreased path length for optical detection, resulting from the use of thinner PMMA. According to Beer's Law, a proportionally higher chromophore concentration was required to achieve the same absorbance level (saturation) with the diminished path length. After making these

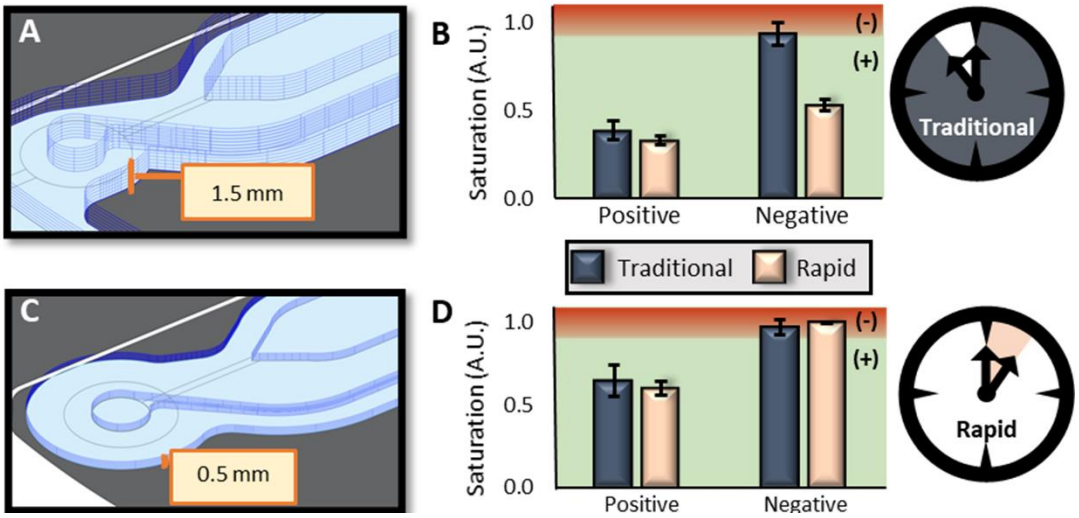

Figure 5-18. LoaD for further decreasing the analytical interval. (A) Schematic depiction of the original LoaD with 1.5 mm thick PMMA. (B) The 2˚ Ab was added to two sets of positive (50 ng/µL morphine) and negative samples in parallel. One was processed in the traditional fashion (overnight) or via the rapid workflow, which included batch mode mixing during an incubation of only 30 minutes. Traditional negatives exhibited saturation values in the negative (red) range, rapid negatives were far less saturated in color, with values well within the positive (green) range. (C) Modified LoaD fabricated using thinner (0.5 mm) PMMA. (D) After scaling reagent concentrations up to account for the diminished detection path length, there was no statistical difference between saturation values between both methods (rapid and traditional) both in terms of positive and negative samples. Adapted from [40].

changes, saturation values obtained from negative controls following rapid 2˚ Ab application were colorimetrically negative and statistically similar to samples processed traditionally ($\alpha = 0.05$, $p = 0.378$) (**Figure 5-18D**). Hence, using the modified architecture and chemistry, batch-mode mixing successfully encouraged all affinity-based interactions with a 90% reduction in required time for 2˚ Ab application. This acceleration, combined with the other expedited on-disc steps, permitted truncation of the sample-to-result interval from multiple days to approximately one hour. Though commercial ELISA kits with comparable analysis times (1.5-2 hours) are available for specific targets, they offer minimal flexibility in terms of either assay protocol or chemistry. This renders them unsuitable for initial assay development and optimization. Further, regardless of their expedited workflow, these commercial methods are open for mat, introducing risk for contamination and/or analyst exposure to dangerous antigens, and remain tethered to

traditional laboratory equipment and facilities. Conversely, the self-contained platform described here offers a more flexible, low-cost, and portable alternative.

When combined with integrated reagent storage, further flow control modalities, and on-board sample preparation, this membrane-modulated centrifugal microfluidic ELISA will permit development of rotationally-driven sample in-answer out LoaD for rapid, automatable, and affordable in-situ opiate immunodetection. Specifically, such a platform would be particularly advantageous in rural hospitals or forensic laboratories that lack infrastructure and/or resources for conventional laboratory-based immunoanalytical testing.

5.4. Conclusions

Here, a novel LoaD platform for rapid, multiplexed opiate immunodetection in up to 8 parallel samples at the microscale is demonstrated in as little as one hour. To our knowledge, this work represents the first demonstration of a centrifugal microdevice with embedded, reversible membrane microvalves to modulate rotationally-driven flow and enable on-board ELISA performance. Balancing centrifugal force with membrane hydrodynamic resistance to flow, or LEP, permitted the cascade of reagent introduction, incubation, and fluid removal steps necessary for successful immunodetection, significantly reducing the manual intervention required, including pipetting steps. Batch-mode mixing supplanted the sole reliance on diffusion-limited immunoaffinity reactions in traditional ELISA formats by actively encouraging binding events. Ultimately, this mixing strategy permitted significant truncation of incubation times relative to traditional formats, from multiple hours to approximately ten minutes each.[57] Even with these changes to the ELISA protocol, comparable colorimetric results were obtained between microfluidic and

traditional methods. However, the LoaD offers drastically increased portability in an enclosed, automatable format that is much more amenable for PoN use. Reduced reagent volumes on-disc also minimizes the cost per test, and associated risks for analyst exposure to harmful substances.

Implementation of empirical image analysis eliminated subjectivity in colorimetric interpretation and permitted opiate detection at the ng/µL range. Detection in this regime was possible in both buffer and artificial urine, which have distinctly different fluidic properties (i.e., ionic strength). These results highlight the robust nature of both assay chemistry and the novel membrane-based microvalving approach. The latter observation was especially important due to 'osmotic de-swelling' of membrane fibers shown to affect membrane penetration and flowthrough.[29, 64-65] However, functional changes in membrane behavior were not observed, highlighting the potential applicability of the ELISA LoaD to urinalysis. Though continued optimization of assay chemistry will likely afford even lower sensitivity, even these pilot studies demonstrate adequate sensitivity for practical implementation. Morphine was detected at 1.6 ng/µL, below both the limit of detection of current ampoule-based field tests (µg level) and the current cutoff recommended in workplace drug testing guidelines.[6, 71] Thus, the ELISA LoaD platform exhibits broad potential applicability, including identifying seized substances suspected to be illicit and urinalysis of clinical/forensic samples.

Specific opiate detection was demonstrated, with no interference observed either from other drug classes, including synthetic opioids, or common adulterants.[12] As expected in using immunodetection, these findings represent improved accuracy relative to existing small-molecule colorimetric tests, which erroneously yield false positive results in the

presence of innocuous, non-controlled substances.[12, 14] Since ELISA specificity relies entirely on the affinity of the mAbs selected, additional mAbs against other controlled substances could be integrated to permit parallel, simultaneous screening for a panel of drugs. Further, the multiplexed device format is well-suited to simultaneous immunodetection of several targets, including drugs (e.g., opiates, amphetamines, cocaine, etc.). Since many current colorimetric field tests require iterative performance of multiple tests,[4] parallel on-disc screening for multiple analytes of interest from a single sample input is capable of expediting presumptive testing further still. Though this work was centered on presumptive drug screening, the novel ELISA format described here has potential for more broad applicability across numerous disciplines simply by changing the identities and affinities of the antigen and antibodies used.

Finally, continued development of an integrated 'lab-on-a-chip' device with automatable fluidics and all reagents preloaded or stored on board will provide sample in – answer out LoaDs capable of performing the entire competitive ELISA workflow autonomously. Comprehensive elimination of manual intervention will allow for affordable, automated immunodetection amenable for use by nontechnical personnel in situ.

5.5. References

1. Scholl, L.; Seth, P.; Kariisa, M.; Wilson, N.; Baldwin, G., Drug and opioid-involved overdose deaths—United States, 2013–2017. *Morbidity and Mortality Weekly Report* **2019,** *67* (51-52), 1419.

2. UNODC, World Drug Report 2020. Global overview of drug demand and supply. **2020,** *2*.

3. Kale, N., Urine drug tests: Ordering and interpreting results. *American Family Physician* **2019,** *99* (1), 33-39.

4. Krauss, S. T.; Woolf, M. S.; Hadley, K. C.; Collins, N. M.; Nauman, A. Q.; Landers, J. P., Centrifugal microfluidic devices using low-volume reagent storage and inward fluid displacement for presumptive drug detection. *Sensors and Actuators B: Chemical* **2019,** *284*, 704-710.

5. Krauss, S. T.; Remcho, T. P.; Lipes, S. M.; Aranda IV, R.; Maynard III, H. P.; Shukla, N.; Li, J.; Tontarski Jr, R. E.; Landers, J. P., Objective method for presumptive field-testing of illicit drug possession using centrifugal microdevices and smartphone analysis. *Analytical Chemistry* **2016,** *88* (17), 8689-8697.

6. Philp, M.; Fu, S., A review of chemical 'spot' tests: A presumptive illicit drug identification technique. *Drug Testing and Analysis* **2018,** *10* (1), 95-108.

7. Fentanyl, carfentanil, heroin testing made safer and more accurate. https://www.fieldforensics.com/press-release-fen-fentanyl-heroin-kit/ (accessed April 1, 2021).

8. Drug Enforcement Agency. Warning to Police and Public: Fentanyl Exposure Kills., Ed. 2016.

9. Kim, S. Y.; Kim, H.; Park, Y.; Lim, J.; Kim, J.; Koo, S. H.; Kwon, G. C., Evaluation of an automated reader and color interpretation-based immunoassays for multiplexed drug-of-abuse testing in urine. *Journal of Analytical Toxicology* **2017,** *41* (5), 412-420.

10. Choodum, A.; Nic Daeid, N., Digital image-based colourimetric tests for amphetamine and methylamphetamine. *Drug Testing and Analysis* **2011,** *3* (5), 277-282.

11. Capitán-Vallvey, L. F.; Lopez-Ruiz, N.; Martinez-Olmos, A.; Erenas, M. M.; Palma, A. J., Recent developments in computer vision-based analytical chemistry: A tutorial review. *Analytica Chimica Acta* **2015,** *899*, 23-56.

12. National Institute of Standards, Technology. Color test reagents/kits for preliminary identification of drugs of abuse. US Department of Justice, Office of Law Enforcement Standards and National Institute of Justice, 2000; Vol. 604.

13. Marquis, E., Über den Verbleib des Morphins im tierischen Organismus. Inaugural-Dissertation, Jurjew (Dorpat) 1896.

14. Gabrielson, R.; Sanders, T., How a $2 roadside drug test sends innocent people to jail. The New York Times 2016, 7.

15. Wang, S.; Zhang, C.; Zhang, Y., Lateral flow colloidal gold-based immunoassay for pesticide. In Biosensors and Biodetection, Springer: 2009; pp 237-252.

16. Snyder, M. L.; Jarolim, P.; Melanson, S. E., A new automated urine fentanyl immunoassay: technical performance and clinical utility for monitoring fentanyl compliance. *Clinica Chimica Acta* **2011,** *412* (11-12), 946-951.

17. Calm, A. M.; Thompson, R.; Betts, K.; Hofmann, R.; Chen, H.; Ford, G.; Ma, J. Testing of Ruggedized Antibodies within a Lateral Flow Immunoassay; Director, ECBC APG United States: 2017.

18. Chen, C. A.; Wang, P. W.; Yen, Y. C.; Lin, H. L.; Fan, Y. C.; Wu, S. M.; Chen, C. F., Fast analysis of ketamine using a colorimetric immunosorbent assay on a paper-based analytical device. *Sensors and Actuators B: Chemical* **2019,** *282*, 251-258.

19. Liu, B.; Si, J.; Zhao, F.; Wang, Q.; Wang, Y.; Li, J.; Li, C.; Li, T., Rapid detection of cow milk adulteration/contamination in goat milk by a lateral flow colloidal gold immunoassay strip. *Journal of Dairy Research* **2019,** 1-4.

20. Koczula, K. M.; Gallotta, A., Lateral flow assays. *Essays in Biochemistry* **2016,** *60* (1), 111-120.

21. Li, Y. F.; Sun, Y. M.; Beier, R. C.; Lei, H. T.; Gee, S.; Hammock, B. D.; Wang, H.; Wang, Z.; Sun, X.; Shen, Y. D., Immunochemical techniques for multianalyte analysis of chemical residues in food and the environment: A review. *TrAC Trends in Analytical Chemistry* **2017,** *88*, 25-40.

22. Gan, S. D.; Patel, K. R., Enzyme immunoassay and enzyme-linked immunosorbent assay. *Journal of Investigative Dermatology* **2013,** *133* (9), e12.

23. Chen, P.; Gates-Hollingsworth, M.; Pandit, S.; Park, A.; Montgomery, D.; AuCoin, D.; Gu, J.; Zenhausern, F., based Vertical Flow Immunoassay (VFI) for detection of bio-threat pathogens. *Talanta* **2019,** *191*, 81-88.

24. Smith, L. C.; Lin, L.; Hwang, C. S.; Zhou, B.; Kubitz, D. M.; Wang, H.; Janda, K. D., Lateral Flow Assessment and Unanticipated Toxicity of Kratom. *Chemical Research in Toxicology* **2018,** *32* (1), 113-121.

25. Jiang, N.; Ahmed, R.; Damayantharan, M.; Ünal, B.; Butt, H.; Yetisen, A. K., Lateral and Vertical Flow Assays for Point-of-Care Diagnostics. *Advanced Healthcare Materials* **2019,** *8* (14), 1900244.

26. Chen, G. H.; Chen, W. Y.; Yen, Y. C.; Wang, C. W.; Chang, H. T.; Chen, C. F., Detection of mercury (II) ions using colorimetric gold nanoparticles on paper-based analytical devices. *Analytical Chemistry* **2014,** *86* (14), 6843-6849.

27. Gong, M. M.; Sinton, D., Turning the page: advancing paper-based microfluidics for broad diagnostic application. *Chemical Reviews* **2017,** *117* (12), 8447-8480.

28. Gubala, V.; Harris, L. F.; Ricco, A. J.; Tan, M. X.; Williams, D. E., Point of care diagnostics: status and future. *Analytical Chemistry* **2012,** *84* (2), 487-515.

29. Woolf, M. S.; Dignan, L. M.; Karas, S. M.; Lewis, H. M.; Hadley, K. C.; Nauman, A. Q.; Geise, G. M.; Landers, J. P., Characterization of a Centrifugal Microfluidic Orthogonal Flow Platform. *Micromachines* **2022,** *13* (3), 487.

30. Gantelius, J.; Hamsten, C.; Neiman, M.; Schwenk, J. M.; Persson, A.; Andersson-Svahn, H., A lateral flow protein microarray for rapid determination of contagious bovine pleuropneumonia status in bovine serum. *Journal of Microbiological Methods* **2010,** *82* (1), 11-18.

31. Oh, Y. K.; Joung, H.-A.; Kim, S.; Kim, M. G., Vertical flow immunoassay (VFA) biosensor for a rapid one-step immunoassay. *Lab on a Chip* **2013,** *13* (5), 768-772.

32. Homann, A. R.; Niebling, L.; Zehnle, S.; Beutler, M.; Delamotte, L.; Rothmund, M. C.; Czurratis, D.; Beller, K. D.; Zengerle, R.; Hoffmann, H., A microfluidic cartridge for fast and accurate diagnosis of Mycobacterium tuberculosis infections on standard laboratory equipment. *Lab on a Chip* **2021,** *21* (8), 1540-1548.

33. Liu, D.; Zhu, Y.; Li, N.; Lu, Y.; Cheng, J.; Xu, Y., A portable microfluidic analyzer for integrated bacterial detection using visible loop-mediated amplification. *Sensors and Actuators B: Chemical* **2020,** *310*, 127834.

34. Brassard, D.; Geissler, M.; Descarreaux, M.; Tremblay, D.; Daoud, J.; Clime, L.; Mounier, M.; Charlebois, D.; Veres, T., Extraction of nucleic acids from blood: unveiling the potential of active pneumatic pumping in centrifugal microfluidics for integration and automation of sample preparation processes. *Lab on a Chip* **2019,** *19* (11), 1941-1952.

35. Van Nguyen, H.; Seo, T. S., High-throughput human DNA purification on a centrifugal microfluidic device for rapid forensic sex-typing. *Biosensors and Bioelectronics* **2021,** *181*, 113161.

36. Woolf, M. S.; Dignan, L. M.; Karas, S. M.; Lewis, H.; Kim, S.; Geise, G.; DeMers, H.; Hau, D.; Gates-Hollingsworth, M.; AuCoin, D.; Landers, J. P., A Centrifugal Microfluidic Approach to Rapid Biothreat Detection via Orthogonal Flow Immunocapture. In Preparation.

37. Ma, L.; Nilghaz, A.; Choi, J. R.; Liu, X.; Lu, X., Rapid detection of clenbuterol in milk using microfluidic paper-based ELISA. *Food Chemistry* **2018,** *246*, 437-441.

38. Lequin, R. M., Enzyme immunoassay (EIA)/enzyme-linked immunosorbent assay (ELISA). *Clinical Chemistry* **2005,** *51* (12), 2415-2418.

39. Noroozi, Z.; Kido, H.; Peytavi, R.; Nakajima-Sasaki, R.; Jasinskas, A.; Micic, M.; Felgner, P. L.; Madou, M. J., A multiplexed immunoassay system based upon reciprocating centrifugal microfluidics. *Review of Scientific Instruments* **2011,** *82* (6), 064303.

40. Dignan, L. M.; Woolf, M. S.; Ross, J. A.; Baehr, C.; Holstege, C. P.; Pravetoni, M.; Landers, J. P., A Membrane-Modulated Centrifugal Microdevice for Enzyme-Linked Immunosorbent Assay-Based Detection of Illicit and Misused Drugs. *Analytical Chemistry* **2021,** *93* (48), 16213-16221.

41. Okamoto, S.; Ukita, Y., Automatic microfluidic enzyme-linked immunosorbent assay based on CLOCK-controlled autonomous centrifugal microfluidics. *Sensors and Actuators B: Chemical* **2018,** *261*, 264-270.

42. Madou, M. J.; Kellogg, G. J. In LabCD: a centrifuge-based microfluidic platform for diagnostics, Systems and Technologies for Clinical Diagnostics and Drug Discovery, International Society for Optics and Photonics: 1998; pp 80-93.

43. Schneider, S.; Gruner, D.; Richter, A.; Loskill, P., Membrane integration into PDMS-free microfluidic platforms for organ-on-chip and analytical chemistry applications. *Lab on a Chip* **2021,** *21*, 1866-1885.

44. Chen, Y. S.; Ma, Y. D.; Chen, C.; Shiesh, S. C.; Lee, G. B., An integrated microfluidic system for on-chip enrichment and quantification of circulating extracellular vesicles from whole blood. *Lab on a Chip* **2019,** *19* (19), 3305-3315.

45. Thompson, B. L.; Ouyang, Y.; Duarte, G. R.; Carrilho, E.; Krauss, S. T.; Landers, J. P., Inexpensive, rapid prototyping of microfluidic devices using overhead transparencies and a laser print, cut and laminate fabrication method. *Nature Protocols* **2015,** *10* (6), 875-886.

46. Birch, C.; DuVall, J. A.; Le Roux, D.; Thompson, B. L.; Tsuei, A.; Li, J.; Nelson, D. A.; Mills, D. L.; Landers, J. P.; Root, B. E., Rapid Fabrication of Electrophoretic Microfluidic Devices from Polyester, Adhesives and Gold Leaf. *Micromachines* **2017,** *8* (1), 17.

47. Baehr, C.; Kelcher, A. H.; Khaimraj, A.; Reed, D. E.; Pandit, S. G.; AuCoin, D.; Averick, S.; Pravetoni, M., Monoclonal antibodies counteract opioid-induced behavioral and toxic effects in mice and rats. *Journal of Pharmacology and Experimental Therapeutics* **2020,** *375* (3), 469-477.

48. Pravetoni, M.; Raleigh, M.; Le Naour, M.; Tucker, A.; Harmon, T.; Jones, J.; Birnbaum, A.; Portoghese, P.; Pentel, P., Co-administration of morphine and oxycodone vaccines reduces the distribution of 6-monoacetylmorphine and oxycodone to brain in rats. *Vaccine* **2012,** *30* (31), 4617-4624.

49. Raleigh, M. D.; Pravetoni, M.; Harris, A. C.; Birnbaum, A. K.; Pentel, P. R., Selective effects of a morphine conjugate vaccine on heroin and metabolite distribution and heroin-induced behaviors in rats. *Journal of Pharmacology and Experimental Therapeutics* **2013,** *344* (2), 397-406.

50. Liu, L.; Shou, L.; Yu, H.; Yao, J., Mechanical properties and corrosion resistance of vulcanized silicone rubber after exposure to artificial urine. *Journal of Macromolecular Science, Part B* **2015,** *54* (8), 962-974.

51. Woolf, M. S.; Dignan, L. M.; Scott, A. T.; Landers, J. P., Digital postprocessing and image segmentation for objective analysis of colorimetric reactions. *Nature Protocols* **2020,** *16* (1), 218-238.

52. Rueden, C. T.; Schindelin, J.; Hiner, M. C.; DeZonia, B. E.; Walter, A. E.; Arena, E. T.; Eliceiri, K. W., ImageJ2: ImageJ for the next generation of scientific image data. *BMC Bioinformatics* **2017,** *18* (1), 529.

53. Schindelin, J.; Arganda-Carreras, I.; Frise, E.; Kaynig, V.; Longair, M.; Pietzsch, T.; Preibisch, S.; Rueden, C.; Saalfeld, S.; Schmid, B.; Tinevez, J. Y.; White, D. J.; Hartenstein, V.; Eliceiri, K.; Tomancak, P.; Cardona, A., Fiji: an open-source platform for biological-image analysis. *Nature Methods* **2012,** *9*, 676-982.

54. Yazgan-Birgi, P.; Ali, M. I. H.; Arafat, H. A., Estimation of liquid entry pressure in hydrophobic membranes using CFD tools. *Journal of Membrane Science* **2018,** *552*, 68-76.

55. Liu, Q.; Zhang, X.; Chen, L.; Yao, Y.; Ke, S.; Zhao, W.; Yang, Z.; Sui, G., A sample-to-answer labdisc platform integrated novel membrane-resistance valves for detection of highly pathogenic avian influenza viruses. *Sensors and Actuators B: Chemical* **2018,** *270*, 371-381.

56. Ducrée, J.; Haeberle, S.; Lutz, S.; Pausch, S.; Von Stetten, F.; Zengerle, R., The centrifugal microfluidic Bio-Disk platform. *Journal of Micromechanics and Microengineering* **2007,** *17* (7), S103.

57. Grumann, M.; Geipel, A.; Riegger, L.; Zengerle, R.; Ducrée, J., Batch-mode mixing on centrifugal microfluidic platforms. *Lab on a Chip* **2005,** *5* (5), 560-565.

58. Xiong, Y.; Leng, Y.; Li, X.; Huang, X.; Xiong, Y., Emerging strategies to enhance the sensitivity of competitive ELISA for detection of chemical contaminants in food samples. *TrAC Trends in Analytical Chemistry* **2020,** *126*, 115861.

59. Cantrell, K.; Erenas, M.; de Orbe-Payá, I.; Capitán-Vallvey, L., Use of the hue parameter of the hue, saturation, value color space as a quantitative analytical parameter for bitonal optical sensors. *Analytical Chemistry* **2010,** *82* (2), 531-542.

60. Cao, S.; Huang, D.; Wang, Y.; Li, G., Phenolphthalein Alkalinity Testing Research Based on Computer Vision Technology and Electronic Technology. In Advances in Mechanical and Electronic Engineering, Springer: 2012; pp 381-386.

61. Dignan, L. M.; Woolf, M. S.; Tomley, C. J.; Nauman, A. Q.; Landers, J. P., Multiplexed Centrifugal Microfluidic System for Dynamic Solid-Phase

Purification of Polynucleic Acids Direct from Buccal Swabs. *Analytical Chemistry* **2021,** *93* (19), 7300-7309.

62. Smith, M. P.; Bluth, M. H., Common interferences in drug testing. *Clinics in Laboratory Medicine* **2016,** *36* (4), 663-671.

63. Cole, C.; Jones, L.; McVeigh, J.; Kicman, A.; Syed, Q.; Bellis, M., Adulterants in illicit drugs: a review of empirical evidence. *Drug Testing and Analysis* **2011,** *3* (2), 89-96.

64. Geise, G. M.; Freeman, B. D.; Paul, D. R., Sodium chloride diffusion in sulfonated polymers for membrane applications. *Journal of Membrane Science* **2013,** *427*, 186-196.

65. Geise, G. M.; Paul, D. R.; Freeman, B. D., Fundamental water and salt transport properties of polymeric materials. *Progress in Polymer Science* **2014,** *39* (1), 1-42.

66. Khare, A. R.; Peppas, N., Swelling/deswelling of anionic copolymer gels. *Biomaterials* **1995,** *16*, 559-567.

67. Sun, S.; Feng, S.; Ji, C.; Shi, M.; He, X.; Xu, F.; Lu, T. J., Microstructural effects on permeability of Nitrocellulose membranes for biomedical applications. *Journal of Membrane Science* **2020,** *595*, 117502.

68. Kainz, D. M.; Früh, S. M.; Hutzenlaub, T.; Zengerle, R.; Paust, N., Flow control for lateral flow strips with centrifugal microfluidics. *Lab on a Chip* **2019,** *19* (16), 2718-2727.

69. Jensen, K. H.; Valente, A. X.; Stone, H. A., Flow rate through microfilters: Influence of the pore size distribution, hydrodynamic interactions, wall slip, and inertia. *Physics of Fluids* **2014,** *26* (5), 052004.

70. Lee, Y. J.; Suh, S. Y.; Song, J.; Lee, S. S.; Seo, A. R.; Ahn, H. Y.; Lee, M. A.; Kim, C. M.; Klepstad, P., Serum and urine concentrations of morphine and morphine metabolites in patients with advanced cancer receiving continuous intravenous morphine: an observational study. *BMC Palliative Care* **2015,** *14* (1), 1-6.

71. Medical Review Officer Guidance Manual for Federal Workplace Drug Testing Programs. Services, Department of Health and Human Services, Ed. 2018.

6. Final Remarks

6.1. Conclusions

Each of the projects described in this dissertation focused on streamlining highly manual, time-intensive workflows used ubiquitously in forensic science and clinical diagnostics. Specifically, the work presented here discussed the development and characterization of microfluidic lab-on-a-disc (LoaD) platforms for nucleic acid (NA) preparation, including lysis and extraction – an area that has remained underdeveloped relative to post-processing methods. Adapting these assays to the microscale systems while incorporating novel fabrication strategies and on-disc unit operations permitted increased automation as well as expedited analysis relative to traditional benchtop methods.

Chapter 2 involved the design and optimization of a microfluidic LoaD capable of performing enzymatic cellular lysis and dynamic solid phase extraction (dSPE). The sequential passage of several solutions through a chamber containing a paramagnetic-cored silica particle solid phase facilitated the 'bind-wash-elute' NAE workflow. The success of this approach was directly contingent upon three key factors. First, the imperative strict temporal control over sequential reagent delivery, incubation, and removal was provided by laser-based closable valves in what was the first demonstration of the technique's compatibility with bioassays. Second, effective retention of the silica nanoparticle solid phase in the central extraction chamber, achieved via careful geometric design, was critical to ensure high and reproducible NA yields at detectable levels. Other microdevices have since leveraged similar designs to retain other solid phases (as in **Chapter 3**) or analytes, such as sperm cells.[1] Third and finally, manipulation of the silica solid phase at the microscale was driven by a bidirectional rotating magnetic field, ultimately encouraging

effective capture of target NAs in solution and mixture with requisite reagents during the assay workflow. The unmodified silica solid phase used here permitted broad implementation of the dSPE LoaD, with demonstrated extraction of both DNA and RNA for forensic and clinical applications.

Conversely, **Chapter 3** details the use of a different, magnetically-susceptible solid phase specifically tailored to the preparation of SARS-CoV-2. Silica particles were supplanted with hydrogel nanoparticles decorated with affinity baits. Instead of capturing NAs after lysis (as seen in Chapter 2), hydrogel particles interacted with viral spike proteins to permit enrichment of intact SARS-CoV-2 virions. Subsequent single-step enzymatic rnaGEM lysis, coupled with the commercial PDQeX system, permitted simplified, hands-free lysis and RNA isolation from patient samples (VTM and saliva) without the repeated washing required in traditional SPE (**Chapter 2**). Enriched rnaGEM isolates were directly compatible with real-time RT-PCR and exhibited comparable yields with 'gold standard' column-based NAE methods. Results demonstrated 100% concordance with clinical outcomes in a double-blind study, a benchmark that highlighted the method's potential for diagnostic use of enriched rnaGEM chemistry. Further, successful SARS-CoV-2 detection in dilutions as high as 20X suggested amenability for pooled sample analysis; related work is ongoing within our group. Combining enriched rnaGEM extraction with isothermal NAATs enabled sample-to-answer analysis in 15 minutes, orders of magnitude below the 2-3 day turnaround time for traditional testing. Finally, the enriched rnaGEM workflow was adapted to a multiplexed LoaD^2 that leveraged architectural features, microvalving patterns, and magnetic manipulation modalities used previously for dSPE (**Chapter 2**) to further automate NAE and minimize risk for analyst exposure.

Unfortunately, extracts in both dSPE (**Chapter 2**) and enriched rnaGEM extraction (**Chapter 3**) were located at the LoaD periphery, which precluded further on-disc processing (e.g., amplification). These observations, juxtaposed with the need for sample-to-answer NA LoaDs outlined in **Chapter 1**, were the impetus for the development and characterization of a method for radially-inward fluid displacement (IFD), described in **Chapter 4**. By harnessing gas generated from an on-board acid-base neutralization reaction, fluid was driven unidirectionally towards the CoR to enable continued rotationally-controlled processing (recovery = 80%). Safe-to-handle solid reagents were stored easily on-board as a mixture stably for up to 6 months under ambient conditions. Effective containment of the gaseous pressure head was achieved using laser-based channel closures, which had previously been applied only to liquid control. To demonstrate NAAT compatibility, a proof-of-concept system was developed that leveraged the enzymatic NA preparation approach described in **Chapter 3** to apply direct-from-swab lysis on-disc followed immediately by IFD. IFD did was not detrimental to downstream post-processing performance, either through sample acidification or mechanical damage to DNA. To our knowledge, this is the first demonstration of gas-based displacement compatibility with NAATs, critical in enabling μTAS platforms. Since LAMP is well-suited for field-forward implementation, a microarchitecture was developed that coupled direct-from-swab lysis, IFD, and LAMP. Continued exploration of combining NA preparation methods with on-disc LAMP are discussed below in Section 6.2.

Finally, **Chapter 5** described the on-disc performance of a different bioanalytical assay that is equally, if not more, labor-intensive than NAE – namely the competitive, indirect ELISA. The portable, fully enclosed, and multiplexed LoaD provided for

objective, empirical colorimetric opiate detection at the ng/µL range in as little as one hour – a significant reduction of the traditional multi-day timeline. Like dSPE (**Chapter 2**), ELISAs require a cascade of reagent introduction, incubation, and fluid removal steps. To enable this, embedded nitrocellulose membranes were employed as reversible microvalves to modulate rotationally-driven flow based on hydrodynamic resistance. Immunoaffinity binding events were expedited from multiple hours to approximately ten minutes by supplanting diffusion with active mixing. The sensitivity of centrifugal microfluidic ELISAs in both buffer and artificial urine was below both the limit of detection of current ampoule-based field tests (µg-level) and sufficient for workplace drug testing. Further, the assay was more accurate than common small-molecule color tests, exhibiting no cross-reactivity with other drug classes, including synthetic opioids, or common adulterants. Further integration of architecture and flow control modalities will enable automatable immunodetection at the PoN.

6.2. Ongoing Studies, Persistent Challenges, and Future Work

The work outlined in this dissertation describe PCL devices capable of performing all or some process chains associated with bioanalytical assays common to forensic and clinical workflows. The majority of projects discussed had a specific focus on NA preparation, a traditionally underdeveloped research area, to expand capabilities for sample-to-answer processing. After successfully optimizing and characterizing these process chains, additional research is needed to integrate on-disc post-processing and reagent storage solutions to yield sample-to-answer systems. Similarly, architectural augmentation of the ELISA LoaD is required for total assay automation and functional PoN use.

6.2.1. Microfluidic Nucleic Acid Processing

The principle remaining challenge in full microfluidic integration of the genetic analysis workflow involves incorporation of on-disc post-processing downstream from extraction methods. Initial efforts to integrate on-disc amplification are centered on LAMP due to amenability for PoN applications and demonstrated compatibility with each of the NAE methods in **Chapters 2-4**.

6.2.1.1. Optimization of On-Disc Loop-Mediated Isothermal Amplification

As mentioned briefly at the conclusion of **Chapter 4**, pilot studies to characterize on-disc LAMP showed that non-specific amplification (NSA) is pervasive in on-disc no template controls (NTCs). This was true for amplification using primers for TPOX (**Chapters 2 and 4**) and SARS-CoV-2 N1 (**Chapter 3**). The observed amplification was not a result of reagent contamination, evidenced by a lack of amplification in parallel, in-tube NTCs. Thus, on-disc amplification conditions must be optimized to ensure accurate, on-target NA detection. Some success was derived from truncating the incubation interval from 45 to 30 minutes; however, a resultant loss in sensitivity is unavoidable. Likewise, increasing temperature reduced NSA frequency, but on-target amplification was somewhat discouraged as well. Thus, continued adjustments to assay chemistry are necessary for mitigating NSA without detriment to on-target detection. One such strategy involves tuning primer concentration; since LAMP incorporates 6 primers instead of only two required for PCR, and thus reducing primer concentration in each reaction could decrease the incidence of NSA, but will also harm sensitivity. In parallel, increasing polymerase concentration could mitigate losses in sensitivity resulting from primer and temperature adjustments by accelerating amplification rate without altering the efficiency of the polymerase itself.

Additional support for this strategy in the context of microfluidics could be supported by the fact that polymerase adsorption to PeT device substrates is understood to occur. Of course, ensuring polymerase activity further in this system, could be increased via passivation of PeT surfaces with BSA (e.g., LAMP chambers).[3] In all probability, careful tuning of each of these factors sequentially will be required for on-disc LAMP performance and optimization. It should be noted also that although IFD and LAMP have been coupled with upstream direct-from-swab prepGEM lysis, these techniques could also be included easily following dSPE (**Chapter 2**) or enriched rnaGEM extraction (Chapter 3). Additionally, the architectures for these LoaDs could also be applied to other bead-based NAE methods, such as pH-modulated chitosan approaches.

6.2.1.2. Indicator Selection

A second factor imperative for practical implementation of on-site genetic analysis is the provision of simple, easily interpreted output. Compatibility of LAMP with colorimetric readout is a key advantage for PoN applications by supplanting reliance on benchtop instrumentation with simple, optical detection. Initial exploratory studies centered on colorimetric LAMP incorporated HNB, used in-tube in **Chapters 2-4**. However, there are known issues in the stability of HNB color over time. Further, in practice, near-complete color fading was occasionally observed on-disc, which suggested sample acidification. This hypothesis was confirmed via LAMP with phenol red as an indicator, which changes from red to yellow with amplification and resultant solution acidification. In initial testing, both negative and positive samples were colorimetrically positive but electrophoretically negative. These results suggested reaction acidification, which likely resulted from LoaD materials. Herein, the chemistry demonstrated its low

buffering capacity to permit the pH-modulated response of phenol red. Importantly, the detriment to amplification performance was not seen in other LAMP chemistries with more standard buffering capacities. Malachite green was also explored as an indicator, but despite excellent discrimination in-tube, the magnitude of the colorless-to-colored transition was too small for reliable on-disc differentiation given the reduced detection path length in microfluidic chambers. Thus, future endeavors should center on the incorporation of indicators independent of absorbance-based measurements. For instance, smartphone-based image capture and subsequent interpretation of calcein's fluorescent response to long-wave UV light could permit simple colorimetric detection with relatively little instrumentation.

6.2.1.3. On-Disc Reagent Storage

In addition to comprehensive integration of each process chain for genetic analysis (lysis, NA extraction, amplification, and detection), on-board reagent storage is essential for true independence from laboratory technology and techniques. As discussed in **Chapter 1**, elimination of all technical manipulation steps, including reagent loading by pipette, is critical for use by non-technical personnel. Liquid reagents (e.g., lysis cocktail, wash buffers, water) may be integrated in pressure-actuated blister packs or stickpacks (discussed in **Chapter 1**) with frangible, rotationally-controlled seals to permit long-term on-disc storage. Other reagents may be stored more stably in solid, dried form. For instance, amplification reagents (e.g., LAMP master mix) have demonstrated stability as lyophilized pellets; RPA reagents are commercially available for shipping and long-term storage in this form. Prior to assay implementation, the pellet could easily be rehydrated in water from a blister or stickpack. Similarly, air-dried primers (and positive control genetic

material) in the appropriate LAMP reaction chambers could be resuspended upon introduction delivery of metered master mix. Characterization of these reagent storage approaches will be necessary to ensure that they do not hinder assay performance.

6.2.1.4. Hardware Improvements

Beyond assay optimization, development of a 'spin stand', or ruggedized, self-contained mechatronic system to automate and regulate fluidic control is required for practical PoN implementation. Minimally, either the PrTZAL system or the integrated mechatronic system currently under development (both discussed in **Chapter 2**) must be encapsulated in a durable encasement (e.g., 3D-printed or injection molded) to protect fragile electronic components, prevent unintended analyst laser exposure during valving, allow for portability, and prevent environmental assay contamination or interference. Currently, these systems are controlled by a laptop, but supplanting this with a smartphone would increase portability and capabilities. A custom-written application could control all required unit operations for assay implementation, including LoaD rotation, laser-valving, and heating. Switching to smartphone-based control will also allow for inclusion of automated optical interpretation of LAMP chromogenesis using the embedded camera; imaging conditions within the enclosure can be carefully controlled using on-board lighting components, such as LEDs, to ensure reproducible imaging and interpretation. One further consideration not yet discussed involves improving heating modalities to permit simultaneous incubation of multiple domains. For true multiplexed analysis, lysis and amplification must occur simultaneously in all LoaD domains. One potential approach involves incorporation of clamped disc-shaped Peltiers at radii corresponding to the positions of swab and LAMP chambers. However, fluid loss from chambers during contact

heating via clamped dual-Peltier systems has been repeatedly observed; thus, transitioning to non-contact heating, modes such as infrared-based methods, may be optimal.

6.2.2. On-Disc Immunodetection

In contrast to the NAE projects discussed above, the detection scheme for the ELISA project has been successfully integrated on-disc; continued research and development is required to incorporate upstream sample preparation and overall automation.

6.2.2.1. Developing a Fully-Integrated Architecture

Proof-of-principle implementation of an integrated microfluidic architecture was shown in **Chapter 5**, but continued characterization and optimization is required to further reduce manual pipetting requirements. Eventual integration of reagent storage (discussed in Section 6.2.1.3) will also be required here prior to PoN use, including lyophilization of Abs stored on board. Additionally, continued architectural development could allow for simultaneous immunodetection of several targets. One method to achieve this involves splitting a single input sample into multiple aliquots, each of which could then be processed in parallel in discrete domains within the multiplexed LoaD. Since many current colorimetric field tests require iterative performance of multiple tests, this multiplexed microfluidic analysis could further expedite on-site presumptive testing.

6.2.2.2. Exploration of Alternative Immunoaffinity Reagents

As noted in **Chapter 5**, the saturation of negative morphine responses in the integrated and rapid assay formats was diminished relative to parallel tests with off-disc sample preparation and sequential reagent loading. Diminished negative saturation values were also observed in exploratory studies probing on-disc fentanyl detection. It was

hypothesized that these unsaturated responses were due, at least in part, to insufficient Ab-Ag interaction during incubation steps. Future endeavors toward expediting immunodetection without detriment to performance could explore supplanting intact Abs with only variable region fragments (F_v). The reduced hydrodynamic radii of these F_v fragments would allow for more efficient, rapid mixing within the ELISA chamber, both in terms of passive (e.g., diffusion) and active processes.

6.2.2.3. Improving ELISA Sensitivity

Currently, colorimetric analysis of negative controls results in saturation values at or near the maximum possible readout of 255 in the 8-bit system used to capture native images. This observation suggests that the detector has been effectively saturated, such that low concentration samples, which may provide readouts that appear visually different than the negative controls are empirically similar. Thus, decreasing the mean signal measured from negatives to some value below that maximum saturation would provide for enhanced discrimination relative to low-concentration positive samples, ultimately improving sensitivity. Sensitivity could be improved further by transitioning from enzyme-catalyzed colorimetric chromogenic readout to fluorescence-based detection. This could also allow for incorporation of real-time detection, advantageous over the endpoint detection possible through colorimetric monitoring of OPD metabolism.

6.3. Summation

Increasing demand for PoN analyses has led to expanding capabilities for centrifugal LoaD technologies for use outside of traditional laboratory settings across numerous sectors, including the forensic and biomedical arenas highlighted in this dissertation. These microfluidic platforms are increasingly capable of performing complex

bioassays with increased autonomy, portability, and cost-efficiency relative to traditional benchtop instrumentation. The preponderance of work here was centered specifically on leveraging these advantages to automate and expedite microfluidic technologies for nucleic acid preparation with the specific goal of lowering the barrier to entry for sample-to-answer LoaDs to be utilized in both forensic and clinical settings. Additionally, preliminary work was demonstrated towards enabling the PoN implementation of ELISAs, which largely remain tethered to centralized facilities and require highly manual processes and trained personnel. This work was centered on improving capabilities for on-site colorimetric drug testing, an area that represents a major technology gap in current law enforcement capabilities. With continued development of the LoaDs described here, chiefly through integration and characterization of on-board reagent storage, each has the potential for practical PoN implementation.

6.4. References

1. Woolf, M. S.; Cunha, L. L.; Hadley, K. C.; Moffett, R. P.; Landers, J. P., Towards an Affinity-Free, Centrifugal Microfluidic System for Rapid, Automated Forensic Differential Extraction. In preparation.

2. Turiello, R.; Dignan, L. M.; Thompson, B.; Poulter, M.; Hickey, J.; Chapman, J.; Landers, J. P., Centrifugal Microfluidic Method for Enrichment and Enzymatic Extraction of Severe Acute Respiratory Syndrome Coronavirus 2 RNA. *Analytical Chemistry* **2022,** *94* (7), 3287-3295.

3. de Oliveira, K. G.; Borba, J. C.; Bailao, A. M.; de Almeida Soares, C. M.; Carrilho, E.; Duarte, G. R. M., Loop-mediated isothermal amplification in disposable polyester-toner microdevices. *Analytical Biochemistry* **2017,** *534*, 70-77.